MARINE SCIENCE & ENGINEERING WITH PLYMOUTH UNIVERSITY

AN ADAPTIVE AUTOPILOT DESIGN FOR AN UNINHABITED SURFACE VEHICLE

ANDY SK ANNAMALAI

A thesis submitted to Plymouth University

in partial fulfilment for the degree of

DOCTOR OF PHILOSOPHY

School of Marine Science and Engineering

Faculty of Science and Environment

In collaboration with
UTC Aerospace Systems

2014

To my Grandparents…

Abstract

An adaptive autopilot design for an uninhabited surface vehicle

Andy SK Annamalai

The work described herein concerns the development of an innovative approach to the design of autopilot for uninhabited surface vehicles. In order to fulfil the requirements of autonomous missions, uninhabited surface vehicles must be able to operate with a minimum of external intervention. Existing strategies are limited by their dependence on a fixed model of the vessel. Thus, any change in plant dynamics has a non-trivial, deleterious effect on performance. This thesis presents an approach based on an adaptive model predictive control that is capable of retaining full functionality even in the face of sudden changes in dynamics.

In the first part of this work recent developments in the field of uninhabited surface vehicles and trends in marine control are discussed. Historical developments and different strategies for model predictive control as applicable to surface vehicles are also explored. This thesis also presents innovative work done to improve the hardware on existing *Springer* uninhabited surface vehicle to serve as an effective test and research platform. Advanced controllers such as a model predictive controller are reliant on the accuracy of the model to accomplish the missions successfully. Hence, different techniques to obtain the model of *Springer* are investigated. Data obtained from experiments at Roadford Reservoir, United Kingdom are utilised to derive a generalised model of *Springer* by employing an innovative hybrid modelling technique that incorporates the different forward speeds and variable payload on-board the vehicle. Waypoint line of sight guidance provides the reference trajectory essential to complete missions successfully.

The performances of traditional autopilots such as proportional integral and derivative controllers when applied to *Springer* are analysed. Autopilots based on modern controllers such as linear quadratic Gaussian and its innovative variants are integrated with the navigation and guidance systems on-board *Springer.* The modified linear quadratic Gaussian is obtained by combining various state estimators based on the Interval Kalman filter and the weighted Interval Kalman filter.

Change in system dynamics is a challenge faced by uninhabited surface vehicles that result in erroneous autopilot behaviour. To overcome this challenge different adaptive algorithms are analysed and an innovative, adaptive autopilot based on model predictive control is designed. The acronym ‘aMPC’ is coined to refer to adaptive model predictive control that is obtained by combining the advances made to weighted least squares during this research and is used in conjunction with model predictive control. Successful experimentation is undertaken to validate the performance and autonomous mission capabilities of the adaptive autopilot despite change in system dynamics.

Table of contents

List of Figures

Chapter 2

Chapter 3

Chapter 4

Chapter 6

Chapter 7

Chapter 8

List of Tables

Acknowledgements

Most of my friends have a PhD, so I had always assumed that, it cannot be that difficult. I realised the mistaken assumption underlying this premise as soon as I started one myself.

I am thankful to my Director of Studies Prof. Robert Sutton for his continued support and the opportunity to pursue research in his group; Dr. Chenguang Yang and Dr. Phillip Culverhouse for their supervision. Sincere thanks to Prof. Neil James, Prof. Pat Pearce and Prof. Arumugam for their timely guidance, support and advice to persevere despite challenging circumstances.

Thanks are extended to Gregory Nash, Bob Williams, William Stephenson and Mike Sloman for their technical support and pragmatic approach.

Many thanks to Ms. Barbara Fuller, Ms. Claire Abbot and Ms. Susan Ackland from the school office admin team; Ms. Lucy Cheetham, Ms. Francesca Niedzielski, Ms. Sarah Kearns and Prof. Mick Fuller from the graduate school office.

I would like to express my gratitude to Denis Kendall, Joan Kendall, Charles Mansfield and Dr. Helena Martensson for their kindness and constant encouragement.

I am also thankful to Ms. Christine Nussey, Ms. Janina Smietanka and Dr. Rachel Wood for their timely support and assistance.

Furthermore, the financial support from EPSRC for this research project under the auspices of Grant EP/I012923/1 is gratefully acknowledged.

Finally, thanks to Amit Motwani, Daniel Roper, Kate Freeman, Kayode Owa, Wathiq Abed and other colleagues at Buckland house and Portland square for enduring the PhD journey when reality resembled Piled Higher and Deeper (also known as PhD Comics).

Although it is not possible for me to name everyone here I am thankful for the support of those who have been involved and contributed to the success of this research.

Author's declaration

At no time during the registration for the degree of Doctor of Philosophy has the author been registered for any other University award without prior agreement of the Graduate Committee.

Work submitted for this research degree at the Plymouth University has not formed part of any other degree either at Plymouth University or at another establishment

This study was financed with the aid of a studentship from the Engineering and Physical Sciences Research Council, United Kingdom.

Relevant scientific seminars and conferences were regularly attended at which work was often presented and the publications are detailed as follows:

Journal papers

- Annamalai, A.S.K., Sutton, R., Yang, C., Culverhouse P., Sharma, S., (2014). Robust Adaptive Control of an Uninhabited Surface Vehicle, Journal of Intelligent & Robotic Systems, Springer Netherlands, issue May.

- Annamalai, A.SK., Motwani, A., Sutton, R., Yang, C., Sharma, SK. and Culverhouse, P., (2013). A robust navigation technique for integration in the guidance and control of an uninhabited surface vehicle, Journal of navigation, 11 October (under review).

- Sharma, S., Sutton, R., Motwani, A. and Annamalai, A.SK., (2013). Nonlinear control algorithms for an unmanned surface vehicle, Proceedings of the Institution of Mechanical Engineers, Part M: Journal of Engineering for the Maritime Environment, 5 November, doi: 10.1177/1475090213503630.

Conference publications and presentations

- Annamalai, A.S.K., Sutton, R., Yang, C., Culverhouse P. and Sharma, S., (2014). Innovative adaptive autopilot design for uninhabited surface vehicles, Twenty fifth Irish Signals and Systems Conference, 26-27 June, Limerick, Ireland.

- Motwani, A. and Annamalai, A.SK., (2013). Autonomous environmental monitoring, Making Waves Conference, 28 November, Plymouth Marine Laboratories, Plymouth, Devon, United Kingdom.

- Annamalai, A.SK., Sutton, R., (2013). An adaptive autopilot design for an uninhabited surface vehicle, Fourth UK Marine Technology Conference, 11-12 June, University College London, United Kingdom.

- Annamalai, A., Motwani, A., Sutton, R., Yang, C., Sharma, SK. and Culverhouse P., (2013). Integrated navigation and control system for an uninhabited surface vehicle based on interval Kalman filtering and model predictive control, Proceedings of the First IET Control and Automation Conference, 4 - 5 June, Conference Aston, Lakeside Centre, Birmingham, United Kingdom.

- Annamalai, A., Yang, C. and Sutton, R., (2013). Closed loop identification of an uninhabited surface vehicle, Proceedings of the 1st IET Control and Automation Conference, 4 - 5 June, Conference Aston, Lakeside Centre, Birmingham, United Kingdom.

- Annamalai, A.SK., (2012). Guidance and control of an USV, Making Waves Conference, 18 December, Plymouth Marine Laboratories, Plymouth, Devon, United Kingdom.

- Annamalai, A.SK., (2012). Guidance and control of an USV, Plymouth University projects showcase, 11 September, Plymouth, Devon, United Kingdom.

Word count of main body of thesis: 32,612

Andy SK Annamalai

30 May 2014

Nomenclature

Abbreviations

AC	Alternating current
ACE	Average controller energy
aMPC	adaptive model predictive control
ANFIS	Adaptive network based fuzzy inference system
ANN	Artificial neural network
ARMAX	Auto-regressive moving average with exogenous input
ARX	Auto-regressive with exogenous input
ASV	Autonomous surface vehicles
AUV	Autonomous underwater vehicle
CLID	Closed loop system identification
COA	Circle of acceptance
CPU	Central processing unit
DC	Direct current
DMC	Dynamic matrix control
DMPC	Distributed model predictive control
DOF	Degrees of freedom
FACE	Function and connectivity extension modules
FFT	Fast Fourier transform
GA-MPC	Genetic algorithm based MPC
GPC	Generalised predictive control
GPS	Global positioning system
HIECON	Hierarchical constraint control
IDCOM	Identification and command
IINA	Intelligent integrated navigation and autopilot
IKF	Interval Kalman filter
IMU	Inertial measurement unit
ITAE	Integral of the absolute error
KF	Kalman filter
KMN	Moments about the x, y and z directions respectively
LOS	Line of sight
LQG	Linear quadratic Gaussian
LQR	Linear quadratic regulator
LS	Least squares
MIMO	Multiple input multiple output
MPC	Model predictive control
MPHC	Model predictive heuristic control
MSE	Mean square error
NASA	National Aeronautics and Space Agency
NGC	Navigation, guidance and control
NMPC	Nonlinear model predictive control
ONR	Office of Naval Research
PC	Personal computer
PFC	Predictive functional control
PID	Proportional integral and derivative
PNG	Proportional navigation guidance
PRBS	Pseudo random binary sequence

QDMC	Quadratic dynamic matric control
QP	Quadratic programming
RHC	Receding horizon control
RHIB	Rigid hull inflatable boat
RMPCT	Robust model predictive technology
ROV	Remotely operated vehicles
rpm	Revolutions per minute
RTO	Real time optimisation
SESAMO	Sea surface autonomous modular unit
SI	System Identification
SISO	Single input single output
SLAM	Simultaneous localisation and mapping
SMOC	Shell multivariable optimising control
STD	Standard deviation
SVM	Support vector machine
SVN	Support vector network
TOC	Time optimal control
USV	Uninhabited surface vehicle
UUV	Unmanned underwater vehicle
wIKF	weighted Interval Kalman filter
WLS	Weighted least squares
XYZ	Forces in the x, y and z directions respectively

Symbols

Δu	Control increments
Δn_d	Rate of change of differential thrust
λ	Line of sight angle (deg)
θ	Pitch
ϕ	Roll of the vehicle in earth fixed reference frame (deg)
α_{GD}	Learning rate
ϕ_k	Regressor
$a(t)$	Innovation sequence
A(z), B(z)	Unknown coefficients of the polynomials
C_A	Coriolis and centripetal effects due to added mass
$\overline{CE_u}$	Average controller energy
C_{RB}	Coriolis and centripetal forces acting on the rigid body
$C(q)$	Controller
$d(t)$	Dither signal
$D_{(v)}$	Hydrodynamic damping matrix
$e(k)$	Error between the reference and actual output
$G_0(q)$	True model of an USV
H_c	Control horizon
H_p	Prediction horizon or output horizon
J	Cost function
K	LQR state feedback gain matrix
K_f	Kalman filter gain matrix
M_{RB}	Rigid body inertia matrix
M	Mass of the vehicle (kg)
N	Total number of time steps

N'	Tuning parameter
n_1	Propeller thrusts of motor one (rpm)
n_2	Propeller thrusts of motor two (rpm)
n_c	Forward thrust velocity
n_d	Differential thrust
N_u	Control horizon
ρ_0	Radius of the circle of acceptance
p	Angular velocity in the *x*-direction (*deg/s*)
Q	State weighting matrix
Q	Weight on the prediction error
q	Angular velocity in the *y*-direction (*deg/s*)
R	Input weighting matrix
R	Weight on the change in the input
r	Angular velocity in the *z*-direction (*deg/s*)
$r(k)$	Distance to the next waypoint from the position of the vehicle were it on the ideal path
$r'(k)$	Distance to the next waypoint from the actual position of the vessel
$r_d(k)$	Deviation from the ideal trajectory
$S_0(q)$	Sensitivity function of the closed-loop system
T_E	Environmental forces and moments acting on the vehicle
T_H	Hydrodynamic forces and moments acting on the vehicle
T_{RB}	Vector of external forces and moments about the origin acting as an input to the rigid body
T_s	Sampling interval
u	Controller output
u	Linear velocity in the x-direction (m/s)
u_{opt}	Optimal controller output sequence
v	Constant forward speed of the vessel
v	Linear velocity in the y-direction (m/s)
V_c	Closing velocity
w	Reference trajectory
w	Linear velocity in the z-direction (m/s)
y_d	Target coordinate of USV along y axis
y_k	Observation / system output
y^{sp}	Set point
$\hat{y}$	Predicted plant output
ψ	Yaw or heading of the vehicle in eaxth fixed reference frame (deg)
$v(t)$	Effect of all unmeasured disturbance
w_k	Noise processes / sequences
x_d	Target coordinate of USV along x axis
x	x coordinate of initial position of USV
y	y coordinate of initial position of USV

Chapter 1

Introduction

"A journey of a thousand miles begins with a single step"

- Lao Tzu

ab initio

The control of a vessel at sea is a complex undertaking. Traditionally in ships, the captain is reliant on the helmsman who has acquired specialised knowledge and expertise over a number of years. Over millions of years of evolution, most *Homo sapiens* have evolved to be intelligent beings. The fact that it takes so long to train such an intelligent being to become a skilled helmsman highlights the complexity of the challenges faced. These challenges become more pronounced when one attempts to design a system that will enable USVs to accomplish required tasks without any human intervention.

1.1 Project objectives

This research project forms an integral part of a research programme with an overall aim of designing and developing a new advanced intelligent integrated navigation and autopilot (IINA) system with adaptive capabilities for an USV. Three PhD research

projects are centred on making this programme aim a reality. A simultaneous localisation and mapping (SLAM) based vision and an intelligent navigation system based on interval Kalman filtering (IKF) are implemented in the other two projects. The significant aim of this PhD investigation is to design and develop an autopilot with accompanying adaptive features for an uninhabited surface vehicle (USV) named *Springer*.

The position data is provided by digital magnetic compasses and speed transducers; the information is further processed by the navigation system to provide an estimate of the vehicles position. This information is utilised in building a guidance and control system suitable to accomplish various missions.

1.2 Aims and objectives of this research

In order to achieve the aims and objectives of this research the thesis will comprise of the following elements:

- To conduct a review of USVs, and understand the system overview of navigation, guidance and control (NGC) systems, trends in marine control, different strategies model predictive control (MPC) and develop further.
- To conduct preliminary trials where the vehicle is operating in semi-autonomous, remote control modes.
- To record and examine the yaw response of *Springer* for a series of step changes in heading.

- To represent a mathematical model of the vehicle derived from system identification (SI) trials, under different operating conditions.
- To conduct the necessary experiments to generate data sets to obtain models that will be used for MPC.
- To design an autopilot that is capable of adapting to a variable vehicular dynamic behaviour with different payloads and prevailing environment conditions.
- To achieve integration between NGC systems.
- To conduct full scale system and integration tests.
- To conduct and evaluate the necessary series of full scale trials and experimental verification to evaluate the performance of autopilot.

1.3 Contributions to knowledge

The following contributions to knowledge are made;

- A new modelling technique to identify the system dynamics of an USV is developed and a generalised model of *Springer* is obtained from experimental results when the vessel is operating under different speeds and variable payload.
- A pioneering autopilot based on a modified linear quadratic Gaussian (LQG) controller that incorporates a linear quadratic regulator (LQR) and an IKF is developed for an USV and is applied to *Springer.*
- An adaptive controller termed the adaptive MPC (aMPC) based on innovative modifications of weighted least squares (WLS) and MPC is utilised as an autopilot for USVs. It is capable of adapting to gradual and sudden change in

mass. Furthermore, the controller automatically adapts to varying disturbance from uncertain weather conditions and the vehicle is kept on course, despite challenging circumstances.

- The performance of the aMPC controller is experimentally verified from field trials conducted at Roadford reservoir, Devon, United Kingdom.

1.4 Thesis overview

The overall aim of the *Springer* project is briefed in this Chapter 1. In particular the aim and objectives of this PhD research which focus specifically on the design development of the adaptive autopilots for an USV are reported.

Recent developments in USV technology, system overview and current trends in marine control systems are explored in Chapter 2. The historical development and the evolutionary path of different generations of MPC are covered in this chapter. Traditionally this controller was developed and applied in oil and refinery industries. However, more recent approaches based on the use of this controller as an autopilot for marine vehicles are detailed here.

The *Springer* and its hardware set up that is used as an experimental research platform are elaborated in Chapter 3. The control of on-board actuators, data transmission and reception and other hardware are also detailed in this chapter. Innovative improvisation and modifications of the *Springer* hardware are discussed in this part of the thesis.

Marine vehicles move in 6 degrees of freedom (6DOF); yaw, pitch, roll and the translational coordinates heave, sway and surge, which is covered in the kinetics and kinematics section in Chapter 4. Subsequently, various modelling methods such as closed loop system identification (CLID), rigid body modelling and SI techniques and its application to *Springer* are presented in the chapter. The data sets collected from experiments conducted at Roadford Reservoir are utilised to obtain auto-regressive with exogenous input (ARX) and auto-regressive moving average with exogenous input (ARMAX) model of the *Springer* under different operating conditions. Finally, an innovative technique to obtain the generalised ARX and ARMAX model of an USV and its application to *Springer* is presented in this chapter.

To fulfil their missions successfully USVs such as *Springer* are totally reliant upon the integrity of their low cost NGC systems. Hence, it is imperative to achieve integration between the NGC systems and analyse performance of the overall system. Furthermore, the integration of contemporary guidance systems with traditional autopilots such as Proportional integral and derivative (PID) and modern controllers such as LQG is detailed in Chapter 5. The overall performance of the vehicle is also examined in this chapter.

The shortcomings of traditional autopilot systems and modern controllers prompted further investigation of advanced controllers, namely MPC in Chapter 6. An MPC design for USVs is proposed and the improvements in performance are also discussed in this chapter.

Autopilots based on MPC use an internal model to keep the vehicle on course. When there is a change in system dynamics owing to a change in mass, external disturbances, *et cetera*; the internal model is no longer valid and results in erroneous behaviour of the controller. This implies that the vehicle is unable to track the desired reference and has serious implications such as damage to other marine crafts in the vicinity, hence many missions are aborted. Thus, the adaptive nature of an autopilot is not an optional, additional luxury rather it is imperative that such a characteristic is an integral part of the autopilot design. The adaptive nature based on innovations to techniques such as gradient descent (GD), least squares (LS) and WLS algorithms in conjunction with MPC is explored and a new adaptive autopilot, aMPC is created by combining the advances to WLS and MPC. This is presented in Chapter 7.

Full scale trials were conducted to verify the results from simulation studies and to examine the performance of the overall system. Furthermore, the adaptive nature of the autopilot is verified experimentally by full scale trials and these results are presented in Chapter 8. Finally, the conclusions and recommendations for further work are detailed in Chapter 9.

Chapter 2

Concomitant Research

2.1 Introduction

Human beings have fantasised about being able to control objects and to perform missions remotely from time immemorial. With the limited knowledge at that time, witchcraft and religions attempted to achieve the same. It was not until 1898 that this fantasy was transformed into reality by an engineer namely, Nikola Tesla. He coined the word ‘tele-automation’. Despite being ahead of his time, Tesla was unable to sell his patent to the US Defense Department (Sosic, 1976). Few other engineers made attempts to interest the business community with their patents for similar systems with very little success. This is an example of how technical advances are shaped by key industries and major users. However, recently, there has been a turn of the tide and there has been increased interest both in academia and industry to develop such systems. As technology progressed, remotely operated vehicles evolved to be capable of performing missions and these are now known as autonomous surface vehicles (ASV) and unmanned surface vehicles (USV). However, the term ‘unmanned’ is being replaced by ‘uninhabited’ in recent literature (Roberts and Sutton, 2012). Currently, USVs are successfully deployed for military operations, search and rescue missions and environmental monitoring, to name a few applications (Motwani, 2012). In the context of military operations USVs are valuable in defence applications such as mine hunting and anti-piracy e.g. by providing a protective perimeter around a vessel. In offensive applications USVs could be armed with missiles and/or automatic weaponry; however

progress in this particular direction is necessarily constrained by ethical considerations. USVs also have considerable potential for civil applications such as structural engineering problems (e.g. bridge scouring and oil platform maintenance issues), search and rescue, firefighting and environmental monitoring. In addition USVs have a number of potential research uses including energy harvesting, cloud creation and environmental sampling applications. Despite the advances in modern electronics, communications and engineering in general, the technologies and the theoretical concepts used in current USVs are still in their infancy. The largest proportion of USVs currently in use are, in fact, remotely operated vessels requiring a human operator in the control loop. Thus autonomous functionality is still a significant research goal in this domain and further development and exploitation of such systems will necessitate the discovery of means to implement autonomous operation for USVs. Before attempting to progress along these lines, one has to be aware of the current and recent developments in this field to identify the gaps in the current literature and to progress the research further to answer worthy research questions.

Hence, recent developments in USVs are provided in the following Section 2.2. Furthermore, this chapter is organised as follows, a system overview is described in Section 2.3 and the current trends in marine control systems are reported in Section 2.4. The use of support vector machine (SVM) inverse model based heading control of an USV is also explored in this section along with the use of predictive and sliding mode cascade control. An overview of model predictive control is given in Section 2.5. Different MPC strategies are given in Section 2.6. Finally, concluding remarks are given in Section 2.7.

2.2 Uninhabited Surface Vehicles

Fifteen years of development of USVs were presented by Manley (2008). Furthermore, a detailed survey of the different USVs used by different military and other research organisations is described in detail by Bertram (2008) and Motwani (2012). Some of the early technologies which enabled the development of USVs and the future outlook of USV technology are described in these papers. During the trials of the first USV (named ARTEMIS) built at Massachusetts Institute of Technology in 1993, it was observed that the small size was a big limitation and it seriously undermined the mission capabilities by reducing its sea-keeping and endurance. Modification and design iterations of the USV resulted in better efficiency and it was able to perform missions in the real world. Around 2003, the US Navy revealed its 'Master Plan' with its focus on development and deployment of USVs. Yet again, it was a demonstration of how end users drive technical advances.

USVs have been successfully utilised in survey missions since 2000 and different experiments have been conducted by different teams around the globe using various hull shapes (Alves et al., 2006). Most of the academic institutions have opted for catamaran type USVs owing to operational flexibility and practicality. *Springer* is an USV developed by Plymouth University around the same time and was slightly ahead of the ROAZ, a catamaran USV built by a Portuguese research team at Instituto Superior de Engenharia does Porto (Ferreira et al., 2006). Prior to this in the late 1990's Dynamical Systems and Ocean Robotics Laboratory in Portugal developed a small autonomous surface craft named *Delfim* and utilised it to perform various proof of concept experiments (Dynamical Systems and Ocean Robotics Laboratory, 2012). More recently, the sea surface autonomous modular unit (SESAMO) project utilised *Charlie*

USV built by an Italian marine robotics research group at Consiglio Nazionale delle Ricerche Istituto di Studi sui Sistemi Intelligenti per l'Automazione (CNR-ISSIA) (Caccia et al., 2005). It is noteworthy to mention that the SESAMO project was conducted in harsh environmental conditions of Antarctica to support ocean research. This last vehicle exemplifies the use of USVs to extend human capabilities by operating in inaccessible and inhospitable environments; enhancing our abilities to understand nature by collecting data under adverse conditions.

Another interesting hybrid is the semi-submersible platform developed by Autonomous Surface Vehicles Ltd. The hull of the vehicle remains submerged underwater and the mast for communication and air exchange remains outside the water level (Phillips et al., 2008). Being submerged underwater enables the vehicle to utilise better propulsion systems and exhibits greater passive stability. However, the electronics have to be encased in a sealed water tight compartment and it is not as flexible and practical as a catamaran hull.

The twin hull design of *Springer* has certain advantages such as positive buoyancy; it is practically unsinkable even if there is a hull penetration. Thus it provides valuable time required to perform rescue or repair, if necessary. Moreover, other marine vehicle designs rely only upon one motor and have rudder mechanisms to control the heading. This inherently increases the risk of failure in case the only available motor malfunctions. The advantage of twin motors present in the catamaran hull is that the vessel can return to base even in the case of a motor failure.

USVs are finding a niche in costal and estuarine systems as a tool for the rapid and cost effective deployment of platforms for environmental monitoring and assessment. One such example is an USV developed by University of South Florida. It has been

developed specifically for environmental monitoring (Steimle and Hall, 2006). Similarly the *Springer* is a unique academic research platform in the UK developed by Plymouth University and is designed for environmental monitoring (Bertram, 2008). Also, Olin College of engineering have developed an USV which is very similar to *Springer*. It also serves as a low cost educational platform for scientific research. Further details about this USV can be found in Holler et al., (2008). Another catamaran style ASV which is similar to *Springer* is presented by Wang et al., (2011). Generally the USVs are reliant upon three basic systems (NGC) which enable them to operate autonomously. An overview of the systems involved is presented in the following section.

2.3 System overview

Navigation, guidance, and control systems are the fundamental blocks that work in conjunction to provide autonomous capability for surface vehicles. The general system overview and the relation between the different systems of an USV are illustrated in Figure 2.1. The navigation system is concerned with determining the current location of the vessel and is achieved by collecting online, real time data from its sensors. The guidance system decides the best possible physical trajectory to be followed by the vehicle. Guiding an automatic vehicle along a desired trajectory has been further explained by Freund and Mayr (1997). The guidance system gets its input from the navigation system and generates the required reference headings. The control system is responsible for keeping the vehicle on course as specified by the guidance processor.

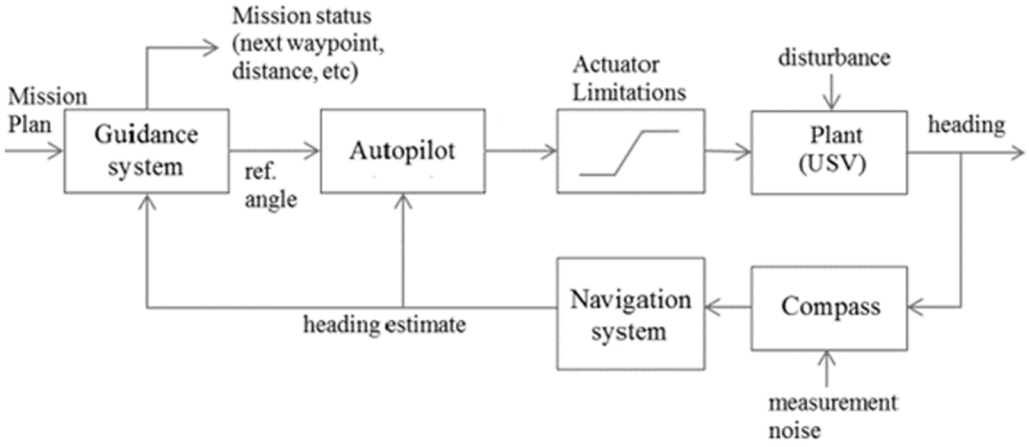

Figure 2.1: General system overview block diagram

Once the functionality of these basic blocks is understood, it was time to investigate the trends in marine control systems.

2.4 Trends in marine control systems

Researchers have made considerable progress in applying intelligent approaches such as fuzzy logic, artificial neural network (ANN) and their combinations into marine systems. Polkinghorne et al., (1995) report the first commercial fuzzy autopilot. Whilst Craven (1999) reports the use of adaptive network based fuzzy inference system (ANFIS) to develop control strategies for UUVs. Though the intelligent systems performed well in simulation studies, application in real life systems produced performance and stability issues. Hence, these techniques are still not widely used in practical applications.

First full scale trials using LQG and H-Infinity controllers for integrated fin rudder roll stabilisation on warships were reported by Roberts et al., (1997). Other developments have included research on control strategies such as the parallel multi-model control system or switch control system. This entails the design of a bank of controllers for

different ship speeds, sea states and encounter angles with a mechanism for automatic switching to the appropriate controller for a given set of conditions (Narendra and Balakrishan, 1997). Further work along the switched control was progressed by Ippolitti et al., (2006) and applied to unmanned underwater vehicles (UUVs).

Roberts (2008) presents a clear picture of the trends in marine control. The only limitation of this study is that the author has considered only the events sponsored by International Federation of Automatic Control. Nevertheless, the study engenders assurance regarding the trends in marine control by considering 750 papers and 13 conferences over a period from 1992 to 2008. Sperry and Minorski developed the first steering autopilots (Roberts, 2008; Sharma et al., 2012). Their pioneering work led to the introduction of PID controllers for automatic ship steering. Also, Fossen (2000) explains that the invention of electrically driven gyrocompass was a pivotal moment. Further advances in this research finally culminated in the development of PID which remains an important advance in ship control.

Further, Roberts (2008) clearly presents the reluctance of industry to overcome the inherent inertia for change from PID controllers and highlights the challenges faced by new autopilot designs to meet high industry standards.

Another area of interest in marine control systems is the control of rudder systems. Stafford and Osborne (2008) report on the technology demonstration projects commissioned by the UK Ministry of Defence (MoD) to realise the all-electric ship concept. They advocate the use of electrical actuation for hydrodynamic control surfaces of rudder systems as it allows faster rudder speed and has significant

advantages over hydraulically operated counterparts. Whilst, most of the advances presented above are concerned with ships and some UUVs, developments related to USVs will be discussed as below.

Passenger comfort and stability of cargo were the driving factors which necessitated the development of control systems designed to achieve roll stabilisation for ships. However, the primary task of reaching desired waypoints still remains a challenging task with respect to USVs. Hence, the heading/yaw control of USV autopilots takes priority in this investigation.

A control methodology based on a SVM inverse model has been used to control the heading of an USV by Qiaomei et al., (2010). It is interesting to note that the support vector network (SVN) was originally proposed by Cortes & Vapnik (1995) as a new learning machine for pattern recognition and early tests entailed optical character recognition study from the US postal service database. Building on initial successes, the use of SVNs was extended to regression analysis and eventually made its way into USV autopilots.

The SVM inverse model direct control is illustrated in Figure 2.2. The SVM inverse model and PID feedback compensation are used to achieve the desired control of heading is shown in Figure 2.3. SVM learning differs from other learning algorithms such as ANNs as the learning here is based on small samples learning. Other benefits of this method include high generalisation ability, avoids over fitting and local minimum point (Qiaomei et al., 2010).

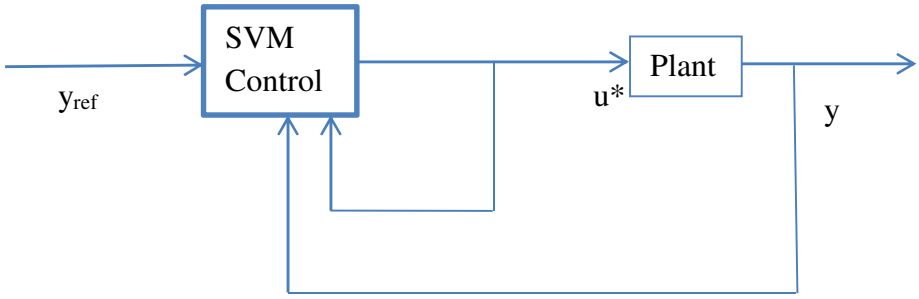

Figure 2.2: SVM inverse model direct control (Qiaomei et al., 2010)

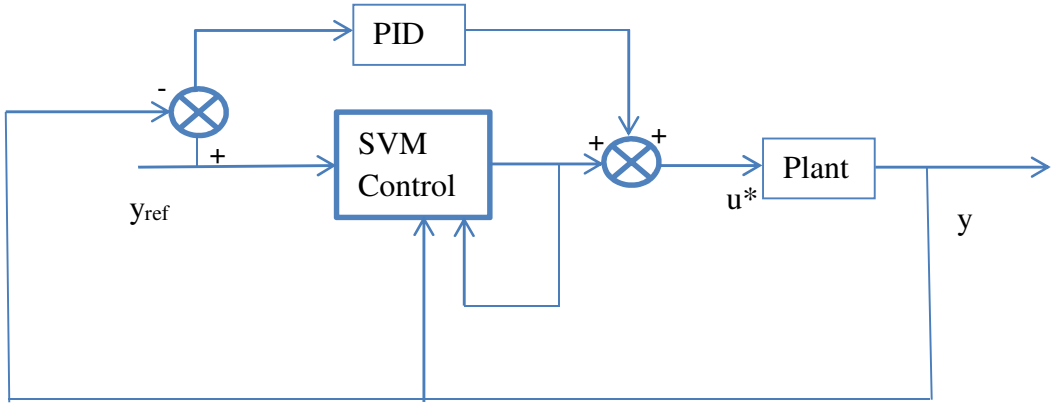

Figure 2.3: SVM inverse model combined with PID feedback (Qiaomei et al., 2010)

Another approach to designing an autopilot for an USV is to use a sliding mode control. Researchers such as McNinch & Ashrafiuon (2011) have obtained marginal improvements by improvising the sliding mode control to a cascade control structure by utilising a discrete time, nonlinear model predictive control (NMPC) to update the parameters of the sliding mode control surfaces to obtain specific performance objectives such as minimum tracking error, minimum time and minimum energy. This simulation study was sponsored by the Office of Naval Research (ONR) which reaffirms the dearth of progress along these lines and need to further research in the areas of designing and building autopilots for USVs. In addition there are growing research interests between UK institutions such as University College London and several universities in the USA including the US Naval Post Graduate School in Monterey CA; the US Naval Academy in Annapolis (MD); Florida Atlantic University (FL) and Steven's Institute of Technology (NJ). This group has received continuous funding from ONR for over 12 years in the field of USVs, in particular for the development of autonomous Wave Adaptive Modular vehicles (WAM V) through the Atlantic Centre for the Control and Design of Small Ships (ACCeSS) sponsored by ONR [Grant N00014-10-1-0652].

2.5 Model Predictive Control Development

This section introduces the topic of MPC, provides an overview of the historical developments in this field and briefly explores the different approaches. MPC refers to a class of algorithms that compute a sequence of manipulated variable adjustments in order to optimise the future behaviour of a plant. The development of MPC dates back to 1978 when Richalet et al. (1978) published a paper on a technique they termed model

predictive heuristic control (MPHC). The approach was originally applied to a fluid catalytic cracking unit main fractionator column and subsequently to a number of other industrial control problems. Cutler and Ramaker (1980) independently developed an MPC technology they termed dynamic matrix control (DMC). In addition Clarke et al. (1987) developed a generalised form of MPC (GPC). These methods differ in the type of model used and the cost function optimised. Zanovello and Budman (1999) present an MPC algorithm with soft constraints. Finite number of weights MPC is based on selecting an appropriate combination of weights even when system constraints are violated. Mayne et al., (2000) present extensive discussion of the issues of stability and optimality of MPC. In addition Morari and Lee (1999) and Qin and Badgwell (2003) present detailed overviews of MPC technologies. The evolution of major MPC algorithms is illustrated by the following Figure 2.4.

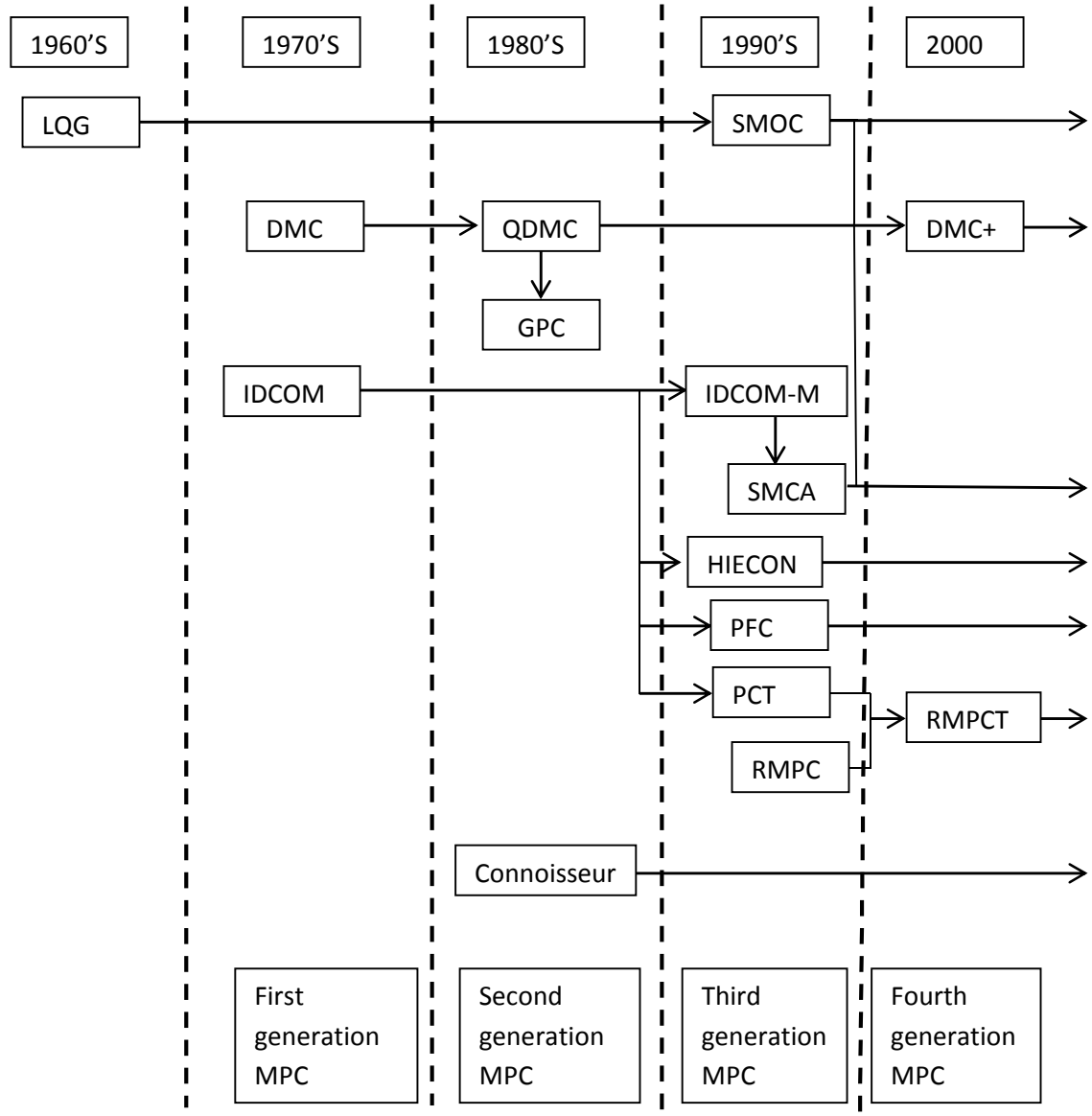

Figure 2.4: Approximate genealogy of linear MPC algorithms

As seen from the above figure, the first generation of MPC technology was dominated by dynamic matric control (DMC) algorithm and identification and command (IDCOM) software. Second generation MPC technologies like quadratic dynamic matric control (QDMC) were able to handle the input and output constraints in a systematic manner (Jounela, 2007). The third generation MPC algorithms such as hierarchical constraint control (HIECON), predictive functional control (PFC), Shell multivariable optimising

control (SMOC) were able to distinguish between the different level of constraints (hard, soft and ranked). Competition and mergers in the industry resulted in two major fourth generation MPC algorithms; robust model predictive technology (RMPCT) is offered by Honeywell and DMC-plus is offered by Aspen Technologies. The fourth generation MPC algorithms are capable of prioritising different control objectives and handling model uncertainties (by using prediction error methods and sub-space methods). The industry is beginning to embrace MPC, despite the high implementation costs. This is owing to the fact that the businesses get a return on their investments under 18 months. Hill (2011) questions this wide spread acceptance of MPC by the industry. He argues that the advanced regulatory control may be better suited than MPC for certain processes in petrochemical industries. Furthermore, Sharma and Sutton (2012) demonstrate the application of MPC in other industries such as automotive, academia and research. The complexity of MPC presents numerous strategies to design the controller based on different design constraints and are evident in the subsequent section.

2.6 Different MPC strategies

MPC is partially limited by the ability to solve optimisation problems in real time. One strategy for improving the computational performance is to formulate MPC using a linear program. While the linear programming formulation seems appealing from a numerical standpoint, the controller does not necessarily yield good closed-loop performance. A combination of penalties on moves, reference trajectory and model filter was used to tune the MPC in a practical way by Wojsznis et al., (2003).

A genetic algorithm based MPC (GA-MPC) that was designed and applied to an AUV is presented by Naeem et al., (2005). It is the first known application of an online genetic algorithm (GA) operating in an underwater vehicle in real time. Also, other researchers such Gabriel Hugh Elkaim (from University of California, Santa Cruz, USA) have succeeded in designing a LQG controller and tested it with the electric trolling motor. The controller demonstrated excellent line-tracking performance, with error standard deviations of less than 0.15m (Elkaim, 2009). The wing-sail propulsion system was fitted, and the same controller was re-tested with the wing providing all propulsive thrust. Line-following performance and disturbance rejection were excellent, with the cross-track error standard deviations of approximately 0.30m, in spite of wind speed variations of over 50% of nominal value (Elkaim, 2009). The controller is able to achieve good performance due to the accurate modelling of the system in discussion. Conversely, such modelling fails to take into account when there is a change in mass of an USV. Performance will deteriorate considerably if such a change were to happen in real life. This problem is dealt with in detail in Chapter 7.

The linear MPC is pretty much a convex optimisation problem and stable results are available. Conversely, for non-linear MPC optimisation problem is more complicated and is in general non-convex. This means that the global optimality cannot be guaranteed (Åkesson and Slätteke, 2006). The solution of the optimisation problem provides the feedback control action, and can be either computed by embedding a numerical solver in the real-time control code, or pre-computed off-line and evaluated through a lookup table of linear feedback gains (Bemporad, 2006).

Other strategies such as fuzzy reasoning techniques and ANN structures are applied to MPC by Tatjewski and Lawrynczuk (2006). The two components of the most commonly used quadratic cost functions in MPC are given by the following Equation (2.1).

$$J(k) = \sum_{p=N1}^{N} ||y^{sp}(k+p|k) - y(k+p|k)||^2 + \lambda \sum_{p=0}^{N_u-1} ||\Delta u(k+p|k)||^2 \quad (2.1)$$

where $y^{sp}(k+p|k)$ is the set point and $y(k+p|k)$ is the predicted output. N_u is control horizon and it must satisfy the constraints $0< N_u \leq N$. The vector of control increments is represented by $\Delta u(k+p|k)$ and λ is the coefficient to scale the sum of squared control increments. The optimal control trajectory is calculated at each sampling instant by minimising the above cost function. The predicted controller outputs are calculated by using the following generalised input-output process model (2.2).

$$y(k+p|k) = f_p\,(\,u(k+p-1|k), \ldots, u(k|k), u(k-1), \ldots, u(k-n_B), y(k), y(k-1), \ldots, y(k-n_A), d(k), p = 1, \ldots, N. \quad (2.2)$$

Nonlinear models result in nonquadratic, nonconvex optimisation problems. Hence the online computation of the MPC algorithm encounters a major problem. Furthermore improvements due to application of neural networks in modelling are also illustrated by Tatjewski and Lawrynczuk (2006).

Richards et al., (2006) offers a completely different perspective to solve the MPC control problem. This paper presents a new analysis tool for predicting the closed-loop performance of a robust constrained MPC scheme. Most other methods use

computationally expensive numerical simulations to investigate the effect of controller parameters like the horizon length, cost of weightings and constraint settings. The computational burden is avoided by analytic method. The expected performance of the controller was predicted using a combination of gains of two linear systems, the optimal control for the unconstrained system and a candidate policy used in performing the constraint tightening. Also, the mismatch between the predicted level of disturbance and the actual disturbance encountered by the system in real time is taken care of in this method.

Sui and Ong (2008) presents two control strategies under the time optimal control (TOC) and MPC frameworks for constrained piecewise linear systems with bounded disturbances (PWLBD systems). Each of the proposed approaches uses an inner convex polytopal approximation of the non-convex domains of attraction and results in simplified control laws which can be determined off-line via multi-parametric programming. These control strategies rely on invariant sets of PWLBD systems. Thereby, approaches for the computation of the disturbance invariant outer bounds of the minimal disturbance invariant set, and convex polytopal disturbance invariant sets are presented. Martensson and Wernrud (2008) overcame the optimal control problem of MPC by proposing to parameterise the control sequence in each sampling instant a dynamic feedback compensator is computed. Hence, the control system runs in a closed loop when the computational delays are present. Whereas, in traditional MPC a finite horizon open loop optimal control problem is solved at each sampling instance which might lead to problems if uncertainties are present.

MPC has slower dynamics. This presents challenges when the plant to be controlled is an USV like *Springer* where the system dynamics tend to be faster (depending on the operational mode and mission desired). Although, the techniques of MPC have been well established in process, petrochemical industries, automotive industries and academic research communities as illustrated by Maciejowski (2002), Rawlings and Mayne (2009), Wang (2009), Allgower, et al., (2010). On the contrary, very few researchers have focussed on the application of MPC concepts to the autonomous marine vehicles. This gap in the research begs further investigation.

Some primitive solutions to overcome the problem of MPC's slower dynamics have been investigated by other researchers as follows. For example, Wang and Boyd (2010) proposed the use of fast MPC which computes the entire control law offline and hence reduces the online controller to a mere look up table. This method works well for system with small state and input dimensions. Fast MPC can compute control actions 100 times faster than generic optimisers. An example problem with 12 states, 30 prediction horizon, and 3 control horizon is solved in less than five msec (hence MPC will be carried out at 200 Hz). It is worth noting that currently MPC used in *Springer* USV operates at 1 Hz. Different authors attempt to solve this problem by different approaches. Explicit MPC is one such approach where in the problem is solved analytically and explicitly. Hence, the control policy involves only searching through a lookup table. Another approach is to solve the optimisation problem efficiently by hand written code. However, drawbacks include substantial development time, specialised knowledge of optimisation and numerical algorithms. Wang and Boyd benefited greatly from the developments in the field of convex optimisation code generation. The MPC policy is specified in a high-level language and the source code is generated for a

custom solver. The custom solver is much faster than generic solvers. This enables the user to utilise MPC polices at KHz rates.

Continuous systems real time optimisation (RTO) has been integrated into MPC by one layer strategy by De Souza, et al., (2010). The cost function of the controller contains the gradient of the economic objective function. Non-linear process model has been used to obtain the optimal conditions of the process at steady state. The plant step test has been used to obtain the linear dynamic model and this linear model has been used to obtain the trajectory to be followed. A quadratic programming routine is used at each sampling step to solve the resulting control / optimisation problem. This approach provides equivalent results instead of solving the entire optimisation problem inside the MPC controller. Solving the full economic optimisation inside the MPC controller results in a non-linear programming problem where the computational power required is much greater. Preview action is used as a standard in MPC. However, feed-forward which is rarely used in the formulation of MPC provides significant improvement when there is an uncertainty with the model and measured noises are presented by Carrasco and Goodwin (2011).

In distributed model predictive control (DMPC), the model is decomposed into N subsystems. Time-varying state-feedback controller has been used for each subsystem to solve the N convex optimisation problem. This has been incorporated into an online algorithm which addresses the problem with model errors in DMPC (Liu, et al., 2011c). The data from MPC vendors have been collected by Liu, et al (2011c) to provide an overview of linear and nonlinear MPC available in the market currently. It also provides

a good summary of identification technology and MPC applications available in the market commercially.

MPC has been combined with an adaptive input disturbance predictor to solve the problem faced by ships which travel in high seas (Liu et al., 2011c). Traditional stabilisation systems performance declines due to the uncertainties in the hydrodynamics as a result of change in sailing conditions and sea states. An autoregressive model of the input disturbance has been used to predict the wave disturbance and the MPC is used to compensate this predicted disturbance. This combination helps the control system to deal with mode uncertainties with robustness. It also enables the ship to adapt to changing sea conditions. This combination solves the problem of performance degradation resulting from state observer estimation errors. Generally the state observers are used with the MPC to estimate output distances (Liu et al., 2011c). Furthermore, subspace methods were used by Privara, et al., (2011) to obtain the multiple input multiple output (MIMO) model of the building heating system to design an MPC controller.

Thus, after investigating the different strategies of MPC the feasibility of utilising MPC as an autopilot for an USV was explored. Kim, et al., (2004) suggest that the accurate control of the autonomous vehicle can be obtained efficiently by using MPC. Moreover, Ghaemi et al., (2010) presents the experimental implementation of MPC strategy for path following on a model ship. The MPC is designed and implemented using both linear and nonlinear models. The experimental test results from *Springer* USV with modified optimal controller show promising results amidst external disturbances and uncertain models (Naeem et al., 2012). Soft computing methodologies have also been

used to develop the subsystems algorithms. A fuzzy LQG autopilot for *Springer* USV was found to perform better than standard LQG and GA-MPC autopilots (Naeem, et al., 2012).

2.7 Conclusions

Historical developments in the field of USVs right from the time of Tesla have been presented. This chapter also highlights the challenges faced by engineers to convince the industry to adapt new techniques/technology. For example, when Tesla demonstrated his tele-automation, the audience were suspicious that he had hidden a well-trained monkey which was capable of reacting when prompted appropriately! Apart from this, the negative publicity inflicted by Thomas Edison ensured that further progress along these lines was stalled during their lifetimes. Engineers need to be aware of the impact of multi various factors to be successful in in their chosen field of research. Despite an unceremonious beginning, the field of USVs has leapt forward considerably, especially after the publication of the 2003 'Master Plan' by the US Navy. Since then, a plethora of USVs have been built by academic/research institutions and marine industries. Under the given circumstances *Springer* has been designed by Plymouth University to serve as a research and test platform. Subsequently, generic overviews of the different functional blocks which make the USV functional at present have been covered in this chapter. Other trends in marine control as discussed in Section 2.4 highlighted the fact that most of the research and progress achieved were applicable mainly to passenger ships, warships and submarines. This called for modernisation of the autopilot systems for USVs such as the *Springer.* Hence, the possibilities of utilising advanced controllers such as MPC as an autopilot for an USV have been explored.

There appears to be no unique way of implementing the MPC. The numerous MPC strategies and their historical developments have been investigated. This investigation emphasised the advantages and the drawbacks of utilising such a controller to be an autopilot for a USV.

Chapter 3

Springer and its hardware setup

3.1 Introduction

The heart of scientific progress rests upon experimentation. Philosophers and artists observe the world around them and try to identify the underlying generalisation in nature. This has been the cornerstone for much of the progress in Science. Whereas, an engineer intervenes in his immediate environment and attempts to change the behaviour to obtain desirable results. The hardware components are the valuable tools that enable engineers to achieve their desired goals. Therefore, this chapter provides an overview of the tools and major components used in the implementation and testing of *Springer*. Section 3.2 describes the *Springer* vessel, its main components, dimensions and propulsion systems. Section 3.3 details the Intense PC Pro used to implement the NGC systems on board *Springer*. The next three Sections: 3.4, 3.5 and 3.6 describe the compasses used (TCM2, HMR3000 and KVH C100). Section 3.7 gives an overview of the RoboteQ controller AX2850. Section 3.8 describes the other hardware used and Section 3.9 presents conclusions.

3.2 *Springer* USV

Some pre-trial experiments were conducted with *Springer* to ensure successful trials. To ensure that the compasses were calibrated correctly and functioning appropriately, the Pelican case enclosing the Intense personal computer (PC) Pro and the sensors was

tested on a mobile platform. In addition, each compass was individually housed in a small waterproof case to provided further isolation and insulation during the full scale trials.

The details of the *Springer's* hardware were published in Sutton et al (2011). However, for the sake of completeness an outline is presented here. The *Springer* USV (as shown in Figure 3.1) was designed as a medium water plane twin hull vessel which is versatile in terms of mission profile and payload. It is 4.2m long and 2.3m wide with a displacement of 0.6 tonnes. Each hull is divided into three watertight compartments. The NGC system is carried in watertight Pelican cases and secured in a bay area between the crossbeams. The batteries which are used to provide the power for the propulsion system and on-board electronics are carried within the hulls, accessed by a watertight hatch. A mast has also been installed to carry the GPS and wireless antennas. The wireless antenna is used as a means of communication between the vessel and its user and is intended to be utilised for remote monitoring purpose, intervention in the case of erratic behaviour and to alter the mission parameters.

Figure 3.1: The *Springer* uninhabited surface vehicle

The *Springer* propulsion system consists of two propellers powered by a set of 24V 74lbs (334N) Minn Kota Riptide transom mounted saltwater trolling motors. As will be seen in Chapter 4, steering of the vessel is based on the differential propeller revolution rates.

The status of the hardware in *Springer* USV was assessed and an initial inventory was carried out in September 2011. RoboteQ controller AX2850 is used to control the two trolling motors. Dry tests were carried out in land to verify the controller's functionality from the project laptop. Different conditions were simulated and the tests were successful. After verifying the motors, batteries and controllers integrity the *Springer* USV was remotely operated to check its sea fitness.

There are two Pelican cases on board in the *Springer* to house the electronics and the processing equipment. Owing to the temperature restrictions inside the Pelican case, it was decided to use the *Intense PC Pro* offered by CompuLab after some deliberations. Further rationale for the choice of Intense PC Pro is detailed in the following section.

3.3 Intense PC Pro

The previous research team had modified the traditional desktop PC's and adapted it for the marine application. The power supply in *Springer* is a direct current (DC) source. This had been converted into an alternating current (AC) source to power the desktop PCs. From the *Springer* technical meetings it was decided to avoid the conversion of the power supply from DC to AC to merely power up the PCs. Moreover, DC supply has the additional advantage of being safer, with a lower risk of electrocution than AC.

Another issue with the traditional desktop PCs and laptops is heat generation. Moreover, the generated heat is not evenly distributed and is contained within hotspot pockets. They are reliant on a fan as a cooling system, which works to acceptable standards under normal terrestrial conditions. However, in *Springer* the PCs are encased in a water tight Pelican case. This compounds the problem of heat dissipation and increases the risk of autopilot and navigation system failure. Initially various modifications to the desktop PC circuitry was considered. It was feasible to circumvent the AC power supply unit and to power it up from a DC source. In spite of this, the cooling system problem was pertinently persistent. Initial thoughts were to design a custom built cooling system. Due to time constraints and efficiency of such a design, this approach

was deemed unfeasible. Hence, it was decided to purchase Intense PC Pro as shown in the following Figure 3.2.

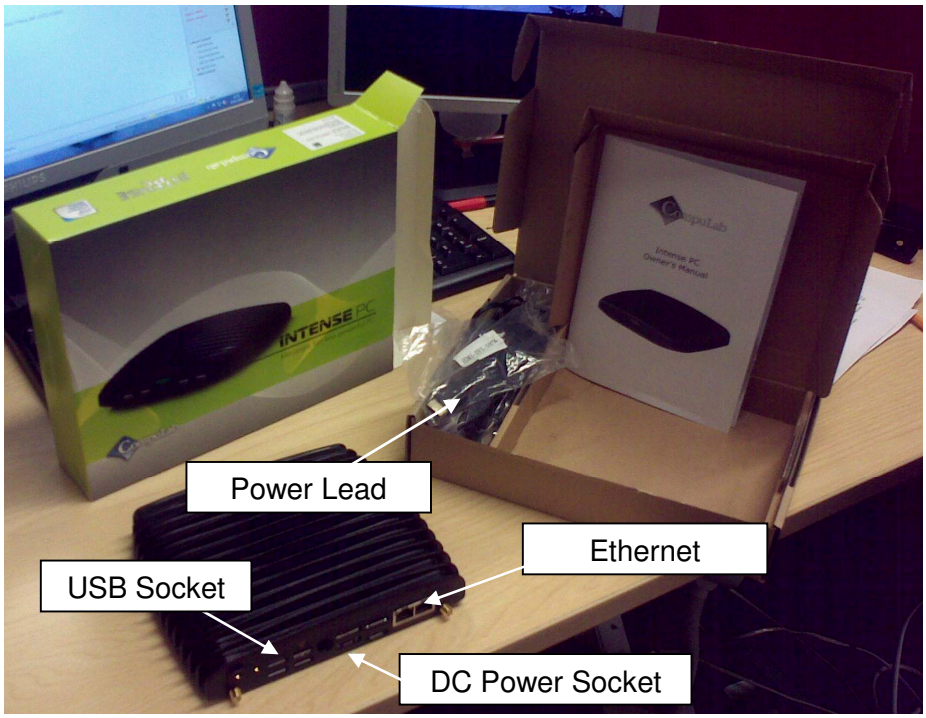

Figure 3.2: Intense PC Pro with Intel i7-3517UE processor

This inherently made the need for external cooling system redundant. Another advantage was that there were no moving parts such as a fan and it had a small form-factor. Static devices increase the robustness and deliver high performance under harsh operational conditions. Furthermore, the central processing unit (CPU) is under-clocked when the temperature inside the Pelican case reaches above the normal operating range of Intense PC Pro. Moreover, the high winds, surface waves and the water undercurrent disturbances cause the *Springer* operational platform to be dynamic. The Intense PC's tough enclosure can handle mechanical shock and operate normally in harsh weather conditions. Some of the key features of the Intense PC Pro from the datasheet are as follows:

- Intel Core CPU up to 1.7GHz dual core
- Low power consumption
- Ruggedised die-cast aluminium shell
- Innovative customisable modular Function And Connectivity Extension Modules (FACE) design

Further technical details of the Intense PC Pro are included in the appendix A1.

3.4 TCM2

Springer was envisaged as a low cost research test platform. Therefore, it was important to develop the systems with low cost components. Hence, TCM2 was chosen as the electronic compass, as shown in the following Figure 3.3. The design of this compass inherently takes care of static magnetic fields by appropriate calibration. However, care should be taken to ensure that the magnetic fields along each of the axis should not saturate more than ±80 μT. It is imperative that this range is not exceeded during operational conditions. If not, the output of the compass will be erroneous.

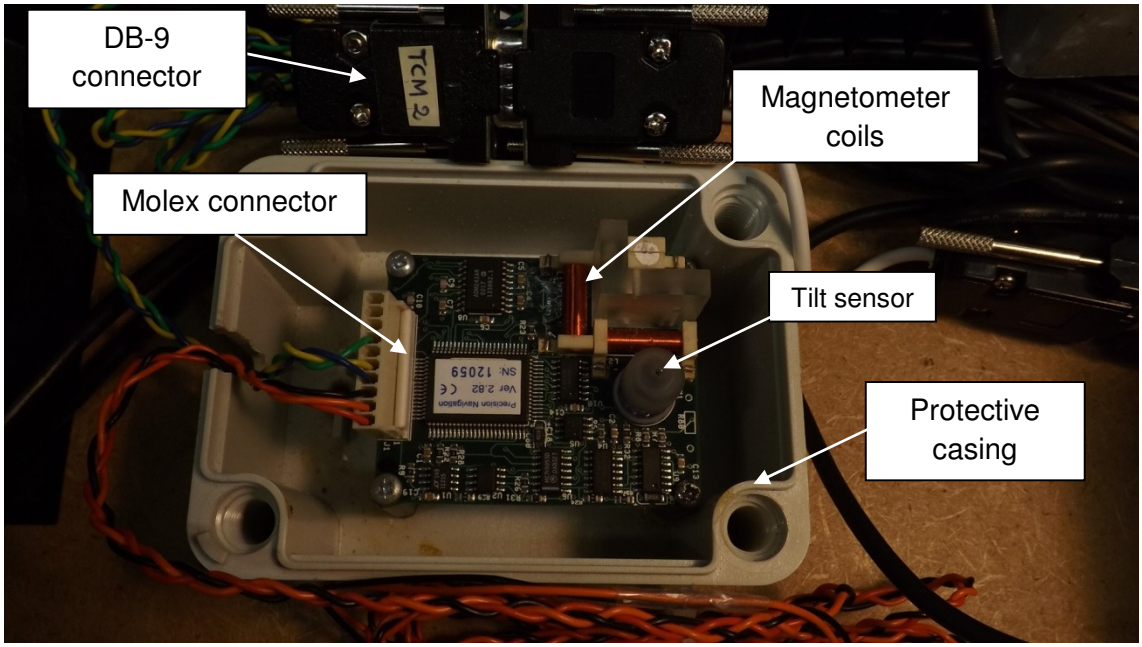

Figure 3.3: TCM2 housed inside the Pelican case on-board *Springer*

Additionally, care should be taken to ensure that interference from transformer's permanent magnetic fields from electric motors *et cetera* in conjunction with the earth's magnetic field do not saturate the compass.

Owing to the sensitive nature of the compass it is vital to mount it in a stable location. For example it would be inappropriate to mount the TCM2 on the mast of the *Springer*, which is prone to excessive vibrations and oscillations. Hence, it was housed inside the Pelican case and secured to the base with a custom built laser cut wooden platform.

The TCM2 Electronic Compass Module User's Manual provides further technical details regarding the data and power connections as illustrated by the following Figure 3.4.

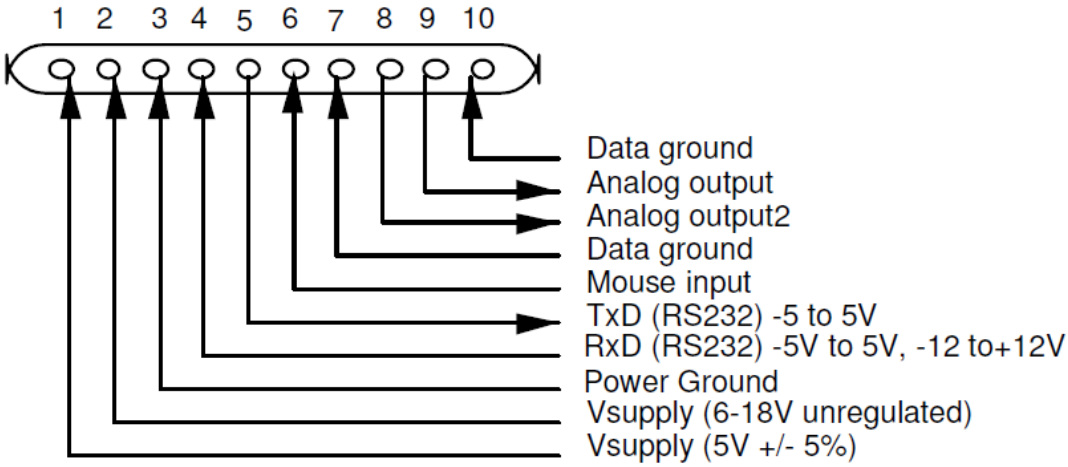

Figure 3.4: Pin-out diagram of the TCM2 connector (source: TCM2 Electronic Compass Module User's Manual)

The sampling rate of TCM2 is between 5-40Hz. However, during the normal operational mode the sensors need a minimum time of 50ms and in fast mode the sensors need a minimum time of 30ms. Further details of TCM2 can be found in appendix A2.

3.5 HMR3000

The HMR3000 is a magneto resistive compass from Honeywell as seen in the following Figure 3.5. It is capable of providing heading, pitch and roll measurements. Two possible outputs from this compass are serial full or half duplex with data rates of 12,000 to 19,200. Similar to TCM2, the HMR3000 is also sensitive to ferrous materials, *et cetera.* Further details of HMR3000 can be found in appendix A3.

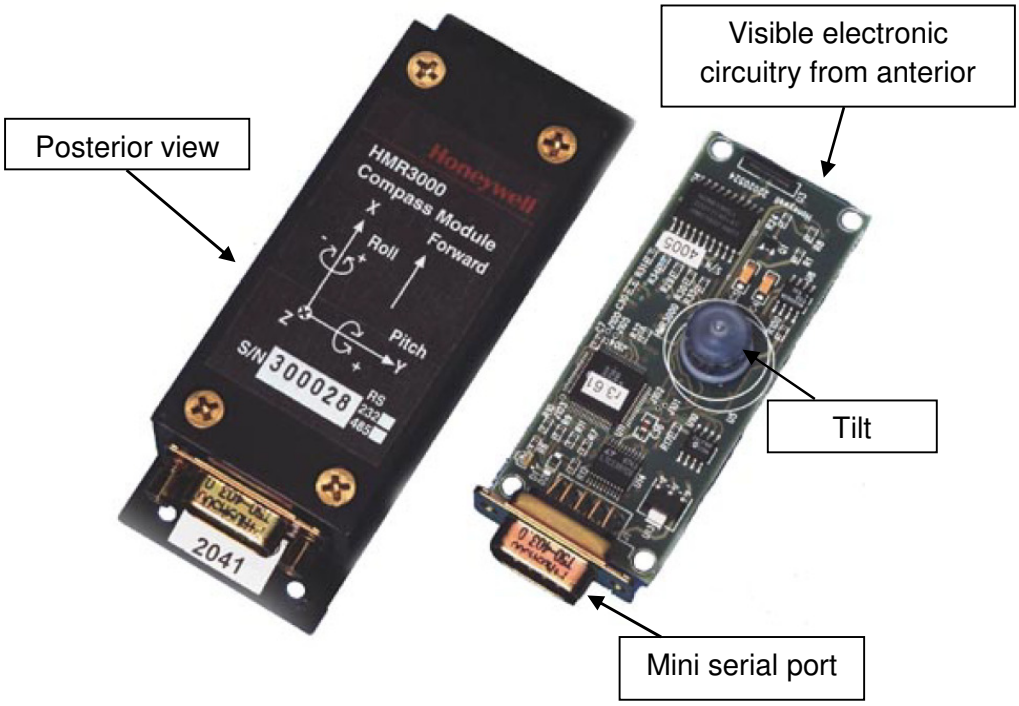

Figure 3.5: HMR3000 posterior and anterior view (source: Honeywell Inc)

3.6 KVH-C100

The KVH C100 as seen in the following Figure 3.6, outputs highly reliable heading data. An in-house custom designed electronics board in conjunction with a toroid fluxgate sensor forms the C100 compass. The saturable ring core freely floats (horizontally with respect to the earth), inside the Lexan cylinder within an inert fluid. Further details of KVH C100 can be found in appendix A4.

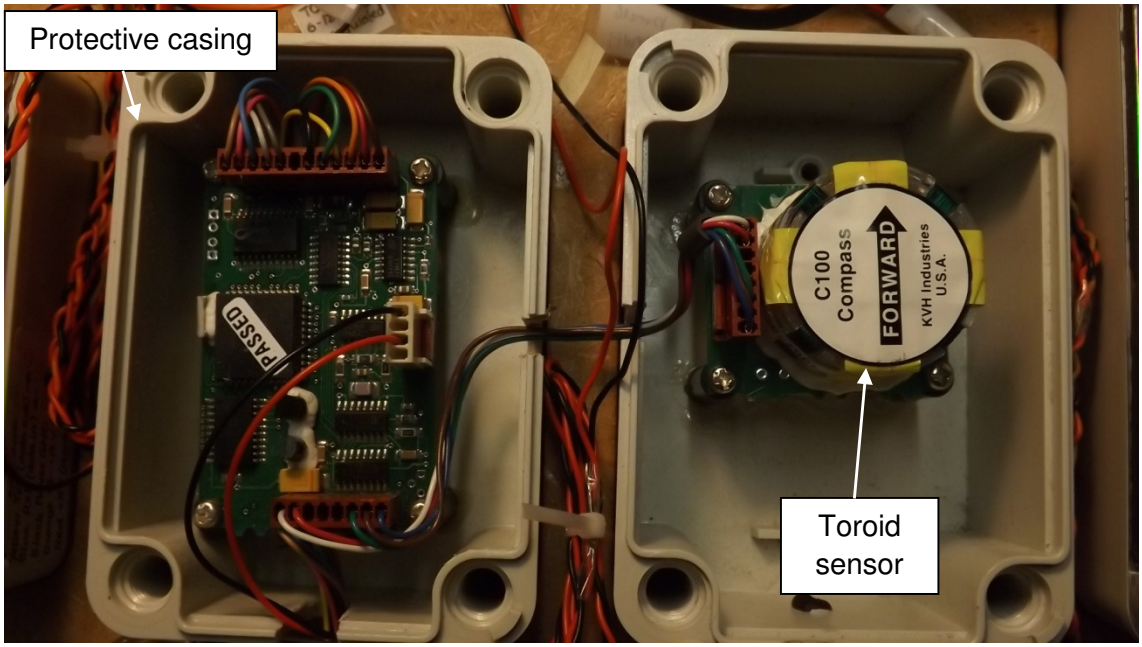

Figure 3.6: KVH C100 on-board *Springer*

Additionally, the significant technical specification of the three compasses can be summarised by the following Table 3.1.

	TCM2	HMR 3000	KVH-C100
Dimension (mm)	73.5x50.8x32.75	114.0x46.0x28.0	74.9x30.5x25.0
Weight (oz)	1.6	0.75	2.25
Baudrate	300 to 38400	300 to 9600	1200 to 38400
Supply Voltage (regulated)(VDc)	+5	+12	+5
Supply Voltage (unregulated)(VDc)	+6 to 18	+6 to 15	+8 to 18
Current (mA)	15 to 20	<40	35
Frequency (Hz)	≈ 10	≈ 10	≈ 10
Temperature (C^o)	-20 to +70	-40 to +65	-20 to +70
Tilt range (degree)	±50	±80	±40
Output	Digital NMEA 0183/Analogue	Digital NMEA 0183/Analogue	Digital NMEA 0183/Analogue

Table 3.1: Technical specifications of the compasses in *Springer*

All the compasses (TCM2, HMR3000 and KVH-C100) on-board *Springer* can output NMEA 0183 standard sentences with special sentence head and checksum. Nevertheless all of these compasses are very sensitive and must be mounted as far as possible from any source of magnetic field and from ferrous metal objects. Electrical and magnetic disturbances become especially pronounced when the marine vehicle is reliant on electric motors for propulsion. This became particularly apparent during the initial trials with the *mini-Springer* and *Sutton* as detailed in appendix A5.

3.7 Roboteq controller AX2850

The RoboteQ controller AX2850 as seen in the following Figure 3.7, is used to provide the differential speed control for *Springer.* RoboteQ is a highly configurable controller but is very sensitive to the settings. Further technical specifications can be found in appendix A6.

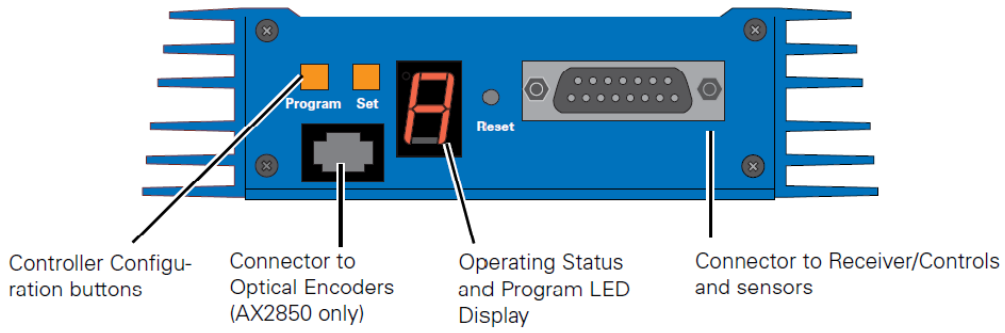

Figure 3.7: Roboteq controller AX2850 display panel (source: RoboteQ Inc)

The Roborun Utility screen layout is presented in Figure 3.8, offers various configurable settings to achieve the desired outcome.

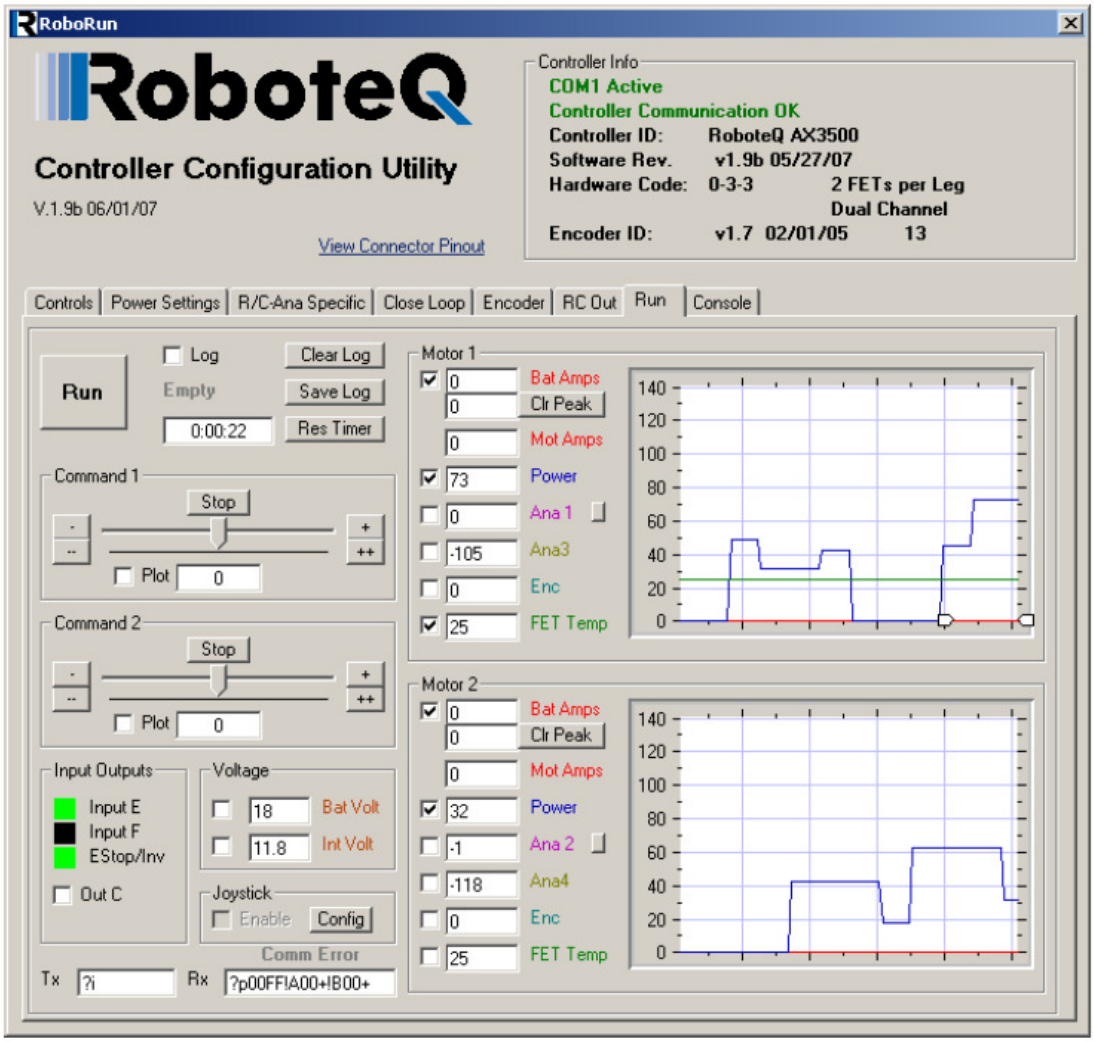

Figure 3.8: Roborun Utility screen layout (source: RoboteQ Inc)

All of the compasses and the Intense PC Pro as described above are housed inside a watertight Pelican case as shown in the following Figure 3.9 (a) and (b):

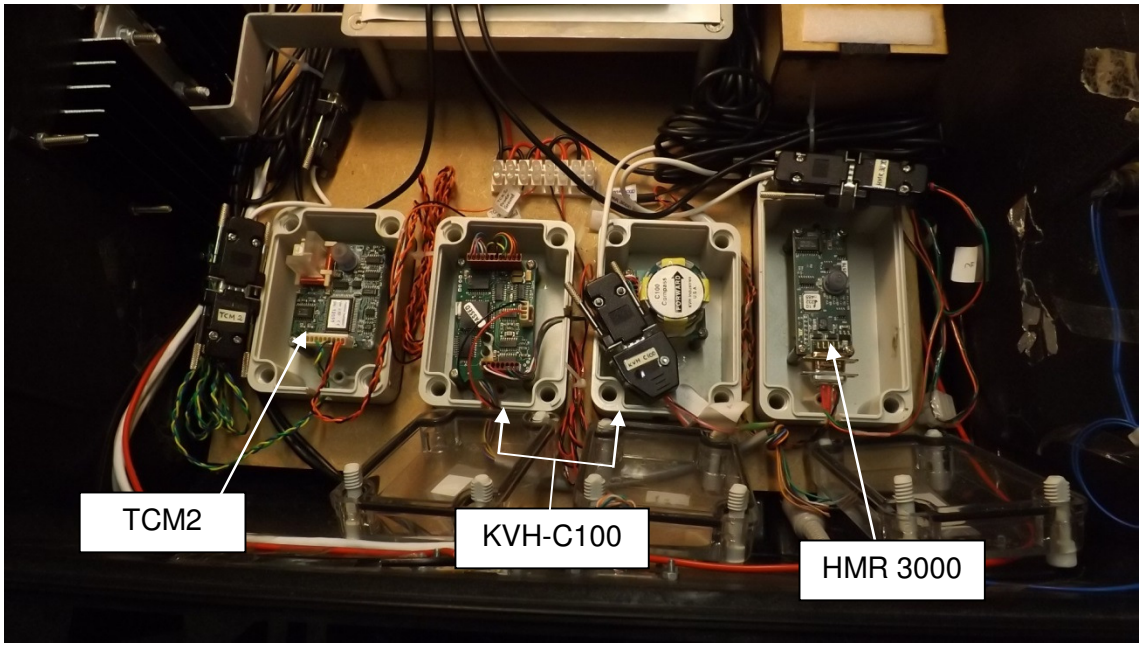

(a)

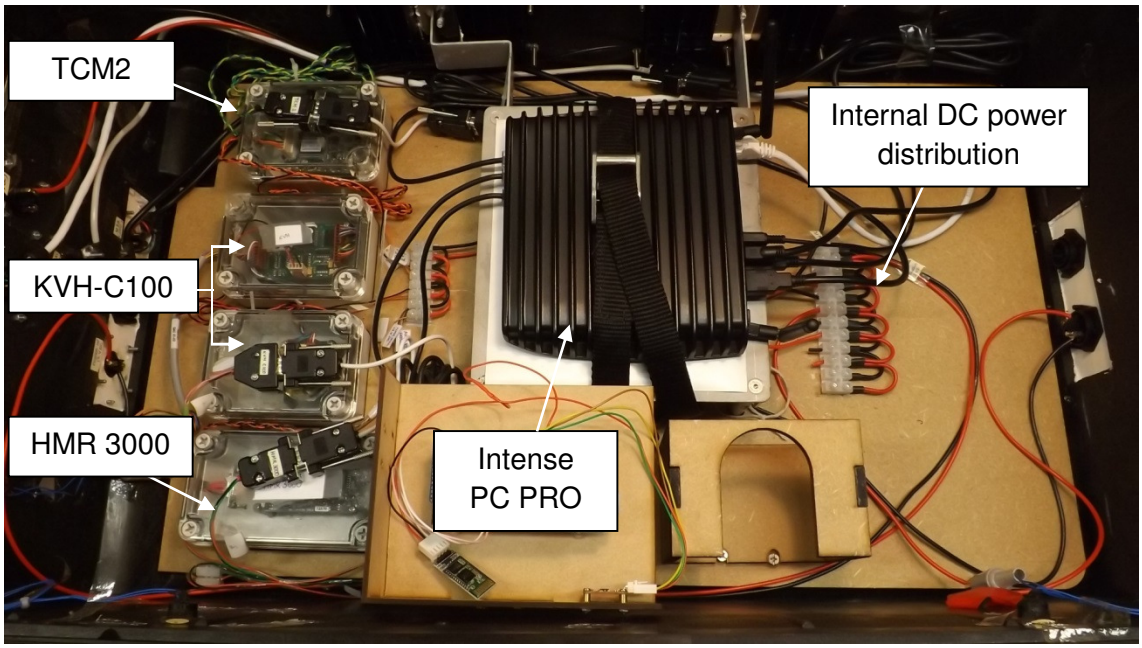

(b)

Figure 3.9: Electronics housed inside the Pelican case on-board *Springer* (a) view of all compasses (b) view of Intense PC Pro and all compasses

3.8 Other Hardware

Other areas of development of electrically powered USVs are to increase the battery life so that the USV could perform missions which require longer operational periods. Long endurance of USVs can be achieved by using solar panels and wave power by Hine and McGillivary (2007). Nevertheless, the speed of such a vehicle is very low and makes it suitable only for passive surveillance missions. To overcome this problem other researchers such as Khare and Singh (2012) have designed a hybrid power system by combining the solar array, an ocean wave energy converter, a fuel cell system, a diesel generator and a lithium ion battery pack. Incorporating all these changes into *Springer* to improve endurance will become another research project in its own right. To achieve a balance between the modernisation of *Springer* and the time spent, it is practical to charge the rechargeable batteries on board via the solar panels to increase the mission durations. Hence, solar panels were initially planned to be installed in *Springer.* However, the marginal gains plausible and the costs involved were disproportionate. Moreover, *Springer* is envisioned as a multi role USV and installation of solar panels would compromise the visibility of the vehicle for covert surveillance and other military operations. Therefore, this approach was abandoned.

Furthermore, the previous research team at Plymouth University had utilised two desktop PCs to act as a NGC system, housed inside the water tight Pelican cases. The PCs were powered by an AC power supply which was obtained by an inverter converting the DC power source on-board *Springer*. As detailed previously in this chapter, the problem of heat dissipation, presence of mechanical moving parts such as

the exhaust fan increases the risk of autopilot and navigation system failure. This problem was solved by utilising Intense Pro PC as detailed previously in this chapter. Owing to this improvisation the presence of the inverter became redundant, as the Intense PC Pro is powered by a DC power supply. Thus, an improved performance and reliability of the NGC system on-board *Springer* was achieved. During the initial stages it became clear that such an approach posed physical challenges during experimentation and accidents could happen should the umbilical cords be caught by the thrusters of the vehicles. This problem was solved by establishing a powerful and reliable wireless connection up to a range of 100 meters. The state of operations inside the Pelican case could be clearly monitored by a remote connection established between a laptop on the rigid hull inflatable boat (RHIB) and the Intense PC Pro. Additionally, the other components in the *Springer* are detailed in the following Figure 3.10.

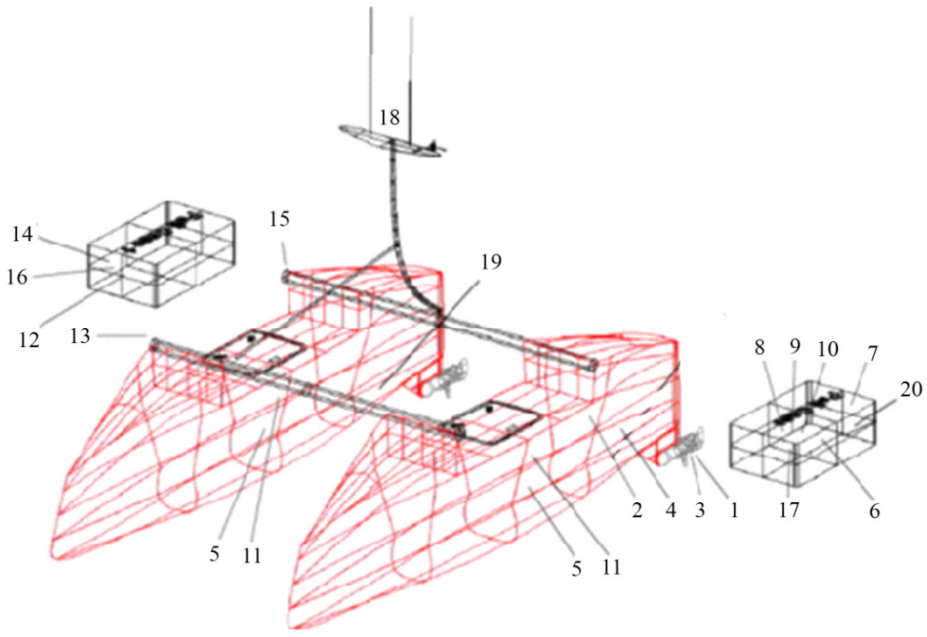

Figure 3.10: Components of the *Springer*

The details of each of these individual components and the reason for why they were selected for this project are summarised in Table 3.2 and the concluding remarks can be found in the subsequent section. Furthermore, details of all hardware components used in this *Springer* project can be found in appendix A7.

Component	Details	Purpose
1. Trolling motors	Minn Kota Riptide	Propulsion
2. RoboteQ motor controller	to be connected via serial link to NGC PC	drives motors and provides digital interface with PC
3. Optical encoders	situated inside motor housings	provide rpm feedback of the motors to RoboteQ controller
4. Power electronics	custom design, connects 1,2,3	to drive the motors, enable remote control operation as well as RoboteQ control
5. Eight 12V Gel batteries	rechargeable gel batteries connected to provide 24V	to power trolling motors
6. NGC PC	Intense PC Pro I/O: 8 USB ports, 2eSATA, 2 ethernet, 1 ultra mini RS232, 1 HDMI, audio. Rated @ 12VDC.	to acquire data from compasses, GPS, RoboteQ (rpm); output control action nc, nd (via RoboteQ)
7. GPS receiver for NGC Peli case	GlobalSat ND-100S USB GPS receiver	to provide GPS localisation data to NGC PC
8. TMC2 compass	can run on 12V DC unregulated supply	to provide heading measurement to NGC PC
9. KVH C100 compass	requires 8-18V DC power input	to provide heading measurement to NGC PC
10. HMR 3000 compass	can run on 12V DC unregulated supply	to provide heading measurement to NGC PC
11. 2 ×12V Gel batteries	Sonnenschein gel batteries, 12V, 24AH, deep cycle, measurements (LWH): 167×176×126mm.	to power NGC PC, visual SLAM laptop, sensors and other onboard electronics

	Terminal type: G-M5	
12. Visual SLAM laptop	Toshiba Satellite P775-10K. Has USB 3 ports for connecting to high speed camera. Rated @ 19VDC, 6.32 A	for acquiring camera data and executing visual SLAM algorithms.
13. High speed camera	PointGrey Flea3 (FL3-U3-32S2C-CS)	for acquiring visual information
14. GPS receiver for SLAM laptop	GlobalSat ND-100S USB GPS receiver	to provide GPS localisation data to visual SLAM laptop
15. IMU	6 DOF IMU provided by UTAS	to assist camera localisation algorithm
16. DC to DC converter	Ansmann DC universal laptop power supply DCPS-50W. Input 12V, Output 9.5 to 20V (adjustable)	to power visual SLAM laptop
17. DC to DC voltage regulator		to power Raymarine transducers
18. Wireless router	Linksys WRT54GX , rated at 12V DC, 800 mA	for establishing communication between NGC PC and visual SLAM laptop, as well as wireless communication with external PCs
19. Speed sensor	paddlewheel, located at bottom of right hull	measure relative speed in forward direction
20. Speed transducer	Raymarine	digital interface for speed sensor

Table 3.2: Description of the components of the *Springer*

3.9 Conclusions

This chapter presents the hardware components which are essential to build the test platform. The obstacles encountered served as a stepping stone to progress the research further. These trials (as in appendix A5) demonstrated the advantages and limitations of

the individual USVs. Moreover, these marine vehicles aided the researchers to enhance their cognizance of the practical aspects of this project. An overview of the technical specifications of the main components such as Intense PC Pro, TCM2, HMR300, KVH C100 and RoboteQ AX2850 has been presented. The rationale for the choice of the components was also discussed.

Chapter 4

Springer Identification and Modelling

4.1 Introduction

As seen in Chapter 2, advanced controllers such as MPC utilise an internal model of the vehicle to compute the appropriate control action. To ensure that the controller behaves as expected it is vital that the model used is as accurate as possible and this requires adaptive capabilities to take account of changes in system dynamics. There are many different approaches to obtain the model of the vehicle. Some of the major approaches such as CLID, rigid body modelling and SI that are applicable to USVs are presented in this chapter. Before venturing into the modelling procedure, an overview of kinetics and kinematics involved in the dynamics of marine vehicles is presented.

4.2 Kinetics and Kinematics

The study of dynamics is divided into two major components; kinetics and kinematics (Perez, 2005). The impact of force on the motion of bodies is dealt by kinetics. The geometrical aspects of motion such as reference frames and transformations are dealt by kinematics.

An USV such as *Springer* moves in six degrees of freedom (6DOF) as illustrated by the following Figure 4.1. Three co-ordinates are necessary to define translation and another set of three co-ordinates are essential to define the orientation of the vehicle. Further

classifications and details of other reference frames have been elaborated by Perez (2005).

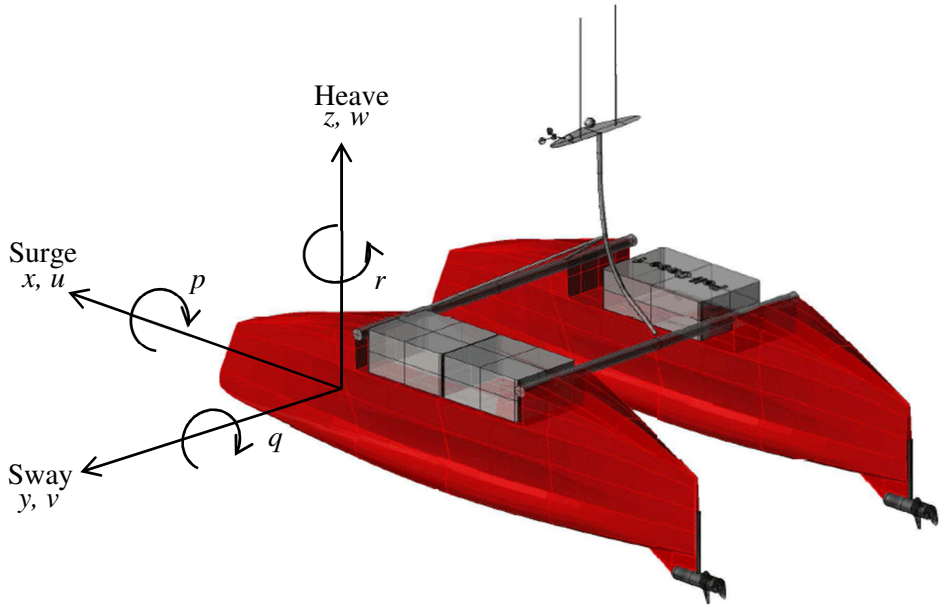

Figure 4.1: *Springer* six degrees of freedom; yaw, pitch and roll plus the translational coordinates heave, sway and surge.

The 3D position of the vessel at any point can be deduced by the *X, Y* and *Z* co-ordinates. The vessel's motion along these axes is described in terms of roll (ϕ), pitch (θ) and yaw (ψ) and the translational coordinates surge, heave and sway. Surge refers to forward motion; heave denotes up/ down movement and sway describes left/right motion. Linear velocity in the *x*-direction (*m/s*) is denoted by *u*, in the *y*-direction is *v* and in the *z*-direction is *w*. Angular velocity in the *x*-direction (*deg/s*) is denoted by *p*, in the *y*-direction is *q* and in the *z*-direction is *r*.

One of the methods to obtain the model of a plant is CLID. The suitability to apply these concepts to *Springer* is discussed in the subsequent section.

4.3 Closed loop system identification

SI in closed loop is presented by Landau and Rolland (1994). The convergence analysis of the parameter estimation algorithm is presented by the authors in this work whereas the effects of a model developed by approximate identification under closed-loop and the model-based control design are presented by Hof and Schrama (1995). Moreover, closed-loop identification appears to produce a better performance for model-based control design (Hjalmarsson et al., 1996). The controller performance is measured as the variance of error between the output of ideal and actual closed loop systems. When the controller is a smooth function of the input-output dynamics and the disturbance spectrum, the best controller performance is achieved by performing the identification in closed loop with an operating controller.

The closed-loop system must be stable which could be unstable in open-loop. Tontiruttananon and Tugnait (1998) proposed two identification algorithms using cyclic-spectral analysis of noisy input-output data. The open-loop transfer function is first estimated using the cyclic-spectrum and cyclic cross-spectrum of the input-output data. These transfer function estimates are then used as "data" for the algorithms investigated by the authors (Tontiruttananon and Tugnait, 1998). Computer simulation examples are presented to support the proposed approaches.

A robust closed-loop identification method is presented by de Klerk and Craig (2002). A new PID tuning rule is used to construct the auto-tuner. The process frequency response is obtained by using fast Fourier transform (FFT) and the inverse FFT is used to obtain the process step response. A simulation concerning the CLID of a

multivariable plant model, where the plant is controlled by a MPC controller, is discussed. A motivation for CLID in this context is given. The identification methodology is further discussed and evaluated (de Klerk and Craig, 2002). Advantages of closed-loop identification are discussed and an MPC is designed by utilising the multivariable and closed-loop identification of industrial processes in this paper. Some main issues regarding CLID are reiterated by de Klerk and Craig (2004). A model obtained from open-loop data is used as a reference to evaluate the CLID approach.

Wang and Sutton (2005) modelled a remotely operated underwater vehicle by using two-stage CLID in a simulation study. A PID controller is used to control the vehicle and a pseudo random binary signal (PRBS) is used to excite the system. Controlled variable of the system does not drift while performing CLID and it also provides an opportunity for online auto tuning of the autopilot. Zhao and Kearney (2007) provide a similar view regarding a tailor made instrumental variable (IV) method for closed loop identification. However, the Hansen Scheme takes a different approach and utilises dual Youla-Kucera parameterisation of all systems stabilised by a given linear controller to transform the closed-loop system identification problems into open-loop equivalents (Bendtsen, et al., 2008). Sotomayor, et al., (2009) deal with a procedure of model re-identification of a process under closed loop with an existing commercial MPC. It is a simulation study of two processes in oil refining industry. Traditionally CLID has been used extensively by the petrochemical and process industries. However, there has not been a tremendous amount of research into the application of CLID to marine control. Hence, it is worthy to investigate the application of CLID to USVs

The purpose of CLID is to identify a mathematical model while the plant is under feedback control. CLID is preferred for economic reasons as it:

- Is less disruptive to normal plant function.
- Provides an opportunity for online auto tuning of the control system.

Another advantage is that the controlled variable of the system does not drift while performing CLID.

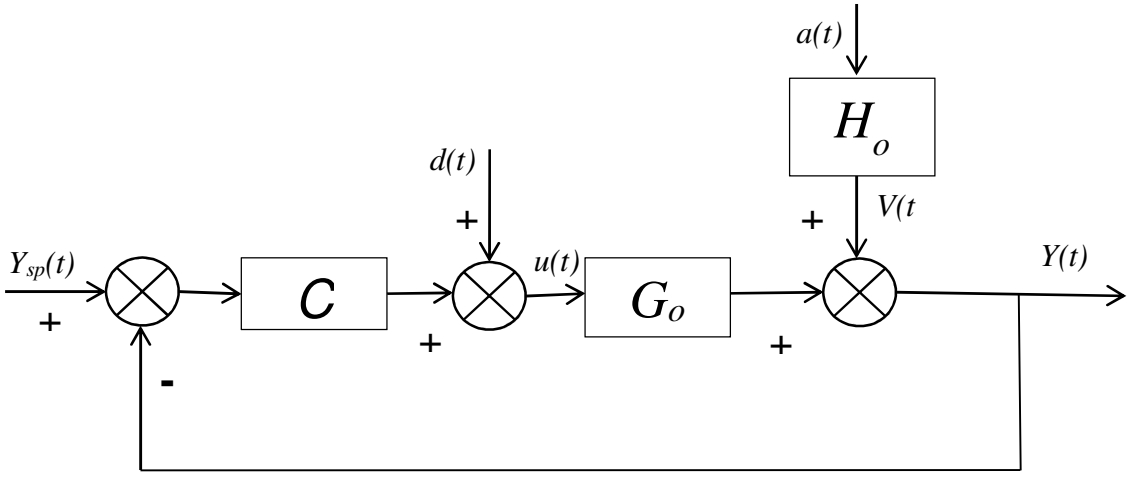

Figure 4.2: Closed loop system identification

The above Figure 4.2 illustrates the concept of single input single output CLID. A PRBS is used to excite the system.

4.4 Comparison of the closed-loop identification methods

A good overview of different closed-loop identification methods such as classical method, 2-step identification and closed-loop output error algorithms are presented by Karimi and Dorã (1998). Bias distribution of the estimates is used to compare the

different methods. Furthermore, closed loop output error identification method has been illustrated by Karimi and Dorã (1998).

The common framework is created by the basic prediction error method, and it is shown that most of the common methods correspond to different parameterisations of the dynamics and noise models. The so-called *indirect methods*, for example, are indeed 'direct' methods employing noise models that contain the regulator. Classification of CLID techniques are based on different assumptions of feedback configuration and it can be summarised as in the following Figure 4.3.

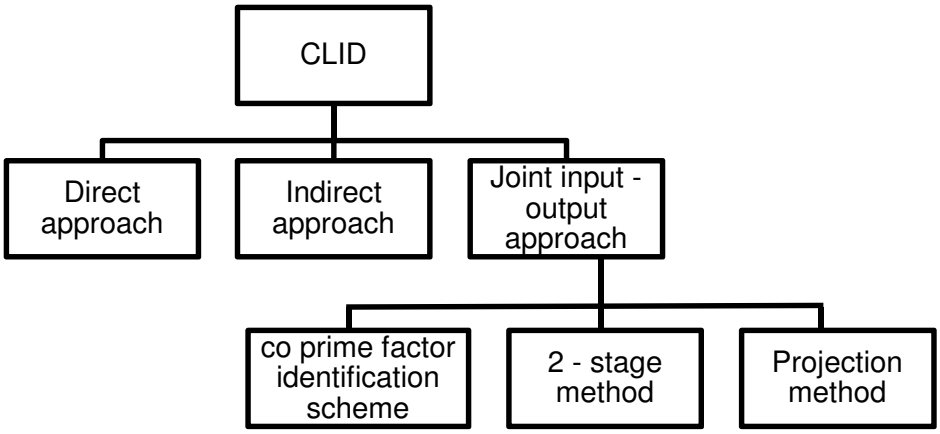

Figure 4.3: Classification of different CLID techniques

4.5 From robust control to adaptive control

Interaction between adaptive control, identification in closed loops and robust control are explored by Landau (1999). The performance of the control system is enhanced by using multiple-model adaptive control based on switching and tuning. Asymptotic and finite data behaviour of some closed-loop identification methods are presented by Landau (1999). Closed-loop identification can generally identify models with smaller variance than open-loop identification.

4.6 Closed-loop system identification via a tailor-made IV method

A bias-correction method for closed-loop identification, introduced in the literature as the bias-eliminated least squares method is presented by Hof and Gilson (2001). This is referred to as the tailor-made IV method for closed-loop identification.

4.7 Closed loop identification with auto-tuning

A robust closed-loop identification method is presented by de Klerk and Craig (2002). A new PID tuning rule is used to construct the auto-tuner. The process frequency response is obtained by using fast Fourier transform (FFT) and the inverse FFT is used to obtain the process step response. A simulation concerning the CLID of a multivariable plant model, where the plant is controlled by a MPC controller, is discussed. A motivation for CLID in this context is given. The identification methodology is further discussed and evaluated (de Klerk and Craig, 2002). Advantages of closed-loop identification are discussed and an MPC is designed by utilising the multivariable and closed-loop identification of industrial processes in this paper.

Some main issues regarding closed-loop system identification are reiterated by de Klerk and Craig (2004). A model obtained from open-loop data is used as a reference to evaluate the CLID approach. Wang and Sutton (2005) modelled a remotely operated underwater vehicle by using the two-stage CLID. PID controller is used to control the vehicle and a PRBS is used to excite the system. Controlled variable of the system does not drift while performing CLID and it also provides an opportunity for online auto tuning of the autopilot. Zhao and Kearney (2007) provide a similar view regarding tailor

made IV method for closed loop identification. However, the 'Hansen Scheme' takes a different approach and utilises dual Youla-Kucera parameterisation of all systems stabilised by a given linear controller to transform the CLID problems into open-loop-like problems (Bendtsen, et al., 2008).

Sotomayor, et al., (2009) deal with a procedure of model re-identification of a process under closed loop with an existing commercial MPC. Basically it is a simulation study of two processes in oil refining industry. Traditionally CLID has been used extensively by the petrochemical and process industries. However, there has not been a lot of research in the application of CLID to USVs. Hence, it is worthy to investigate the application of CLID to USVs.

4.8 Results and discussion for closed loop system identification

The general system as illustrated in Figure 4.2 can be summarised by the following Equation (4.1).

$$y(t) = G_0(q)u(t) + H_0(q)a(t) \tag{4.1}$$

where $G_0(q)$ represents the true model of an USV and the effect of all unmeasured disturbance is given by $v(t) = H_0(q)a(t)$ where q represents the forward shift operator. The plant input is given by the following Equation (4.2).

$$u(t) = C(q)\left(y_{sp}(t) - y(t)\right) + d(t) \tag{4.2}$$

where $y_{sp}(t)$ is the set-point, $d(t)$is the dither signal and $C(q)$ is the controller. When $y_{sp}(t) = 0$, then *d(t)* becomes the only input and the above feedback equation becomes

$$u(t) = -C(q)y(t) + d(t) \tag{4.3}$$

At this juncture, it is worthy to note that the system model (4.1) can be more precisely represented as the following Equation (4.4).

$$y(t) = G(q.\rho)u(t) + H(q.\eta)a(t) \tag{4.4}$$

where ρ and η vectors of parameters and *a(t)* is the innovation sequence. The challenging task here is to identify the plant under feedback. External excitation is provided to the system by $d(t)$embed in u(t). From Equation (4.1) and (4.3), the sensitivity function of the closed-loop system can be obtained by

$$S_0(q) = \frac{1}{1+G_0(q)C(q)} \tag{4.5}$$

The Equations (4.1) and (4.3) become the following by using the Equation (4.5)

$$y(t) = G_0(q)S_0(q)d(t) + S_0(q)v(t) \tag{4.6}$$

$$u(t) = S_0(q)[d(t) - C(q)v(t)] \tag{4.7}$$

Equations (4.6) and (4.7) can be further expanded as follows:

$$y(t) = G_0(q)S_0(q)d(t) + S_0(q)H_0(q)a(t) \tag{4.8}$$

$$u(t) = S_0(q)d(t) - C(q)S_0(q)H_0(q)a(t) \tag{4.9}$$

In Equation (4.9), $d(t)$ and $a(t)$ are uncorrelated, hence $S_0(q)$ can be identified in an open loop way. Further in Equation (4.8) assume that $u^d(t) = S_0(q)d(t)$ and it reduces to the following form as in Equation (4.10)

$$y(t) = G_0(q)u^d(t) + S_0(q)H_0(q)a(t) \tag{4.10}$$

From Equation (4.10), $G_0(q)$ can be identified in an open loop way after obtaining $u^d(t)$. This is feasible as $u^d(t)$ and $a(t)$ are uncorrelated.

From Figure 4.2, it is clear that there are three possible inputs: $y_{sp}(t), d(t)$ and $a(t)$. The presence of each of these inputs in the absence of the other two inputs produces an output and the outputs are further illustrated in Annamalai et al., (2013).

From the above equations (4.1) to (4.10), the sensitivity function S_0 of the *Springer* USV was found to be

$$S_{0(cal)} = \frac{z^3 - 1.997\,z^2 + 0.9965\,z}{z^3 - 1.909\,z^2 + 1.056\,z - 0.1445} \tag{4.11}$$

$$S_{0(ident)} = \frac{0.9996 - 1.507\,z^{-1} + 0.564\,z^{-2} - 0.05709\,z^{-3}}{1 - 1.424\,z^{-1} + 0.6707\,z^{-2} - 0.119\,z^{-3}} \tag{4.12}$$

and the CLID model of the *Springer* USV was found to be

$$G_{0(CLID)(cal)} = \frac{-5.443 * 10^{-6} + 0.0001463\,z^{-1}}{1 - 1.038\,z^{-1} + 0.03598\,z^{-2}} \tag{4.13}$$

$$G_{0(CLID)(ident)} = \frac{-4.649 * 10^{-6} + 0.0001428\,z^{-1}}{1 - 1.061\,z^{-1} + 0.05925\,z^{-2}} \tag{4.14}$$

Additional results regarding CLID has been explored in Annamalai et al., (2013). Despite the promising initial results, there were many challenges to implement this in reality on-board the *Springer*. This was owing to the approach being computationally expensive and it was not feasible to implement in conjunction with MPC during trials. Conventionally CLID is applied in chemical and petrochemical industries where system dynamics change more slowly and disturbance is not very great, in addition it is mainly applied to processes which are inherently unstable in open loop. Whereas here the *Springer* dynamics are stable in open loop and thus CLID does not provide any great advantage in this case but does increase computational cost. In this project emphasis was placed on practically feasible approaches that could be implemented on-board *Springer*, within the available time period. Hence, alternative approaches to model the *Springer* were undertaken as discussed in the subsequent section.

4.9 Rigid body modelling approach

Fossen (2011) suggests that the generalised six degree of freedom rigid body Equations of motion for the vehicle can be taken as follows:

$$\mathrm{M}_{RB}\dot{v} + \mathrm{C}_{RB}(v)v = \tau_{RB} \tag{4.15}$$

Here $v = [u\ v\ w\ p\ q\ r]^T$ represents the linear and rotational motions of the rigid body in a body-fixed coordinate system. M_{RB} is the rigid body inertia matrix satisfying

$$\mathrm{M}_{RB} = \mathrm{M}^{\mathrm{T}}{}_{RB} > 0, \quad \dot{\mathrm{M}}_{RB} = 0 \tag{4.16}$$

and the C_{RB} corresponds to the Coriolis and centripetal forces that can be parameterised to a skew symmetric matrix, which can be expressed as follows:

$$\mathrm{C}_{RB}(v) = -\mathrm{C}^{\mathrm{T}}{}_{RB}(v) \tag{4.17}$$

$\tau_{RB} = [X\ Y\ Z\ K\ M\ N]^T$ is a generalised vector of external forces and moments about the origin acting as an input to the system where X, Y and Z represent forces in the x,y and z directions respectively and K,M and N represent the moments about the x, y and z directions respectively. For many USVs, the depth z and pitch θ variables are not applicable. Also the roll ϕ variations were found to be negligible and thus ignored. Therefore expanding Equation (4.17) with reference to the above statements results in the following four Equations:

$$m[\dot{u} - vr - x_G(r^2) - y_G\dot{r}] = X$$

$$m[\dot{v} + ur - y_G(r^2 + p^2)] = Y$$

$$\mathrm{rpl_x} - \dot{\mathrm{p}}\mathrm{l_{xy}} - \mathrm{mx_G(vp)} = \mathrm{N} \qquad (4.18)$$

It can be noted that by coinciding the centre of gravity with the origin, the above equations can be simplified further. Nevertheless, the intention as always is to model the yaw dynamics of the vehicle and thereby gain an insight to the behavioural characteristics of the system.

Unfortunately hydrodynamic modelling is usually very expensive, time consuming and requires the use of specialist equipment in the form of a tank testing facility. However, the approach does produce detailed models based upon hydrodynamic derivatives. In addition, costs can also rise further if vehicle configurations change and thus, the tank testing and modelling procedure have to be repeated. Since the hiring and running costs for such a facility were deemed to be prohibitive, it was considered more appropriate to model the vehicle dynamics using Black box identification techniques, which will be explored in the following section.

4.10 System Identification

SI methods compose a mathematical model, or a series of models, from measurements of inputs and outputs of dynamic systems. The extracted models allow the characterisation of the response of the overall system or component subsystem (Tischler, 1995), (Fossen et al, 1996). To build an efficient controller it is essential to capture the dynamics of the operating vehicle as accurately as feasible.

Basically, the SI approach is a Black box modelling technique used extensively in the general control systems engineering community (Ljung, 1999). Ljung (2010) offers a comprehensive perspective on SI and argues that though SI is a very large topic, with different techniques that depend on the character of the models to be estimated: linear, nonlinear, hybrid, nonparametric, *et cetera*. Ljung (2010) recommends that one's main focus should be concerned with obtaining a sustainable description by proper decision in the triangle of model complexity, information contents in the data and effective validation.

Moreover, SI has also been detailed in Sutton, et al., (2011), only a brief note on this approach is given here. It consists of the subsequent steps:

- Data collection: During this first phase the input/output data of the system to be identified is gathered.
- Characterisation: Here the aim is to define the structure of the system to be identified and the selection of suitable model architecture.

- Identification/estimation: This involves determining the numerical values of structure parameters that minimise the error between the system to be identified and its model.
- Validation: Model validation consists of relating the system to the identified model in the time or frequency domain to instil confidence in the model obtained.

This approach is applied to obtain the model of the *Springer* in the following section.

4.11 System identification for *Springer*

Several trials were carried out to collect data whilst the vessel was driven for calculated manoeuvres at Roadford Reservoir, Devon, United Kingdom. The vehicle has a differential steering mechanism and hence requires two inputs to adjust its course. This can be simply modelled as a two input, single output system in the form depicted in Figure 4.4.

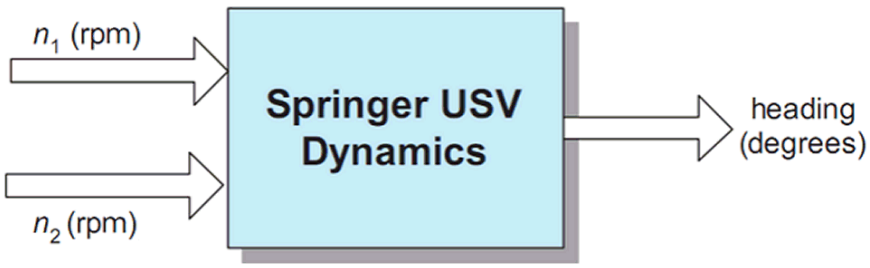

Figure 4.4: Block diagram representation of a two-input USV

In the above Figure 4.4, n_1 and n_2 represent the two propeller thrusts in revolutions per minute (rpm). Clearly, straight line manoeuvres require both the thrusters running at the same speed whereas the differential thrust is zero in this case. In order to linearise the

model at an operating point, it is assumed that the vehicle is running at a constant speed of 1.5 m/s (3 knots). This corresponds to both thrusters running at 900 rpm. To clarify this further, let n_c and n_d represents the common mode and differential mode thruster velocities defined to be

$$n_c = \frac{n_1 + n_2}{2} \tag{4.19}$$

$$n_d = \frac{n_1 - n_2}{2} \tag{4.20}$$

In order to maintain the forward velocity of the vessel, n_c must remain constant at all times. The differential mode input, however, oscillates about zero depending on the direction of the manoeuvre. For data acquisition, several inputs were superimposed with PRBS to make the signals persistently exciting and were applied to the thrusters to obtain a range of data, instead of constant values. SI was then applied to the acquired data set and a dynamic model of the vehicle is obtained in the following form (Ljung, 2010).

$$x(k+1) = \mathrm{A}\ x(k) + \mathrm{B}\ u(k) \tag{4.21}$$

$$y(k) = \mathrm{C}\ x(k) \tag{4.22}$$

where $u(k)$ represents the differential thrust input in rpm and $y(k)$ the heading angle in radians, A is the system matrix, B is the input matrix, C is the output matrix and the sampling time is 1s (Loebis et al., 2006). The open loop model is utilised by the controller / autopilot to keep the vehicle on course.

4.12 Identification results

Prior to the trials, several *Springer* technical meetings were convened and a plan was agreed by the team (appendix B). The following steps were taken to acquire trial results:

- To ensure that the systems were operative and to solve any arising issues a series of initial tests on remote control operation were conducted. The data was obtained from the compasses, GPS and motors.
- To obtain an understanding of the current and wind speed, direction and its variability along the reservoir the drift speed of the vehicle was measured under no motor thrust. This was different for each trial. Hence, an average was taken into account.
- To manoeuvre the vessel a connection between a laptop and the RoboteQ controller was established. Moreover, relationships between n_1, n_2 and n_c, n_d (to ensure that the sign of n_d as a function of n_1 and n_2 is valid) were verified.
- To model the relationship between n_c and the forward speed of the vehicle, dynamic steering models were obtained for different constant values of n_c. These trials also enabled the range of n_c to be determined.
- To obtain steering dynamic models whilst maintaining n_c constant, data was collected.
- To realise some basic manoeuvres pre-programmed on the intense PC Pro

From the initial trials, the technical challenges were overcome and the sea worthiness of the vehicle was established. Further trials were conducted at Roadford Reservoir between the 17 and 19 of June 2013 and selected few data sets are presented in this section (in Figures 4.5 - 4.9) and a comprehensive range of data sets under different operating conditions is included in appendix C.

It is worth mentioning that the value of n_c and n_d is expressed as a percentage of maximum, heading angle (in degrees) from TCM2 compass, heading angle (in degrees) from HMR3000 compass module, heading angle (in degrees) from KVH C100 compass, GPS latitude (degrees and minutes), GPS longitude (degrees and minutes). The sampling time of the data is 1s.

The data set 1 was collected under the following conditions: n_c = 10%, n_d varied manually with a superposition of PRBS signal of ±2%, wind speed 0.5 – 2 m/s (1-4 knots) in a northerly direction. The results can be found from the following Figure 4.5.

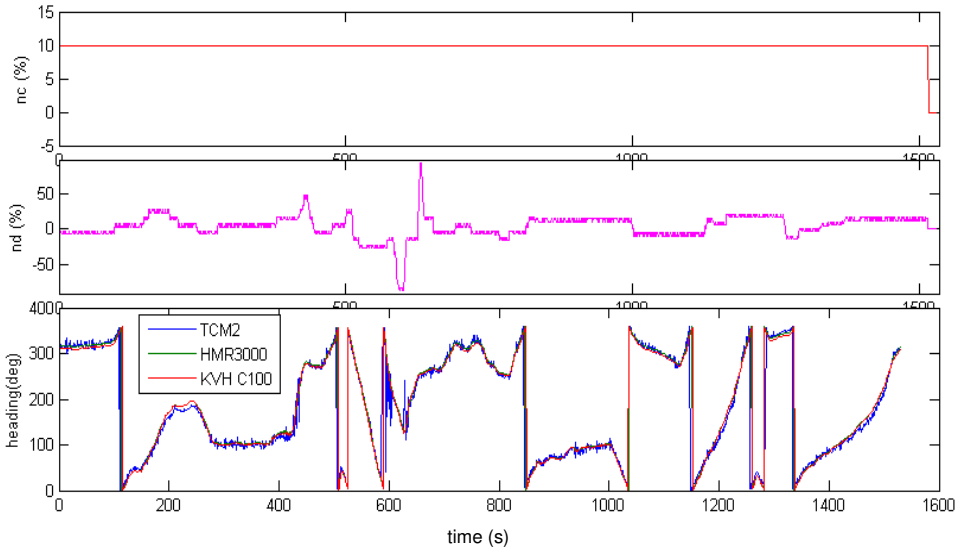

(a)

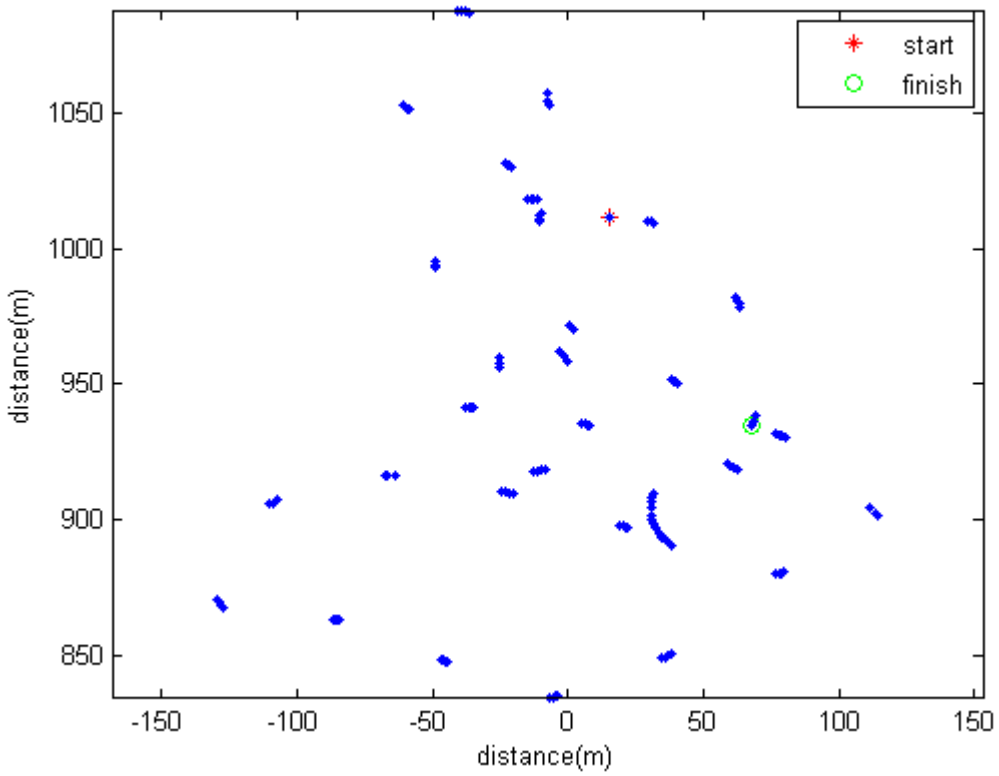

(b)

4.5: Data set 1 (a) n_c, n_d and heading (b) actual trajectory

Data set 2 was collected under the following conditions: n_c = 20%, n_d variable + PRBS.

The results can be found from the following Figure 4.6.

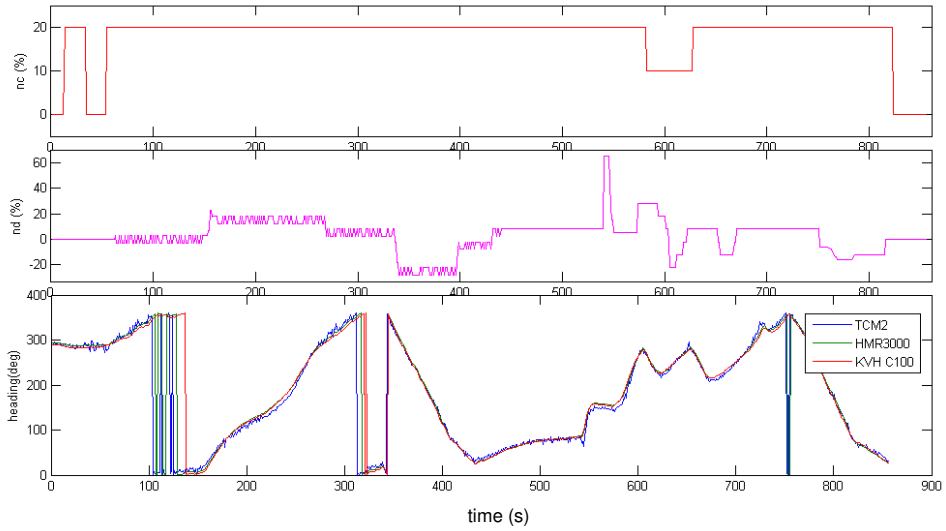

(a)

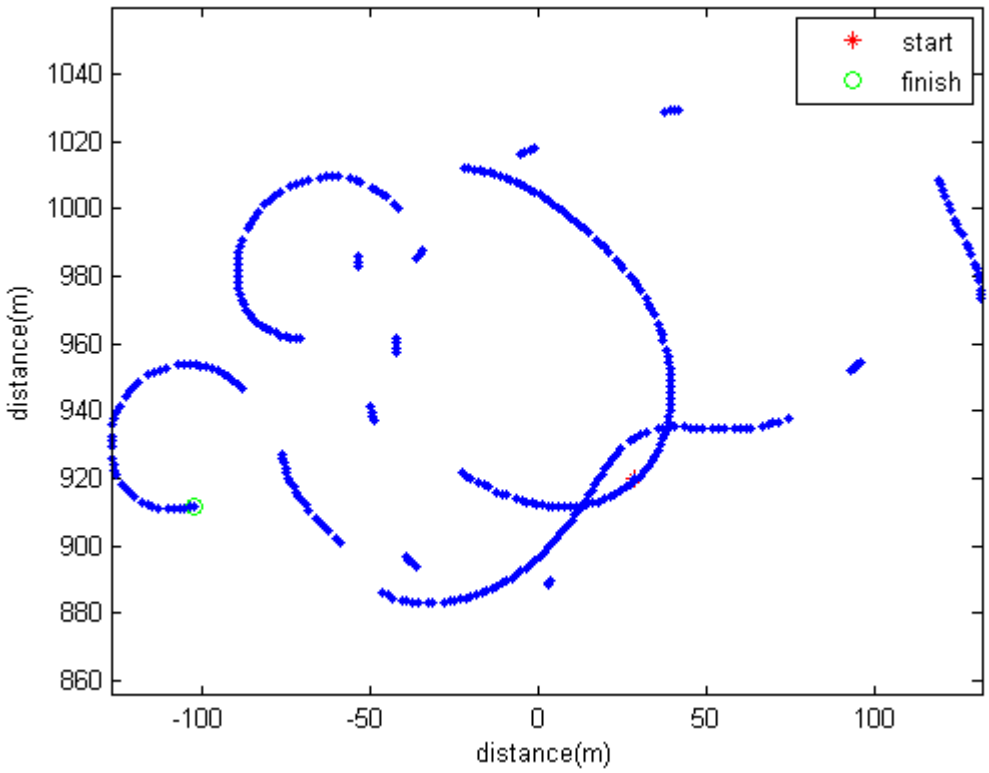

(b)

Figure 4.6: Data set 2 (a) n_c, n_d and heading (b) actual trajectory

Data set 3 was collected under the following conditions: n_c = 30%, wind speed of 2-5 m/s (4-10 knots) in a south westerly direction. The results can be found from the following Figure 4.7.

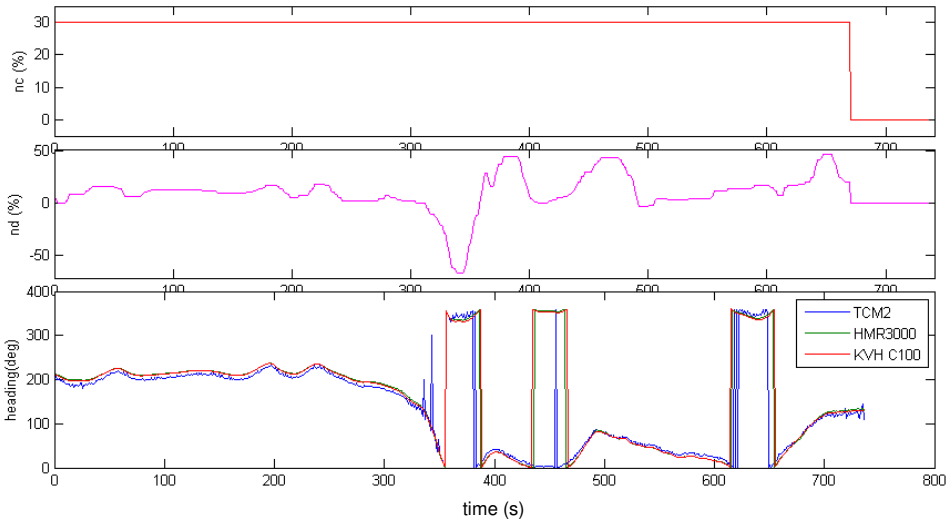

(a)

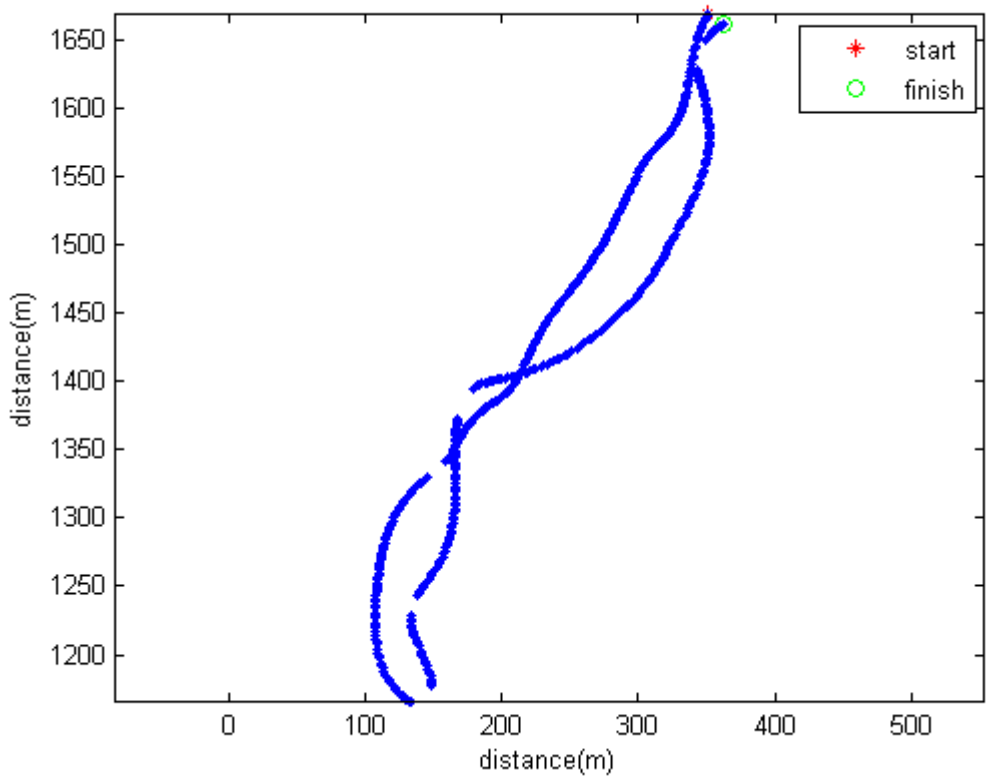

(b)

Figure 4.7: Data set 3 (a) n_c, n_d and heading (b) actual trajectory

Data set 4 was collected under the following conditions: n_c = 50%, wind speed of 2-5 m/s (4-10 knots) in a south westerly direction. The results can be found from the following Figure 4.8.

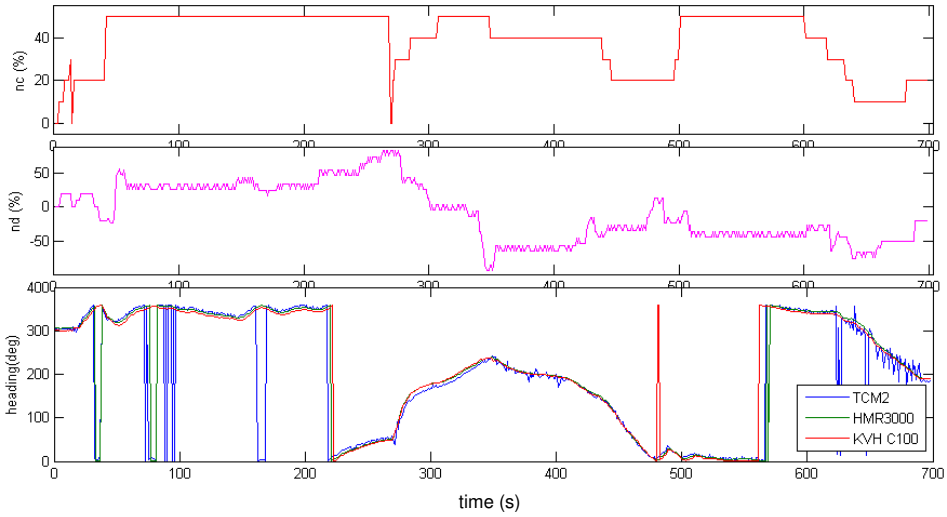

(a)

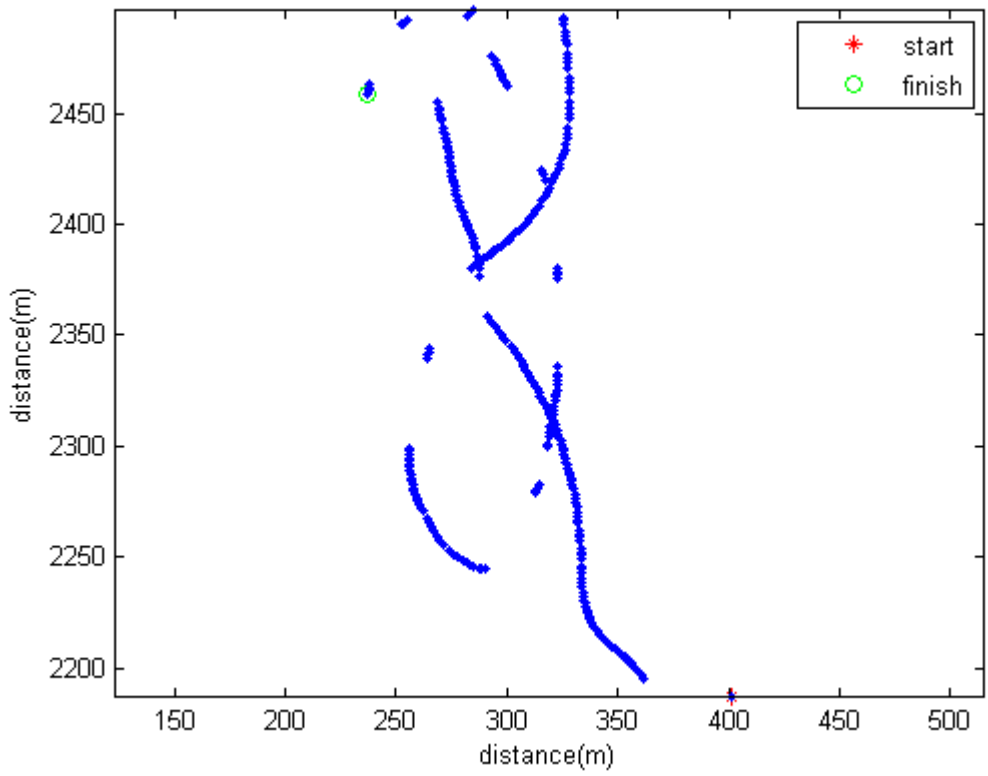

(b)

Figure 4.8: Data set 4 (a) n_c, n_d and heading (b) actual trajectory

Data set 5 was collected attempting to go at full thrust capacity under the following conditions: n_c = 100%, wind speed of 3-6 m/s (6-12 knots) in a south westerly direction. The results can be found from the following Figure 4.9.

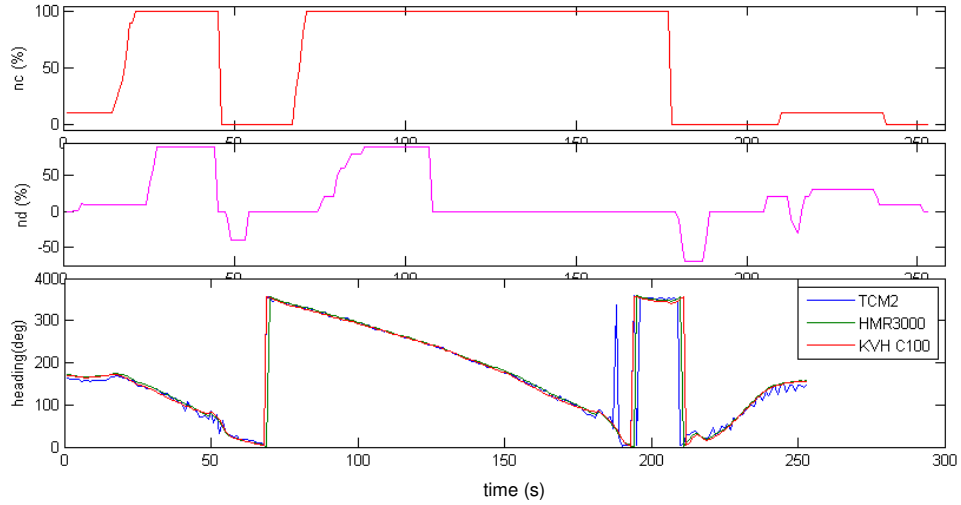

(a)

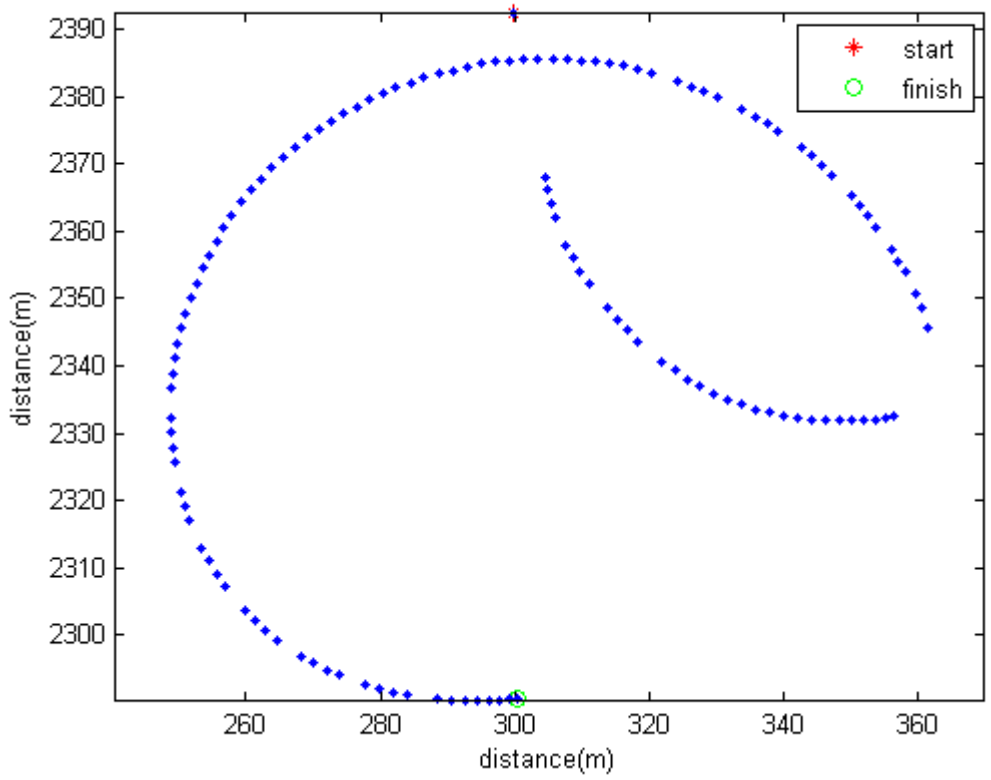

(b)

Figure 4.9: Data set 5 (a) n_c, n_d and heading (b) actual trajectory

One of the issues encountered was that the demanded n_c was not available for motor set points and encoder readings, when n_c = 1800rpm. The issue was traced to the saturation of individual motors A and B which is illustrated by the following Figure 4.10.

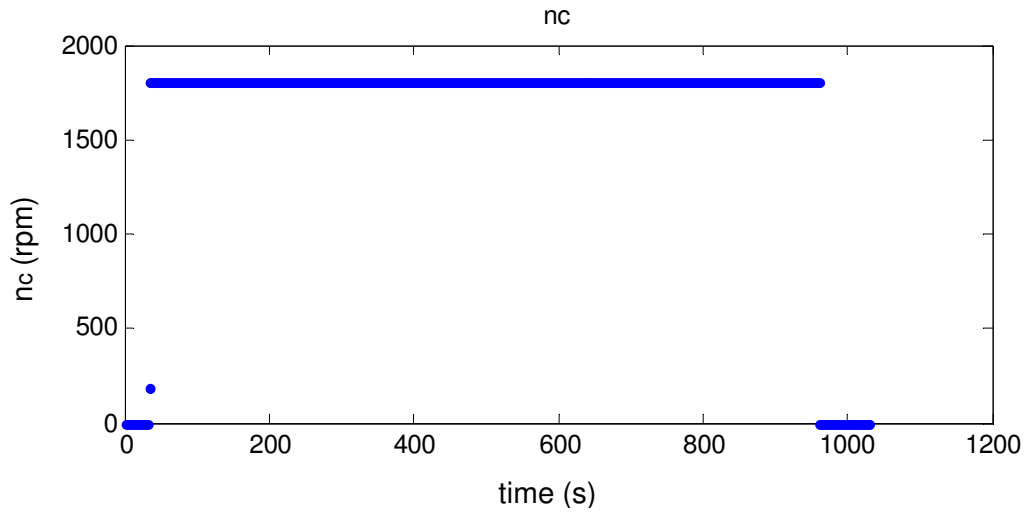

(a)

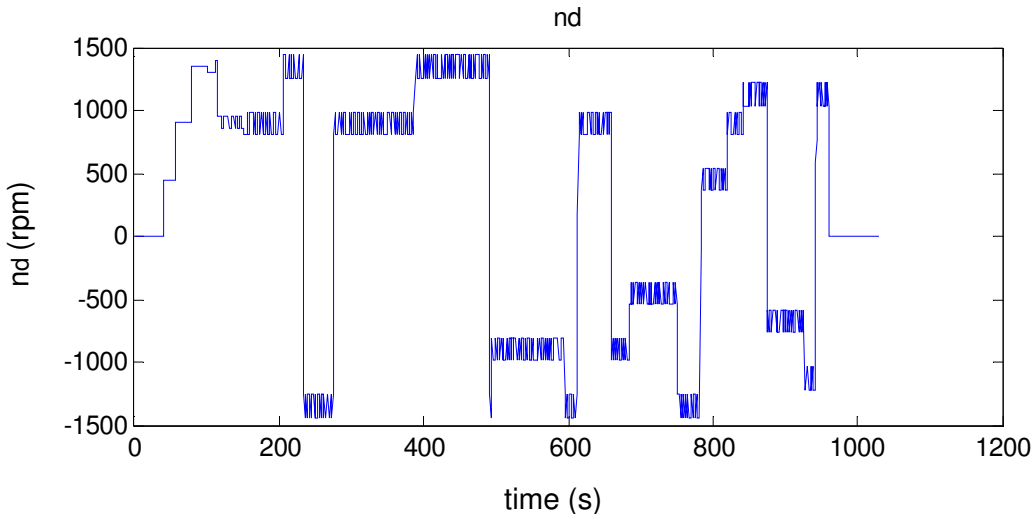

(b)

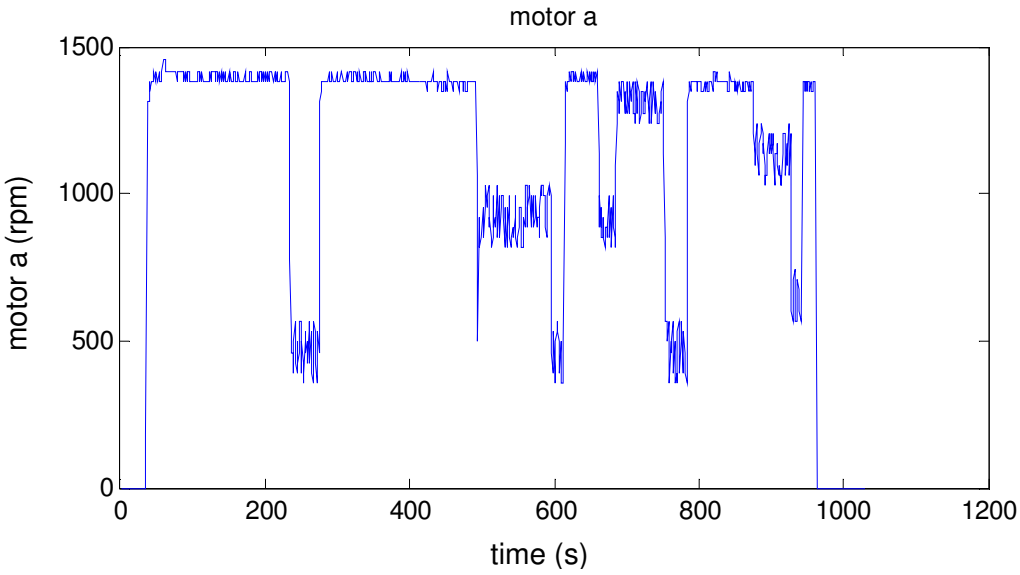
motor a
motor a (rpm)
time (s)
0
500
1000
1500
0
200
400
600
800
1000
1200

(c)

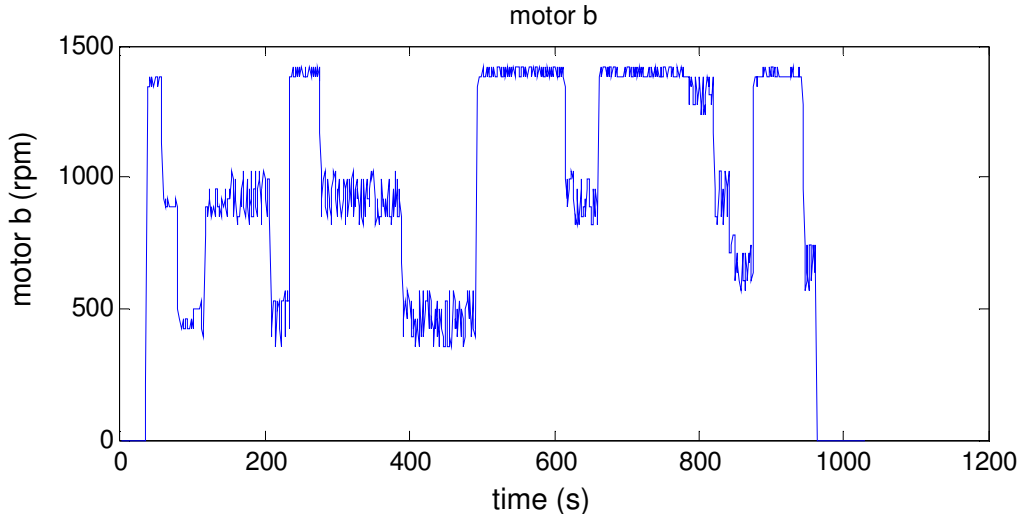
motor b
motor b (rpm)
time (s)
0
500
1000
1500
0
200
400
600
800
1000
1200

(d)

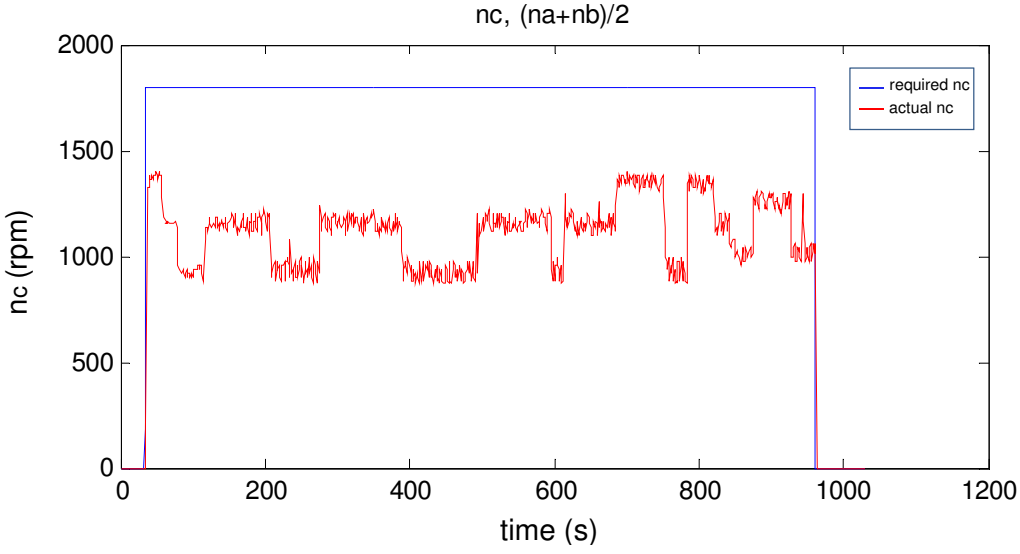
nc, (na+nb)/2
required nc
actual nc
nc (rpm)
time (s)
0
500
1000
1500
2000
0
200
400
600
800
1000
1200

(e)

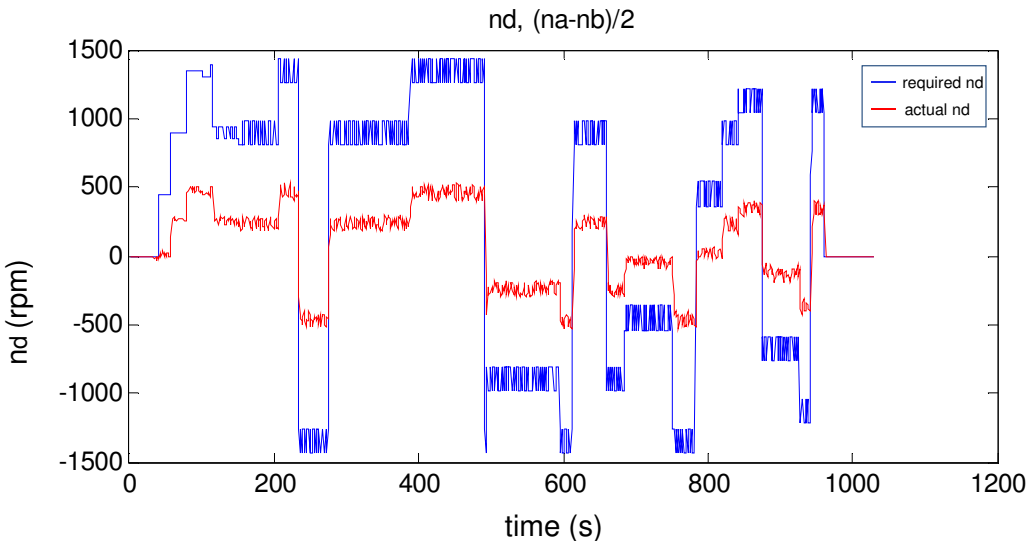

(f)

Figure 4.10: Data set (a) n_c, (b) n_d (c) motor A (d) motor B (e) actual n_c (f) actual n_d

After obtaining the model of full scale *Springer* without any modifications, it was soon realised that any change in mass would have an impact on the model obtained. In real life situations a change of mass is inevitable as *Springer* is envisaged to be used for multiple purposes. The test equipment on-board is bound to have varying mass for different purposes. Additionally, a change of mass occurs when there is a payload deployment. Adaptive autopilots to tackle this issue have been discussed in detail in Chapter 7. At this stage the discussion will be limited to quantify the change in the model owing to the change in mass and speed. Though the change in mass and speed occurs frequently in real life situations, it was difficult to design the test environments to measure the appropriate changes. During several discussions many ideas were brainstormed to design an appropriate test environment. Ideas such as designing a mechanism to release cast iron weights attached to floats were explored. It soon became evident that there would be practical challenges to operate such a mechanism, as *Springer* would be in motion when the change in mass occurs. Furthermore, there was a

risk of losing the cast iron weights in the reservoir which threatened to prevent any subsequent trials from taking place.

As the technologies developed for *Springer* have the potential to be applied to search and rescue missions, for a change of mass could thus be induced through the acquisition of people or objects that are rescued from open waters for return to a secure base. Hence, it was considered that it might be plausible to have persons on board and that they could drop into the water at pre-defined locations. The Health and Safety regulations and restrictions placed by insurance cover prevented the implementation of such ideas. Although initially disappointing, the validity of such safety concern was later reaffirmed by a serious accident occurring at sea, in broadly similar circumstances and with the loss of two lives (British Broadcast Corporation, 2013).

A drop mechanism to release sand bags was also considered. However, the Roadford Reservoir provides drinking water to the City of Plymouth and nearby towns. Hence, the South West Water authorities were reluctant to drop material into the reservoir that could contaminate the water supplies. Therefore, this approach was abandoned and it was decided to use water for the change of mass scenario. It was thus necessary to contain the water without there being any risk of damage to sensitive electronics and electrical circuits on board *Springer*. Suitable containers were obtained and figures illustrating the setup mounted on *Springer* are presented in Chapter 8. Accordingly, a test environment to obtain the models for a change of mass in *Springer* was designed successfully.

Henceforth, the following data-sets were collected from *Springer* for different speeds and masses on 2 and 3 September 2013 at Roadford Lake, Devon, United Kingdom. Details regarding other hardware used have already been discussed in Chapter 3 and in Annamalai and Motwani (2014).

The data-sets consist of input data in the form of differential speed of the thrusters in rpm (n_d), and the corresponding change in the heading of the vehicle in degrees from one time sample to the next (Δh). The heading angle of the vehicle at sampling time k is thus calculated as $h(k) = h(k\text{-}1) + \Delta h(k)$. Data-sets were recorded for three common thrust speed values of the motors, namely 450, 900 and 1200rpm, and for each of these, three different payloads of 0, 50 and 100 kg were added to the mass of the vehicle and were evenly distributed. In each case, the data-sets available were divided into training and validation sets for modelling purposes, and are shown in the following Figures 4.11 – 4.19. The input was differential thrust (n_d in rpm) and the output was change of heading (Δh in deg).

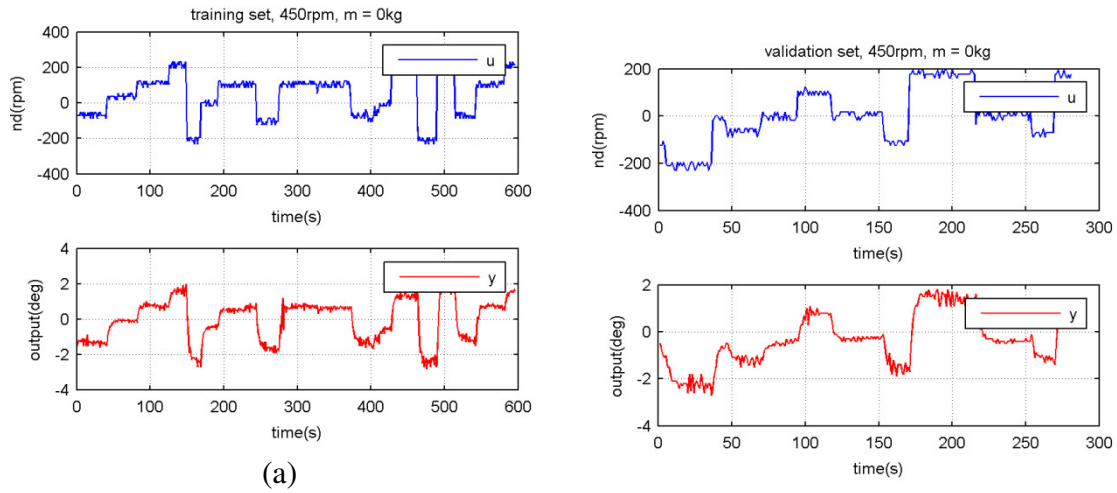

(a) (b)

Figure 4.11: Data set for 450rpm, 0kg (a) training set (b) validation set

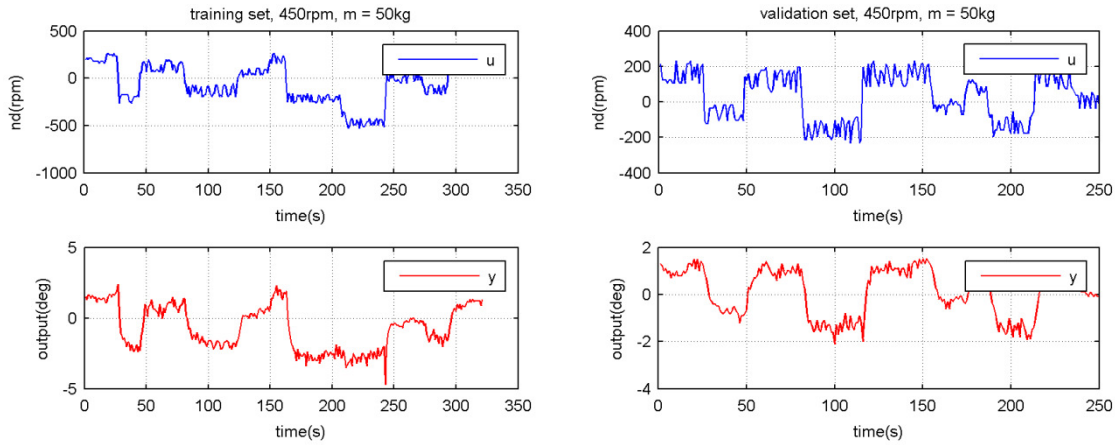

(a) (b)

Figure 4.12: Data set for 450rpm, 50kg (a) training set (b) validation set

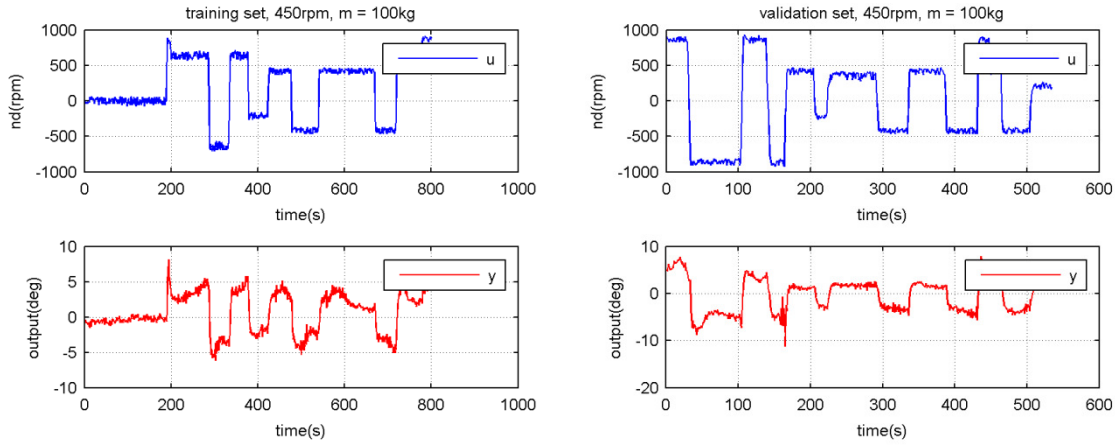

(a) (b)

Figure 4.13: Data set for 450rpm, 100kg (a) training set (b) validation set

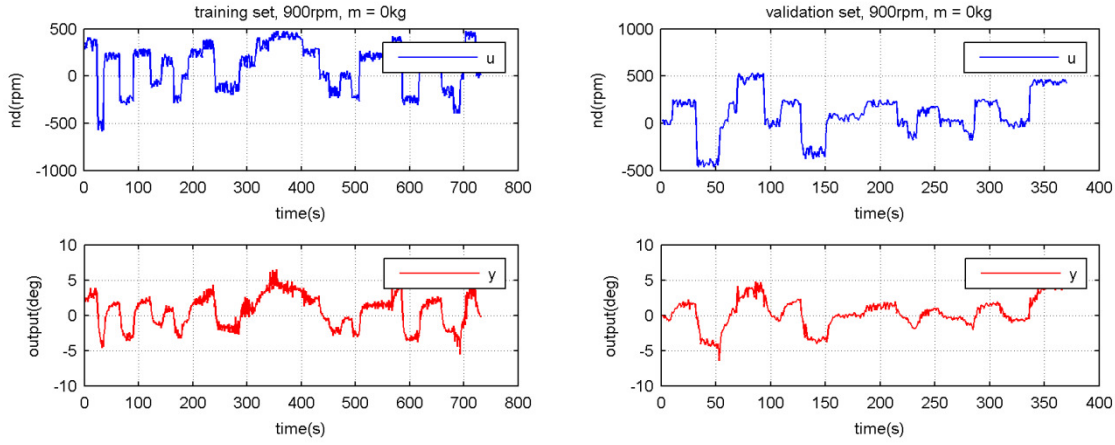

(a) (b)

Figure 4.14: Data set for 900rpm, 0kg (a) training set (b) validation set

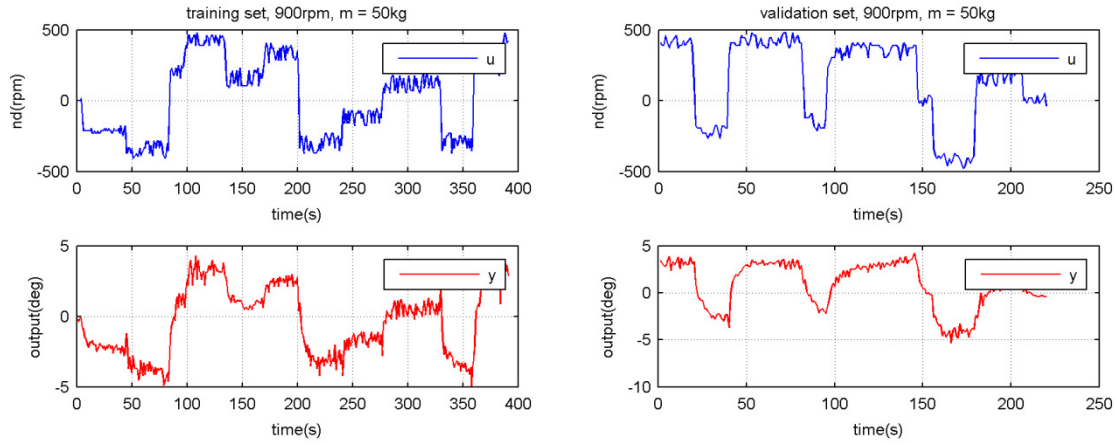

(a) (b)

Figure 4.15: Data set for 900rpm, 50kg (a) training set (b) validation set

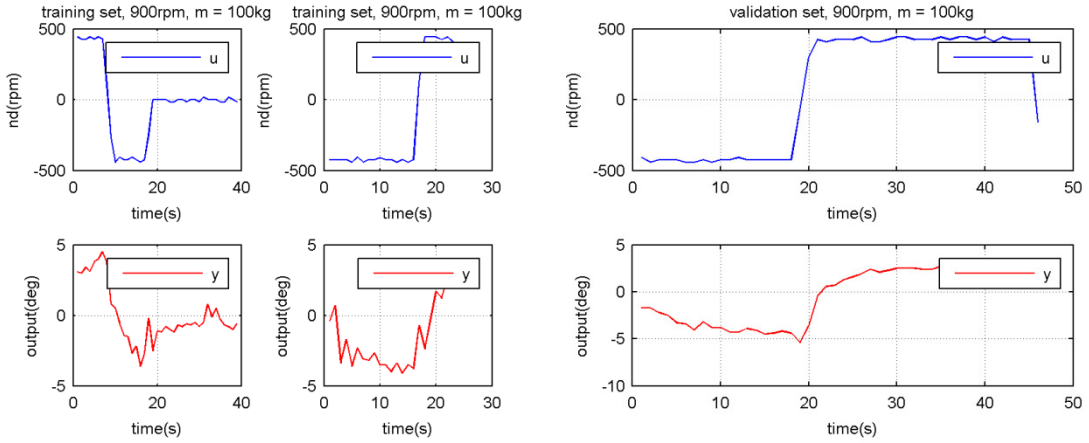

(a) (b)

Figure 4.16: Data set for 900rpm, 100kg (a) training set (b) validation set

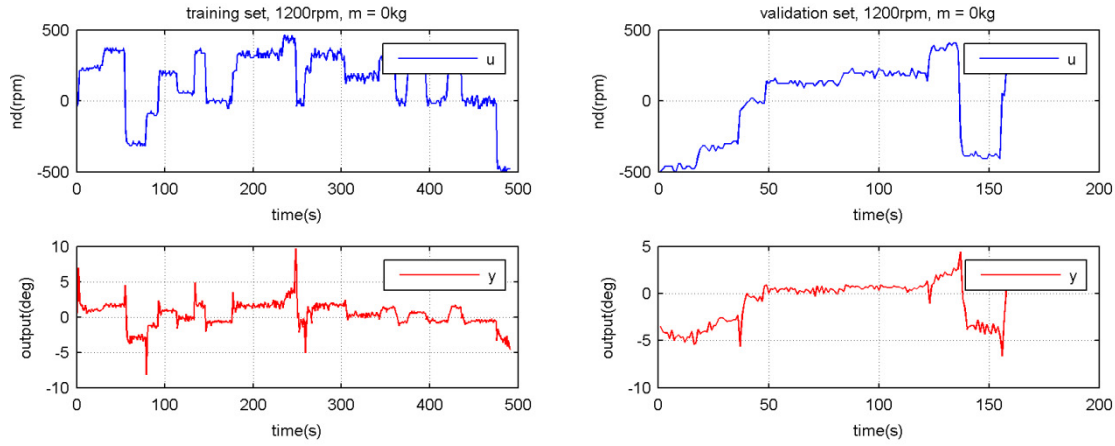

(a) (b)

Figure 4.17: Data set for 1200rpm, 0kg (a) training set (b) validation set

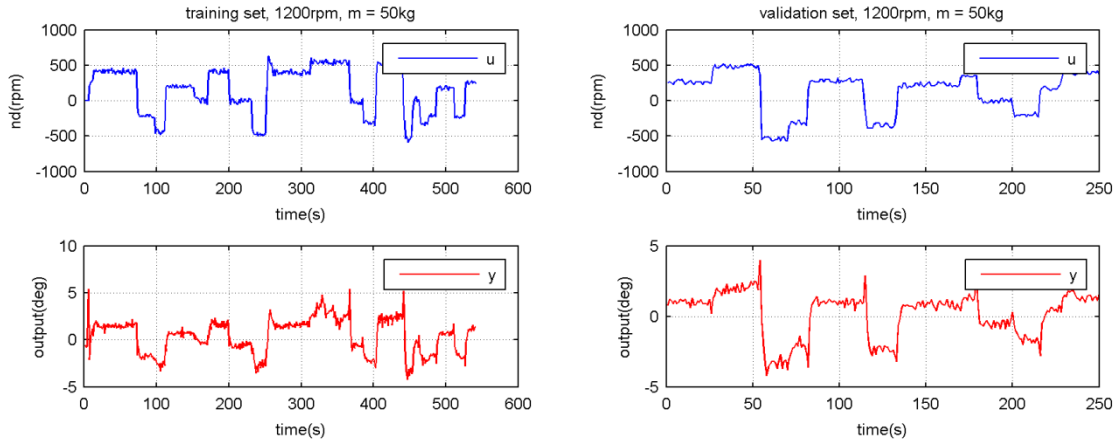

(a) (b)

Figure 4.18: Data set for 1200rpm, 50kg (a) training set (b) validation set

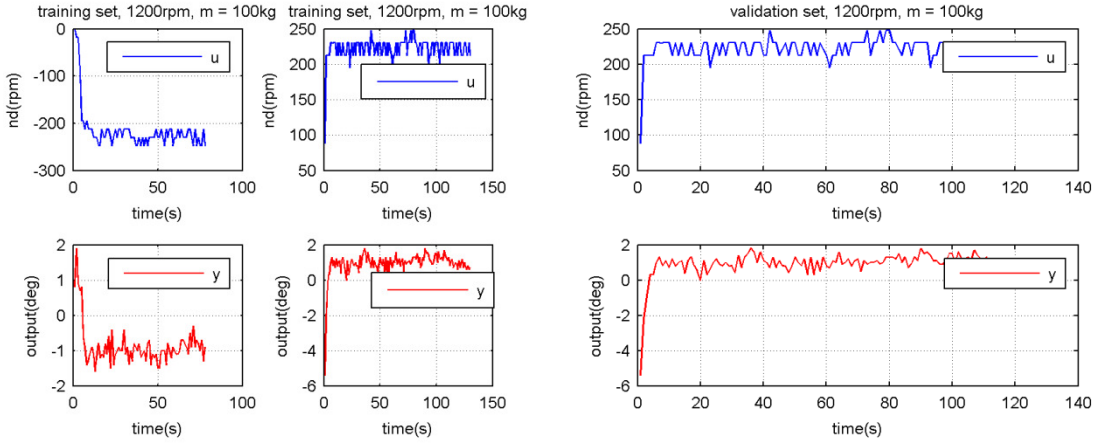

(a) (b)

Figure 4.19: Data set for 1200rpm, 100kg (a) training set (b) validation set

The data obtained from experiments proved invaluable to construct respective models. The general autoregressive with exogenous input (ARX) model is of the form (Ljung, 2010):

$$A(q)y(t) = B(q)u(t) + e(t) \tag{4.23}$$

where

$$A(q) = 1 + a_1 q^{-1} + \cdots a_{na} q^{-na}$$
$$B(q) = b_1 q^{-1} + \cdots b_{nb} q^{-nb} \tag{4.24}$$

and $e(t)$ is a white-noise stochastic process that captures the random disturbances in the data.

The order of the ARX models was chosen as four. This was based on analysis of the residuals for different model orders as presented in the subsequent figures. Once the parameters of the model were estimated and applied to the validation data-set, together with the consideration that all individual models should have the same order, which facilitates the development of generalised parametric models.

The parameter estimation method used is the prediction error approach (Ljung, 1987), in which the difference between the model's predicted output and the measured output is minimised. The residual correlations are shown for each individual model adopted, and for the most part, the correlations lie within the 99% confidence regions shown. Where this is not the case, it was verified that higher order models did not offer significant improvements and so did not warrant their usage; in such cases, other model structures may offer better results.

The individual models for each of the 9 cases, pertaining to specific forward speed (n_c) and mass are given in the following:

ARX case 1: 450 rpm, 0 kg

$$A(q) = 1 - 0.3151q^{-1} - 0.5621q^{-2} - 0.2652q^{-3} + 0.2179q^{-4}$$
$$B(q) = 0.004322q^{-1} + 0.0005432q^{-2} - 0.001399q^{-3} - 0.002634q^{-4} \quad (4.25)$$

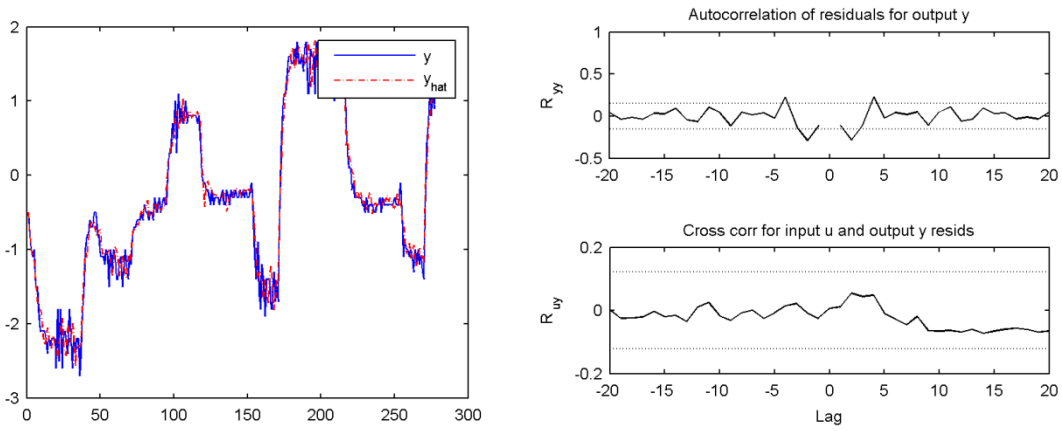

(a) (b)

Figure 4.20: ARX case 1 (a) comparison of target and one-step ahead model prediction (b) residual analysis: error autocorrelation and error-input cross correlation based on one-step ahead prediction for validation data-set

ARX case 2: 450 rpm, 50 kg

$$A(q) = 1 - 0.3853q^{-1} - 0.3652q^{-2} - 0.3216q^{-3} + 0.1710q^{-4}$$

$$B(q) = 0.003802q^{-1} + 0.0004513q^{-2} - 0.001021q^{-3} - 0.002401q^{-4} \quad (4.26)$$

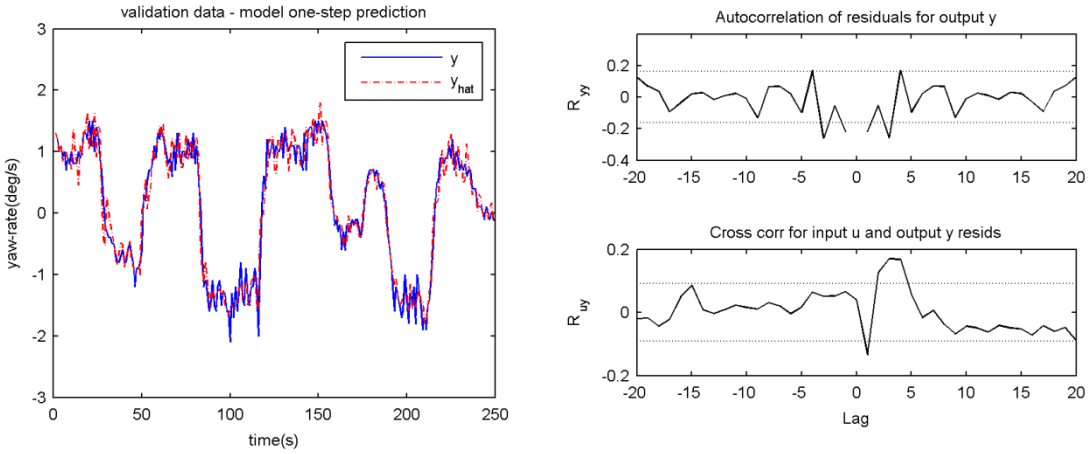

(a) (b)

Figure 4.21: ARX case 2 (a) comparison of target and one-step ahead model prediction (b) residual analysis: error autocorrelation and error-input cross correlation based on one-step ahead prediction for validation data-set

ARX case 3: 450 rpm, 100 kg

$$A(q) = 1 - 0.3080q^{-1} - 0.5347q^{-2} - 0.2015q^{-3} + 0.1459q^{-4}$$

$$B(q) = 0.002914q^{-1} + 0.0005894q^{-2} - 0.0007062q^{-3} - 0.002202q^{-4}$$

(4.27)

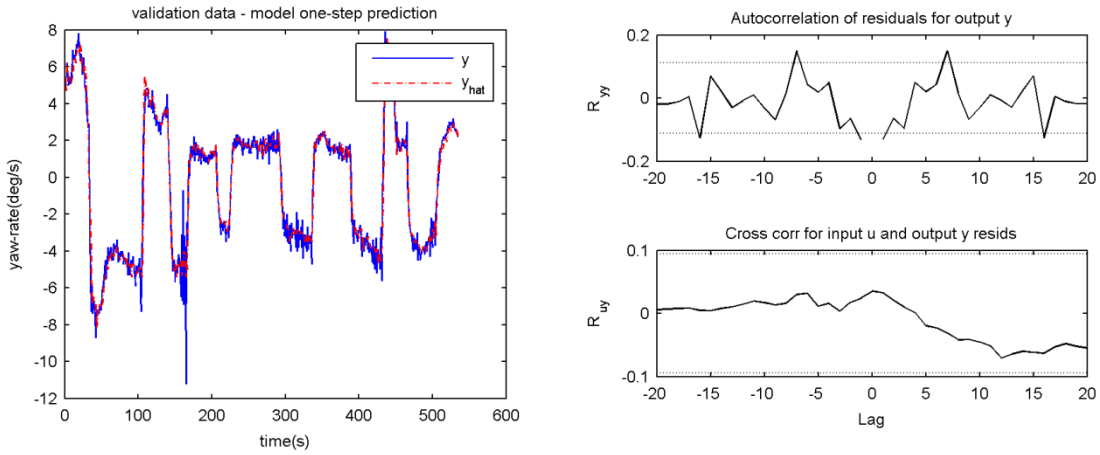

(a) (b)

Figure 4.22: ARX case 3 (a) comparison of target and one-step ahead model prediction (b) residual analysis: error autocorrelation and error-input cross correlation based on one-step ahead prediction for validation data-set

ARX case 4: 900 rpm, 0 kg

$$A(q) = 1 - 0.06588q^{-1} - 0.2937q^{-2} - 0.3265q^{-3} - 0.008445q^{-4}$$

$$B(q) = 0.003619q^{-1} + 0.0006259q^{-2} + 0.0008716q^{-3} - 0.002256q^{-4}$$

(4.28)

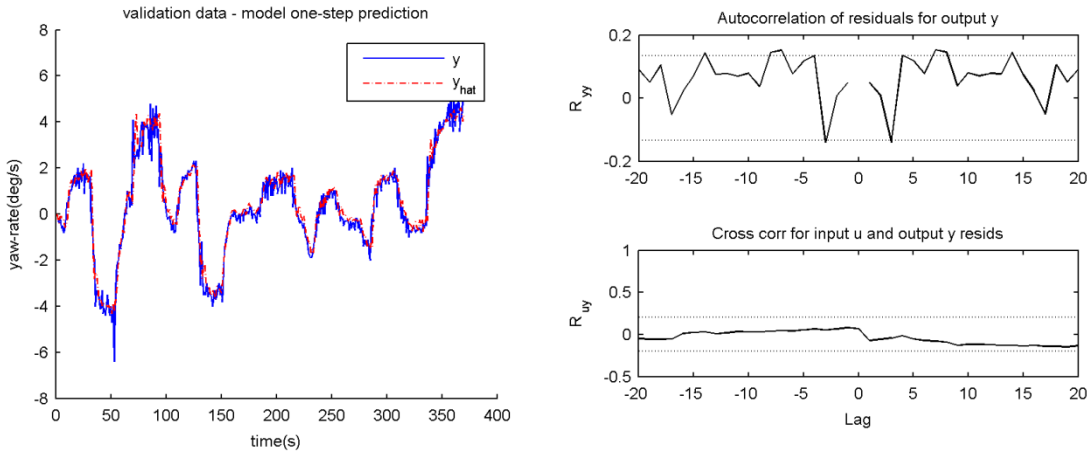

(a) (b)

Figure 4.23: ARX case 4 (a) comparison of target and one-step ahead model prediction (b) residual analysis: error autocorrelation and error-input cross correlation based on one-step ahead prediction for validation data-set

ARX case 5: 900 rpm, 50 kg

$$A(q) = 1 - 0.2082q^{-1} - 0.3039q^{-2} - 0.3060q^{-3} + 0.006661q^{-4}$$

$$B(q) = 0.005065q^{-1} - 0.0005560q^{-2} - 0.0004378q^{-3} - 0.002238q^{-4}$$

(4.29)

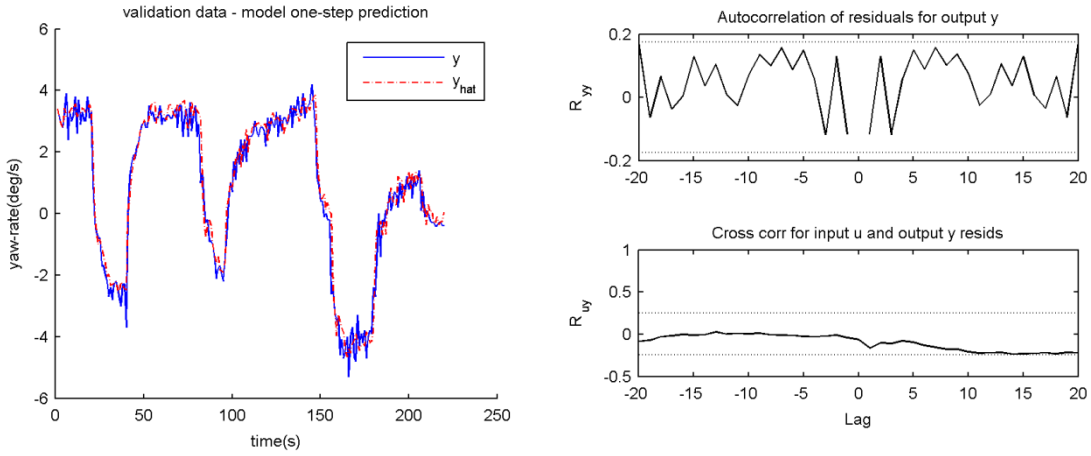

(a) (b)

Figure 4.24: ARX case 5 (a) comparison of target and one-step ahead model prediction (b) residual analysis: error autocorrelation and error-input cross correlation based on one-step ahead prediction for validation data-set

ARX case 6: 900 rpm, 100 kg

$$A(q) = 1 - 0.01618q^{-1} - 0.2819q^{-2} - 0.1155q^{-3} - 0.01304q^{-4}$$

$$B(q) = 0.004055q^{-1} - 0.001740q^{-2} + 0.002781q^{-3} - 0.0008156q^{-4}$$

(4.30)

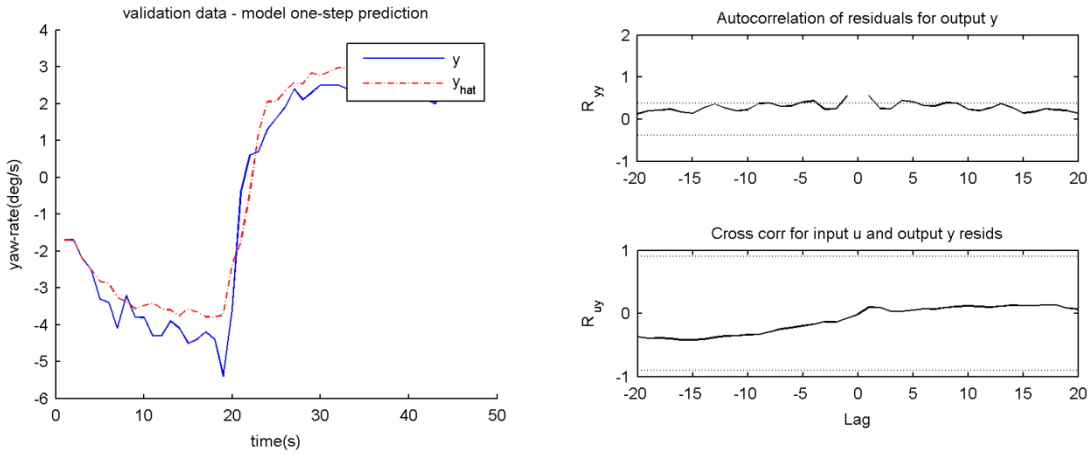

(a) (b)

Figure 4.25: ARX case 6 (a) comparison of target and one-step ahead model prediction (b) residual analysis: error autocorrelation and error-input cross correlation based on one-step ahead prediction for validation data-set

ARX case 7: 1200 rpm, 0 kg

$$A(q) = 1 - 0.4218q^{-1} - 0.1039q^{-2} - 0.1180q^{-3} - 0.04697q^{-4}$$

$$B(q) = 0.004270q^{-1} - 0.0003095q^{-2} - 0.0002728q^{-3} - 0.001971q^{-4}$$

(4.31)

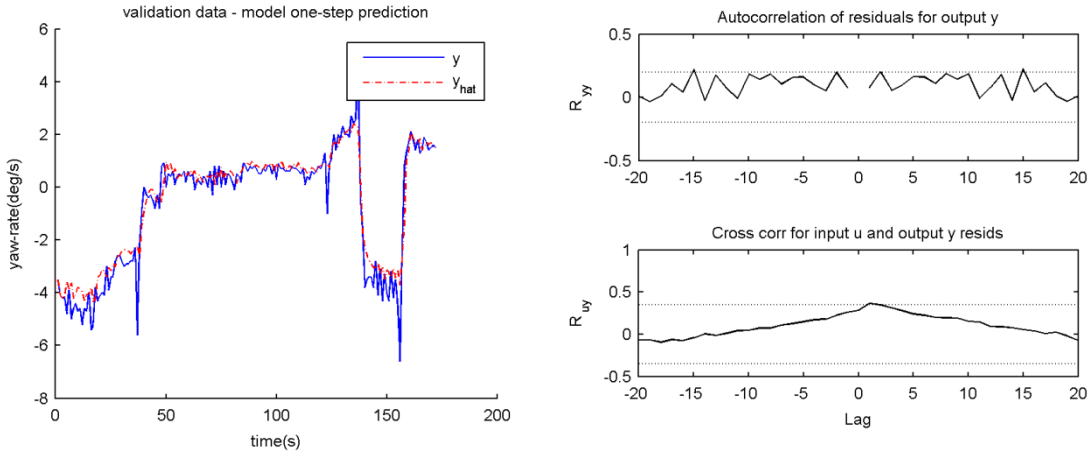

(a) (b)

Figure 4.26: ARX case 7 (a) comparison of target and one-step ahead model prediction (b) residual analysis: error autocorrelation and error-input cross correlation based on one-step ahead prediction for validation data-set

ARX case 8: 1200 rpm, 50 kg

$$A(q) = 1 - 0.4028q^{-1} - 0.08644q^{-2} - 0.1520q^{-3} - 0.03760q^{-4}$$

$$B(q) = 0.002313q^{-1} + 0.001249q^{-2} - 0.0003404q^{-3} - 0.001683q^{-4}$$

(4.32)

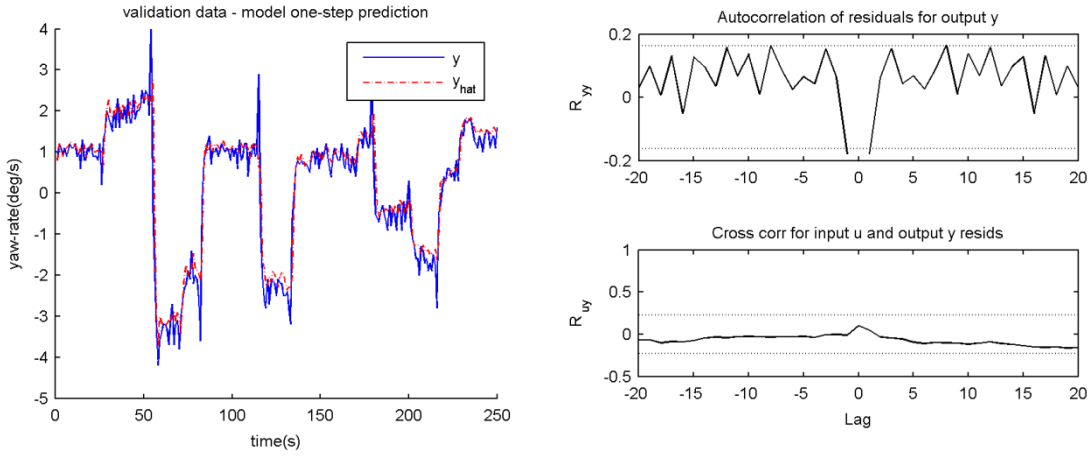

(a) (b)

Figure 4.27: ARX case 8 (a) comparison of target and one-step ahead model prediction (b) residual analysis: error autocorrelation and error-input cross correlation based on one-step ahead prediction for validation data-set

ARX case 9: 1200 rpm, 100 kg

$$A(q) = 1 - 0.06822q^{-1} - 0.3485q^{-2} - 0.07227q^{-3} + 0.04317q^{-4}$$

$$B(q) = 0.001671q^{-1} + 0.002578q^{-2} + 0.0006505q^{-3} - 0.002397q^{-4}$$

(4.33)

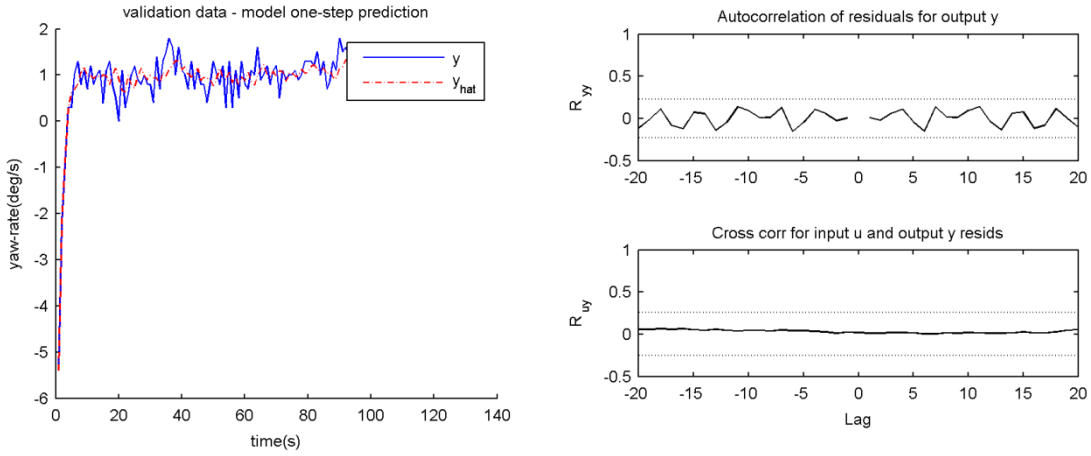

(a) (b)

Figure 4.28: ARX case 9 (a) comparison of target and one-step ahead model prediction (b) residual analysis: error autocorrelation and error-input cross correlation based on one-step ahead prediction for validation data-set

Furthermore, the model coefficients for each of the payload and common-mode speed combinations may be correlated to obtain a generalised model, in which the said coefficients become functions of the payload and speed. The individual values for each coefficient are fitted to a quadratic surface, given by the following Equation (4.34), in which n_c is in rpm and m in kg:

$$\mathrm{A}(q)\,y(t) = \mathrm{B}(q)u(t) + e(t)$$

$$\mathrm{A}(q) = 1 + a_1 q^{-1} + a_2 q^{-2} + a_3 q^{-3} + a_4 q^{-4}$$

$$\mathrm{B}(q) = b_1 q^{-1} + b_2 q^{-2} + b_3 q^{-3} + b_4 q^{-4}$$

$$a_1 = \text{-}1.602\text{e-}06\, n_c^2 + 4.329\text{e-}06\, n_c \times m + 5.315\text{e-}05\, m^2 + 0.002478 n_c - 0.007627 m - 1.064$$

$$a_2 = \text{-}\,7.037\text{e-}08\, n_c^2 - 3.367\text{e-}06\, n_c \times m - 4.092\text{e-}05\, m^2 + 0.0006947 n_c + 0.00627 m - 0.8529$$

$$a_3 = 5.614\text{e-}07\, n_c^2 + 3.717\text{e-}08\, n_c \times m + 3.069\text{e-}05\, m^2 - 0.00073 n_c - 0.002032 m - 0.07498$$

$$a_4 = 5.035\text{e-}07\, n_c^2 + 2.109\text{e-}06\, n_c \times m + 3.889\text{e-}06\, m^2 - 0.001192 n_c - 0.002136 m + 0.656$$

$$b_1 = \text{-}8.328\text{e-}09\, n_c^2 - 1.139\text{e-}08\, n_c \times m - 1.007\text{e-}07\, m^2 + 1.307\text{e-}05\, n_c + 7.847\text{e-}06\, m - 0.0002346$$

$$b_2 = 1.09\text{e-}08\, n_c^2 + 3.066\text{e-}08\, n_c \times m - 1.748\text{e-}10\, m^2 - 1.866\text{e-}05\, n_c - 2.415\text{e-}05\, m + 0.007235$$

$$b_3 = \text{-}1.097\text{e-}08\, n_c^2 + 4.962\text{e-}09\, n_c \times m + 3.682\text{e-}07\ m^2 + 1.926\text{e-}05\, n_c - 2.928\text{e-}05\, m - 0.007668$$

$$b_4 = \text{-}\,3.005\text{e-}09\, n_c^2 - 8.764\text{e-}09\, n_c \times m + 2.449\text{e-}08\, m^2 + 5.923\text{e-}06\, n_c + 9.821\text{e-}06\, m - 0.004866$$

(4.34)

The quadratic surfaces are fitted to the data-points (9 models obtained from the 9 cases above) using least squares and they are shown graphically in Figure 4.29 and Figure 4.30.

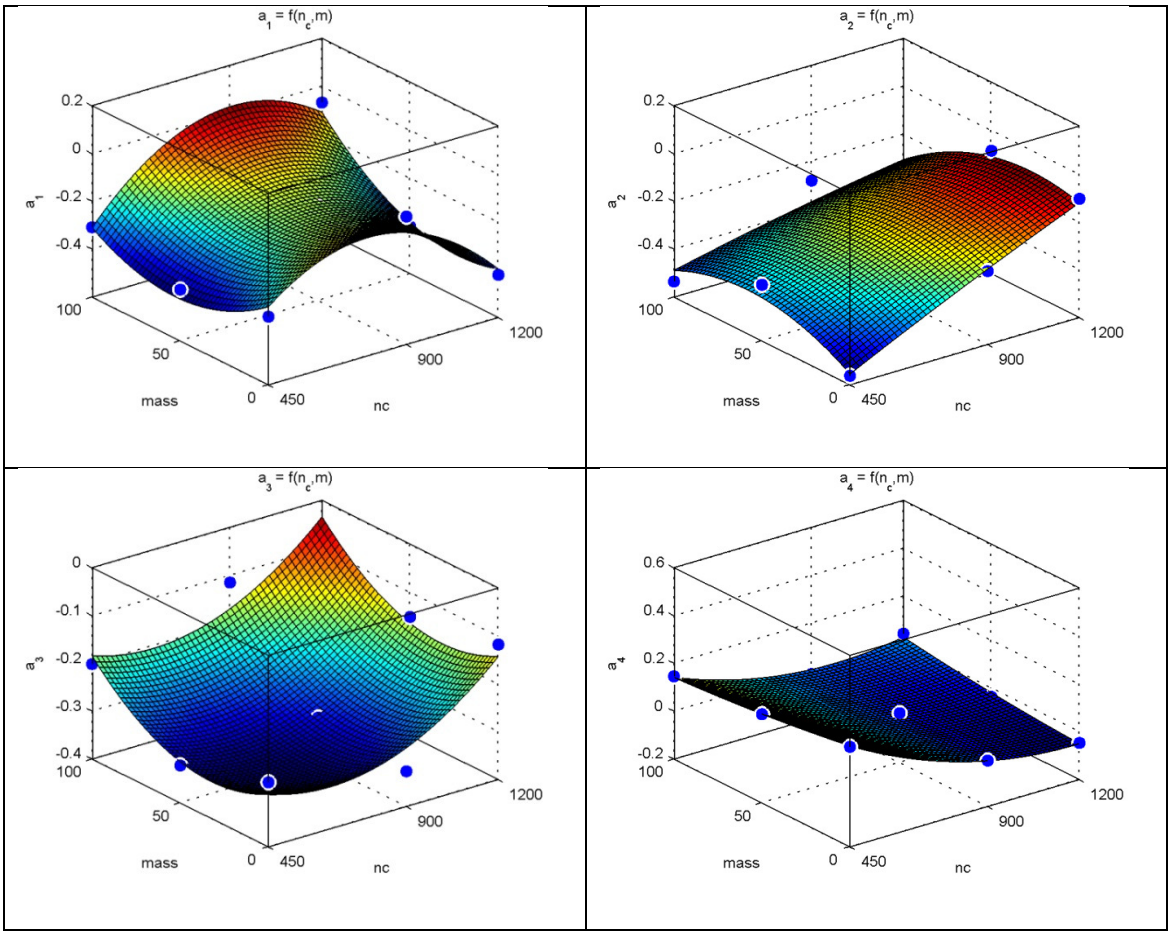

Figure 4.29: Quadratic surfaces for the coefficients a_i of the ARX models.

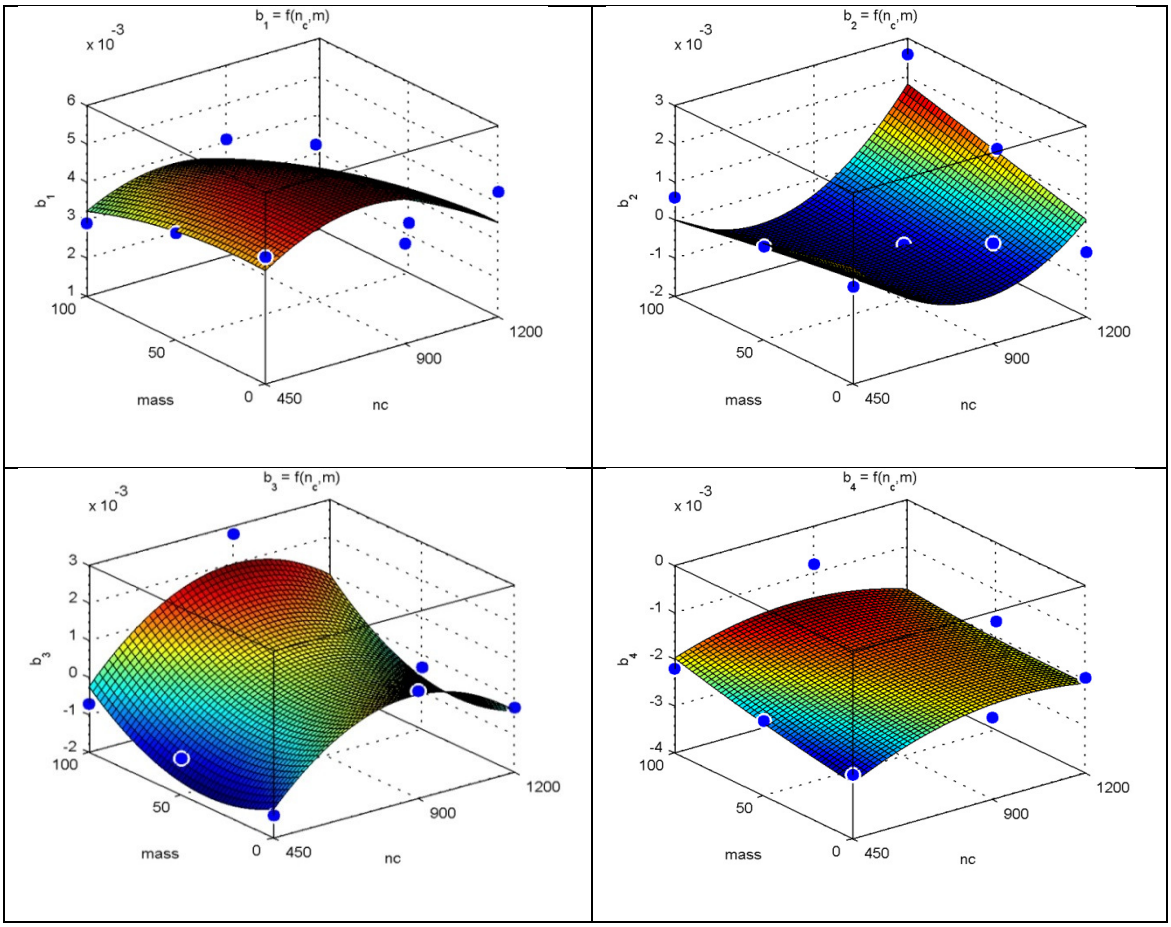

Figure 4.30: Quadratic surfaces for the coefficients b_i of the ARX models.

Thus, the ARX model for different cases of forward speed and variable mass was obtained and a generalised model was derived, as in Equation (4.34). As suggested by Ljung (1999), the ARX model provided acceptable results (as the residual values are within the confidence regions). However, further refinements and improvements for a model that more accurately represents the dynamics of the vehicle was necessary. Hence, ARMAX was investigated.

Additionally, the general autoregressive moving average with exogenous input (ARMAX) model is of the form:

$$A(q)y(t) = B(q)u(t) + C(q)e(t) \tag{4.35}$$

where

$$A(q) = 1 + a_1 q^{-1} + \cdots a_{na} q^{-na}$$

$$B(q) = b_1 q^{-1} + \cdots b_{nb} q^{-nb}$$

$$C(q) = 1 + c_1 q^{-1} + \cdots c_{nc} q^{-nc} \tag{4.36}$$

and $e(t)$ is a white-noise stochastic process that captures the random disturbances in the data.

The fourth order of the ARMAX models were chosen for the reasons discussed in the previous section. The parameter estimation method used is, as before, based on the prediction error approach. The residual correlations are shown for each individual model adopted along with the 99% confidence regions.

ARMAX case 1: 450 rpm, 0 kg

$$A(q) = 1 - 0.7828q^{-1} - 0.8869q^{-2} + 0.7405q^{-3} - 0.06941q^{-4}$$

$$B(q) = 0.003962q^{-1} - 0.001048q^{-2} - 0.003501q^{-3} + 0.005944q^{-4}$$

$$C(q) = 1 - 0.8515q^{-1} - 0.6227q^{-2} + 0.87982q^{-3} - 0.3316q^{-4} \quad (4.37)$$

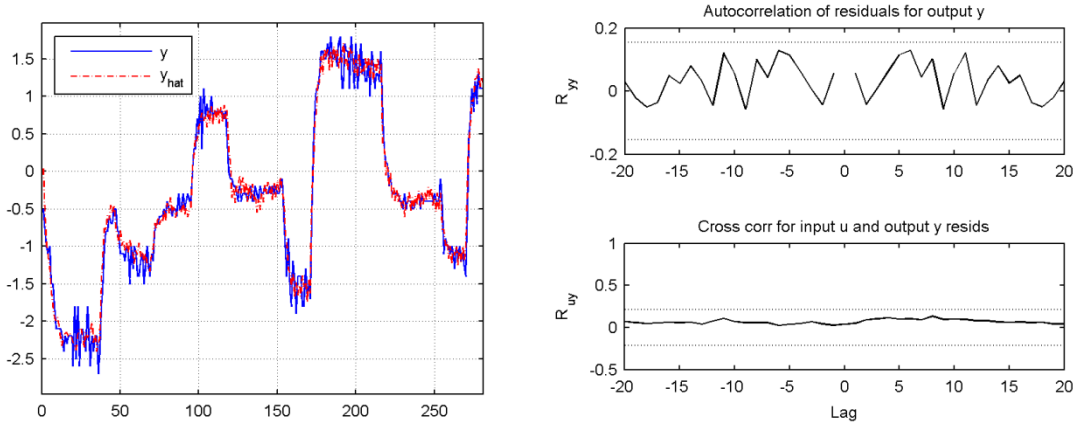

(a) (b)

Figure 4.31: ARMAX case 1 (a) comparison of target and one-step ahead model prediction (b) residual analysis: error autocorrelation and error-input cross correlation based on one-step ahead prediction for validation data-set

ARMAX case 2: 450 rpm, 50 kg

$$A(q) = 1 - 0.4107q^{-1} - 0.2163q^{-2} - 0.8611q^{-3} + 0.5422q^{-4}$$

$$B(q) = 0.003840q^{-1} + 0.00004715q^{-2} - 0.0001600q^{-3} - 0.003309q^{-4}$$

$$C(q) = 1 - 0.2361q^{-1} + 0.08703q^{-2} - 0.6538q^{-3} + 0.6019q^{-4}$$

(4.38)

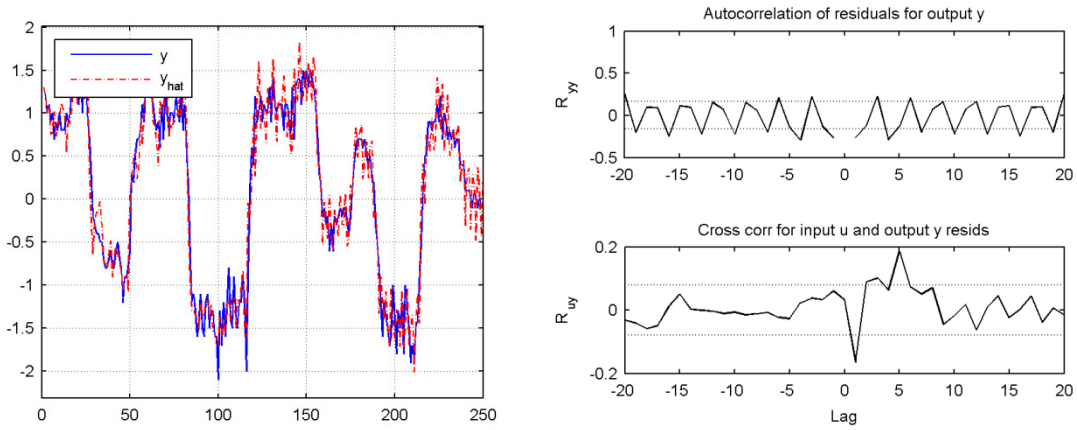

(a) (b)

Figure 4.32: ARMAX case 2 (a) comparison of target and one-step ahead model prediction (b) residual analysis: error autocorrelation and error-input cross correlation based on one-step ahead prediction for validation data-set

ARMAX case 3: 450 rpm, 100 kg

$$A(q) = 1 - 0.2390q^{-1} - 0.8609q^{-2} - 0.1052q^{-3} + 0.2646q^{-4}$$

$$B(q) = 0.002955q^{-1} + 0.0008783q^{-2} - 0.001861q^{-3} - 0.001651q^{-4}$$

$$C(q) = 1 - 0.006975q^{-1} - 0.4091q^{-2} + 0.02662q^{-3} + 0.07620q^{-4}$$

(4.39)

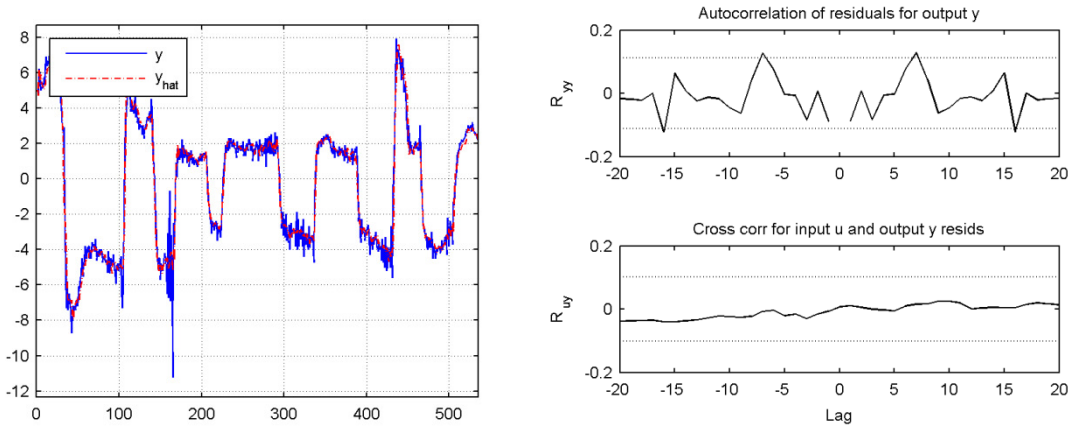

(a) (b)

Figure 4.33: ARMAX case 3 (a) comparison of target and one-step ahead model prediction (b) residual analysis: error autocorrelation and error-input cross correlation based on one-step ahead prediction for validation data-set

ARMAX case 4: 900 rpm, 0 kg

$$A(q) = 1 - 1.113q^{-1} - 0.3519q^{-2} + 0.4221q^{-3} + 0.04596q^{-4}$$

$$B(q) = 0.004301q^{-1} - 0.003881q^{-2} - 0.001648 + 0.001247q^{-4}$$

$$C(q) = 1 - 1.214q^{-1} - 0.1037q^{-2} + 0.6224q^{-3} - 0.2639q^{-4} \quad (4.40)$$

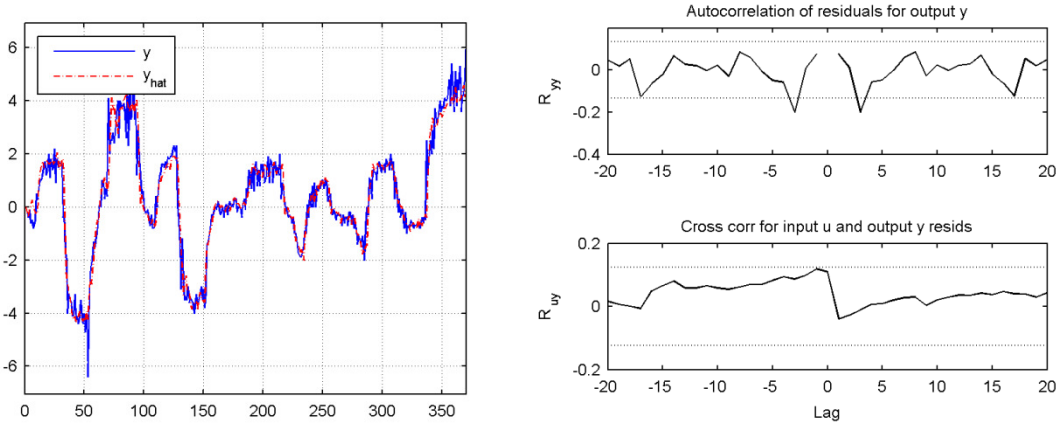

(a) (b)

Figure 4.34: ARMAX case 4 (a) comparison of target and one-step ahead model prediction (b) residual analysis: error autocorrelation and error-input cross correlation based on one-step ahead prediction for validation data-set

ARMAX case 5: 900 rpm, 50 kg

$$A(q) = 1 - 0.7902q^{-1} - 0.9527q^{-2} + 0.7211q^{-3} + 0.02280q^{-4}$$

$$B(q) = 0.005037q^{-1} - 0.002781q^{-2} - 0.005380 + 0.003138q^{-4}$$

$$C(q) = 1 - 0.7618q^{-1} - 0.8428q^{-2} + 0.7875q^{-3} - 0.1315q^{-4}$$

(4.41)

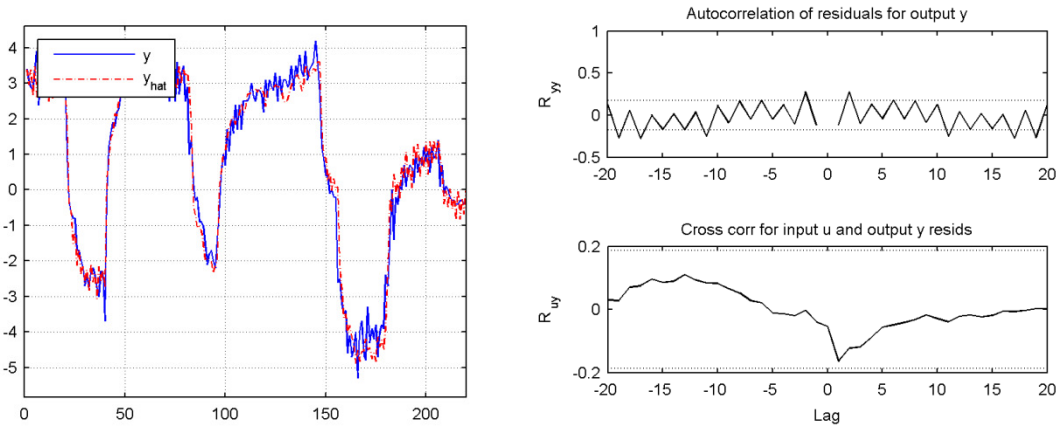

(a) (b)

Figure 4.35: ARMAX case 5 (a) comparison of target and one-step ahead model prediction (b) residual analysis: error autocorrelation and error-input cross correlation based on one-step ahead prediction for validation data-set

ARMAX case 6: 900 rpm, 100 kg

$$A(q) = 1 + 0.2109q^{-1} - 0.1182q^{-2} - 0.5894q^{-3} - 0.1344q^{-4}$$

$$B(q) = 0.009923q^{-1} - 0.008453 + 0.006235 - 0.003660q^{-4}$$

$$C(q) = 1 + 0.3546q^{-1} - 0.3834q^{-2} - 0.2879q^{-3} - 0.54990q^{-4} \quad (4.42)$$

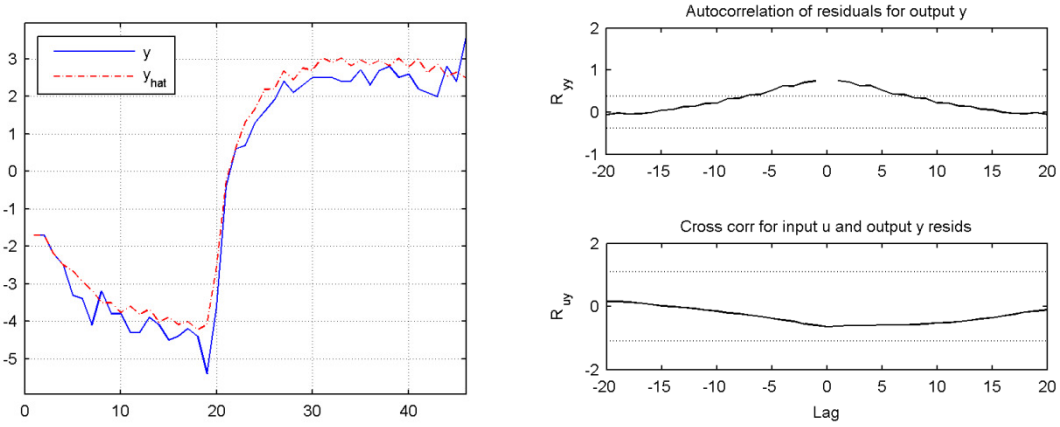

(a) (b)

Figure 4.36: ARMAX case 6 (a) comparison of target and one-step ahead model prediction (b) residual analysis: error autocorrelation and error-input cross correlation based on one-step ahead prediction for validation data-set

ARMAX case 7: 1200 rpm, 0 kg

$$A(q) = 1 - 0.4622q^{-1} - 0.1223q^{-2} - 0.8189q^{-3} + 0.4208q^{-4}$$

$$B(q) = 0.004535q^{-1} - 0.0007611q^{-2} - 0.001204q^{-3} - 0.002516q^{-4}$$

$$C(q) = 1 - 0.1283q^{-1} - 0.09675q^{-2} - 0.8484q^{-3} + 0.1564q^{-4} \quad (4.43)$$

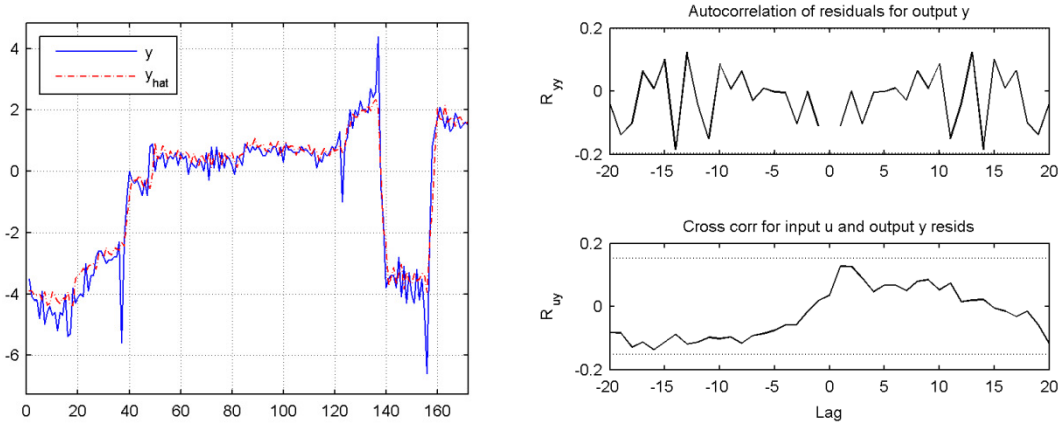

(a) (b)

Figure 4.37: ARMAX case 7 (a) comparison of target and one-step ahead model prediction (b) residual analysis: error autocorrelation and error-input cross correlation based on one-step ahead prediction for validation data-set

ARMAX case 8: 1200 rpm, 50 kg

$$A(q) = 1 - 1.472q^{-1} + 0.3053q^{-2} + 0.3144q^{-3} - 0.1383q^{-4}$$

$$B(q) = 0.002463q^{-1} - 0.001448q^{-2} - 0.001937q^{-3} + 0.0009625q^{-4}$$

$$C(q) = 1 - 1.186q^{-1} - 0.04049q^{-2} + 0.4182q^{-3} - 0.1180q^{-4} \quad (4.44)$$

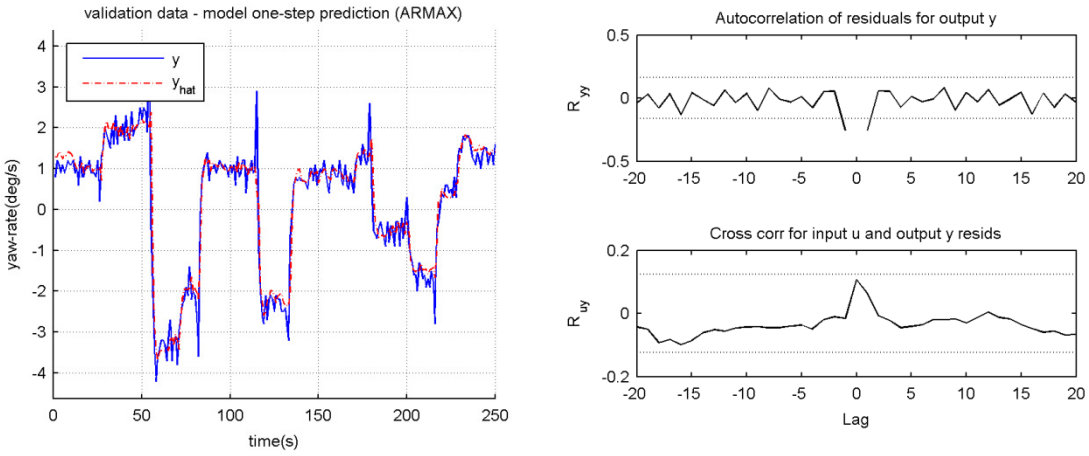

(a) (b)

Figure 4.38: ARMAX case 8 (a) comparison of target and one-step ahead model prediction (b) residual analysis: error autocorrelation and error-input cross correlation based on one-step ahead prediction for validation data-set

ARMAX case 9: 1200 rpm, 100 kg

$$A(q) = 1 - 0.8089q^{-1} + 0.6663q^{-2} - 0.05899q^{-3} - 0.07505q^{-4}$$

$$B(q) = 0.0008776q^{-1} + 0.0008629q^{-2} + 0.001638q^{-3} - 0.0001176q^{-4}$$

$$C(q) = 1 - 0.8013q^{-1} + 1.045q^{-2} - 0.1615q^{-3} + 0.1909q^{-4} \tag{4.45}$$

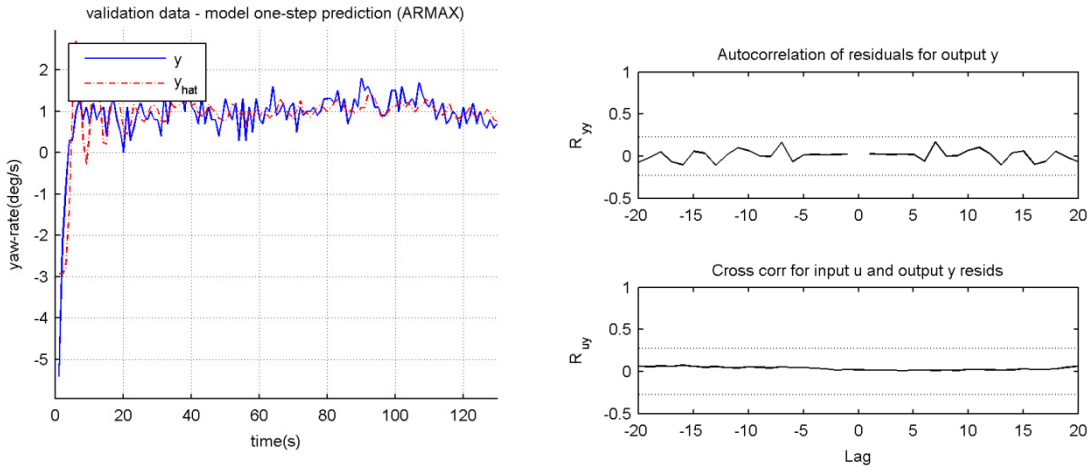

(a) (b)

Figure 4.39: ARMAX case 9 (a) comparison of target and one-step ahead model prediction (b) residual analysis: error autocorrelation and error-input cross correlation based on one-step ahead prediction for validation data-set

As developed for the ARX models, a generalised ARMAX model may be constructed from the individual models obtained as in the following Equation (4.46). Quadratic fits to the coefficients yield the following functional expressions, in which n_c is in rpm and m in kg:

$$\mathrm{A}(q)y(t) = \mathrm{B}(q)u(t) + \mathrm{C}(q)e(t)$$

$$\mathrm{A}(q) = 1 + a_1 q^{-1} + a_2 q^{-2} + a_3 q^{-3} + a_4 q^{-4}$$

$$\mathrm{B}(q) = b_1 q^{-1} + b_2 q^{-2} + b_3 q^{-3} + b_4 q^{-4}$$

$$\mathrm{C}(q) = 1 + c_1 q^{-1} + c_2 q^{-2} + c_3 q^{-3} + c_4 q^{-4}$$

$$a_1 = \text{-}1.301\text{e-}06\, n_c^2 - 9.568\text{e-}06\, n_c \times m + 0.0001434\, m^2 + 0.002042\, n_c - 0.001139\, m - 1.458$$

$$a_2 = 2.831\text{e-}06\, n_c^2 + 9.73\text{e-}06\, n_c \times m + 3.558\text{e-}06\, m^2 - 0.003908\, n_c - 0.005132\, m + 0.5534$$

$$a_3 = \text{-}2.425\text{e-}06\, n_c^2 + 1.943\text{e-}05\, n_c \times m - 5.058\text{e-}05\, m^2 + 0.00288\, n_c - 0.01511\, m - 0.3509$$

$$a_4 = 1.198\text{e-}06\, n_c^2 - 1.109\text{e-}05\, n_c \times m - 2.672\text{e-}05\, m^2 - 0.001657\, n_c + 0.01096\, m + 0.5618$$

$$b_1 = \text{-}2.527\text{e-}08\, n_c^2 - 2.093\text{e-}08\, n_c \times m + 2.582\text{e-}07\, m^2 + 4.145\text{e-}05\, n_c - 4.841\text{e-}06\, m - 0.01031$$

$$b_2 = 3.521\text{e-}08\, n_c^2 - 1.511\text{e-}08\, n_c \times m - 2.691\text{e-}07\, m^2 - 5.788\text{e-}05\, n_c + 3.635\text{e-}05\, m + 0.01852$$

$$b_3 = \text{-}5.721\text{e-}09\, n_c^2 + 2.572\text{e-}08\, n_c \times m + 9.742\text{e-}07\, m^2 + 9.94\text{e-}06\, n_c - 7.807\text{e-}05\, m - 0.00589$$

$$b_4 = \text{-}8.58\text{e-}09\, n_c^2 + 5.236\text{e-}08\, n_c \times m - 5.124\text{e-}07\, m^2 + 1.274\text{e-}05\, n_c - 9.11\text{e-}06\, m - 0.004036$$

$$c_1 = \text{-}2.131\text{e-}07\, n_c^2 - 1.737\text{e-}05\, n_c \times m + 0.0001147\, m^2 + 0.0007663\, n_c + 0.009091\, m - 1.208$$

$$c_2 = 3.695\text{e-}06\, n_c^2 + 1.053\text{e-}05\, n_c \times m + 6.811\text{e-}05\, m^2 - 0.0058\, n_c - 0.01218\, m + 1.635$$

$$c_3 = \text{-}3.398\text{e-}06\, n_c^2 + 1.881\text{e-}05\, n_c \times m - 5.819\text{e-}05\, m^2 + 0.00429\, n_c - 0.01376\, m - 0.6511$$

$$c_4 = 3.016\text{e-}06\, n_c^2 - 5.801\text{e-}06\, n_c \times m - 9.512\text{e-}05\, m^2 - 0.004738\, n_c + 0.01496\, m + 1.416$$

(4.46)

The quadratic surfaces are fitted to the data-points (9 models obtained from the 9 cases above) using least squares and they are shown graphically in Figures 4.40 - 4.42.

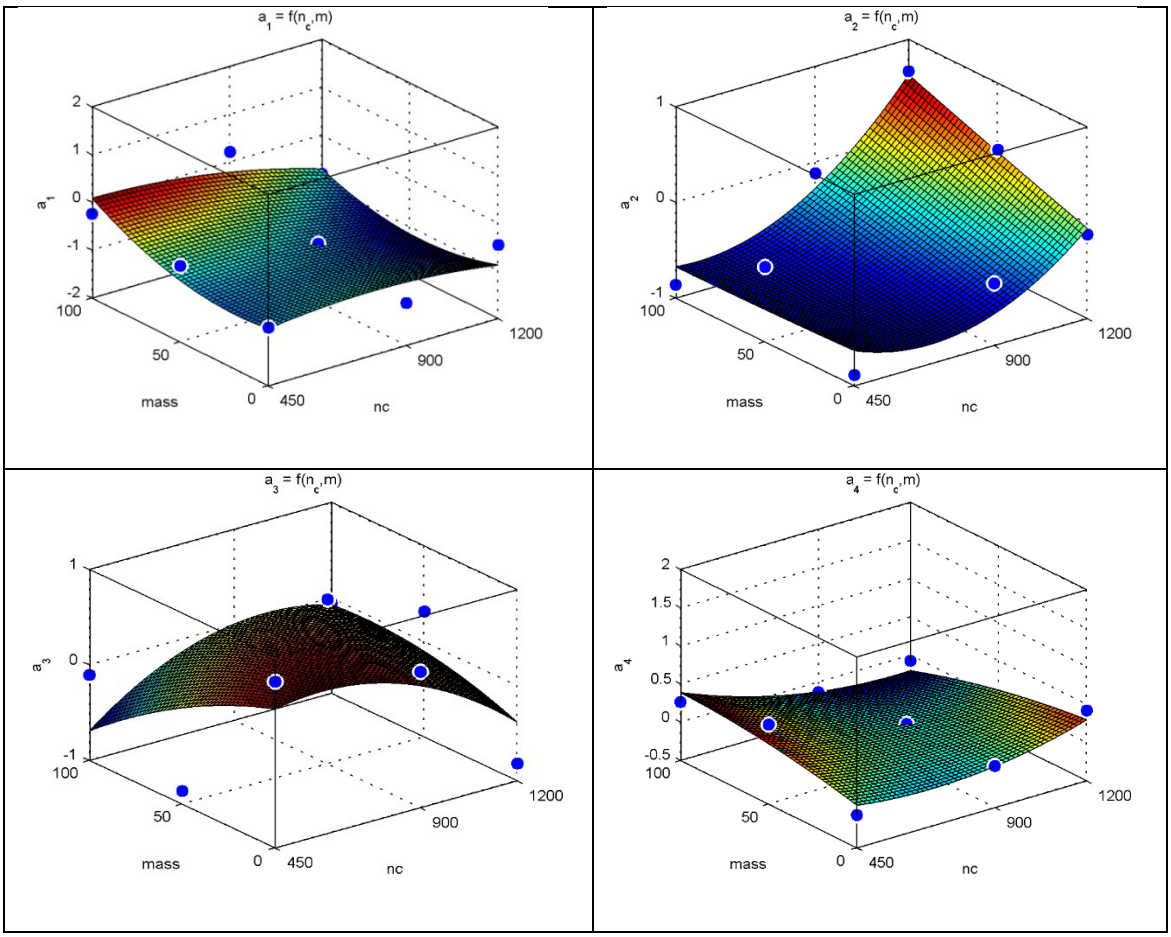

Figure 4.40: Quadratic surfaces for the coefficients a_i of the ARMAX models.

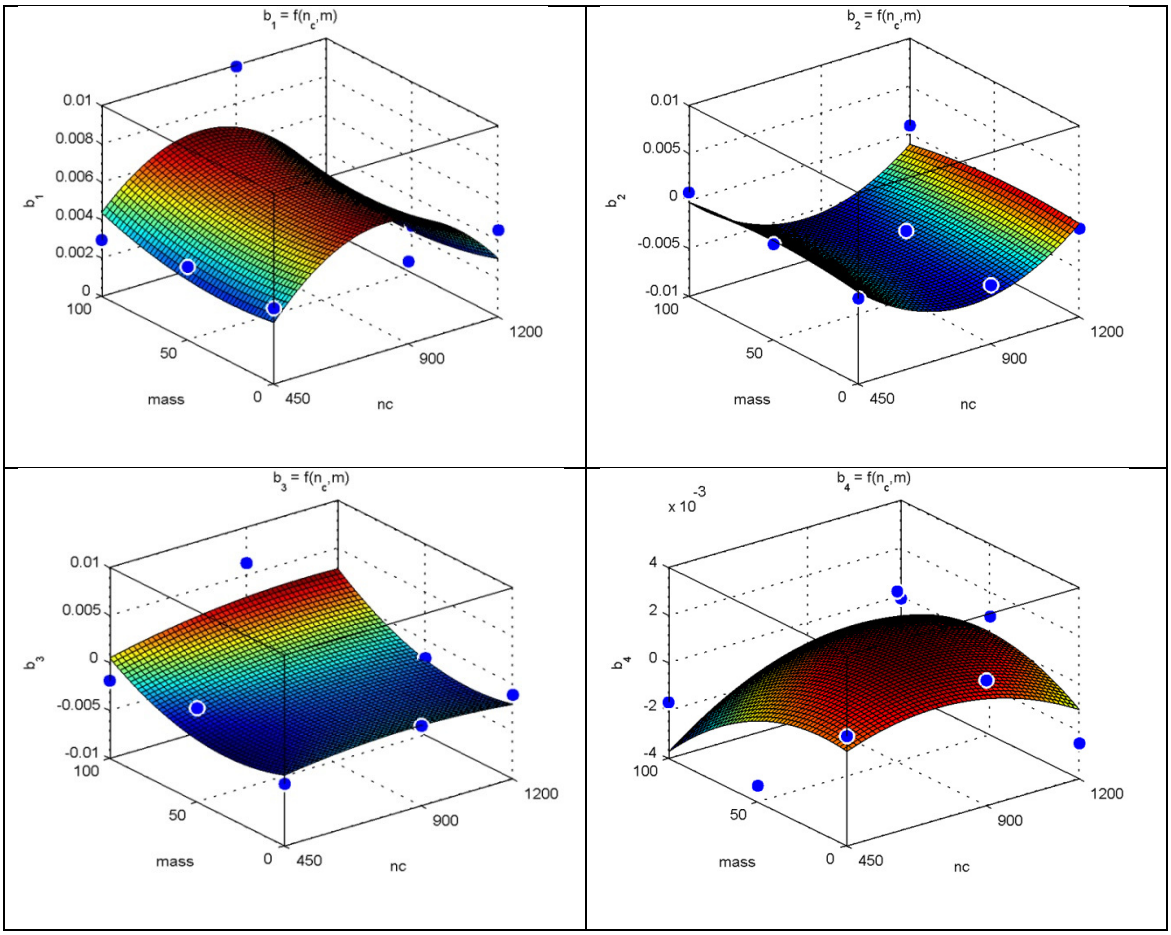

Figure 4.41: Quadratic surfaces for the coefficients b_i of the ARMAX models.

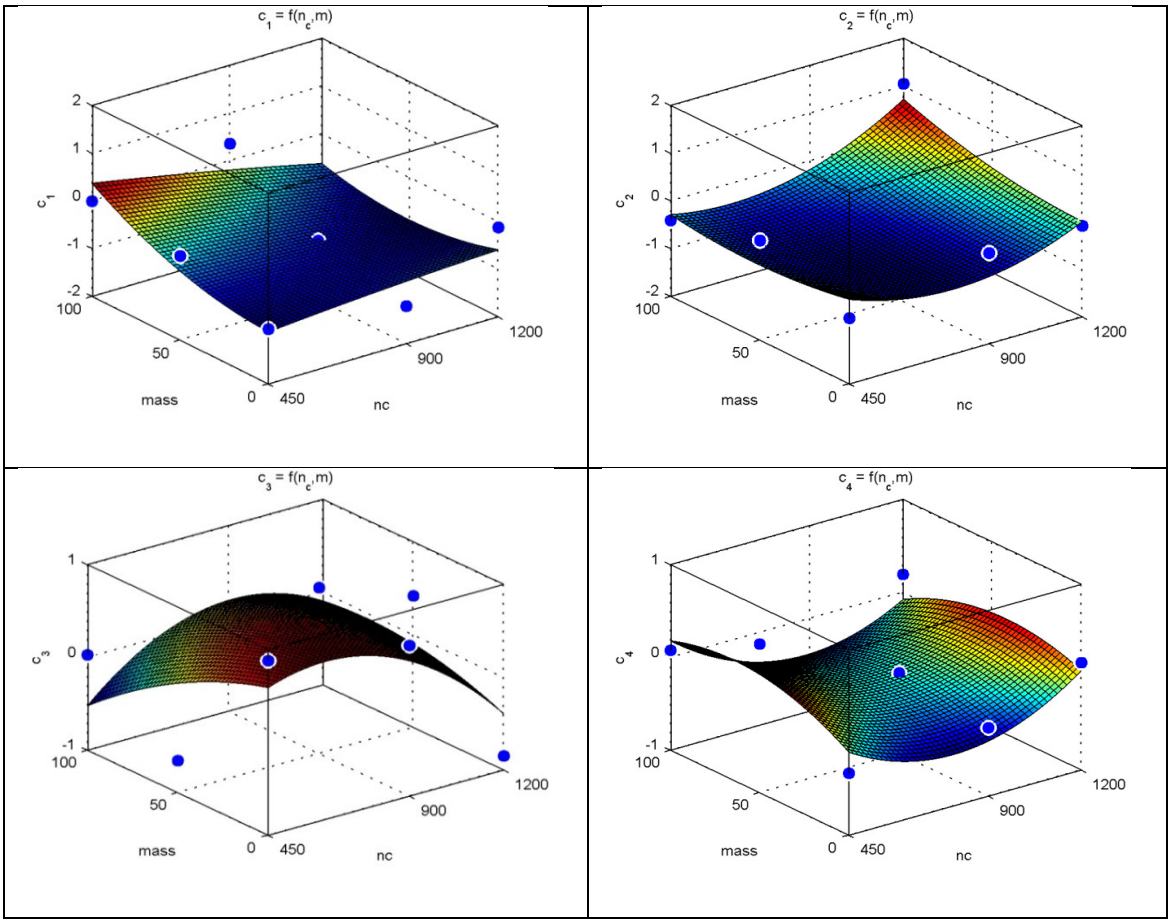

Figure 4.42: Quadratic surfaces for the coefficients c_i of the ARMAX models.

4.13 Conclusions

The reference frames involved in defining the translation and orientation of the *Springer* USV vehicles was discussed in the kinetics and kinematics section of this chapter. This provides the background information necessary to understand the particular challenges faced by autopilots due to the six degrees of freedom in motion inherent to marine vehicles. This adds an extra element of complexity to course keeping and way point following missions (especially when compared to similar tasks in land based vehicles). The need for obtaining an accurate model of an USV under different operating conditions, to design an autopilot is emphasised. This chapter includes some exploration

pertaining the use of CLID to find the dynamic model of *Springer* USV. Though this approach was initially promising, there were practical limitations to utilise this in conjunction with advanced controllers such as MPC. Hence, a traditional method such as rigid body modelling that is used by the shipping industry was considered. However, the time frame and costs involved were prohibitive for the use of such an approach for *Springer* USV. Therefore, a more practical approach of system identification was investigated further. Subsequently, these procedures were applied to *Springer* USV for various forward speeds and variable payloads. The challenges and rationale for the design of a successful test environment to obtain a model of *Springer*, for various forward speeds and masses are discussed and the results obtained from experiments conducted at Roadford Reservoir, Devon, United Kingdom presented. A generalised model of the *Springer* was derived by an innovative technique from the trials data.

Chapter 5

Contemporary guidance and autopilot designs

5.1 Introduction

Automatic marine control systems for ships of all sizes are being designed and developed to meet the needs of both the military and civil marine industries. Although automatic systems for modern ships are endowed with a high degree of expensive control sophistication, they also possess manual override facilities in case of emergencies and unforeseen events. However, when functioning in a truly autonomous mode, USVs such as *Springer* do not have the luxury of manual override. The application of USVs is continually expanding in naval, commercial and scientific sectors such as surveying (Majohr et al., 2000), environmental data gathering (Caccia et al., 2007), mine-counter measures (Yan et al., 2010), and search and rescue operations (Annamalai, 2012), to name but a few. In the absence of manual override such systems are totally reliant upon the integrity of their low cost NGC systems in order to fulfil their missions successfully.

To accomplish this task, guidance and navigation systems are essential. In this chapter guidance systems that generate the reference trajectory are discussed. Thereafter PID, LQG autopilots and innovations to LQG technology are presented here. A generalised integrated NGC system for the *Springer* USV is represented by the following block

diagram in Figure 5.1. The predetermined trajectory that the vehicle must follow is provided by the guidance system. The plant input-output relationship is given by the steering model previously described in Chapter 4. The guidance system is presented in Section 5.2, thereafter way-point guidance by means of LOS is discussed in Section 5.3. Contemporary autopilot technologies are elaborated in Section 5.4. PID and LQR are discussed in the subsequent Sections 5.5 and 5.6. Simulations and conclusions are presented in Sections 5.7 and 5.8.

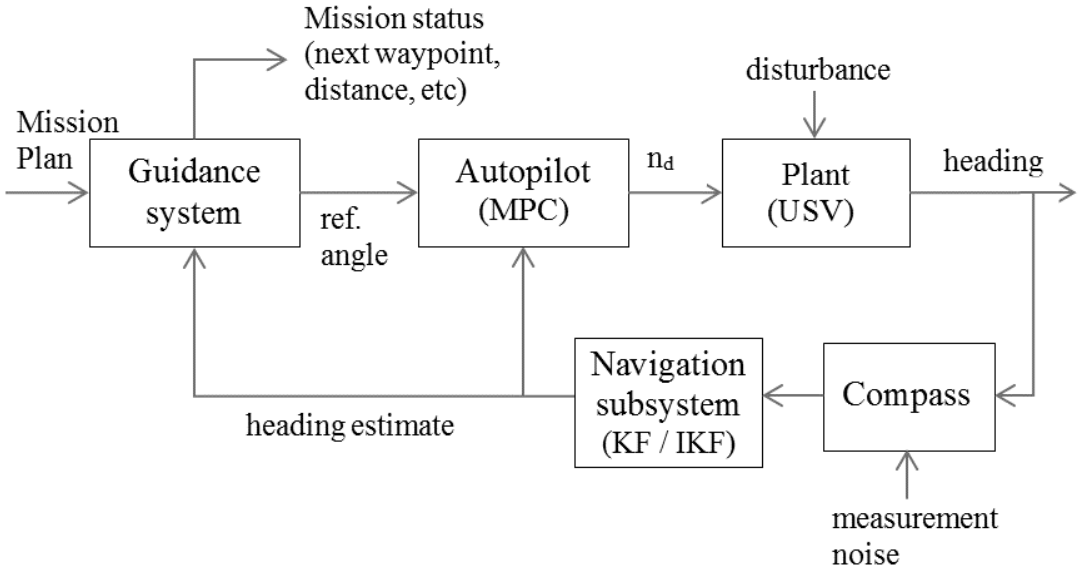

Figure 5.1: NGC system block diagram

5.2 Guidance system

The guidance system decides the best possible physical trajectory to be followed by the vehicle. Freund and Mayr (1997) explain how automated vehicles could be guided along a desired trajectory. The guidance system receives its input from the navigation system and generates the required reference headings. The control system is responsible

for keeping the vehicle on course as specified by the guidance processor. The suitability of different control systems for *Springer* have been analysed and their performances evaluated in Chapters 5 and 6. This chapter explores recent developments of USV guidance strategies and navigation systems. A survey of different guidance strategies is discussed in detail by Naeem et al., (2003). A decentralised controller based on a receding horizon control (RHC) scheme was designed by Borrelli et al., (2004) for collision avoidance. A predictive control and guidance strategy for a nonlinear unmanned aerial vehicle has been presented by Anderson and Stone (2007). A way-point guidance scheme based on a LOS algorithm has been presented by Moreira et al., (2007). Research and design aspects of *Springer*'s NGC systems and their implementation in the USV are presented by Naeem, et al., (2008). Experimental results for multiple waypoints following algorithm is also discussed in this paper. Oh and Sun (2010) present an MPC scheme with LOS path generation capability for a way-point tracking of under actuated surface vessels. The inclusion of a LOS decision variable into the MPC design results in path performance improvement. Whereas, biologically inspired strategies for the guidance of autonomous vessels are presented by Srinivasan (2011). Whilst a model reference adaptive control algorithm in parallel with an analytic MPC is presented for path following of under actuated ships along a predefined path at a constant forward speed by Xiaofei, et al., (2011).

Different strategies used in marine environments to guide the vehicles are further illustrated in Annamalai (2012). Two of the main strategies presented here will be discussed as follows:

- LOS
- Proportional navigation

LOS guidance is the commonly used simple guidance strategy. The line of sight angle between the target and the vehicle can be easily obtained by the following Equation (5.1):

$$\lambda = \tan^{-1}\left[\frac{y_2 - y_1}{x_2 - x_1}\right] \tag{5.1}$$

where (x_1,y_1) is the current location of the *Springer* and (x_2,y_2) is the target position required for the *Springer*.

Proportional navigation guidance (PNG) was initially used in the guidance of missile systems and it can be mathematically represented as show in the following Equation (5.2):

$$\eta_c = N' V_c \lambda \tag{5.2}$$

where V_c is the closing velocity and λ is the LOS angle, and N' is the tuning parameter. The advantage of this law is that the variation of N' results in better performance. More variations of PNG law and a comprehensive view of other different guidance systems can be found in Naeem, et al., (2003).

5.3 Waypoint guidance by LOS

The most common guidance scheme used in autonomous vehicles is waypoint guidance by LOS (Naeem, et al., 2003). In this scheme the guidance between two points [x_d (t_o),y_d (t_o)] and [x_d (t_f), y_d (t_f)] is achieved by splitting the path between them into a number of way points [x_d (k), y_d (k)] for $k = 1, 2, \ldots, N$ as shown in the following Figure 5.2:

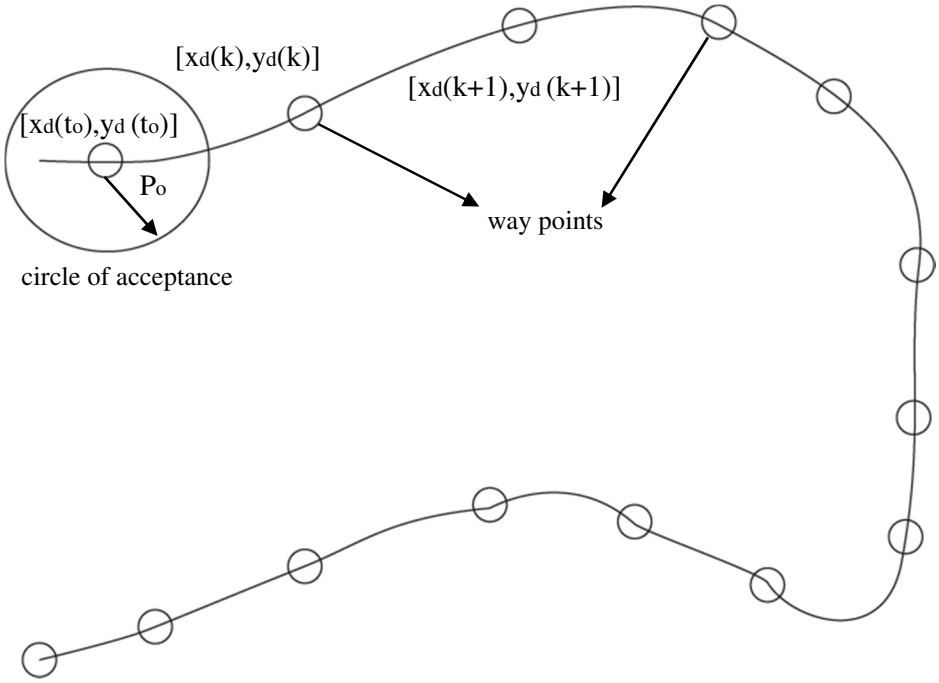

Figure 5.2: Way point guidance by LOS (Naeem, 2004)

In the above Figure 5.2, based on the current estimated position of the USV and the coordinates of the next waypoint to be reached, the desired or reference heading angle based on LOS is calculated as follows in Equation (5.3):

$$r(k) = tan^{-1}\left[\frac{y_d(k)-y(k)}{x_d(k)-x(k)}\right] \tag{5.3}$$

where (x,y) is the current location of the vessel and (x_d,y_d) the target coordinates. In practice, because the inverse of the tangent is restricted to (-90°, 90°), the four quadrant inverse tangent, $arctan2(y_d(k)-y(k), x_d(k)-x(k))$ which takes into account the signs of both arguments, is used instead.

Care is also taken to ensure that the vessel is directed to turn toward the updated reference angle from its present heading in the direction of rotation that requires the lesser change in angle with respect to its present heading angle, since two possibilities always exist.

The guidance system keeps track of the mission status constantly, which includes a log of the waypoints reached or missed and the current target waypoint, as well as the total distance travelled, deviation from the ideal trajectory, and controller energy consumed. These are updated at every sampling instant given the updated estimates of the position and heading of the USV.

In order to decide whether a waypoint has been reached or not, the guidance system considers a circle of acceptance (COA) around each of the waypoints. Healey and Lienard (1993) suggest that the COA should be at least twice the length of the vehicle. During experimentation at Roadford Reservoir, this made more sense as the vehicle approached the waypoints from various different angles, as shown in the following Figure 5.3.

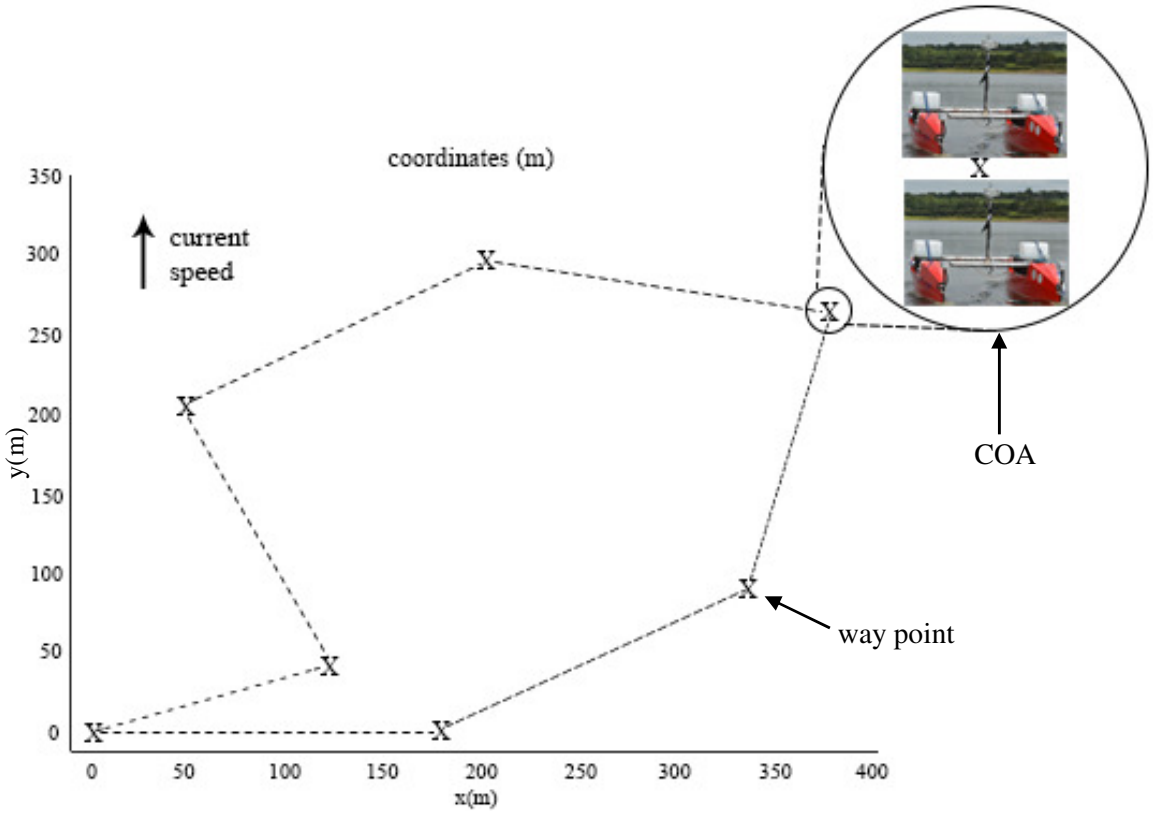

Figure 5.3: Circle of acceptance

For *Springer* the length is approximately 4m, thus the COA is 8m in diameter. At each sampling instant, the guidance system calculates the distance to be covered to reach the next waypoint according to the following Equation (5.4):

$$\rho = \sqrt{[x_d(k) - x(t)]^2 + [y_d(k) - y(t)]^2} \leq \rho_0 \tag{5.4}$$

where ρ_0 is the radius of the COA. When this condition is met then it is concluded that the waypoint is reached, and the guidance system directs the vessel to the following waypoint. As a practical consideration during implementation, note that the vessel's coordinates may not be within the COA at the sampling instants of time, though it may have entered and left it in between sampling instants. The criterion used here is that if

the straight line between two position estimates penetrates the COA even though the two estimates do not, then it is considered that the waypoint in question has been reached.

However, the vessel might pass by the vicinity of a waypoint without entering the COA. This condition is determined by checking the derivative $d\rho/dt$, which when switches from positive to negative, indicates that the vessel has missed the waypoint. In this case, the guidance system also directs the vessel toward the next waypoint.

The vessel normally follows a path different from the ideal one. Several performance indices are used to assess the trajectories followed, which the guidance system computes at each time step and keeps track of. The deviation from the ideal trajectory can be measured by the following Equation (5.5).

$$r_d(k) = \sqrt{r^2(k) + r'^2(k) - 2r(k)r'(k)\cos\alpha} \tag{5.5}$$

where $r(k)$ is the distance to the next waypoint from the position of the vehicle were it on the ideal path, and $r'(k)$ the distance to the next waypoint from the actual position of the vessel, α being the angle between the two vectors, as shown in Figure 5.4.

The average controller energy $\overline{CE_u}$ is defined by the following Equation (5.6).

$$\overline{CE_u} = \frac{\sum_{k=0}^{N} [u_c(k)/60]^2}{N} \tag{5.6}$$

where N is the total number of time steps and u_c the controller effort at time k in *rpm*.

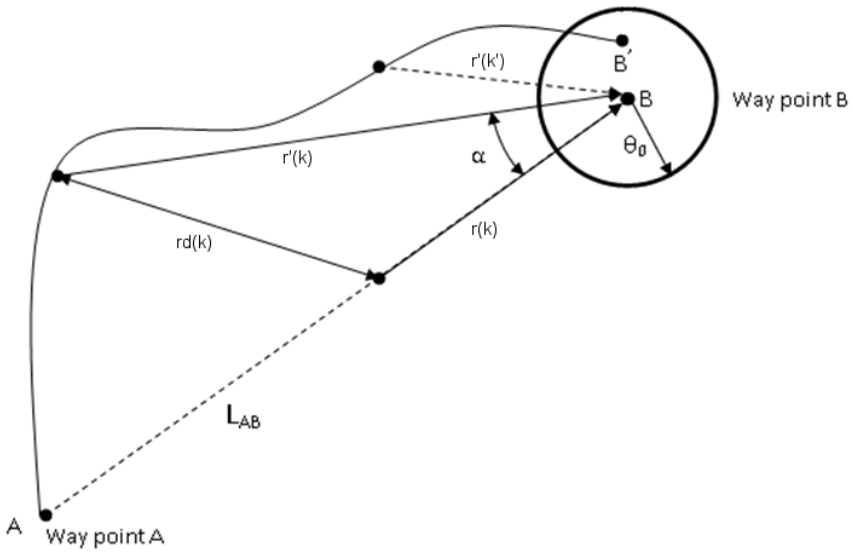

Figure 5.4: Deviation at time *k*

The guidance system described so far enables *Springer* to generate the reference trajectory required to achieve the desired missions. This reference trajectory is utilised by the autopilot to keep the vehicle on course and is described in the subsequent section.

5.4 Autopilot methodologies

In previous work with the *Springer*, data from digital compasses are combined using various data-fusion architectures based on the KF (Xu, 2007). The use of redundant data (by using three separate compasses simultaneously) allows for the construction of fault-tolerant navigation systems. Another example is the USV *Charlie* that is equipped solely with a GPS and a magnetic compass which uses an extended KF (Caccia et al., 2008). In this chapter, the suitability of the design of two autopilots (PID and LQG) is analysed for application in *Springer*.

The following Figure 5.5 shows the overall structure of the system which has been discussed in detail in previous chapters. It is presented here for reasons of clarity and continuity however the main focus of this chapter will be the design and development of autopilots.

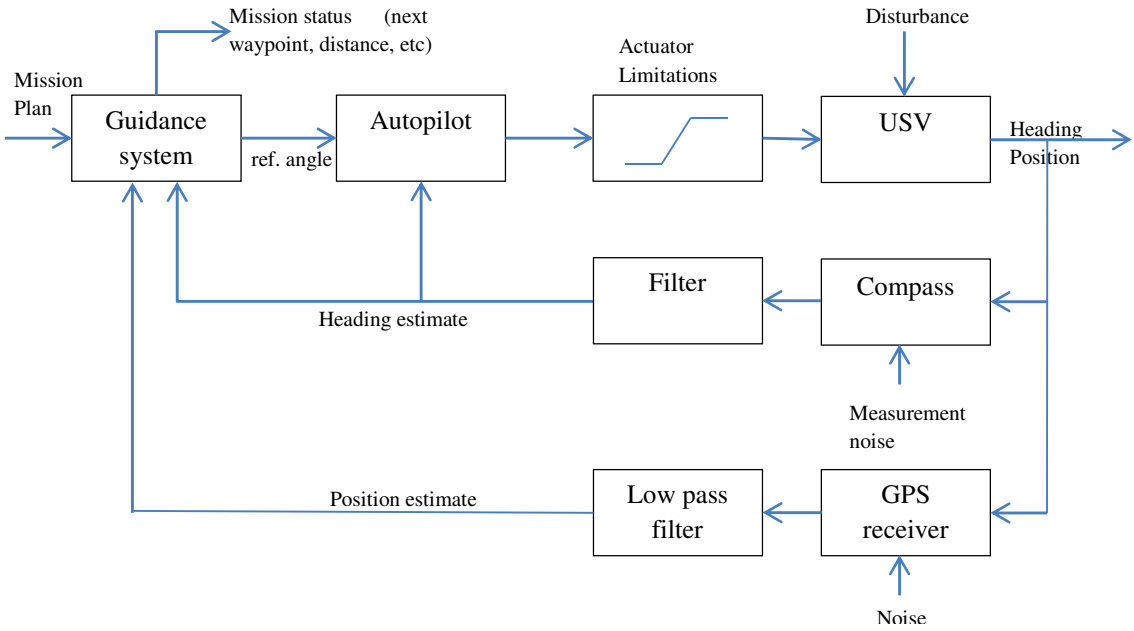

Figure 5.5: General Block Diagram

5.5 Proportional integral and derivative autopilot

PID control has been the workhorse in the process industry for over forty years; it has been used here to benchmark the performance of modern controllers such as a linear quadratic state feedback regulator (LQR) discussed in this chapter. The PID algorithm used here is given by the following Equation (5.7):

$$u(k+1) = u(k) + K_p\left[\left(1 + \frac{\Delta t}{T_i} + \frac{T_d}{\Delta t}\right)e(k) + \left(-1 - 2\frac{T_d}{\Delta t}\right)e(k-1) + \frac{T_d}{\Delta t}e(k-2)\right] \quad (5.7)$$

where $u(k)$ is the output of the PID and $e(k)$ the error between the reference and actual output, and K_p is the proportional gain, T_i is the integral time and T_d is the derivative time which are the parameters of the PID controller. The NGC diagram containing the PID autopilot is shown in the following Figure 5.6.

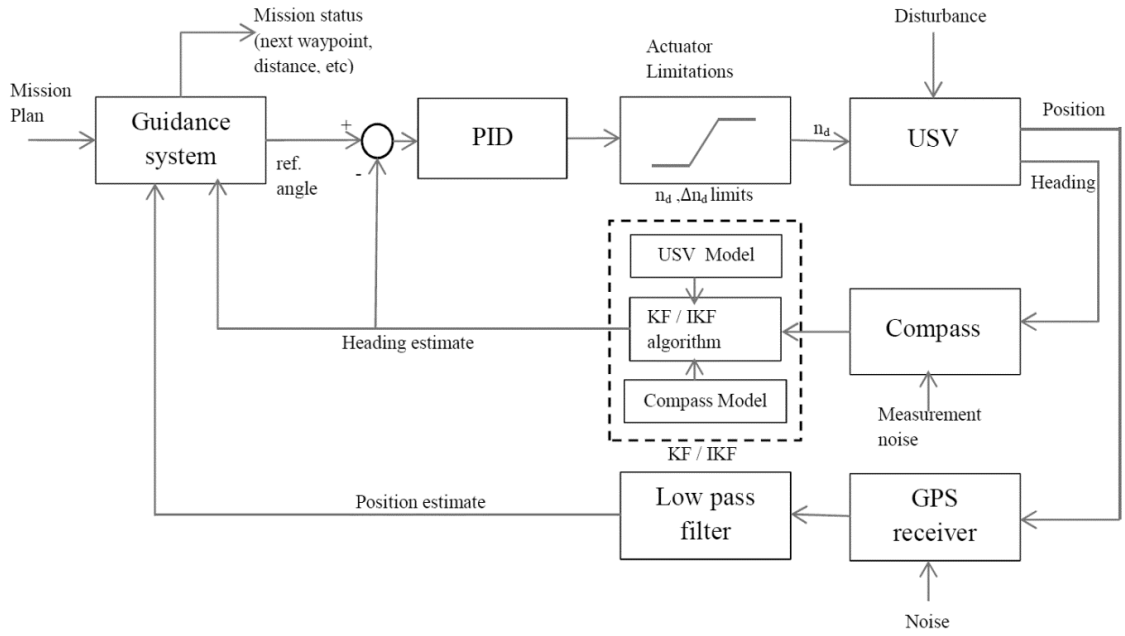

Figure 5.6: NGC system with PID autopilot

5.6 Linear quadratic Gaussian autopilot design and further innovations

In a conventional optimal autopilot design, an LQG controller is generally selected, this consists of LQR and KF which are developed independently and then combined to form the controller, an approach based on the *separation principle* (Naeem, 2004). The LQG controller is inherently multivariable therefore modification to a multi-input, multi-output model is rather straightforward. To construct the autopilot, an LQR problem is solved which assumes that all states are available for feedback. However, this is not always true because either there is no available sensor to measure that state or the measurement is very noisy. A KF can be designed to estimate the unmeasured states.

The following three approaches were applied to *Springer* and will be discussed briefly subsequently:

1. Kalman Filter (KF)
2. Interval Kalman Filter (IKF)
3. weighted Interval Kalman Filter (wIKF)

5.6.1 Kalman Filter

In this project, a dynamic model of one of *Springer's* compasses (as described in Chapter 3), a TCM2 digital magnetic compass, is made use of in the KF. Obtained through SI techniques as described in Chapter 4, the model of the compass is given by Xu (2007) as shown in the following Equations (5.8 and 5.9):

$$x(k+1) = \mathrm{A}\, x(k) + Bu(k) + \omega(k) \tag{5.8}$$

$$y(k) = \mathrm{C}\, x(k) + v(k) \tag{5.9}$$

It is important to note that the KF requires a precise dynamic model however 100% precision is not possible, thus erroneous location estimations of the USV will result. In order to increase the robustness of the KF method the Interval Kalman Filter was developed, this is explored in the subsequent section.

5.6.2 Interval Kalman Filter

The details of the IKF are published in Motwani et al. (2014). However, for the sake of completeness an outline is presented here. As often occurs in practice, the dynamic model of the plant is not known exactly. If an inaccurate model is used for prediction, then the KF estimate is no longer optimal. However, if the model parameters are known to lie within certain bounds, then the model can be described in terms of intervals (as seen in Figure 5.7), and a version of the KF, known as the IKF (Chen et al., (1997)), may be applied. As opposed to the KF, the IKF provides estimates in terms of intervals rather than point values. Chen et al. (1997) show that the interval estimates contain all the possible KF estimates that would be obtained using a model contained in the interval model. Thereby, the IKF estimate provides guaranteed bounds to a statistically optimal KF estimate, as long as the interval model contains the true model of the plant.

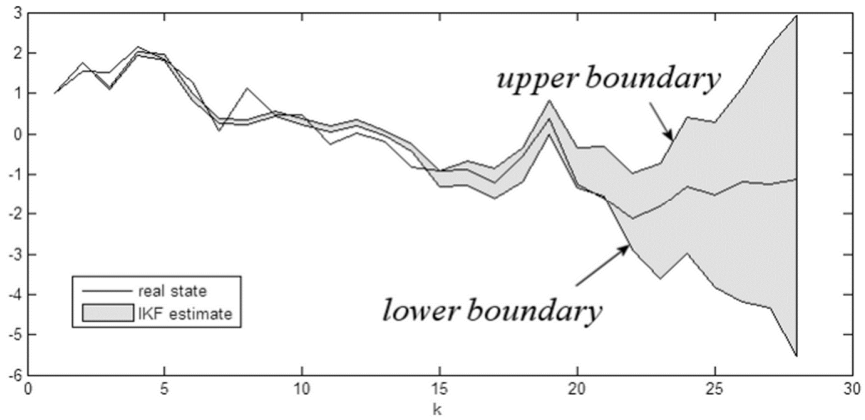

Figure 5.7: IKF estimate consisting of an interval at each time step, resulting in upper and lower estimation boundaries

Let it be assumed that the compass model contains an uncertain parameter on which the value of K is dependent. Concretely, assume that owing to this it is only certain that the true value of K lies within five per cent of the nominal value. Then the interval $K^I = [0.95\times K, 1.05\times K]$ can be used instead of K, and $\mathrm{C}^{\mathrm{I}} = K^I\,[1,0]$ instead of C. The IKF can then be applied to the interval model. More generally, given an interval model described by the following Equations (5.10 and 5.11):

$$x(k+1) = \mathrm{A}^{\mathrm{I}}x(k) + \mathrm{B}^{\mathrm{I}}u(k) + \omega(k) \tag{5.10}$$

$$y(k) = \mathrm{C}^{\mathrm{I}}x(k) + \upsilon(k) \tag{5.11}$$

where $\mathrm{M}^{\mathrm{I}} = [\mathrm{M} - |\Delta\mathrm{M}|, \mathrm{M} + |\Delta\mathrm{M}|]$ for $\mathrm{M} \in \{\mathrm{A}, \mathrm{B}, \mathrm{C}\}$, $\omega(k)$ and $\upsilon(k)$ are white noise sequences with zero-mean Gaussian distributions with known covariances $cov(\omega) = \mathrm{Q}$, $cov(\upsilon) = \mathrm{R}$, and $\mathrm{E}[\omega(l)\,\upsilon^T(k)] = 0\ \forall\, l,k$, $\mathrm{E}[x(0)\,\omega^T(k)] = 0$, $\mathrm{E}[x(0)\,\upsilon^T(k)] = 0\ \forall\, k$, then the IKF algorithm is summarised by the following recursive Equations (5.12 - 5.16):

Prediction:

$$\hat{x}^{\mathrm{I}-}(\mathrm{k}+1) = \mathrm{A}^{\mathrm{I}}\,\hat{x}^{\mathrm{I}+}(\mathrm{k}) + \mathrm{B}^{\mathrm{I}}u(k) \tag{5.12}$$

$$\mathrm{P}^{\mathrm{I}-}(\mathrm{k}+1) = \mathrm{A}^{\mathrm{I}}\mathrm{P}^{\mathrm{I}+}(\mathrm{k})\mathrm{A}^{\mathrm{I}^{\mathrm{T}}} + \mathrm{Q} \tag{5.13}$$

Kalman Gain:

$$\mathrm{K}^{\mathrm{I}}(\mathrm{k}) = \mathrm{P}^{\mathrm{I}-}(\mathrm{k})\mathrm{C}^{\mathrm{I}^{\mathrm{T}}}\left\{\mathrm{C}^{\mathrm{I}}\,\mathrm{P}^{\mathrm{I}-}(\mathrm{k})\mathrm{C}^{\mathrm{I}^{\mathrm{T}}} + \mathrm{R}(\mathrm{k})\right\}^{-1} \tag{5.14}$$

Correction:

$$\hat{x}^{\mathrm{I}+}(\mathrm{k}) = \hat{x}^{\mathrm{I}-}(\mathrm{k}) + \mathrm{K}^{\mathrm{I}}(\mathrm{k})[z(k) - \mathrm{C}^{\mathrm{I}}\,\hat{x}^{\mathrm{I}-}(\mathrm{k})] \tag{5.15}$$

$$\mathrm{P}^{\mathrm{I}+}(\mathrm{k}) = [\mathrm{I} - \mathrm{K}^{\mathrm{I}}(\mathrm{k})\mathrm{C}^{\mathrm{I}}]\,\mathrm{P}^{\mathrm{I}-}(\mathrm{k}) \tag{5.16}$$

in which $z(k)$ is the measurement at time *k* rather than the output predicted by (10), and the interval $\hat{x}^{\mathrm{I}}(k)$ is the predicted state at time step *k*. Initial values required are $\hat{x}^{\mathrm{I}}(0)$ (the initial estimate) and $\widehat{\mathrm{P}}^{\mathrm{I}}(0) \stackrel{\text{def}}{=} var[\hat{x}^{\mathrm{I}}(0)]$.

Though IKF provides a good interval bounds based on simple arithmetic average, further improvements could be obtained by wIKF as explained below.

5.6.3 weighted Interval Kalman Filter

In this approach an ANN is trained offline and is utilised to provide the weight parameters. In turn these parameters were employed to obtain an improved performance by wIKF which can be summarised by the following set of Equations (5.17 and 5.18):

$$y^{wIKF}(k) = y^{IKF-}(k) + w(k)[y^{IKF+}(k) - y^{IKF-}(k)] \tag{5.17}$$

where

$$y^{IKF+}(k) = \max\{y^{IKF}(k)\} and\ y^{IKF-}(k) = \min\{y^{IKF}(k)\} \tag{5.18}$$

Further details about this work can be found in Motwani et al. (2014).

The individual components and the functional blocks of a NGC system applicable to *Springer* obtained from a combination of LQR with KF/IKF is depicted in the following Figure 5.8.

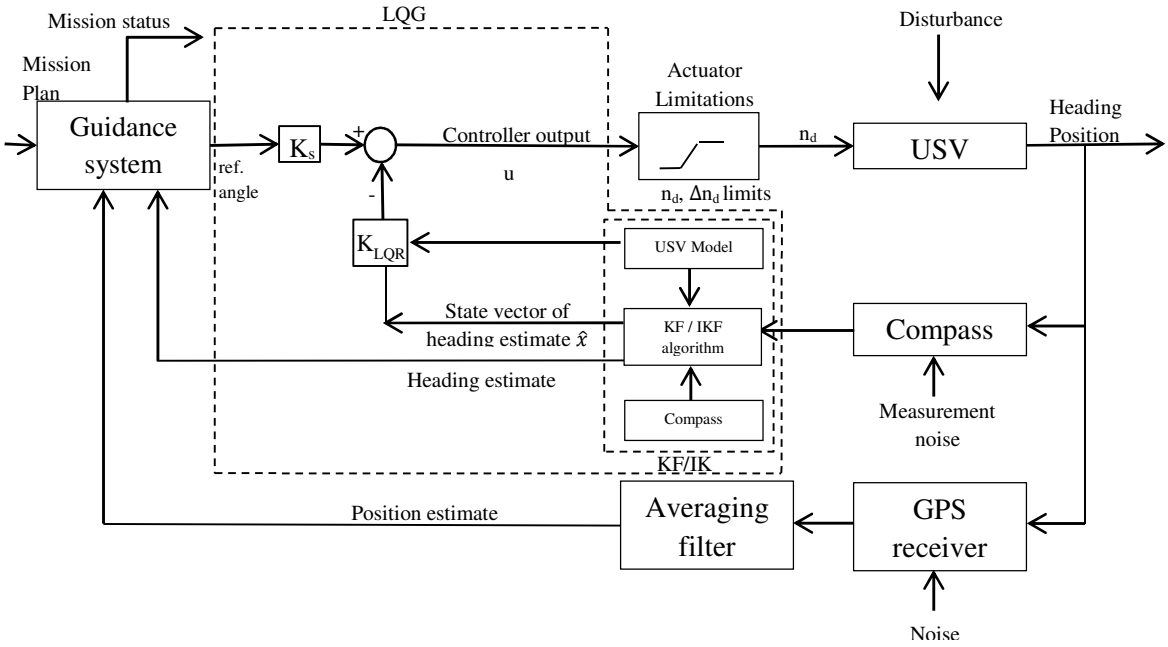

Figure 5.8: NGC system with LQR, KF/IKF controller

The LQG controller requires a state space model of the system in the form specified by the following Equation (5.19):

$$x(k+1) = Ax(k)+Bu(k)$$

$$y(k) = Cx(k) \tag{5.19}$$

where

$$A = \begin{bmatrix} 0.0372 & 1 & 0 & 0 \\ 0.1002 & 0 & 1 & 0 \\ 0.3781 & 0 & 0 & 1 \\ 0.471 & 0 & 0 & 0 \end{bmatrix}, \; B = \begin{bmatrix} 0.3235 \\ -0.8218 \\ 0.8819 \\ -0.3031 \end{bmatrix},$$

$$C = \begin{bmatrix} 1 & 0 & 0 & 0 \end{bmatrix}, \qquad D = [0] \tag{5.20}$$

The controller output of the LQG is defined as follows in Equation (5.21):

$$u(k) = -K_{LQR}\,\hat{x}(k) + K_s\,r(k) \tag{5.21}$$

where K_{LQR} is a function of A,B,Q,R. Hence, the model of the system has an impact in the calculation of K_{LQR}. Additionally, K_s is the scaling gain to ensure that the closed loop system has unit steady state gain and K_s can be computed as follows:

$$K_s = \frac{1}{steady\ state\ gain\ (closed\ loop\ system)} \tag{5.22}$$

Furthermore, concerning the choice of parameters Q and R. Q = C^TC, R being a scalar thus the cost function takes the following form (Equation 5.23):

$$J = \sum \|y\|^2 + R \sum \|u\|^2 \tag{5.23}$$

5.7. Simulation, results and discussion

In order to compare autopilots, each one must be tuned to offer the best possible performance. In the case of PID controllers, there is widespread literature on tuning rules based on the transient step-response of a plant, and in all cases, it would be

straightforward to tune the parameters based on optimising some performance measure of the step-response, such as minimisation of the integral of the absolute error (ITAE) (Sharma et al., 2013). Here, the system under consideration contains non-linear elements (actuator saturation limits) and performance is based not only on tracking the reference heading angle but overall on how well the vessel follows the desired trajectory. Performance measurement is based not just on the deviation from the ideal trajectory but also upon other criteria such as energy used. Thus it was decided to tune each controller based on the evaluation of a cost function over simulations of the actual NGC system for the mission plan under consideration.

In addition to random disturbance affecting the yaw dynamics of the vessel, a disturbance consisting of an imposed variation in the vessel speed was applied in order to recreate a more realistic scenario in which surface currents exist, transporting the vessel as if on a conveyor belt. The magnitude of this variation, though not constant, was nominally around 25% of the constant forward speed of the vessel (Figure 5.9) with a constant direction given by the positive direction of the *y*-coordinate axis. Furthermore, this disturbance solely affects the position of the vessel without affecting its heading.

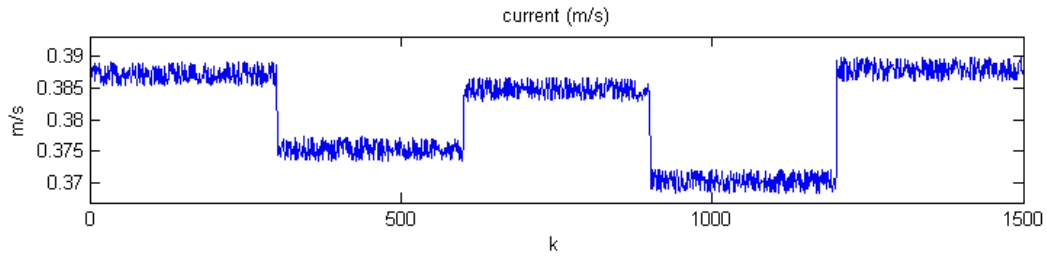

Figure 5.9: Disturbance signal

The performance of LQG autopilot is discussed in this section. A disturbance of 15% current acting in a northerly direction is added throughout the simulation to recreate realistic environments.

The position of the USV is updated using a dead-reckoning method. If *x(k)* and *y(k)* represent the position at time *k,* then the position at this sample time is calculated by the following Equations (5.24) and (5.25):

$$x(k) = x(k-1) + v * T_s * \cos(\theta) \tag{5.24}$$

$$y(k) = y(k-1) + v * T_s * \sin(\theta) + 0.15v * T_s \tag{5.25}$$

where v is the constant forward speed of the vessel (3 knots), T_s is the sampling interval of 1s, θ is the actual heading angle of the vessel at time k, and the disturbance of $0.15v * Ts$ has been added to the y component as in the following Figure 5.10:

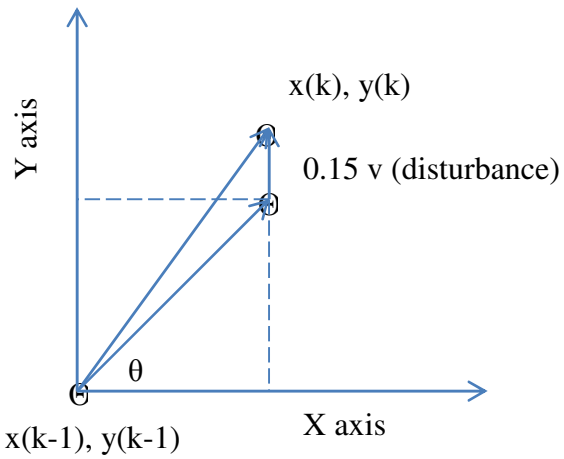

Figure 5.10: Effect of disturbance on calculation of position of the USV

Once the impact of disturbance was considered, it was time to define the parameters that will saturate the devices on-board the *Springer*. These have been imposed as expressed by the following Equation (5.26):

$$|n_d| < 300rpm \text{ and } |\Delta n_d| < 20rpm \tag{5.26}$$

that is, a limitation both on the maximum absolute value and the rate of change of the *rpm* of the motors.

Under this scenario, the mission plan was simulated using the NGC with the two controllers for different values of their respective parameters. The simulations were carried out using an ordinary KF as state estimator for the yaw-dynamics model. The performance indices measured were: number of waypoints reached (out of 7), total distance travelled, average deviation and average controller energy. Owing to the random nature of the disturbance that acts on the USV, the simulation results were different for each run which made the comparison difficult. To overcome this problem and to approximate the effect of randomisation Monte Carlo analysis was used. For each set of values of the parameters, the simulation was repeated ten times and the graphs shown reflect the mean values obtained.

Figure 5.11 shows the values obtained of each measure for each triplet (K_p,T_i,T_d), which are colour based. The optimal parameter values for each measure, based on minimum *J* are indicated on the graph by a purple circle. Because, as can be expected, the optimum parameters are different for each measure of performance, in order to obtain a single performance value a single cost function that takes each of these into account can be

constructed. The cost function chosen is simply a weighted average of the four performance measures as shown in the following Equation (5.27):

$$J = -\rho_1 \frac{wp\ reached}{7} + \rho_2 \frac{distance}{1500} + \rho_3 \frac{av.deviation}{30} + \rho_4 \frac{av.energy}{5} \tag{5.27}$$

Each measure is divided by a representative value in order to normalise it. The values of the weights were chosen as $\rho_1 = 100$, $\rho_2 = 75$, $\rho_3 = 75$, $\rho_4 = 50$, whereby the fraction of waypoints reached is given the most importance, and the controller energy the least. The values of PID parameters that minimise J are found to be K_p = 130, T_i = 13, T_d = 0.

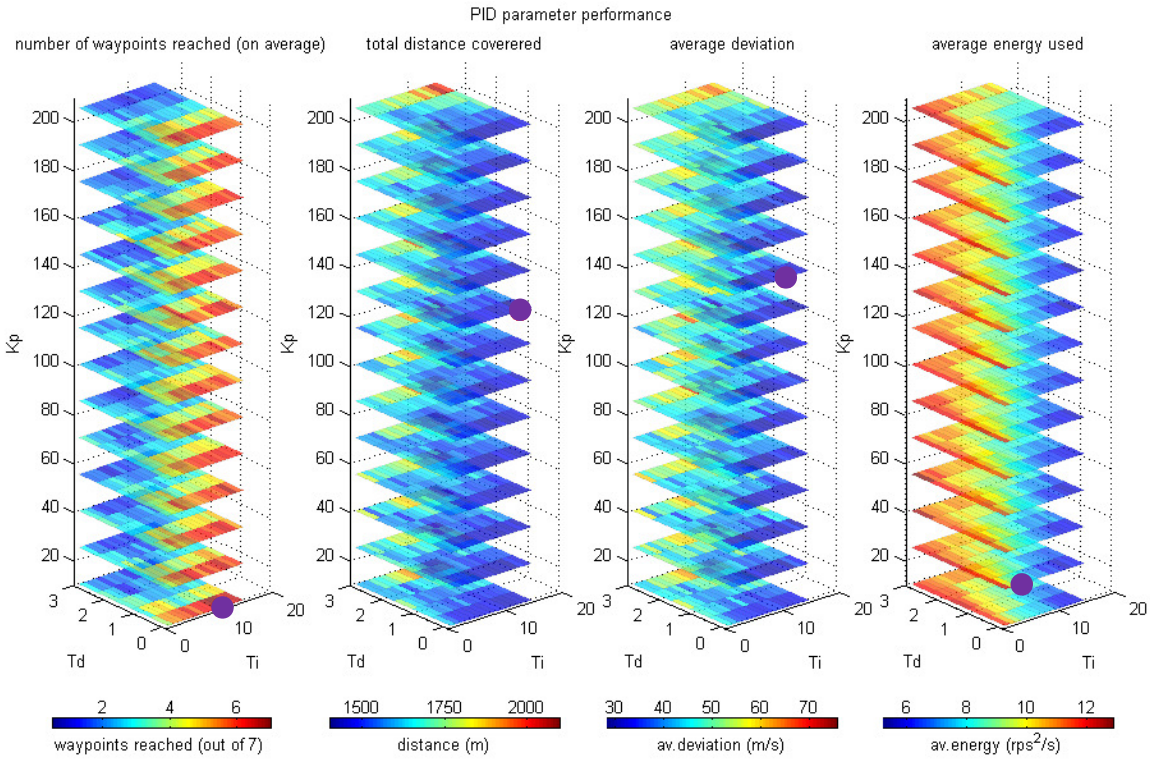

Figure 5.11: PID parameter performance.

In the case of the LQR controller, the only parameter is R. Figure 5.12 shows the average performances for different values of R. Similarly, a single value of R is obtained that minimises the cost function *J*, and this value was found to be R = 0.0049.

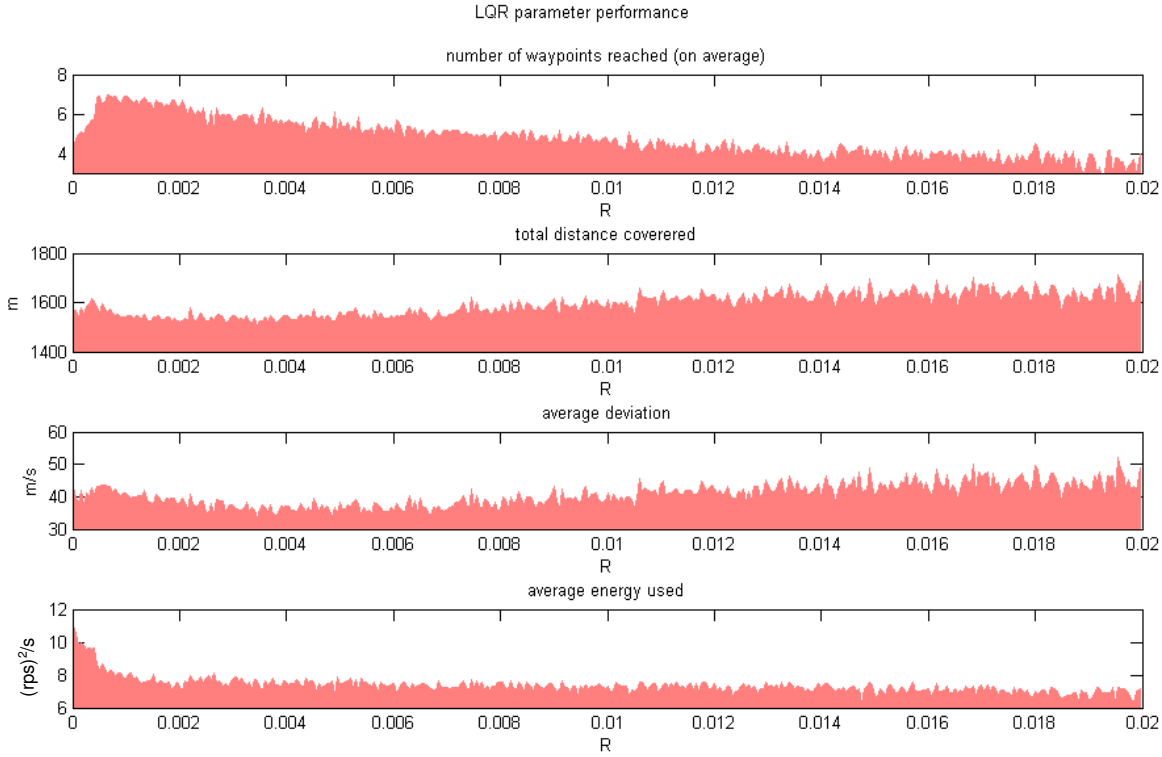

Figure 5.12: LQR parameter performance.

The following Figures show typical simulations of each of the controllers using IKF feedback information. Figures 5.13 and 5.17 depict the position of the USV, both the actual position and the one estimated by the filtered GPS data, as well as information provided by the guidance system. Figures 5.14 and 5.18 compare plots of the true heading of the USV with the estimated heading. As discussed previously, the IKF provides interval estimates, represented on the plots as upper and lower boundaries. The average of these bounds is also plotted and it is the value fed back to the guidance and control systems in practice. Notice that the width of the intervals increases over time,

and the advantage of the guaranteed estimates is lost in practice. However, the average value still provides the same effectiveness as an estimate as that of an ordinary KF estimate. However, should tighter bounds be available, then the guaranteed heading estimate could be combined with a dead-reckoning system to provide guaranteed bounds of the trajectory estimate. If this is sufficiently narrow, it could be very useful to feedback such information to the guidance system which could generate a trajectory that is guaranteed being clear of submerged sandbanks and shoals. The figures also provide plots of the compass heading measurements, and the reference heading angle computed by the guidance system.

Figures 5.15 and 5.19 show the output of the respective controllers, and Figures 5.16 and 5.20 the derivative of these. The derivative term is obtained by $\frac{\Delta n_d}{\Delta t}$ and in this case Δt= T_s (sampling time) = 1 sec. Hence, it is expressed by the units (rpm/s). It can be seen how these are limited due to the actuator saturation limits considered. These have been imposed as in the following Equation (5.28):

$$|n_d| < 300rpm \text{ and } |\Delta n_d| < 20rpm \tag{5.28}$$

that is, a limitation both on the maximum absolute value and the rate of change of the *rpm* of the motors.

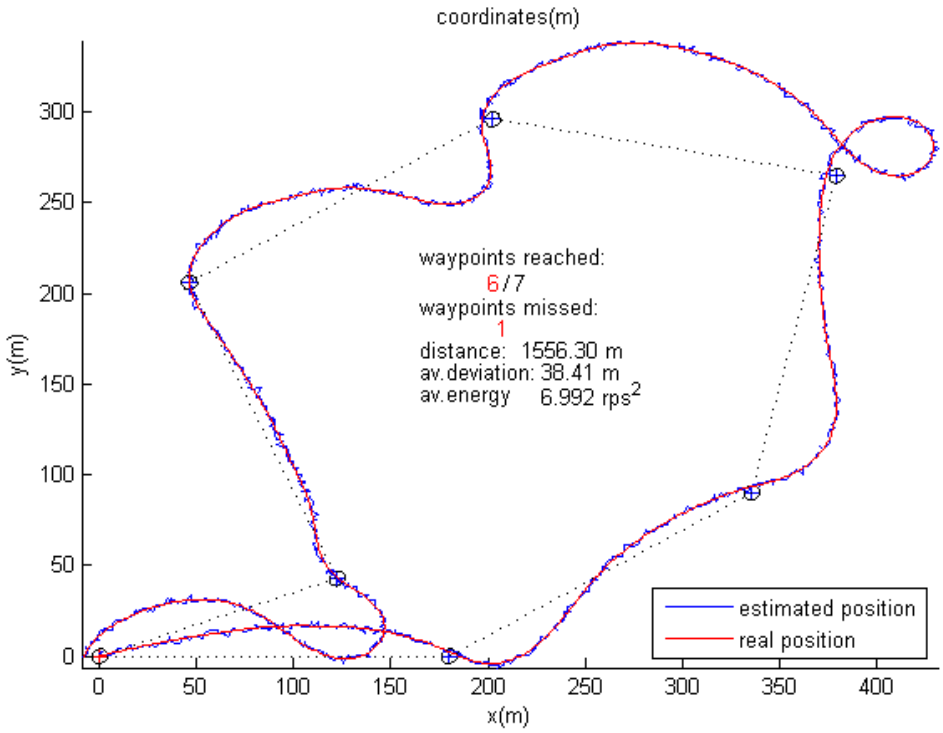

Figure 5.13: Waypoint tracking using PID-IKF based NGC (Kp = 130, Ti = 13, Td = 0).

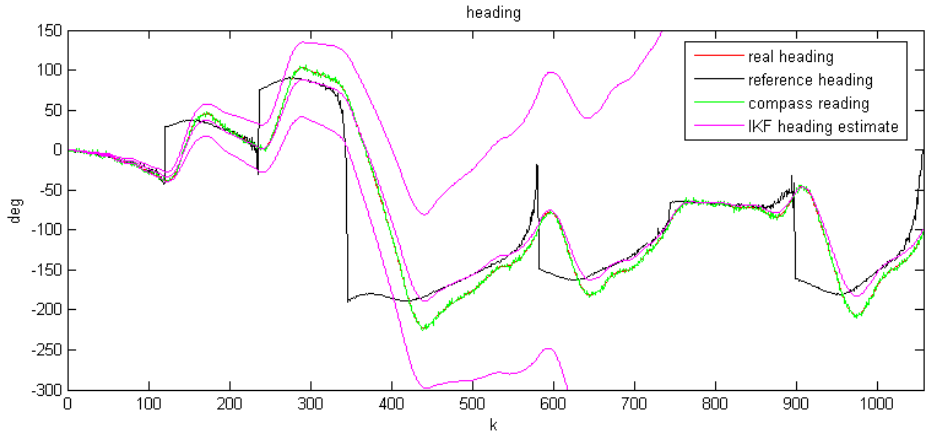

Figure 5.14: Heading using PID-IKF based NGC (Kp = 130, Ti = 13, Td = 0).

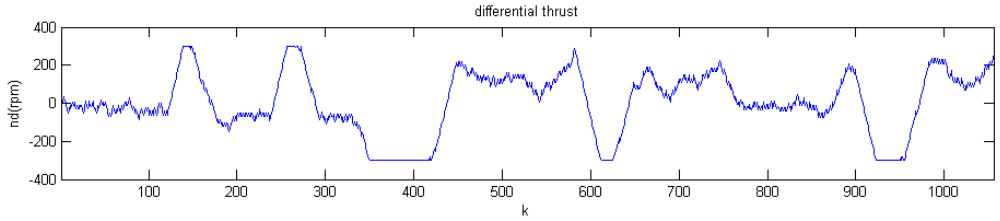

Figure 5.15: Controller action using PID-IKF based NGC (Kp = 130, Ti = 13, Td = 0).

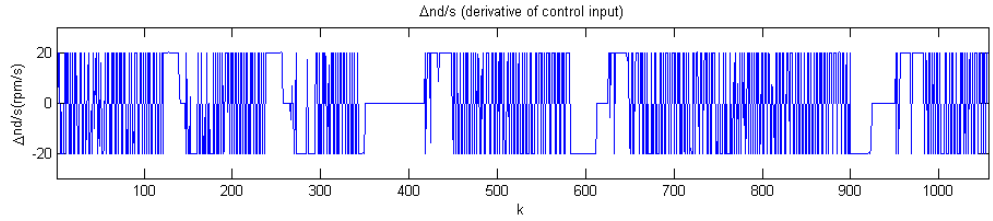

Figure 5.16: Derivative of controller action using PID-IKF based NGC (Kp = 130, Ti = 13, Td = 0).

The PID controller was able to reach an average of 6.5 waypoints with a standard deviation of 0.641. Moreover, the LQR controller was able to reach 6.1 waypoints on average with a standard deviation of 0.939. Furthermore, the mean total distance travelled, mean deviation from the ideal trajectory and the mean of average controller energy consumed is shown in the following table 5.1 that summarises the results obtained for the optimal parameter values for PID and LQR controllers.

Case	No. of waypoints reached mean (std)	Total distance (m) mean (std)	$\overline{r_d}$ (m/s) mean (std)	$\overline{CE_u}$ (rps)^2/s mean (std)
PID (K_p = 130, T_i = 13, T_d = 0)	6.5 (0.641)	1409 (41.219)	28.78 (3.751)	5.41 (0.615)
LQR (R = 0.0049)	6.1 (0.939)	1521 (40.157)	36.78 (3.278)	6.72 (0.901)

Table 5.1: Average performance measures for NGC systems using KF estimation.

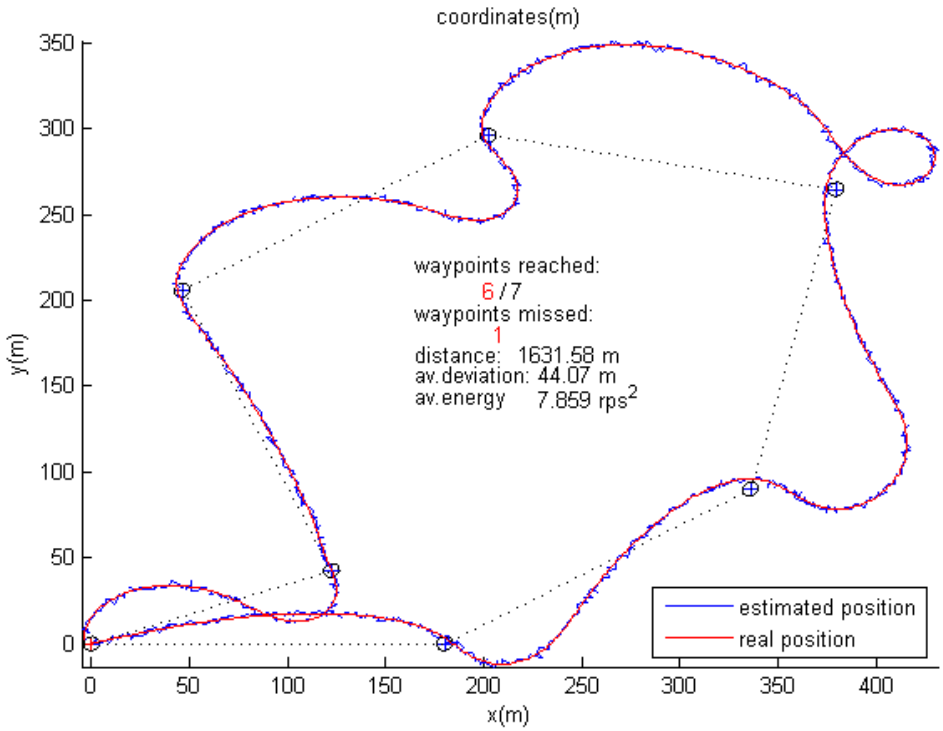

Figure 5.17: Waypoint tracking using LQR-IKF based NGC (R = 0.049).

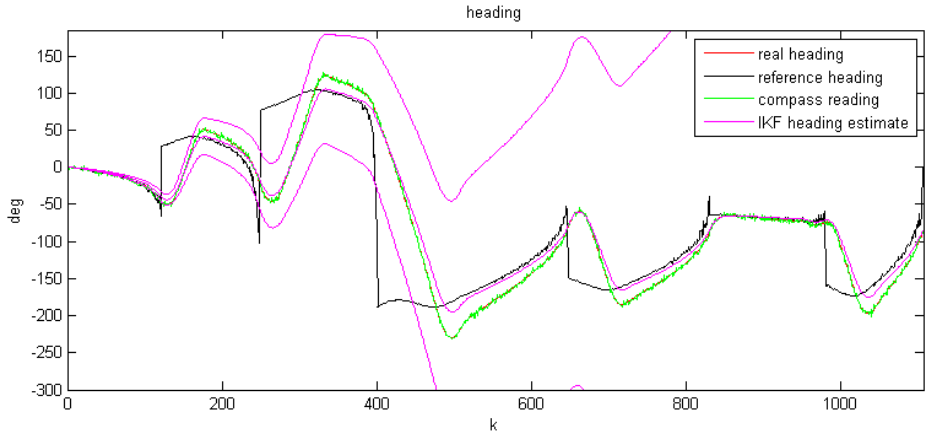

Figure 5.18: Heading using LQR-IKF based NGC (R = 0.049).

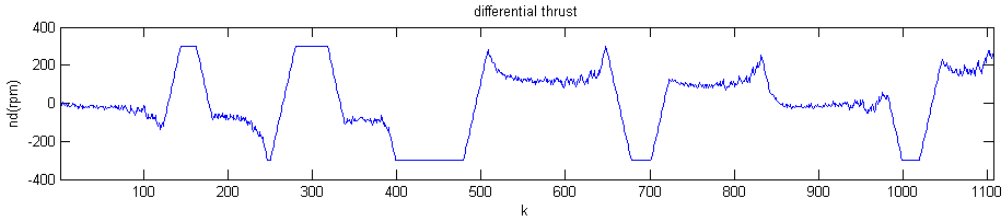

Figure 5.19: Controller action using LQR-IKF based NGC (R = 0.049).

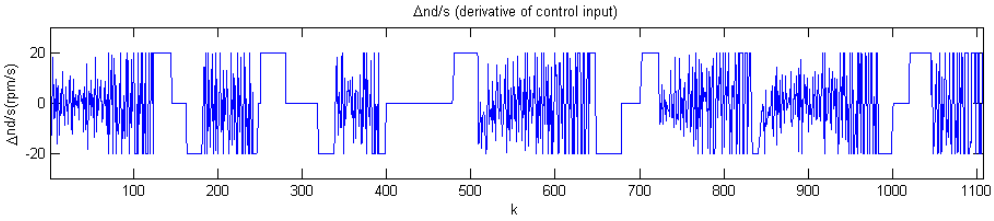

Figure 5.20: Derivative of controller action using LQR-IKF based NGC (R = 0.049).

Using the optimal parameters found for each of the controllers, the following Table 5.2 shows the results obtained by simulating the mission plan using the NGC with an IKF rather than a standard KF to estimate the heading angle. As before, ten simulations were carried out for each case and the table presents the mean and standard deviation for each one.

Case	No. of waypoints reached mean (std)	Total distance (m) mean (std)	$\overline{r_d}$ (m/s) mean (std)	$\overline{CE_u}$ (rps)^2/s mean (std)
PID (K_p = 130, T_i = 13, T_d = 0)	6.7 (0.674)	1429 (40.258)	31.09 (3.824)	5.52 (0.652)
LQR (R = 0.0049)	5.7 (0.948)	1526 (41.905)	35.57 (3.730)	7.21 (0.891)

Table 5.2: Average performance measures for NGC systems using IKF estimation.

The difference in results between Tables 5.1 and 5.2 are within the standard deviations and so indicate that there is no significant difference as far as performance goes in using a KF or an IKF in the NGC system.

In order to investigate the effect of the saturation limits, the restriction in the derivative of the motor speed was lifted and the mission plan simulated using the same controllers as previously used. The results are presented in Table 5.3.

Case	No. of waypoints reached mean (std)	Total distance (m) mean (std)	$\overline{r_d}$ (m/s) mean (std)	$\overline{CE_u}$ (rps)^2/s mean (std)
PID (K_p = 130, T_i = 13, T_d = 0)	4.1 (1.101)	1385 (66.418)	23.60 (5.233)	12.04 (0.439)
LQR (R = 0.0049)	5.7 (0.675)	1441 (36.341)	27.81 (3.191)	7.12 (0.376)

Table 5.3: Average performance measures for NGC systems using IKF estimation, without actuator rate of change saturation.

Whereas with the imposed restriction in the derivative of the differential thrust the PID controller seems to outperform the LQR autopilot, this is not the case when the restriction on Δn_d is lifted, in which case the LQR based autopilot produces better results. The LQR-based autopilot is capable of producing superior control manoeuvres as suggested by the results of Table 5.3.

5.8. Conclusions

In this study an NGC system is built based on an LQG and a modified LQG autopilot and was benchmarked against a standard PID control algorithm. This highlighted challenges in integration because IKF provides bounds that are too wide to provide any additional benefit over the traditional KF estimate. With regard to the autopilots, the LQG requires that the nonlinearities of the physical limitations (actuator limits) be incorporated into the optimisation algorithms in order to achieve better performance. This is evidenced by the results obtained when such limitations were partially lifted.

In addition to the innovative modifications to LQG, this study has also shown the feasibility of integrating an IKF-based navigation system with LQG and PID based autopilots and an LOS guidance system, with reasonably good results being achieved (the worst case still achieving over 5 waypoints reached successfully on average out of the 7 waypoints, even though the vessel's position was distorted by the effect of adding 25% of its nominal speed along a constant direction to simulate a current along that direction).

The results presented in this chapter show that the LQG and PID autopilots combined with both KF and IKF state estimates offer similar performances despite LQG being an optimal control algorithm. This can be understood owing to the persistent nature of disturbance acting on the system being controlled. Hence, the more sophisticated MPC approach was investigated to improve upon the former for USV autopilots.

Chapter 6

Model predictive control autopilot for *Springer*

6.1 Introduction

The investigation conducted in the previous chapter demonstrates that the modified LQG is a viable alternative to PID based autopilots. Historically PID has been extensively used in passenger ships to supplement manual control, whereas LQG was developed as a stepping-stone towards optimal control. Conversely, MPC was developed in the petrochemical industries. The majority of USVs currently in use by industry and the military are remotely controlled from a mother ship or a safe/secure base. The *Springer* project is specifically aimed at taking a further step towards true autonomy and some of its work packages are specifically focused on exploration of the potential to use MPC as an autopilot for autonomous operation.

As noted in Chapter 2, the success MPC has enjoyed is attributed to the fact that it was developed in the industry, by the industry and for the industry. A comparison between both theoretical and practical aspects of MPC has been undertaken by Carlos et al., (1989) whilst a general overview of MPC technology from the past through to future applications has been provided by Morari and Lee (1999). The concepts and techniques of MPC have developed over the past three decades and are shown to be widely applied in many sectors such as the process and automotive industries, and in theory development and simulation studies since it offers the advantage of enforcing various

types of constraints on the plant process as illustrated in Maciejowski (2002), Rawlings and Mayne (2009), Wang (2009), Allgower et al., (2010) and Annamalai (2012). While MPCs have not been much used in marine control system designs, Naeem et al (2005) have successfully exploited this technology in UUVs. Perez (2005) focuses on application to ship autopilot design. While there is a relative dearth of research into the use of MPCs in marine autopilots, some very recent work has evidenced growing interest in this approach and specifically in the use of MPCs with USVs as seen in Oh and Sun (2010), Liu et al (2011), and Li and Sun (2012). It is worth mentioning that these authors have published simultaneously with the development of the *Springer* project. These researchers have focussed on utilising MPC solely as an autopilot which parallels the approach taken in this chapter. However, Chapter 7 and 8 present modifications to the standard MPC algorithm that provides adaptive capabilities to respond to changes in system dynamics of the USV.

This chapter has the following sections: First, a discussion of important concepts in MPC is presented. Subsequently the challenges in adapting MPC to *Springer* are introduced. The results of simulation studies carried out using the same set of way points (as in Chapter 5) and comparable parameters are then presented and the performance of the autopilot is evaluated. Some concluding remarks pertaining to the application of MPC to *Springer* are made in the final section of the chapter.

6.2 Important concepts in MPC

In a standard MPC, the process output is predicted by using a model of the process to be controlled. Any model that adequately describes the relationship between the input and the output of the process can be used. Further, if the process is subject to disturbances, a disturbance or noise model can be added to the process model. In the context of marine vessel control, to define how well the predicted process output tracks the reference trajectory, a criterion function is used. Typically the criterion is the difference between the predicted process output and the desired reference trajectory. A simple criterion function is shown in Equation (7.1),

$$J = \sum_{i=1}^{H_p} [\hat{y}(k+i) - w(k+i)]^2 \tag{6.1}$$

where $\hat{y}$ is the predicted process output, w is the reference trajectory, and H_p is the prediction horizon or output horizon. The general structure of an MPC is shown in the following Figure 6.1.

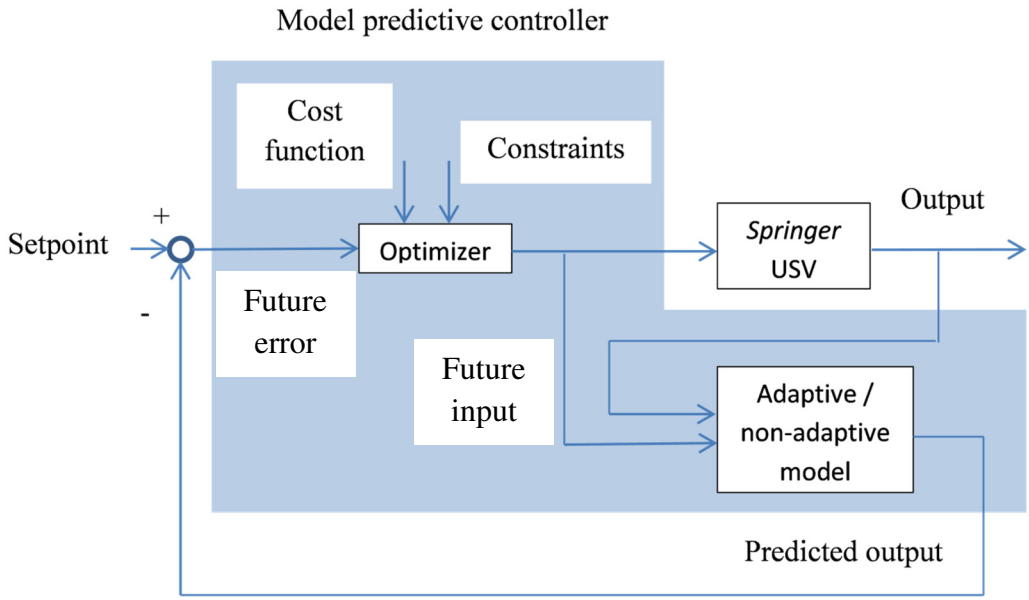

Figure 6.1: General structure of a model predictive controller

The optimal controller output sequence over the prediction horizon is obtained by minimisation of J with respect to u. As a result the future tracking error is minimised. If there is no model mismatch, for example if the model is identical to the process and there are no disturbances and constraints, the process will track the reference trajectory exactly on the sampling instants.

The MPC algorithm consists of three major steps. The first entails prediction of the plant output for a future period of time termed the prediction horizon. An internal model is used explicitly to achieve this. The second step involves computation of a control sequence for a pre-defined period of time in the future to optimise an index of performance. This time window is commonly known in the literature as the Control

Horizon (H_c), e.g. see Maciejowski (2002), Naeem, (2005), Rawlings and Mayne (2009).

Upon application of the first step of the control sequence, at each sampling point the calculations for computation of the prediction and control horizons are updated based on a receding horizon strategy. These three steps are illustrated in Figure 6.2 where *y(k)* is the actual output from the plant. For any given instant of time (*k*) the MPC endeavours to compute a sequence of predicted output $\hat{y}(k)$ over the prediction horizon (H_p). Subsequently the control sequence *u(k)* is computed along the time frame of the control horizon H_c to optimise a pre-defined performance index. At time *K+1* the whole operation in repeated and so on until the desired objectives are met.

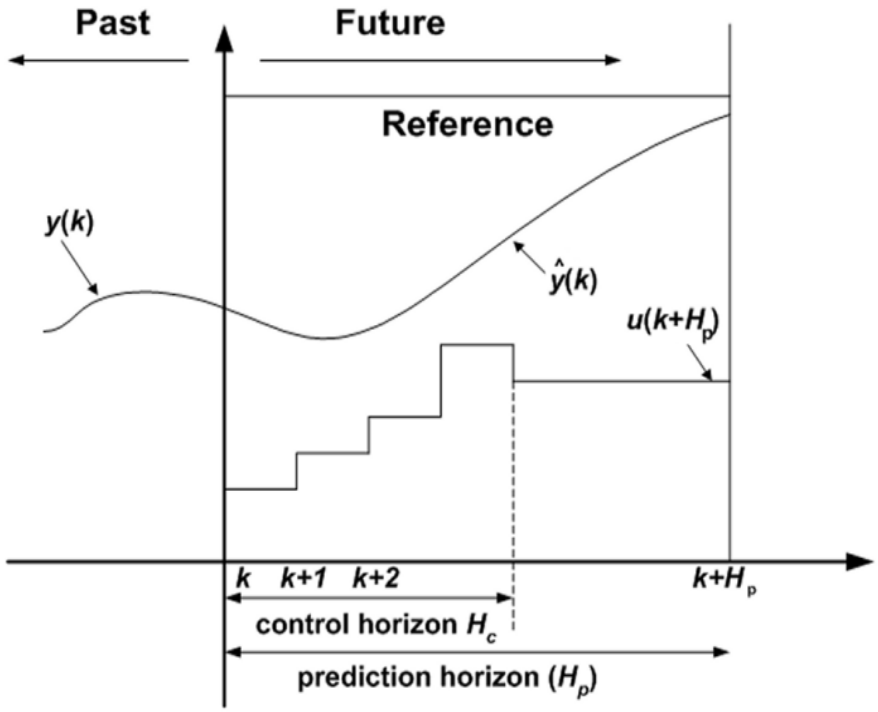

Figure 6.2: General strategy of a model predictive controller (Naeem, 2004)

Having looked at key concepts in MPC it is useful to note the features of this approach which make it an especially promising candidate mechanism for USV control. MPC is applicable to both linear and non-linear systems and has the capacity to handle both single-input, single-output (SISO) and MIMO. In addition, MPC has the capacity to handle constraints systematically (Naeem, 2004). The controller is not fixed and is designed at every sampling instant based on actual sensor measurements so disturbances can easily be dealt with as compared to fixed gain controllers. Thus, autopilots based on MPC have a significant advantage over fixed gain approaches as the controller is designed at every sampling instant.

Moreover, it also offers considerable benefits through the way that constraints imposed by the physical system are inherently handled by the MPC design. The recent adaption of MPC to marine control system design is exemplified by authors such as Li and Sun (2012), Liu, et al., (2011c), Oh and Sun (2010), Naeem, et al., (2005), Perez (2005).

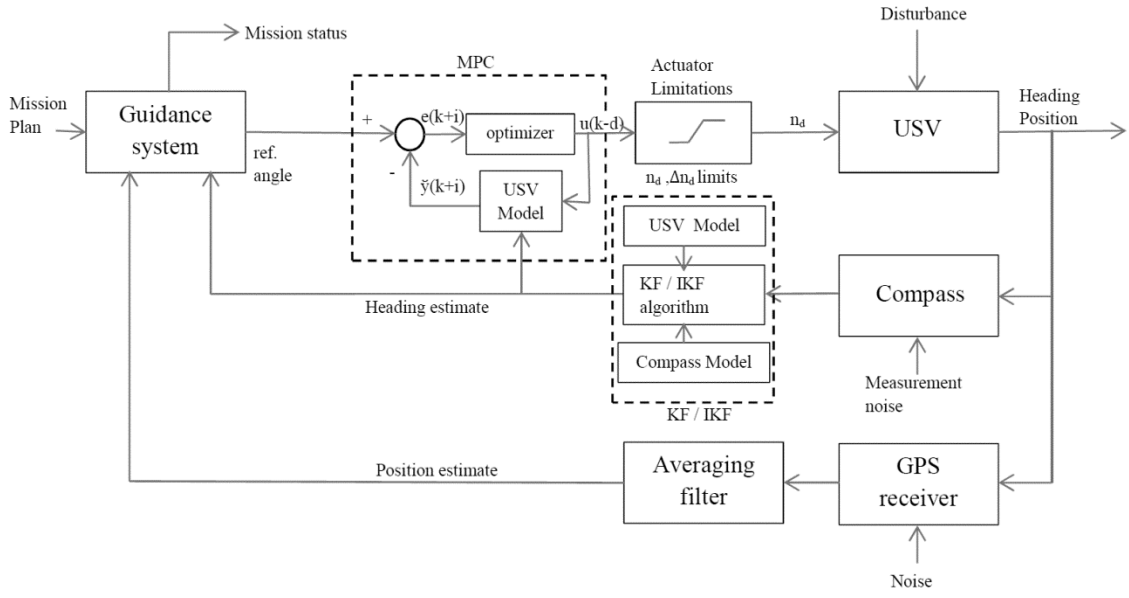

Figure 6.3: NGC system with MPC controller

6.3 Application of Model Predictive Control to *Springer*

Since management and monitoring of the environment is a major issue worldwide, *Springer* has been specifically built and continues to be developed to be a cost effective and environmentally friendly vehicle primarily for undertaking pollutant tracking, environmental, hydrographical surveys in rivers, reservoirs, inland waterways and coastal waters, particularly where shallow waters prevail. An equally important secondary role is also envisaged for *Springer* as a test bed platform for other academic and scientific institutions involved in environmental data gathering, sensor and instrumentation technology, control systems engineering and power systems based on alternative energy sources. In this study, the plant output $y(k)$ is obtained from the KF estimate and the integration of the NGC system is detailed in Chapter 5.

MPC employs a model of the vessel internally to predict the output (as shown in Figures 6.2 and 6.3). The accuracy of the model determines the efficiency of the controller and the controller output required to keep the vehicle on course with a minimum effort (Ljung, 1999). When there is a sudden change in the plant dynamics, employing a static internal model would have a fatal flaw in the autopilot design and severely undermine the success of the missions undertaken by the USV. To overcome this problem, adaptive algorithms, as mentioned previously, were employed to construct an internal model of the vessel (which reflects the vessels current dynamics as accurately as possible) at any given point in time.

This model was utilised to generate predicted output against set reference trajectories. A cost function of the following form as shown in Equation (6.2) and (6.3) used to define how well the predicted vessel output was able to track the set reference point.

$$J = \sum_{i=1}^{H_p} e(k+i)^T Q e(k+i) + \sum_{i=1}^{H_c} \Delta u(k+i)^T R \Delta u(k+i) \tag{6.2}$$

subject to,

$$\Delta u^l \leq \Delta u(k+i) \leq \Delta u^u \tag{6.3}$$

where $e(k) = \hat{y}(k) - r(k)$ is the prediction error, or difference between the predicted vessel output $\hat{y}$ and the reference trajectory r. The superscripts l and u represent the lower and the upper bounds respectively. Q is the weight on the prediction error, and R the weight on the change in the input Δu. H_p is the prediction horizon or output horizon, and H_c the control horizon. Minimisation of J with respect to u yields the optimal controller output sequence u_{opt} over the prediction horizon. Quadratic programming was utilised to obtain these optimal values; this ensures that the future error is minimised.

Previous studies by Annamalai and Motwani (2013) and Annamalai et al., (2013) demonstrate the improved performance of MPC in comparison with standard approaches such as quadratic Gaussian based controllers. The MPC controller also incorporates the actuator limitations of the vessel as optimisation constraints. These are specified as below in Equation (6.4):

$$\left|n_d\right| \leq 300 \ rpm \ \text{ and } \left|\Delta n_d\right| \leq 20 \, rpm \tag{6.4}$$

that is, a limitation both on the maximum absolute value and on the change of the *rpm* of the motors from one sampling instant to the next. The parameters of the MPC algorithm used are H_p = 50 and H_c = 3, as these values were necessary to tune the controller, and the weights Q = 1 and R = 0.1 for the cost function were chosen.

6.4 Simulation results

The performance of the MPC autopilot is discussed in this section. The performance indices measured to compare the autopilots were: number of waypoints reached (out of 7), total distance travelled, average deviation and average controller energy. As in Chapter 5 a disturbance of 15% to 25% current acting in a northerly direction is added throughout the simulation to recreate realistic environments. With the exception of the autopilot itself, all other attributes of the simulation studies described here are the same as those presented in Chapter 5. This was done to facilitate comparison of the results obtained with PID, LQG and MPC.

For the MPC controller, the four performance measures are shown as a function of the prediction horizon H_p and the control horizon H_c. In the below Figure 6.4 (a) shows the results of multiple combinations of control (H_c) and prediction (H_p) horizons (Figure 6.2) on the number of waypoints reached. This is done to extract the optimum parameters for (H_c) and (H_p). Figure 6.4 (b) shows results of the same procedure on distance covered. Figure 6.4 (c) shows average deviation from the ideal trajectory generated by the guidance system with multi-various combinations of control (H_c) and prediction (H_p) horizons (as above). Figure 6.4 (d) shows the average energy output of the controller.

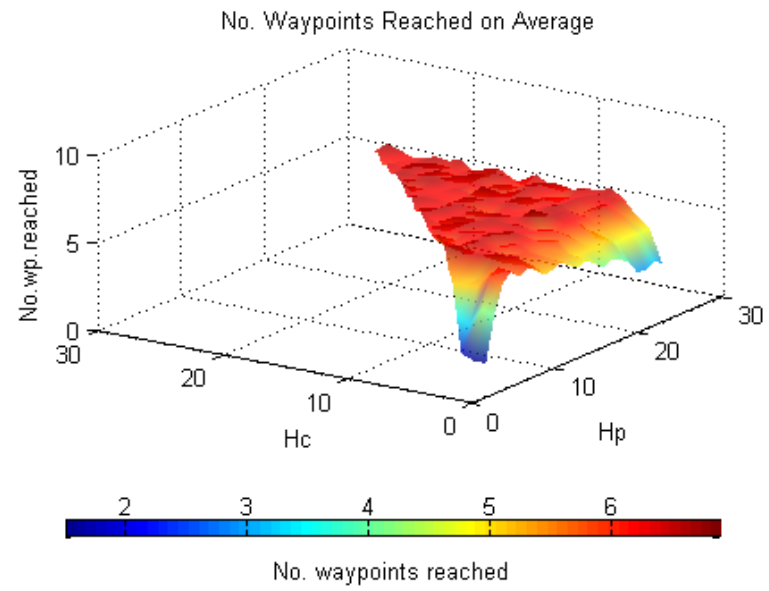
No. Waypoints Reached on Average
No.wp.reached
10
5
0
30
20
10
0
Hc
0
10
20
30
Hp
2
3
4
5
6
No. waypoints reached

(a)

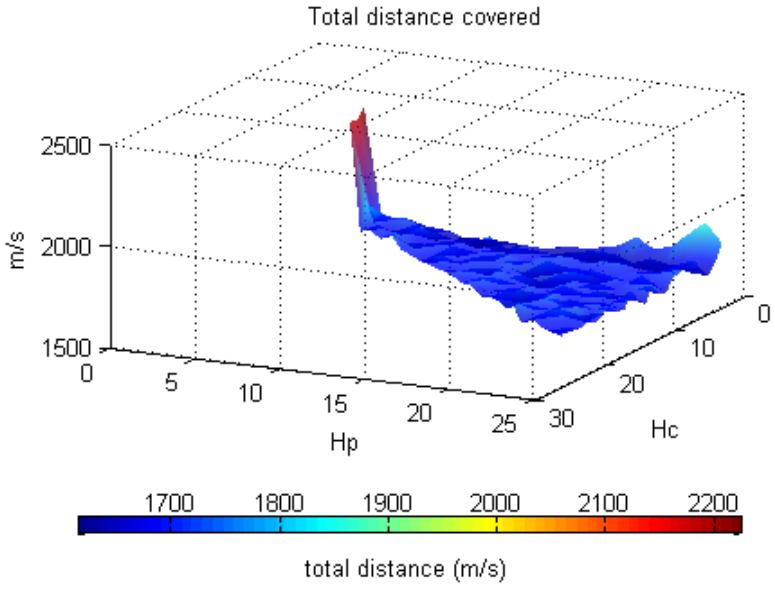
Total distance covered
m/s
2500
2000
1500
0
5
10
15
20
25
Hp
30
20
10
0
Hc
1700
1800
1900
2000
2100
2200
total distance (m/s)

(b)

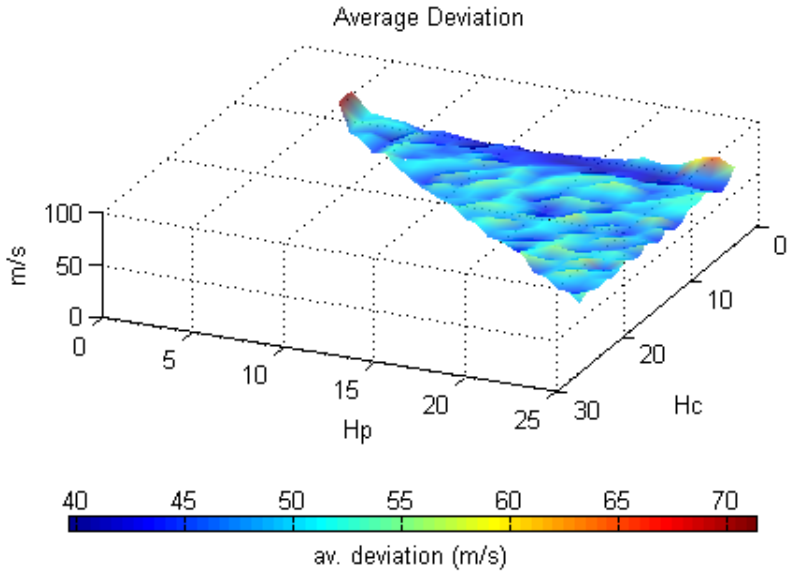

(c)

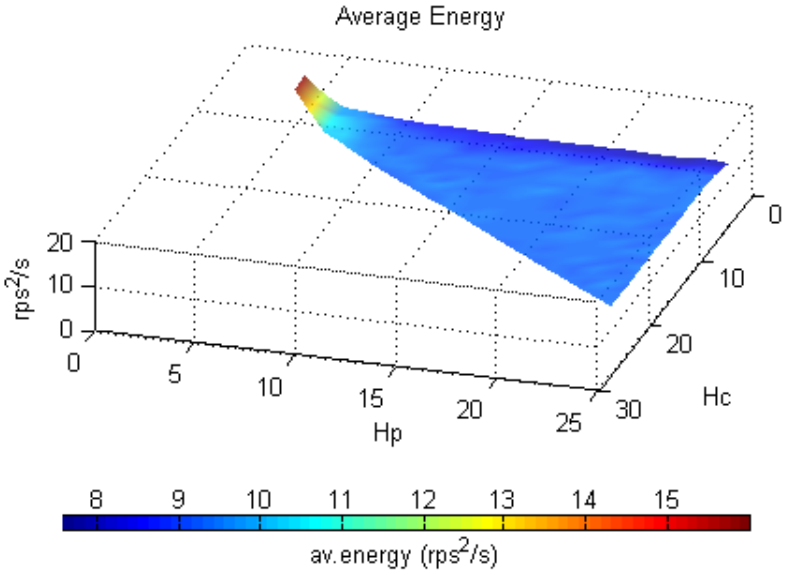

(d)

Figure 6.4: MPC parameter performance (a) number of way points reached on average (b) total distance covered (c) average deviation (d) average energy

The colour scheme in the above Figure 6.4 represents an ascending scale, thus in the case of the number of waypoints reached the red shaded areas indicate the best

combinations of H_c and H_p. In the remaining plots dark blue shaded areas indicate the most effective parameter values for the achievement of desired performance. Depending on the circumstances and the USV missions involved, performance of some parameters become more important than others. MPC controller offers this choice to the end users, to be able to specify parameters to suit the mission requirements. Additionally, the overall impact owing to the choice of H_p and H_c on the number of way points reached, total distance covered, average deviation and average controller energy consumption are clearly illustrated in Figure 6.4. The optimum values that minimise J (as in equation 6.2) were found to be $H_p = 10$, $H_c = 2$. Using the optimal parameters obtained, the following Table (6.1) shows the results obtained by simulating the mission plan using the NGC with a KF to estimate the heading angle.

Case	No. of waypoints reached mean (std)	Total distance (m) mean (std)	$\overline{r_d}$ (m/s) mean (std)	$\overline{CE_u}$ $(\text{rps})^2/\text{s}$ mean (std)
MPC ($H_p = 10$, $H_c = 2$)	5.5 (0.768)	1616 (70.61)	39.65 (10.144)	8.70 (0.189)

Table 6.1: Average performance measures for NGC systems using KF estimation.

As in the studies described in Chapter 5, ten simulations were carried out for each case and the following Table 6.2 presents the mean and standard deviation for each one.

Case	No. of waypoints reached mean (std)	Total distance (m) mean (std)	$\overline{r_d}$ (m/s) mean (std)	$\overline{CE_u}$ $(\text{rps})^2/\text{s}$ mean (std)
MPC ($H_p = 10$, $H_c = 2$)	5.8 (0.788)	1651 (69.64)	43.91 (10.144)	8.65 (0.189)

Table 6.2: Average performance measures for NGC systems using IKF estimation

As in Chapter 5, the following figures show typical simulations of the MPC controller using KF and IKF feedback information with a disturbance of 25%. Figure 6.5 shows the position of the USV, both the actual position and the one estimated by the filtered GPS data, as well as information provided by the guidance system. Figure 6.6 compares plots of the true heading of the USV with the estimated headings provided by the compasses.

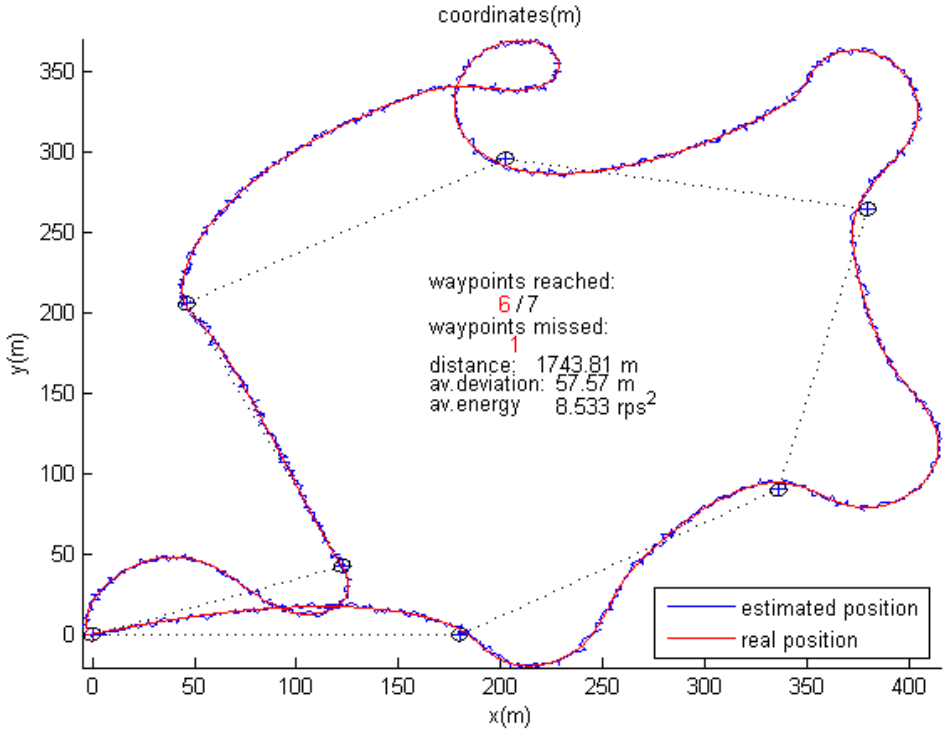

Figure 6.5: Waypoint tracking using MPC-IKF based NGC (Hp=10, Hc=2).

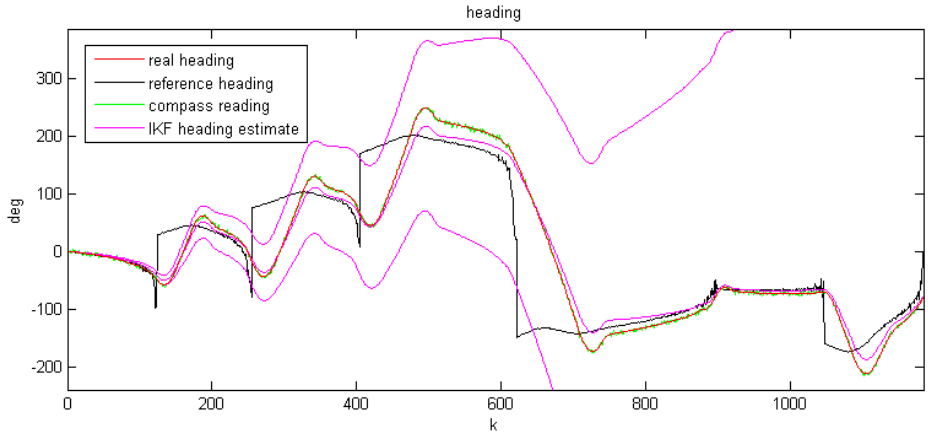

Figure 6.6: Heading using MPC-IKF based NGC (Hp=10, Hc=2).

Figures 6.7 and 6.8 show the controller output (u) and the derivative of controller action over time.

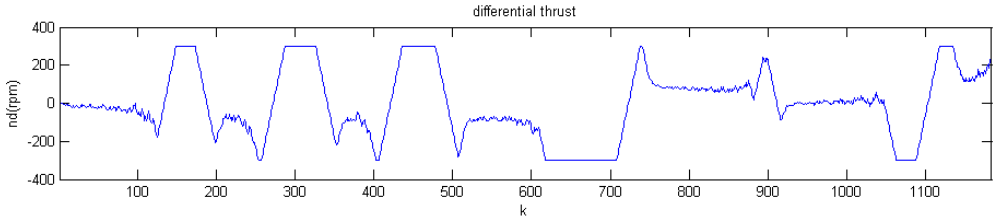

Figure 6.7: Controller action using MPC-IKF based NGC (Hp=10, Hc=2).

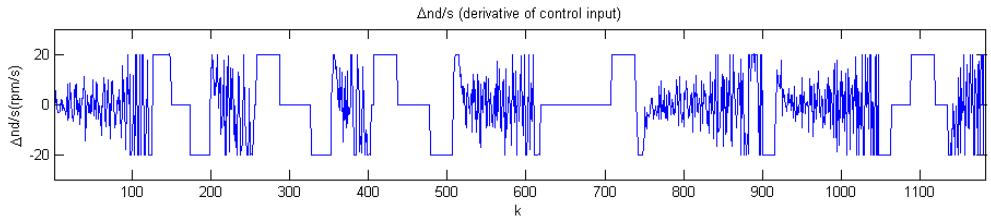

Figure 6.8: Derivative of controller action using MPC-IKF based NGC (Hp=10, Hc=2).

In order to investigate the effect of the saturation limits, the restriction in the derivative of the motor speed was lifted and the mission plan simulated using the same controller as previously described. The results are presented in Table 6.3.

Case	No. of waypoints reached mean (std)	Total distance (m) mean (std)	$\overline{r_d}$ (m/s) mean (std)	$\overline{CE_u}$ $(\text{rps})^2/\text{s}$ mean (std)
MPC ($H_p = 10$, $H_c = 2$)	6.5 (0.527)	1453 (61.362)	29.29 (4.168)	7.46 (0.580)

Table 6.3: Average performance measures for NGC systems using IKF estimation, without actuator rate of change saturation.

Whereas with the imposed restriction in the derivative of the differential thrust the PID controller seems to outperform both LQG (see Chapter 5) and MPC autopilots, again this is not the case when the restriction on Δn_d is lifted where the MPC provides the best results, followed by the LQR based system. It is thought that this is because the restriction on Δn_d was not explicitly taken into account by the MPC's optimiser but rather imposed afterwards. The MPC-based autopilot is capable of producing superior control manoeuvres as suggested by the results of Table 6.3, further experimentation (as in Chapter 8) confirmed this supposition.

After initial field trial with the vessels discussed in Chapter 3 it became clear that 25% disturbance was excessive whereas under most normal conditions there was a disturbance of a maximum of 15%. Thus it was decided to run a series of simulations with disturbance set to this value and the results are shown in Figure 6.9 (below).

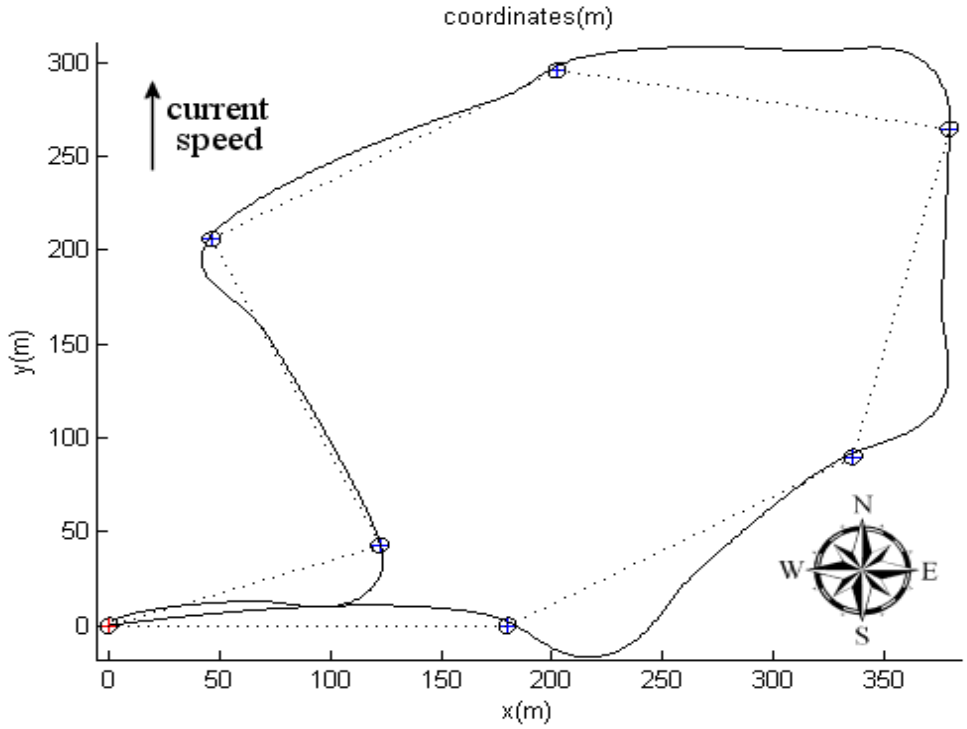
coordinates(m)
current
speed
y(m)
x(m)
N
W
E
S
0
50
100
150
200
250
300
350

(a)

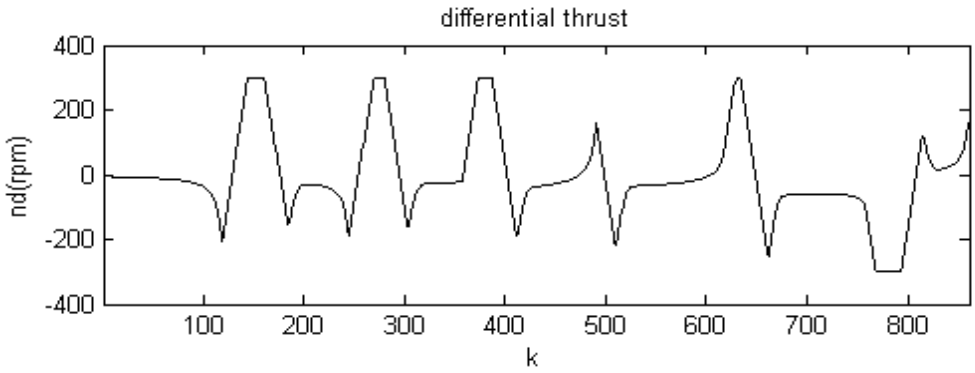
differential thrust
nd(rpm)
k
400
200
0
-200
-400
100
200
300
400
500
600
700
800

(b)

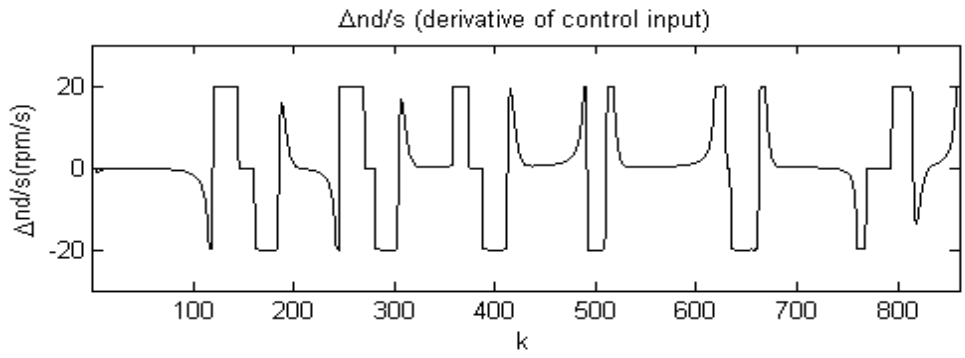

(c)

Figure 6.9: Waypoint tracking (a) MPC autopilot trajectory (b) differential thrust (c) derivative of control input.

The Figure 6.9 (a) illustrates an anticipated improvement in waypoint tracking performance obtained with reduced disturbance. More interestingly, a comparison of Figures 6.5 and 6.9 (b) illustrates reduced duration of controller output saturation, thus indicating reduced response latency. The results are summarised in the following Table 6.4.

Parameters	**MPC**
Number of waypoints reached	7
Total distance travelled	1305.39 m
Average deviation	19.09 m
Average energy	4.536 $(rps)^2/s$

Table 6.4: MPC Autopilot

6.5 Conclusions

The MPC, LQG and PID autopilots are compared for inclusion in an integrated navigation, guidance and control system for an USV. Various parameters of the autopilots performance were analysed and the results were discussed in this and the previous chapter. Kalman filtering was used to provide the navigation estimates and the line of sight guidance system was utilised to generate the reference heading to be achieved by the control subsystems. With regard to the autopilots, the MPC clearly outperforms the LQG and PID with respect to the performance parameter measures used. Hence, MPC is recommended as a suitable autopilot for USVs such as *Springer*.

This chapter and the previous one have shown the feasibility of integrating an IKF based navigation system with MPC, LQG and PID based autopilots and an LOS guidance system. Good results were achieved; the worst case still achieving over 5 waypoints successfully on average out of the 7 waypoints, even though the vessel's position was distorted by the effect of adding up to 25% of its nominal speed along a constant direction to simulate a current along that direction. The efficiency of the MPC control depends upon accurate description of the system model. Additionally, in practice, the dynamics can be varying especially for USVs as discussed in the introduction. So, to take this into account and provide robustness against such model uncertainty or variation, an adaptive MPC based on online model identification was developed and is described in the next chapter.

Chapter 7

Adaptive Autopilot

7.1 Introduction

On 11 March 2011, a tsunami and an earthquake struck Japan. It is one of the countries that are frequently tormented by natural calamities. Hence, they are best equipped and well prepared to face disasters than most other countries. High walls of 10.1m were in place to restrict and limit the damage, in case of a sea breach. This height had been sufficient to protect a nuclear facility when faced with individual natural disasters. However, on this occasion a combination of a tsunami and an earthquake triggered the sea waves to rise above 10.2m and nullified the designed protection. Consequently, radioactive coolants were deliberately leaked into the sea to prevent a full blown explosion. Dispersion of this radioactive contamination can be seen in Figure 7.1.

The range of radioactive contamination from a single incident is really shocking. It almost reached the coastlines of United States of America. Whether it is a radiation leak like this or it is oil spills or hazardous materials release in the sea, it is imperative to collect samples and monitor the level of contamination to make informed decisions about preventing further damage and to manage the situation responsibly. Nevertheless, it is too dangerous for human beings to be involved directly under these circumstances and it is constantly necessary to change the load bearing capacity of the operating vehicle to replace the collected samples and other appropriate equipment. Under these

circumstances success of the mission is reliant on an accurate and robust vessel autopilot.

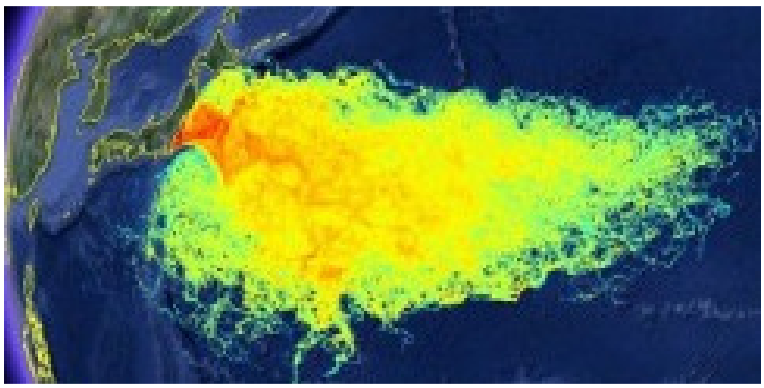

Figure 7.1: Radioactive contamination, Fukushima (source: ASR Ltd).

Furthermore, for a number of years *Predator* unmanned air vehicles have been involved in strike missions using air-to-ground *Hellfire* missiles. Surprisingly, the first missiles were launched by the US Navy from an USV took place during trials in late October 2012 (Eshel, 2012). During the trials, in total six Rafael *Spike* missiles were fired which equates to a total payload displacement of approximately 204 kg. Clearly, if a pod of such missiles was to be launched (as illustrated by an artistic impression in Figure 7.2) in a salvo then there would be an abrupt change in the dynamic characteristics of the vehicle owing to the sudden decrease in its overall mass. However, the mass of the vehicle would gradually alter over a period of time if such missiles were to be fired periodically.

Figure 7.2: Strike missions (source: zyvextech.com).

Besides coping with changing payloads, as illustrated above, multi-role USVs also have to contend with amendments to mission requirements and objectives, and varying environmental conditions whilst being employed in the commercial, naval and scientific sectors. Hence, all USVs have a common need for robust adaptive control (autopilot) systems. Thus, to date, in order to meet the testing demands being imposed by these various sectors, autopilots have been designed based on fuzzy logic (Park et al., 2005) gain scheduling (Alves et al., 2006) H-infinity method (Elkaim and Kelbley, 2006) linear quadratic Gaussian (Naeem, et al., 2006) sliding mode (Ashrafiuon, et al., 2008) neural network (Qiaomei, et al., 2011) and local control network (Sharma, et al., 2012) techniques that have met with varying degrees of success.

Currently most USVs are reliant on a static model of the vehicle to generate the appropriate controller action. However, in real life the USVs are faced with situations where change of mass is inevitable. Under these circumstances the autopilot will generate erroneous control action as the internal model of the plant is invalid. This results in personnel intervention to take charge of the vehicles operation remotely. Conversely, the need for such human intervention defeats the whole purpose of designing a USV, where the processes should be automated as much as possible with the help of currently available technology. As a last resort missions need to be aborted to avoid damage to the USV and the nearby marine environment. The challenge of designing an automated system becomes more complex as there is no *a priori* knowledge of when these events are likely to happen. Thus for the reasons outlined above, this chapter reports a study into the application of gradient descent, least squares and weighted least squares in-conjunction with MPC techniques in an attempt to design an adaptive autopilot for the *Springer* vehicle. In particular this chapter investigates the

performance, endurance and capabilities of such autopilots to cope with sudden change in the mass of the vehicle.

With regards to the structure and content of this chapter, on completion of this introductory material, Section 7.2 describes the autopilot designs. Subsequently Section 7.3 outlines the gradient descent algorithm, Section 7.4 outlines the least squares algorithm and Section 7.5 outlines the weighted least squares algorithm. The results and discussion are presented in Section 7.6. Finally concluding remarks are given in Section 7.7.

7.2 Autopilot Designs

The autopilot is concerned with keeping the vehicle on course. Soft computing techniques such as adaptive fuzzy has been utilised by Li, et al., (2011), Liu, et al., (2013), Li, et al., (2013), and adaptive neural techniques has been utilised by Liu, et al., (2011a), Liu, et al., (2011b), Li and Su (2013). The combination of fuzzy / neural approaches has been dealt with by Chen, et al., (2013). As this research area has been well investigated, it leaves room for only marginal improvement by adopting soft computing techniques in this project. Other adaptive and robust control techniques are dealt by Chen, et al., (2011) and Li, et al., (2010). Furthermore, the control strategies required to perform co-ordinated, complex tasks by multiple units of autonomous vehicles are explored by Cui, et al., (2010) and Cui, et al., (2012) However, the scope of this research is concerned with improving the control and capabilities of a single autonomous marine vehicle at present. Hence, relevant control strategies were explored

further. To cope with the sudden change in dynamics, adaptive MPC schemes based on three of the following adaptive algorithms were investigated:

(i) Gradient descent

(ii) Least squares

(iii) Weighted least squares

An outline of each of these algorithms is covered individually by the following three sub Sections 7.3, 7.4 and 7.5 respectively.

7.3 Gradient Descent

The gradient descent algorithm tries to minimise a function by following its slope in small steps and provides an updated model of the *Springer* online. It can be visually summarised in Figure 7.3.

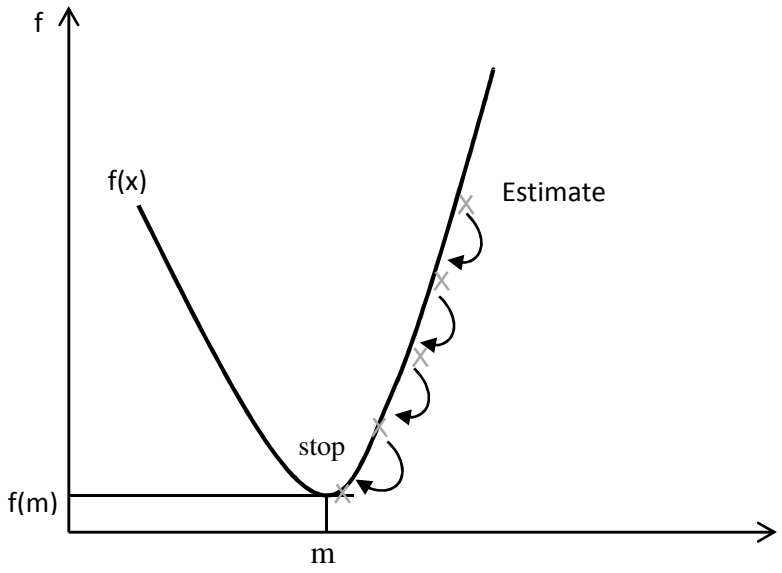

Figure 7.3: General steps involved in a gradient descent algorithm

The steps involved in a gradient descent algorithm can be summarised as follows:

i. Start with an estimated point
ii. Determine a descent direction
iii. Choose step size
iv. Update (until stopping criteria are reached)

An ARX model of the plant can be represented by the following set of equations:

$$A(z)y_k = B(z)u_k \qquad k \geq 0$$
$$A(z) = 1 + a_1 z + \cdots + a_p z^p, \qquad p \geq 0$$
$$B(z) = b_1 z + \cdots + b_q z^q, \qquad q \geq 1 \tag{7.1}$$

where A(z) and B(z) are the unknown coefficients of the polynomials and u_k represents the system input. The unknown parameters can be grouped together as follows:

$$\theta = [-a_1 \ldots . -a_p b_1 \ldots b_q]^\tau \tag{7.2}$$

The parameter θ is estimated by minimising the following cost function

$$J_k(\theta) = \frac{1}{2k}\sum_{i=0}^{k}(y_{i+1} - \theta^\tau \phi_i)^2 \tag{7.3}$$

Gradient descent is utilised to obtain the values of θ based on the following Equation (7.4):

$$\theta_{k+1} = \theta_k - \alpha_{GD} \nabla J(\theta_k) \text{ for k = 0 to number of iterations} \quad (7.4)$$

where α_{GD} is the learning rate and

$$\nabla J(\theta_k) = \begin{bmatrix} \frac{\partial J(\theta)}{\partial \theta(1)} \\ \vdots \\ \frac{\partial J(\theta)}{\partial \theta(p+q)} \end{bmatrix} \quad (7.5)$$

The gradient is calculated from the partial derivative of cost function at θ with respect to the corresponding component of θ. The numerical approximation to the partial derivative $\frac{\partial J(\theta)}{\partial \theta(l)}$ is given by the following Equation (7.6).

$$\frac{\partial J(\theta)}{\partial \theta(l)} = \frac{J(\theta_l^+) - J(\theta_l^-)}{2\delta_{GD}} \quad (7.6)$$

where $J(\theta_l^+)$ and $J(\theta_l^-)$ is the cost of θ_l^+ and θ_l^- correspondingly and the values of θ_l^+ and θ_l^- are computed as follows:

$$\theta_l^+ = \begin{bmatrix} \theta_{(1)} \\ \vdots \\ \theta_{(l)} + \delta_{GD} \\ \vdots \\ \theta_{(p+q)} \end{bmatrix} \qquad \theta_l^- = \begin{bmatrix} \theta_{(1)} \\ \vdots \\ \theta_{(l)} - \delta_{GD} \\ \vdots \\ \theta_{(p+q)} \end{bmatrix} \quad (7.7)$$

Calculate

$$\Delta\theta = |\theta_{k+1} - \theta_k| \quad (7.8)$$

While $\Delta\theta \cong 0$ convergence is reached (or) reached maximum number of iterations, the last best value is taken. This can be visually represented by a flow chart as shown in Figure 7.4.

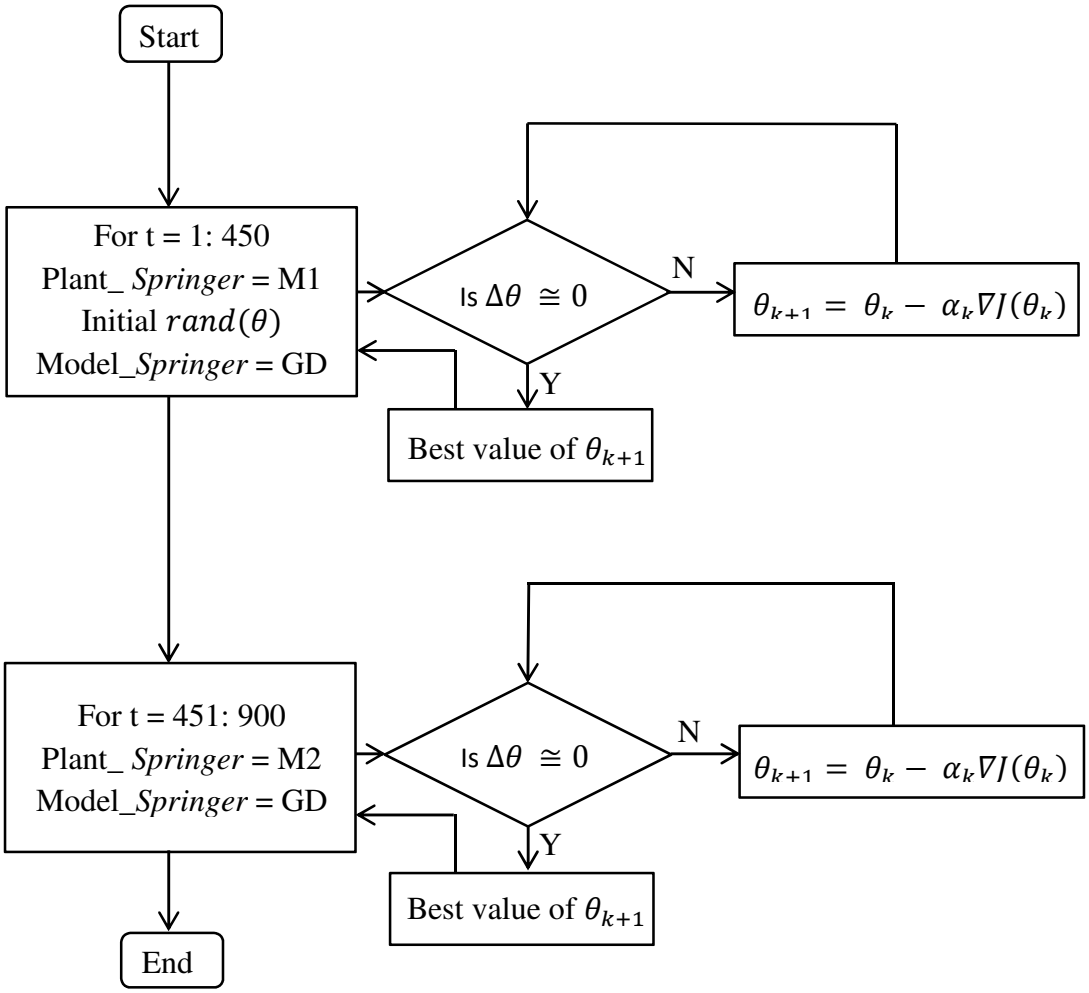

Figure 7.4: Gradient descent algorithm flow chart for *Springer* USV

A wide range of parameters were tested for gradient descent. The optimum parameters of gradient descent which provided a valid model of the *Springer* are shown in Table 7.1 as follows:

Parameters	Values
α_{GD} learning rate (Gradient Descent)	0.000000001
Max no iterations	15000
δ_{GD}	1e-15

Table 7.1: Parameters of Gradient descent for *Springer* USV

Gradient descent provides a simple solution. However, it has certain drawbacks as follows (Ljung, 1999):

1. Starting point: the starting point determines, how long the algorithm takes to converge to a solution and usually this point is chosen arbitrarily.
2. Step size: if large step sizes are chosen, the algorithm might miss the minimum point and provide a bad result. On the other hand, if too small step size is chosen, too many unnecessary steps of computation have to be repeated and the whole process becomes inefficient.
3. Despite all these issues, the major drawback of this method is that the solution can get stuck in local minima at times and there is no guarantee that the solution reached was the global minima.

Hence, further algorithms such as least squares (LS) were explored to overcome these difficulties.

7.4 Least Squares

A common and natural way to obtain a model from a set of data is least squares (Ljung, 1999). The model of the plant can be expressed by the following linear regression model

$$y_{k+1} = \theta^{\tau}\phi_k + w_{k+1} \tag{7.9}$$

where θ is the unknown parameter vector,

y_k = observation / system output

ϕ_k = regressor

w_k = noise processes / sequences

The parameter θ is estimated by minimising the following criterion

$$J_k(\theta) = \frac{1}{2}\sum_{i=0}^{k}(y_{i+1} - \theta^{\tau}\phi_i)^2 \tag{7.10}$$

An ARX model of the plant can be represented by the following set of equations:

$$\begin{aligned} &A(z)y_k = B(z)u_k \qquad k \geq 0 \\ &A(z) = 1 + a_1 z + \cdots + a_p z^p, \quad p \geq 0 \\ &B(z) = b_1 z + \cdots + b_q z^q, \quad q \geq 1 \end{aligned} \tag{7.11}$$

where A(z) and B(z) are the unknown coefficients of the polynomials and u_k represents the system input. The unknown parameters can be grouped together as follows:

$$\theta = [-a_1 \ldots . -a_p b_1 \ldots b_q]^{\tau} \tag{7.12}$$

The following recursive LS algorithm is employed to estimate the value of θ defined above

$$\theta_{k+1} = \theta_k + L_k(y_{k+1} - \theta_k^{\tau}\phi_k) \tag{7.13}$$

$$L_k = \frac{P_k\phi_k}{1+\phi_k^{\tau}P_k\phi_k} \tag{7.14}$$

$$P_{k+1} = P_k - \frac{P_k\phi_k\phi_k^{\tau}P_k}{1+\phi_k^{\tau}P_k\phi_k} \tag{7.15}$$

$$\phi_k = [y_k \ldots . y_{k-p+1}\, u_k \ldots u_{k-p+1}\ ]^{\tau} \tag{7.16}$$

The standard parameter of least squares α_{LS} is one and it has been utilised with *Springer* for further simulation studies conducted.

Some of the issues regarding the standard LS are as follows (Guo, 1996):

1. The estimates may not converge (or even may not be bounded). i.e., LS does not have self-convergence property.
2. The estimated models may not be uniformly controllable.

To overcome these problems weighted least squares were investigated further.

7.5 Weighted least squares

One of the key advantages of weighted least squares (WLS) is that it has a self-convergence property (Guo, 1996). Irrespective of the control law design, this algorithm

converges to a particular arbitrary vector. The 'universal convergence' result eliminates the analysis of stochastic adaptive control systems. This is achieved by slowly decreasing the weights of the system. Then the model hence obtained is uniformly controllable and enables to create a general framework for an adaptive robust control system design for *Springer*. In this method, the parameter θ is estimated by minimising the following criterion

$$J_k(\theta) = \frac{1}{2}\sum_{i=0}^{k} \propto_i (y_{i+1} - \theta^{\tau}\phi_i)^2 \tag{7.17}$$

where $\propto_i \geq 0$ is a weighting sequence. It enables allocation of different weights to different measurements. In a closed loop, the values of actual observation (y_k), $\text{regressor}(\phi_k)$ are unknown. Decreasing $\propto_i$ decreases the effect of instability and lack of excitation. Moreover, decreasing the rate of $\propto_i$ ensures that WLS enjoys similar good asymptotic properties as the standard LS (Guo, 1996).

The recursive WLS algorithm as follows is employed here:

$$\theta_{k+1} = \theta_k + L_k(y_{k+1} - \theta_k^{\tau}\phi_k) \tag{7.18}$$

$$L_k = \frac{P_k\phi_k}{\alpha_k^{-1} + \phi_k^{\tau}P_k\phi_k} \tag{7.19}$$

$$P_{k+1} = P_k - \frac{P_k\phi_k\phi_k^{\tau}P_k}{\alpha_k^{-1} + \phi_k^{\tau}P_k\phi_k} \tag{7.20}$$

$$\phi_k = [y_k \ldots . y_{k-p+1}\, u_k \ldots u_{k-p+1}\ ]^{\tau} \tag{7.21}$$

$$\alpha_k = \frac{1}{f(r_k)} \tag{7.22}$$

$$\text{where } r_k = \|P_o^{-1}\| + \sum_{i=0}^{k}\|\phi_i\|^2 \tag{7.23}$$

and f(x) is a slowly increasing function and satisfies the following condition

$$\int_N^{\infty} \frac{dx}{xf(x)} < \infty \; for\ some\ N > 0 \tag{7.24}$$

The function employed here is $f(x) = log^{1+\delta}x \ \ where\ \delta > 0$ (7.25)

Other similar functions can be found in (Guo, 1996). Various simulation studies were conducted and the optimum parameters of WLS which provided a valid model of the *Springer* were obtained heuristically and are detailed in Table 7.2, as follows:

Parameters	Values
α_{WLS}	0.5
δ_{WLS}	1

Table 7.2: Parameters of WLS for *Springer* USV

7.6 Results and discussion

As stated earlier, *Springer* offers a standard displacement of 0.6 tonnes. Under the present circumstances, the dynamic model of the *Springer* vehicle is given in Chapter 4. For the sake of completeness it is represented by the following Equations (7.26) and (7.27):

$$x(k+1) = Ax(k) + Bu(k)$$
$$y(k) = Cx(k) + Du(k) \tag{7.26}$$

where

$$A = \begin{bmatrix} 0.0372 & 1 & 0 & 0 \\ 0.1002 & 0 & 1 & 0 \\ 0.3781 & 0 & 0 & 1 \\ 0.471 & 0 & 0 & 0 \end{bmatrix}, \quad B = \begin{bmatrix} 0.3235 \\ -0.8218 \\ 0.8819 \\ -0.3031 \end{bmatrix},$$

$$C = \begin{bmatrix} 1 & 0 & 0 & 0 \end{bmatrix}, \qquad D = \begin{bmatrix} 0 \end{bmatrix} \tag{7.27}$$

The problem with this model is that it does not reflect the true dynamics of the system at all times during its operation. Environmental changes, wear and tear and mass changes all attribute to the change in system dynamics and can offset the autopilot performance if it is based on an offline model obtained from prior trials. Hence, to improve the overall performance, it was contemplated to update the model of the plant at each sampling instant. This section illustrates how this is achieved and implemented on *Springer* USV.

The objective of this study has been to develop a robust adaptive autopilot for the *Springer* USV which will be capable of handling changes in the mass of the USV. Hence, the adaptive nature of algorithms (GD, LS, WLS) discussed in the above

sections are investigated further. As discussed in the earlier sections, in the event of change in mass of the system, usually it ranges from 0% to 20% of the total mass of the USV. However, during extreme weather conditions or sudden change in mass of the USV as in search and rescue operation (or payload deployment from USV) the worst case scenario could offset the system parameters considerably. Whilst it is imperative to push the limits of robustness of the autopilot, it will become a fallacy to endeavour a solution for practically impossible situations (such as 100% change in mass for example). Hence, to test the endurance of the robust adaptive autopilot, different changes were studied. Initial trials conducted at Roadford Reservoir, Devon, UK indicate that the following system matrix A represented by Equation (7.28) represents a case for 50% change in mass of the *Springer*. This system matrix was chosen to highlight the effectiveness of different methods to cope with such a change (should such a severe change occur in reality).

$$A = \begin{bmatrix} 0.0186 & 1 & 0 & 0 \\ 0.0501 & 0 & 1 & 0 \\ 0.1891 & 0 & 0 & 1 \\ 0.4710 & 0 & 0 & 0 \end{bmatrix} \tag{7.28}$$

Additionally, it can be observed from the following figures that a negative value of n_d is required to keep the vehicle on course to follow a desired reference trajectory. This is primarily owing to the utilisation of model obtained by Sharma and Sutton (2012) in these simulation studies. This issue was resolved during full scale trials experimentation and improved performance and results were obtained in the subsequent Chapter 8. However, in this chapter, the ability of the GD, LS and WLS algorithms to converge to the true value despite the random initialisation and the feasibility of real time application is examined. Innovative modifications to these algorithms, in an attempt to obtain improved performance are detailed as follows.

7.6.1 Gradient descent and MPC

Gradient descent algorithm as described in the previous Section 7.2 was utilised in conjunction with the MPC as illustrated in Figure 7.1(a). The initial θ values were randomly initialised during initiation of the algorithm. As the initial values were randomly chosen, several runs were carefully examined and the following two cases are presented here to illustrate the range of outputs obtained from this course of action.

The following Figures 7.5 and 7.6 extol the impact of initial values of θ. As explained in the flowchart (Figure 7.3), the algorithm obtains a new model of the USV at every sampling instant. In effect, it runs 15,000 iterations for every sampling instant and hence to complete one set of algorithm; it took 1 hour and 18 minutes approximately.

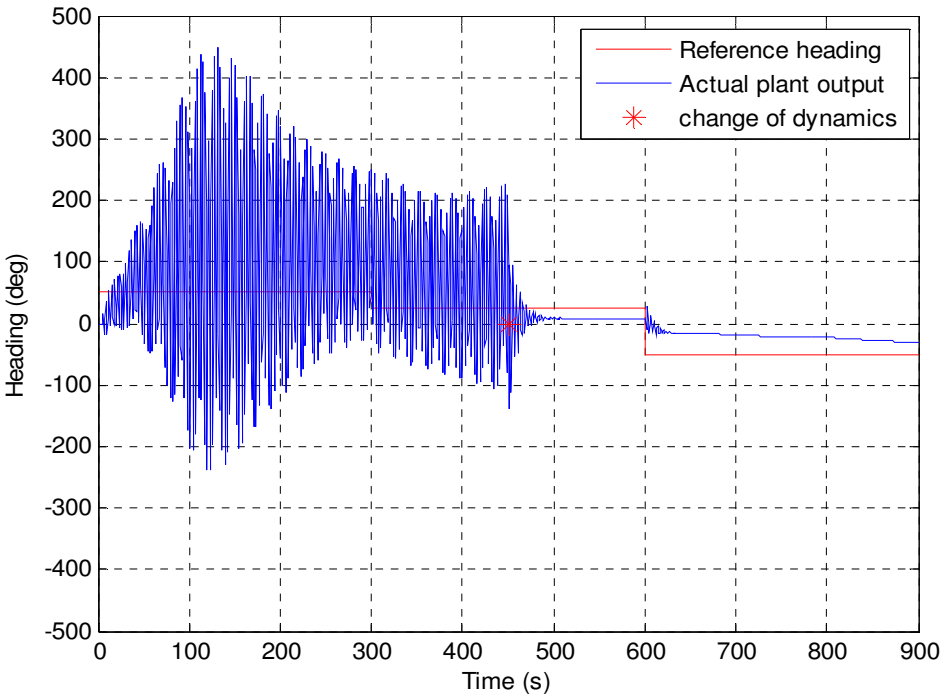

(a)

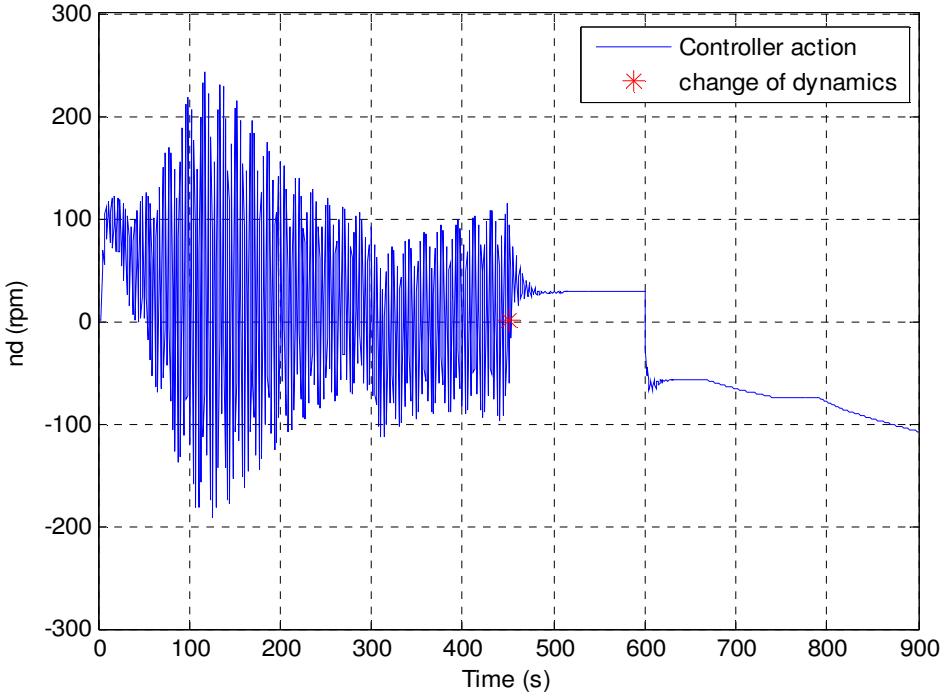

(b)

Figure 7.5: Gradient descent and MPC controller (a) plant output

(b) controller action (case 1)

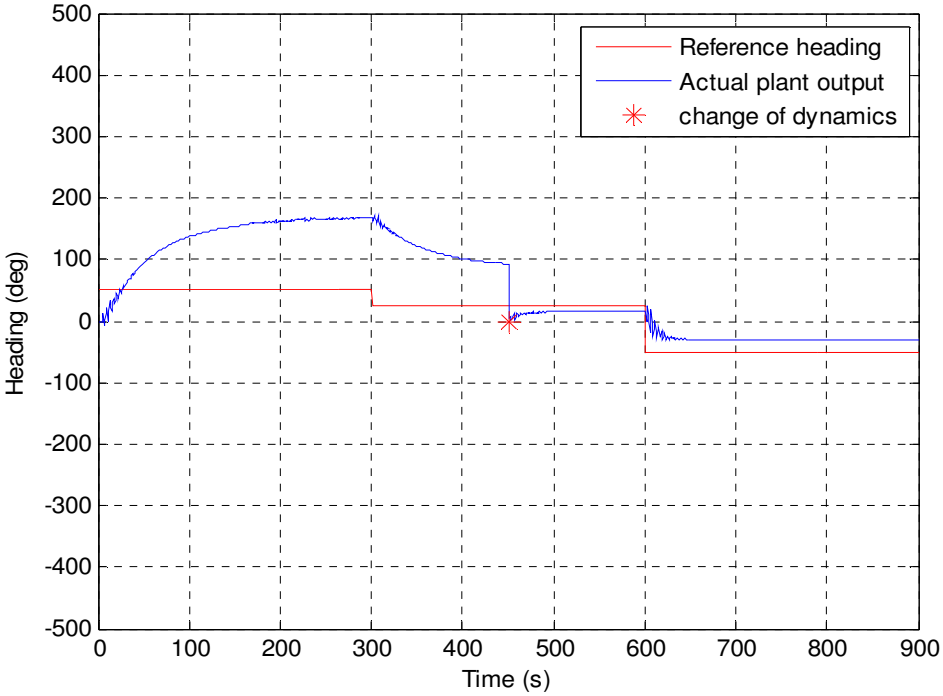

(a)

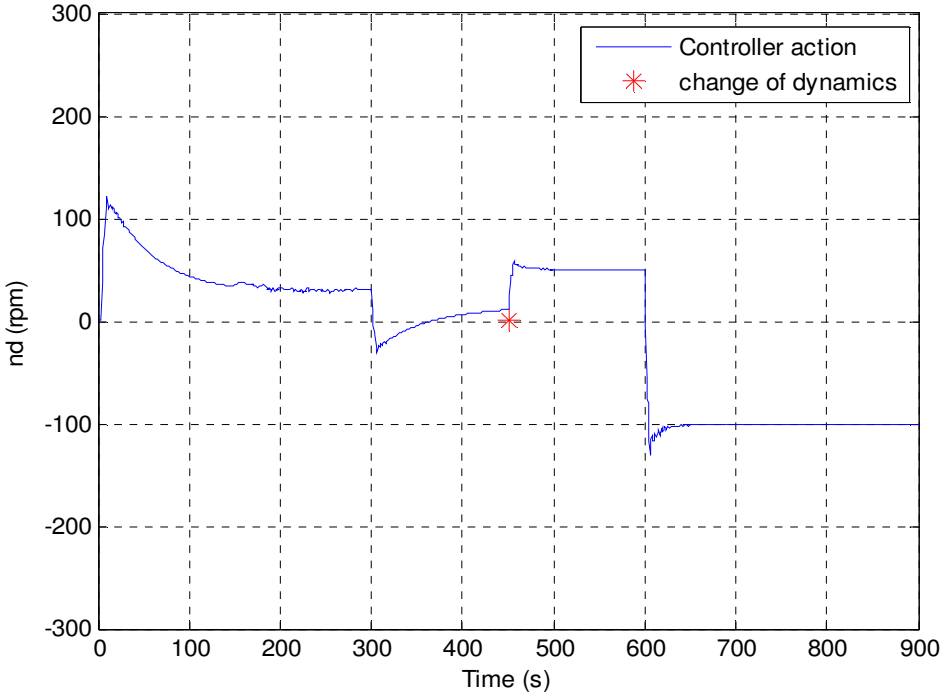

(b)

Figure 7.6: Gradient descent and MPC controller (a) plant output (b) controller action (case 2)

Despite being computationally expensive, the results from the gradient descent were not promising. Owning to the true random nature of the initial values chosen, no two runs were the same. The impact of the initial random values can be clearly illustrated in the 2 above cases represented in Figure 7.5 and 7.6. This implied that the initial θ value assignment had a significant effect on subsequent behaviour. Hence, the standard gradient descent was modified slightly as follows. Instead of total random assignments of the initial θ values, 25% of the true values of the original plant were chosen as initial θ. This implies that the system will still cope with 75% error in the initial θ values. Moreover, instead of computing the gradient algorithm for every sampling instant, it was initiated only once for every 100 seconds. The changes in the results were dramatic as can be seen in the following Figure 7.7.

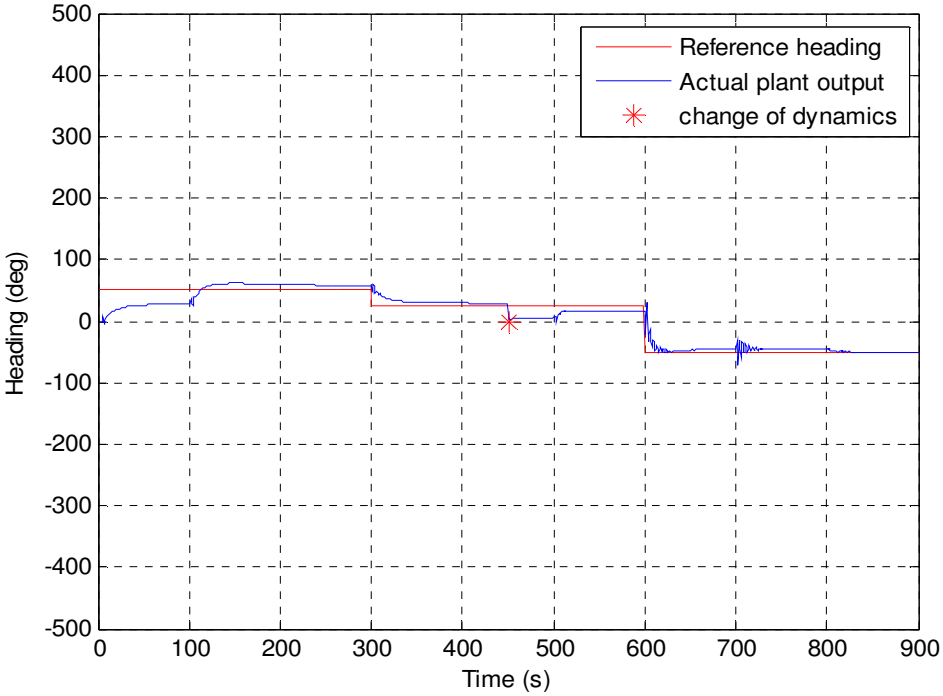

(a)

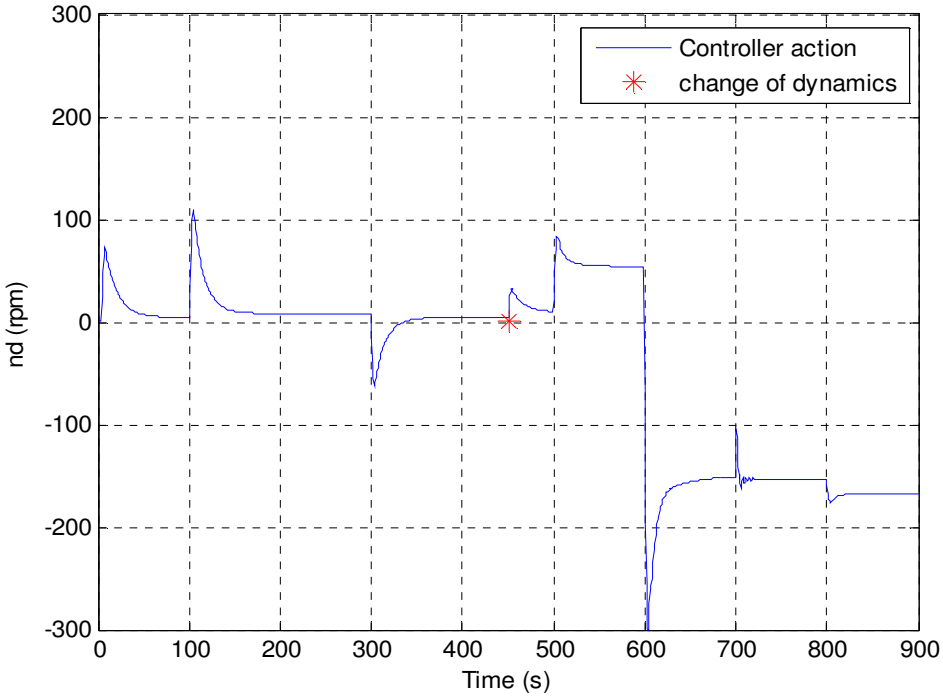

(b)

Figure 7.7: Modified gradient descent and MPC controller (a) plant output (b) controller action

The improvements in the performance of the autopilots are visually evident from Figures 7.5 – 7.7. However, to measure the improvements numerically, the average controller energy (ACE) and mean square error (MSE) were utilised. In a discrete form, these two parameters can be calculated by the following equations:

$$ACE = \frac{1}{M}\sum_{t=1}^{M}[u(k)]^2 \tag{7.29}$$

where *u(k)* is the controller effort at an instant of time *k*, *M* is the total number of samples,

$$MSE = \frac{1}{M}\sum_{k=1}^{M}[y(k) - r(k)]^2 \tag{7.30}$$

where *y(k)* is the output from the USV in degrees and *r(k)* is the reference angle which the USV is supposed to track in this study. The corresponding values of ACE and MSE were calculated for the different options illustrated by Figures 7.5 – 7.7 and the results are summarised along with the other approaches in the Table 7.3. In pursuit of further improvements, the next subsection details the results obtained by utilising LS with MPC.

7.6.2 Least squares and MPC

Given, its simplicity and lean computation, least square is seen as a natural choice to obtain model of the vessel for a given set of input, output data. Initial performance was satisfactory and was able to work well in conjunction with MPC controller. However, as soon as there was a change in the dynamics of the plant, then it was no longer able to

track the reference in a satisfactory manner. This can be clearly observed from the following Figure 7.8. The corresponding values of ACE and MSE were calculated for LS and MPC combination and the results are summarised in the Table 7.3.

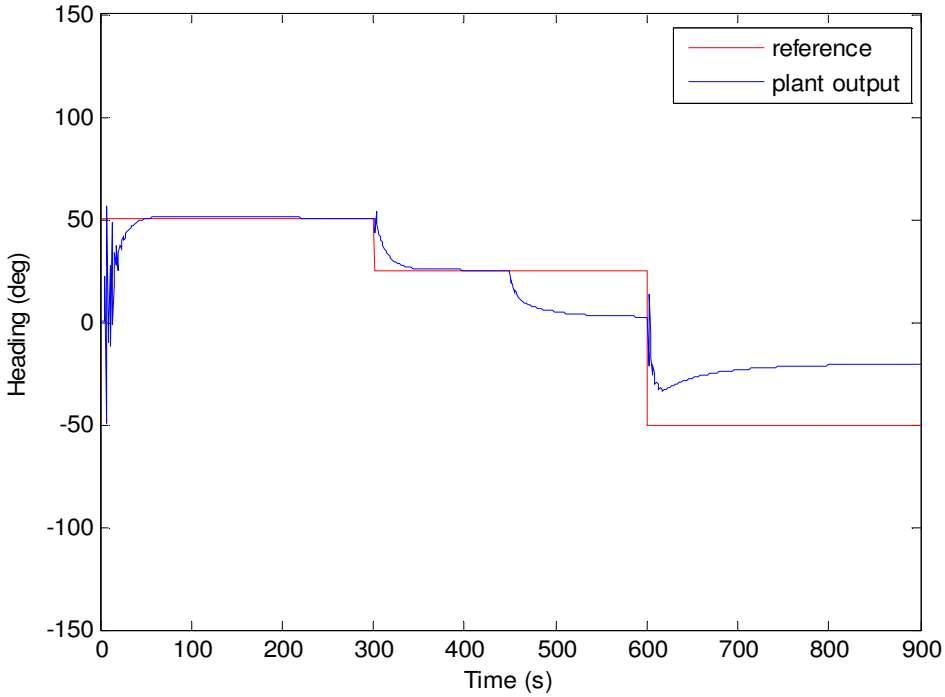

(a)

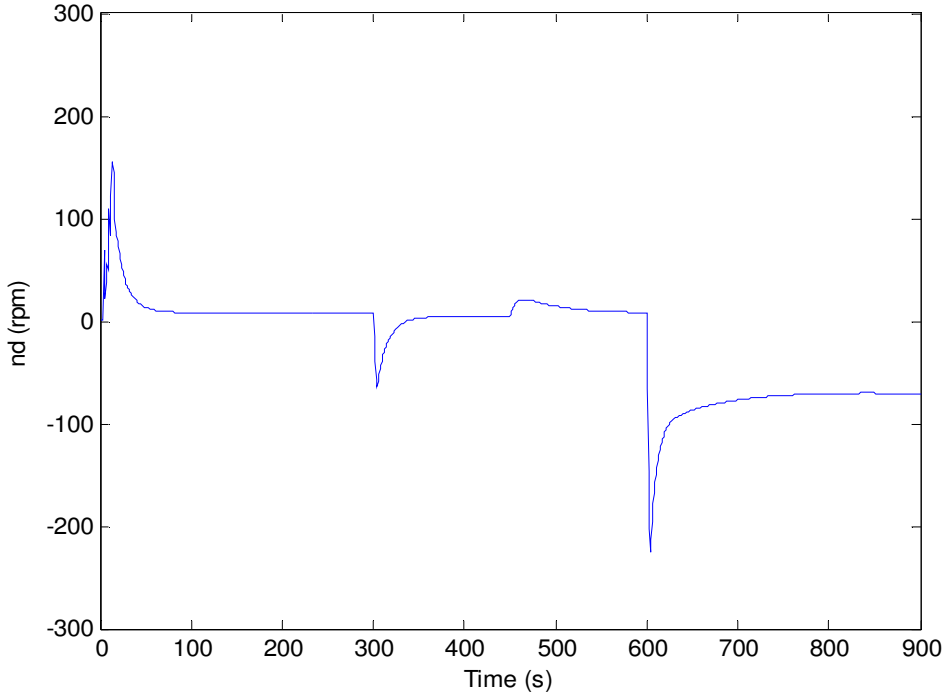

(b)

Figure 7.8: Least squares and MPC controller (a) plant output (b) controller action

7.6.3 Weighted least squares and MPC

Weighted least squares certainly have theoretical advantages over the least squares, as mentioned in previous Section 7.6.2. In reality, there was only a marginal improvement of the results and hitherto, the change in the dynamics had offset the reference tracking ability of the autopilot. This can be seen from Figure 7.9.

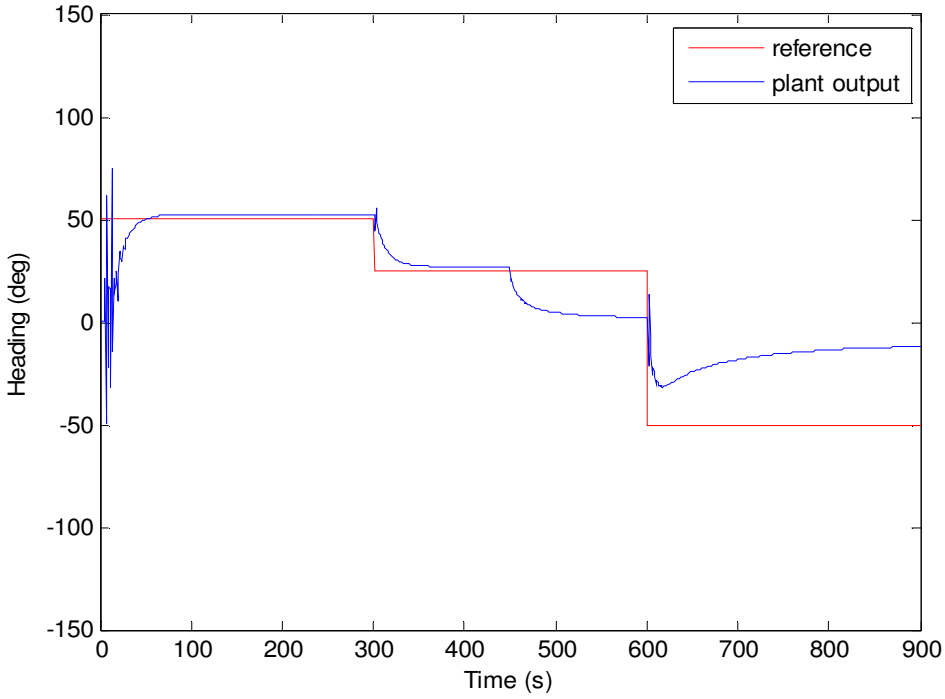

(a)

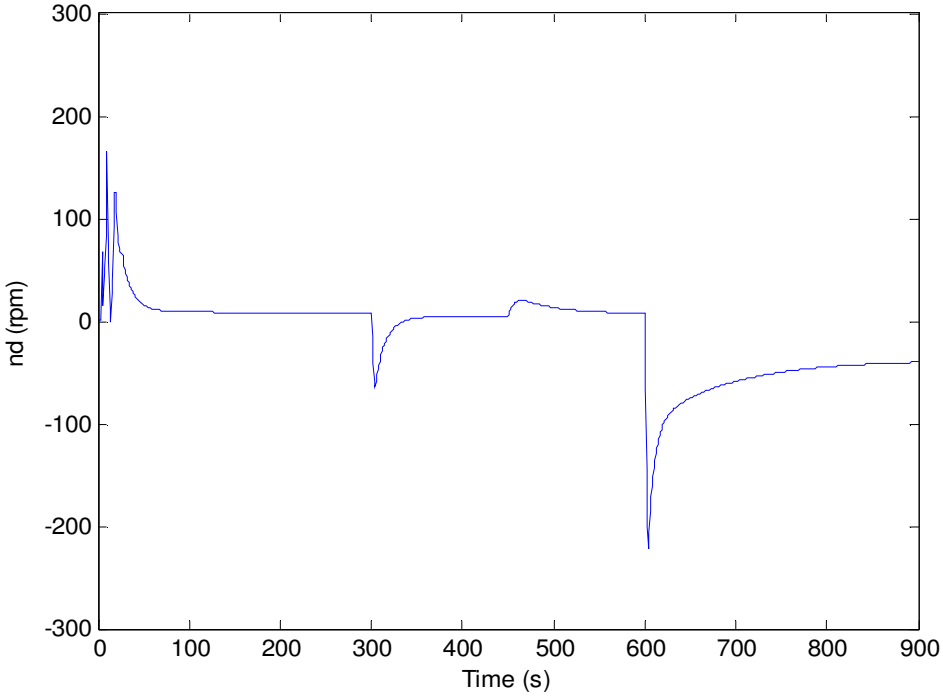

(b)

Figure 7.9: Weighted least squares and MPC controller (a) plant output (b) controller action

To tackle this problem, the WLS algorithm was reinitiated when there was a change in the dynamics of the system. In the real world it may not be possible to have *a priori* knowledge of the change in the system dynamics. Hence, decision making logic was implemented to detect the change in the dynamics and reinitialise the WLS algorithm, only when these conditions were satisfied:

$$\Delta\theta_k = \theta_k - \theta_{k-1} > 80 \text{ to } 120\ \% \tag{7.31}$$

From the values of the individual components of θ, it was observed that a change of 80 to 120% or more signified a sudden change in system dynamics. At the same time, the system was still being initialised with random θ values and huge changes of $\Delta\theta$ were common during the initialisation. If this was wrongly detected as change in system

dynamics, the algorithm will be reset continuously and yield very poor results. Hence, to ensure that the algorithm was only reinitialised when there was a change in system dynamics, the above criteria of $\Delta\theta$ was used in conjunction with the following two additional criterions:

$$\Delta\theta_{k-1} = \theta_{k-1} - \theta_{k-2} \cong 0 \; or < 10\,\% \tag{7.32}$$

$$\Delta\theta_{k-2} = \theta_{k-2} - \theta_{k-3} \cong 0 \; or < 10\,\% \tag{7.33}$$

The values of $\Delta\theta_{k-1}$ and $\Delta\theta_{k-2}$ was usually detected to be approximately zero or it reached a maximum value of 10% in some cases. Once the above three conditions were satisfied, it was deemed appropriate to reinitialise the WLS algorithm.

This allows time for the WLS algorithm to reach a steady state with the random initial conditions and reinitiates the algorithm when there is a change in the dynamics. This is indicated by the following Figure 7.10 where the norm (P) indicates that it has been reset only once after initialisation.

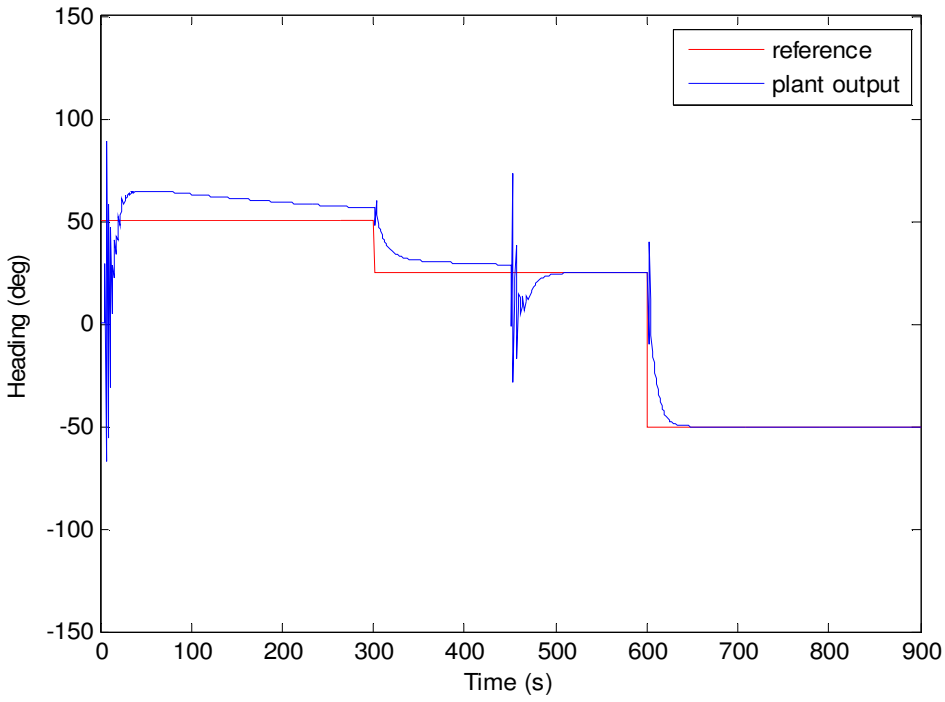
reference
plant output
Heading (deg)
Time (s)
150
100
50
0
-50
-100
-150
0
100
200
300
400
500
600
700
800
900

(a)

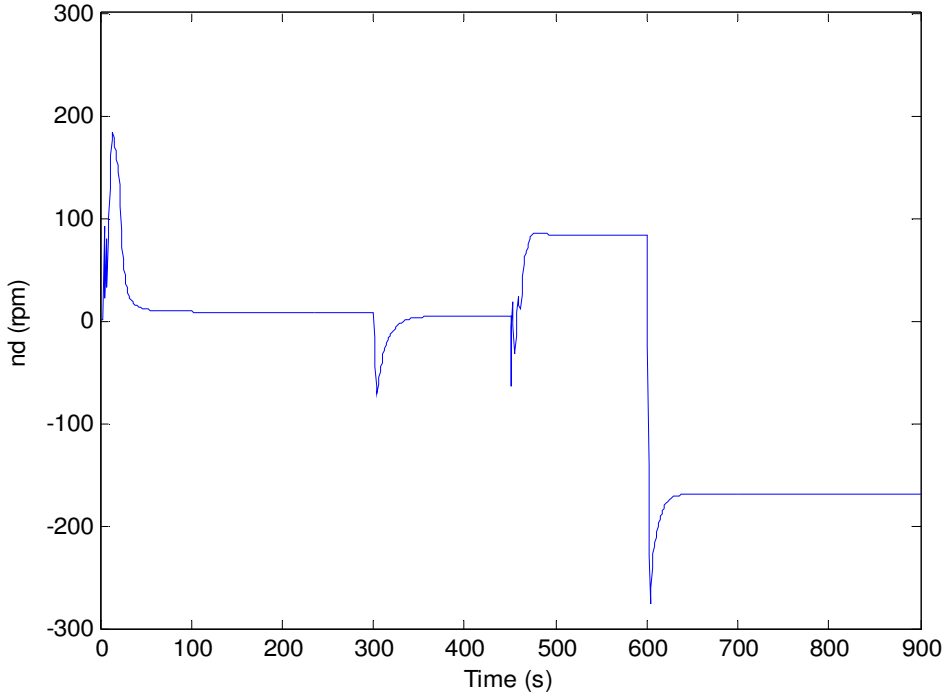
nd (rpm)
Time (s)
300
200
100
0
-100
-200
-300
0
100
200
300
400
500
600
700
800
900

(b)

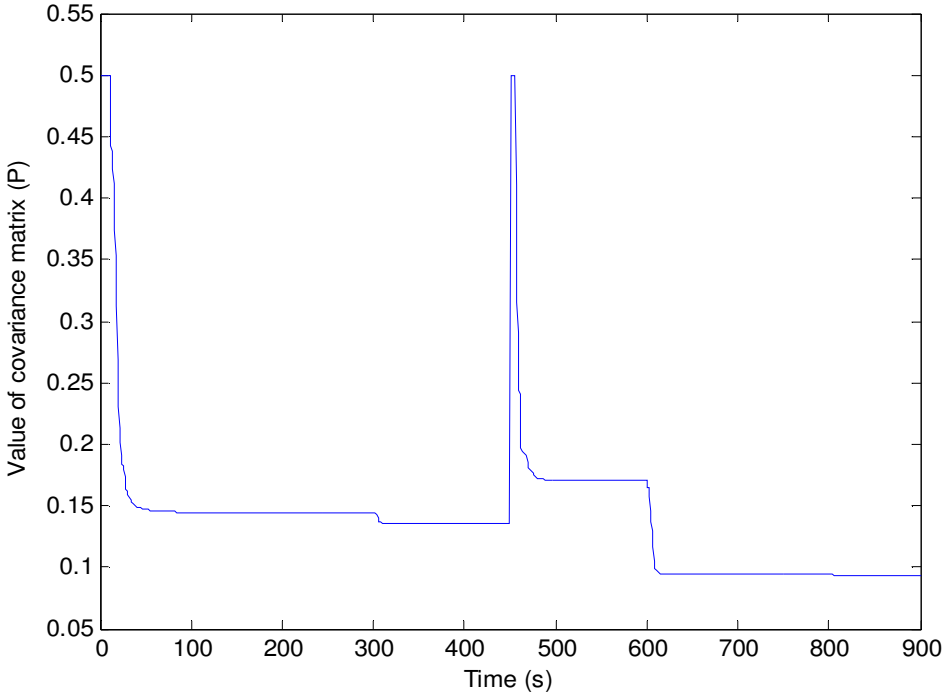

(c)

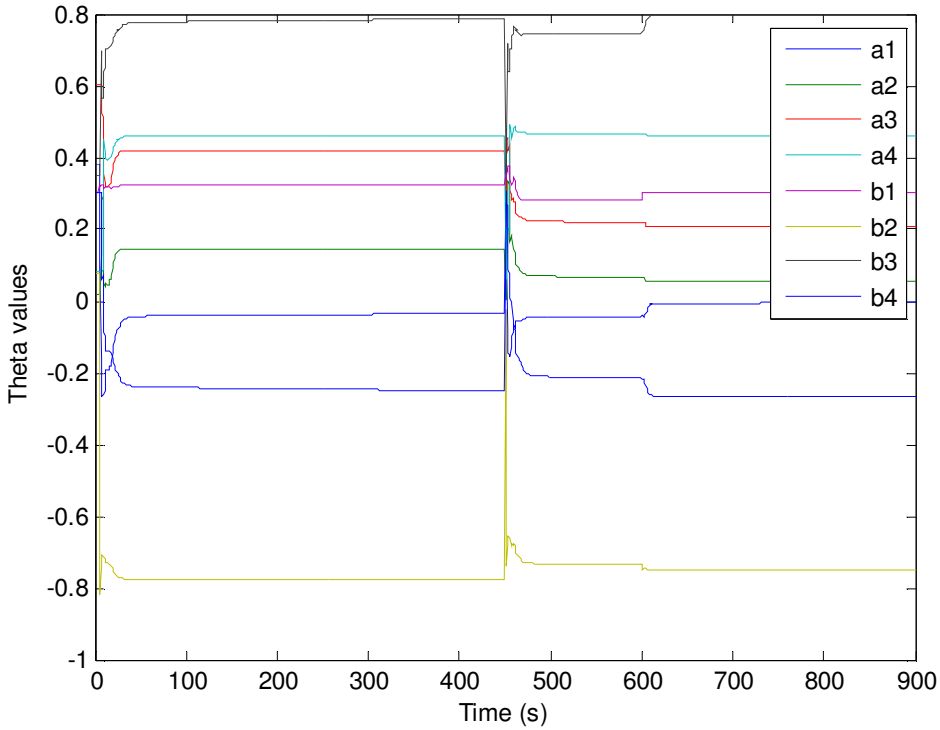

(d)

Figure 7.10: Weighted least squares and MPC controller (a) plant output (b) controller action (c) re-initialised covariance matrix (P) (d) θ values

Once improved results were obtained by reinitialising the algorithm, it was contemplated, if reinitialising the algorithm periodically might improve the performance further. These results can be seen in the following Figure 7.11, where the system was reset periodically for every 50 s. Re-initialisation caused the θ values and the covariance matrix P (Equation (7.18)) to be reset every time. Hence, spikes at change of dynamics reached values more than 100. So this approach was deemed unfit for real-time application. Nevertheless, it paved the way to obtain the subsequent steps.

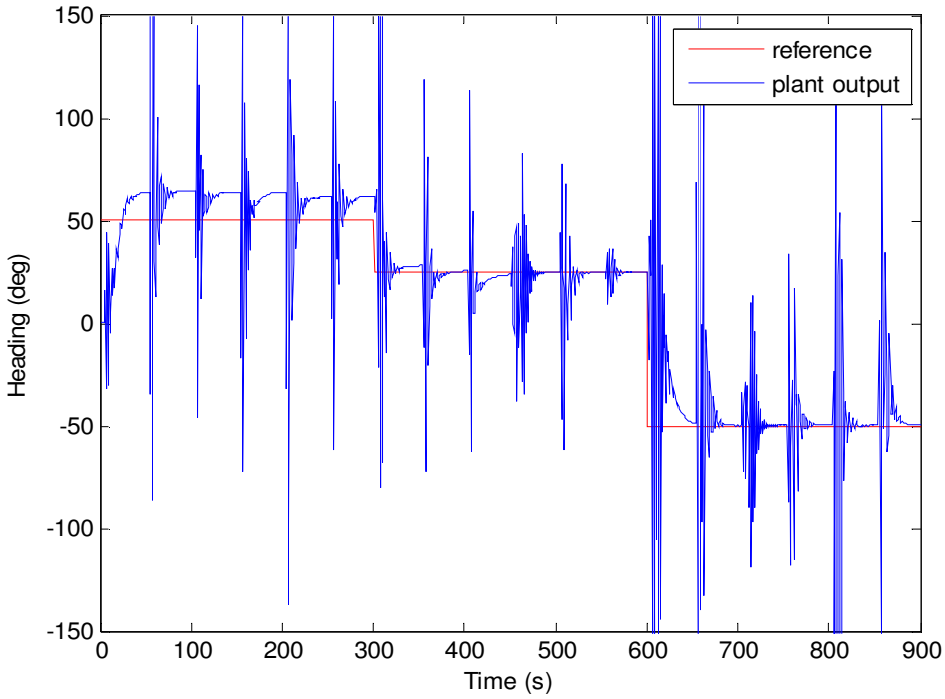

(a)

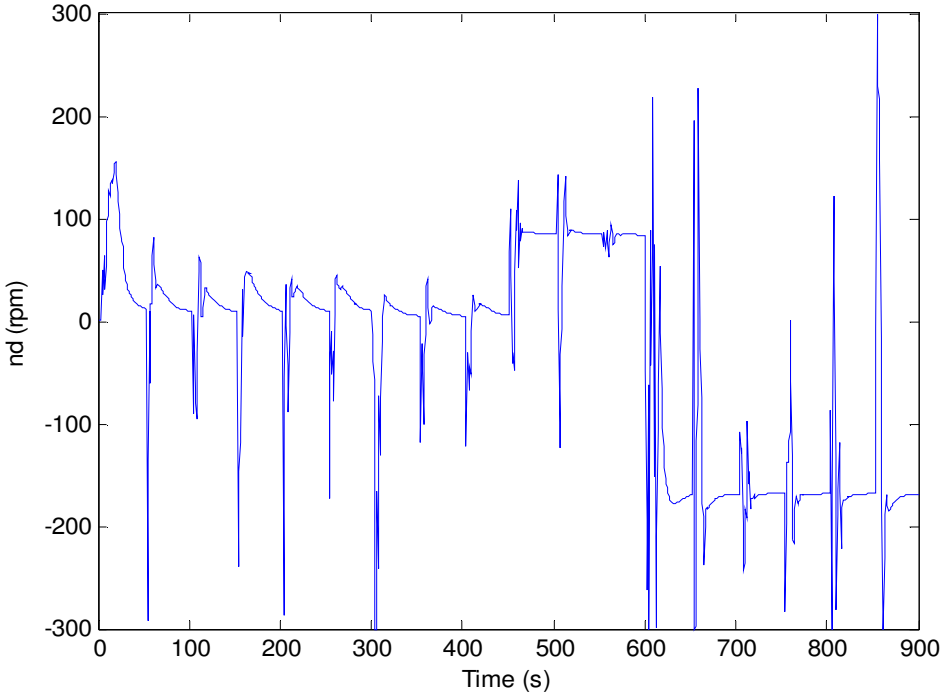
300
200
100
0
-100
-200
-300
nd (rpm)
0
100
200
300
400
500
600
700
800
900
Time (s)

(b)

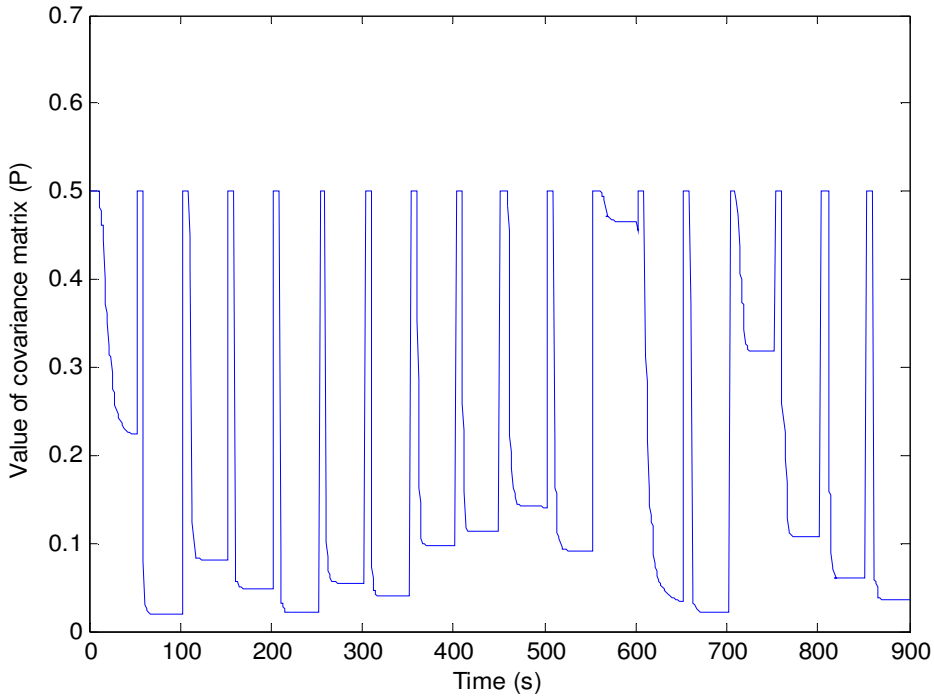
0.7
0.6
0.5
0.4
0.3
0.2
0.1
0
Value of covariance matrix (P)
0
100
200
300
400
500
600
700
800
900
Time (s)

(c)

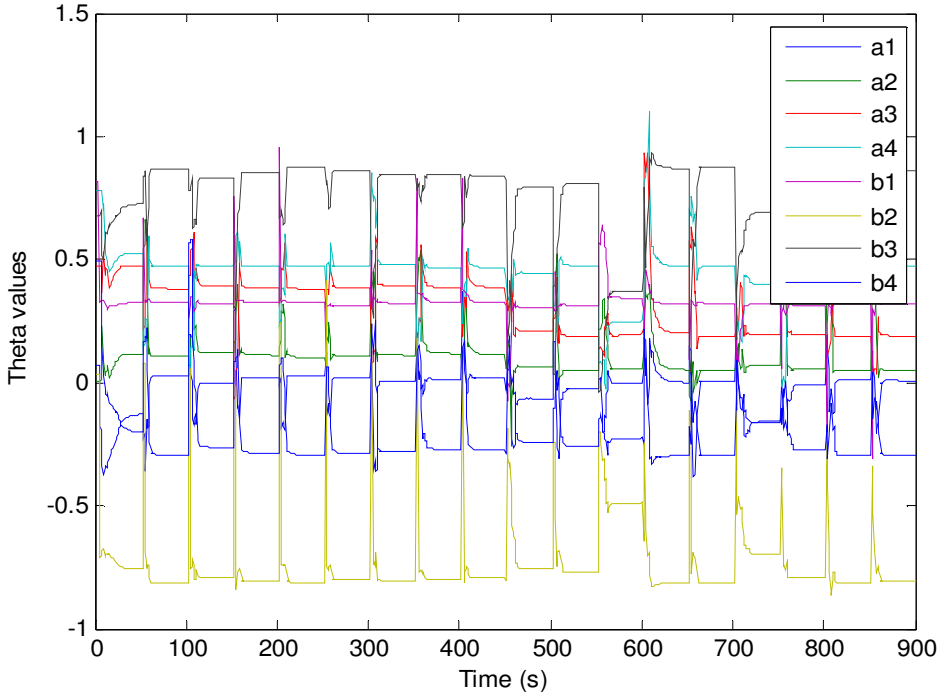

(d)

Figure 7.11: WLS reinitialised for every 50 sec (a) plant output (b) controller action (c) re-initialised covariance matrix (P) (d) θ values

Instead of re-initialising the entire algorithm, much better performance was obtained by resetting the values of the covariance matrix P, at periodic intervals and by keeping the θ values continuous. The results are obvious from the following Figure 7.12. Additionally this approach eliminates the need for having a decision making process (which inherently carries the risk of resetting the system inadvertently). Thus by the above said modifications, the robust adaptive autopilot capable of handling changes in the system dynamics has been realised.

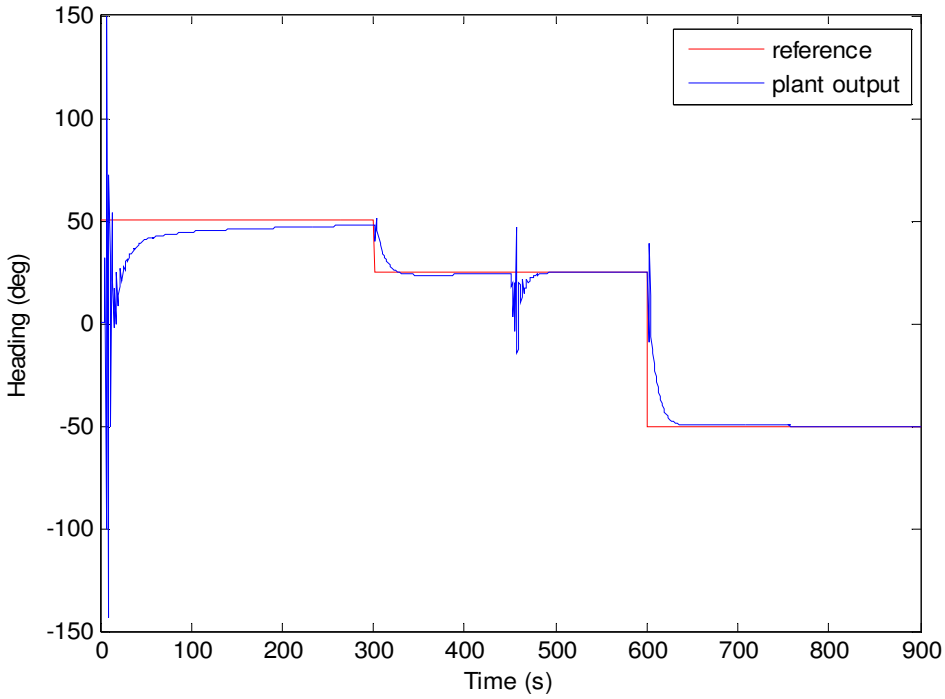

(a)

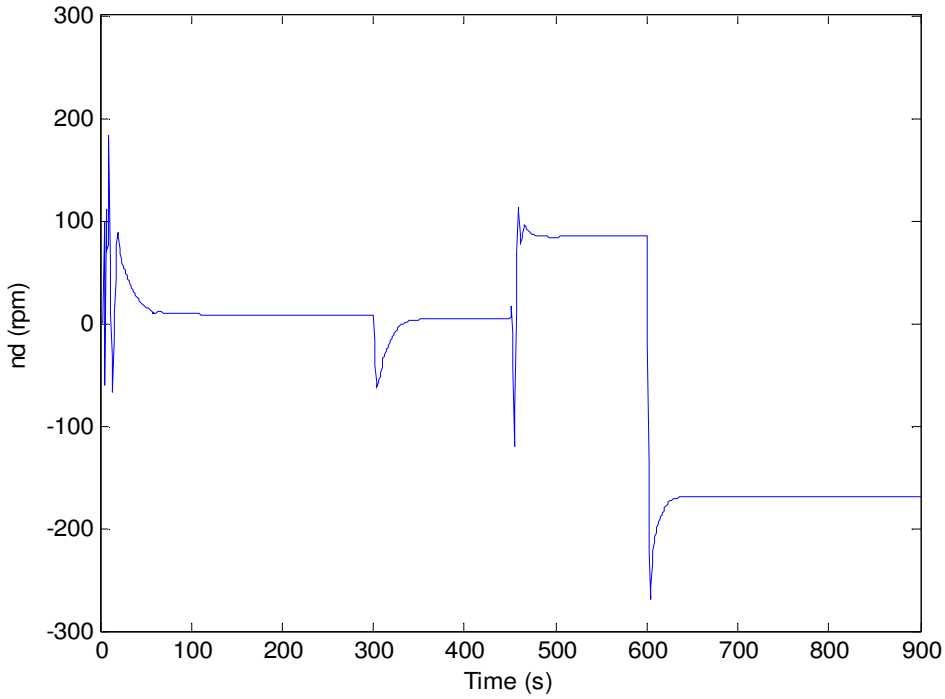

(b)

Figure 7.12: Covariance matrix (P) reinitialised for every 50 sec, with continuous θ

(a) plant output (b) controller action

Once this approach yielded satisfactory results, it was time to retune the periodic intervals at which the covariance matrix (P) was reset. When the window length was increased to 100 seconds the performance deteriorated as can be seen from the following Figure 7.13. Then the window of time was reduced to different time periods and the performance deteriorated below 25 seconds. Hence, the optimum time to reset the covariance matrix for *Springer* USV was found to be 25 seconds. The results can be found as follows in Figure 7.14. These results from the modified WLS, as in Figure 7.15 were benchmarked against the real values of θ and the results were strikingly very similar. This modified form of WLS in conjunction with MPC will referred to as adaptive MPC (aMPC), here afterwards. Moreover, the aMPC handled the change in the dynamics better than providing the real values to the controller directly.

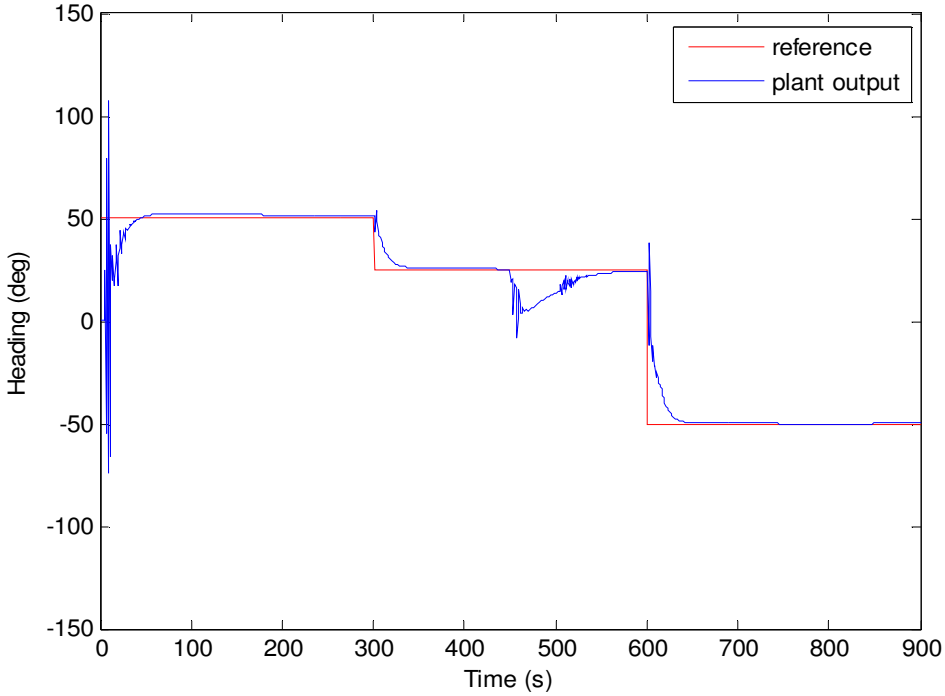

(a)

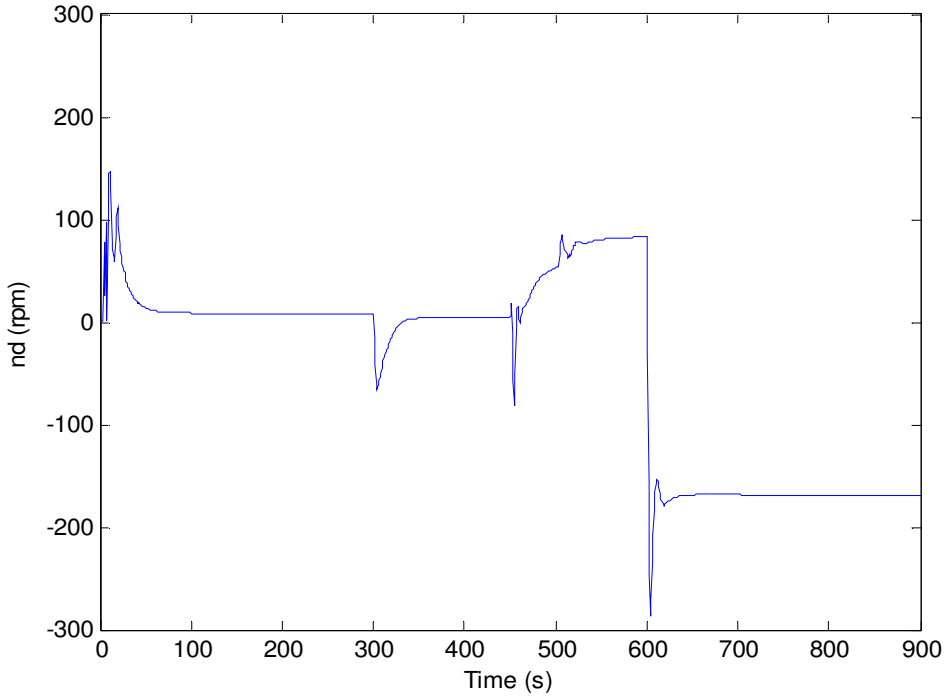

(b)

Figure 7.13: Covariance matrix (P) reinitialised for every 100 sec, with continuous θ

(a) plant output (b) controller action

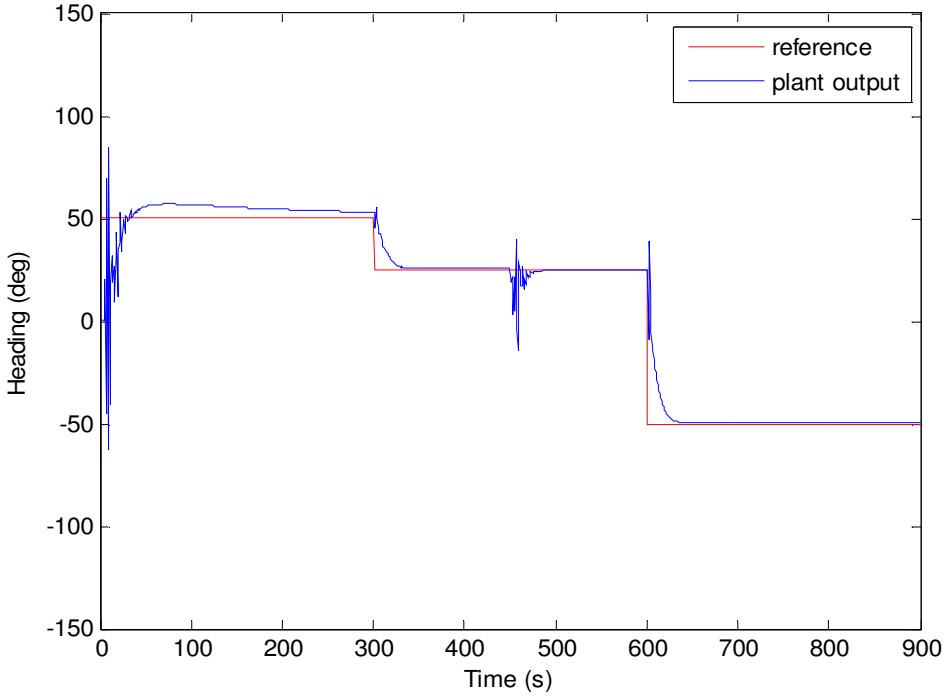

(a)

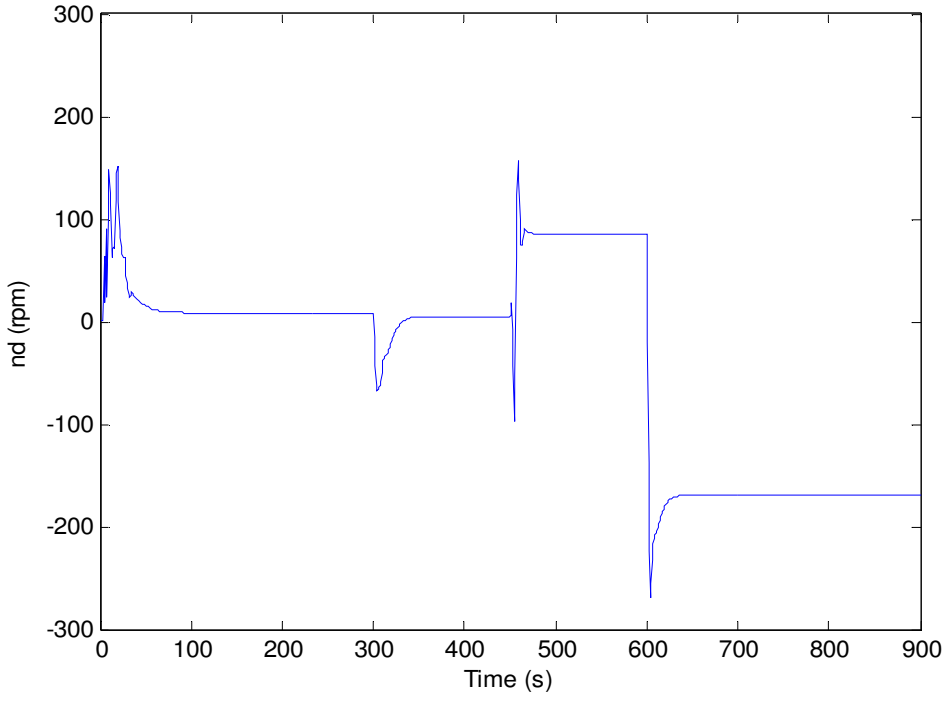

(b)

Figure 7.14: Covariance matrix (P) reinitialised for every 25 sec, with continuous θ

(a) plant output (b) controller action

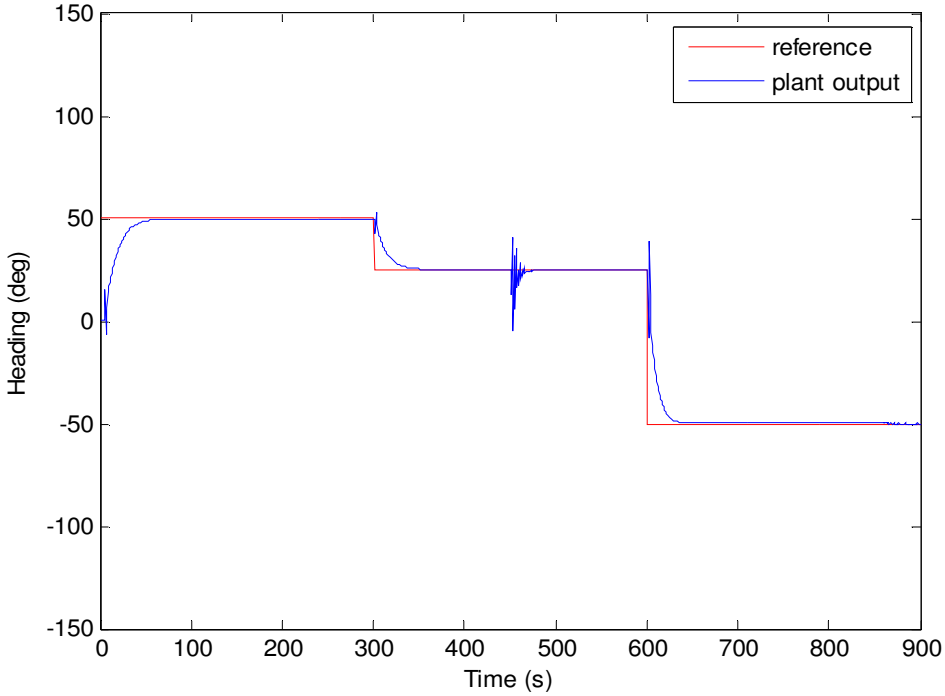

(a)

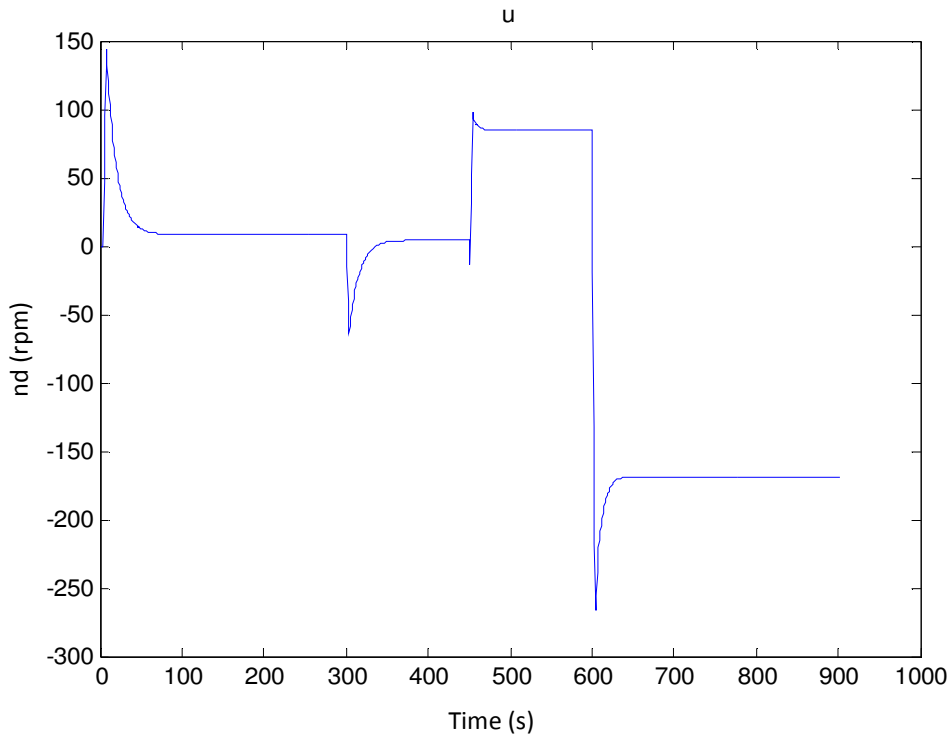

(b)

Figure 7.15: Weighted least squares with real θ and MPC controller (a) plant output (b) controller action

The corresponding values of ACE and MSE were calculated for the different options illustrated by Figures 7.5 - 7.15 and the results are summarised in Table 7.3 as follows.

Main algorithm used	Different cases	ACE $(rps)^2/s$	MSE (deg^2)
Gradient descent	Gradient descent (case 1)	1.8273	1.1968e+04
	Gradient descent (case 2)	1.3253	4.6621e+03
	Modified gradient descent (case 3)	2.6839	189.0032
Least squares	Standard Least squares	0.6253	408.6256
Weighted least squares	Standard weighted least squares	0.4827	517.1449
	Reinitialised during a change in dynamics	3.1483	148.2021
	Reinitialised for every 50 sec	3.4617	1.8671e+03
	Covariance matrix (P) reinitialised for every 50 sec, with continuous θ	3.1026	179.6000
	Covariance matrix (P) reinitialised for every 100 sec, with continuous θ	2.9731	125.5104
	Covariance matrix (P) reinitialised for every 25 sec, with continuous θ	3.1332	107.5875
	WLS with real θ	3.1126	68.9770

Table 7.3: Comparison of performance of autopilots (for *Springer* USV)

From the above Table 7.3, it is clear that the gradient descent algorithm suffers from its inherent disadvantages and performs poorly. Case 1 and 2 in gradient descent further illustrate the huge discrepancies in performance due to the arbitrary initial values. Significant improvements are gained by the proposed modifications to the standard gradient descent. In pursuit of further improvements, LS algorithm was investigated and the performance was not satisfactory. Hence, WLS was investigated further. It can be observed that WLS with no modifications clearly has a large tracking error. This is considerably reduced by reinitiating the algorithm during a change in dynamics of the USV. Further attempts were made to improve the performance by reinitialising the algorithm periodically. On the outset, it seemed counterproductive as the error values increased significantly. On closer analysis, it became clear that such behaviour was due to frequent random initialisation and the transient response characteristics. Instead of solving a problem, now it served as additional burden on the system. Significant improvements were achieved by keeping the θ values continuous and reinitialising only the covariance matrix. Once this behaviour was understood, then marginal gains were made by varying the size of the time frame window to carry out the initialisation. The values from these cases are also summarised in the above table 7.3. A time frame of 25 seconds seems to be the optimum time frame to the reinitialise the parameters discussed above.

This novel approach enables the autopilot to cope well with significant changes (approximately 50%) in the system dynamics. Under normal circumstances, the changes in the system dynamics are likely to be 0 to 20%. Hence, it is deemed appropriate for *Springer* and is highly recommended to design a robust adaptive autopilot for other such USVs by utilising this innovative approach.

7.7 Conclusions

The sudden change in the dynamics of a plant causes considerable deterioration (in case of non-adaptive techniques) in the controller performance and remains a major obstacle in accomplishing a desired mission. This problem has been suitably dealt in this study by designing a robust adaptive autopilot for the *Springer* USV. Initially the basic structure of the controller and the performance of the original offline plant dynamics were established. Subsequently, the performance was compared with three suitable methods namely: gradient descent, LS and WLS. Gradient descent is able to provide a solution with very bad tracking performance. Additionally, there is a risk that it might get stuck in the local minima. Hence, LS was investigated further. The system stabilises even after the change in dynamics. However, the self-convergence is not guaranteed by the LS approach and the autopilot was not able to cope with change in dynamics. Therefore, WLS was investigated further. Conversely, applying WLS to solve this problem posed several, severe, initial challenges. To overcome these issues a new approach has been presented here. Random initialisations of θ values and periodically reinitialise the covariance matrix P at intervals of 25 seconds, whilst keeping the intermittent θ values continuous offers a new approach to deal with change in dynamics. It is also worth mentioning that in a standard WLS the recent values are given more weightage and it will make the system unstable if the changes in the immediate values are large. Stability and controllability are guaranteed by giving less weightage to the immediate values and giving more weightage to the past values. Subsequent to these suitable modifications it was found to be the most appropriate to be incorporated in the design of a robust adaptive autopilot by utilising aMPC. Moreover, this approach also eliminates the need for implementing a decision making algorithm / logic to detect the

change in dynamics. Hence, by implementing such a technique further problems such as false trigger or no detection of changes is comprehensively circumvented successfully. This approach checks for changes periodically and at the same time manages to be computationally efficient by keeping the continuous θ values. This inventive approach will enable the *Springer* USV and other USVs to cope with change in dynamics and still accomplish the desired missions effectively. Practical experimentation was undertaken at Roadford Reservoir, Devon, UK and the results will be presented in the following Chapter 8.

Chapter 8

Full scale trials and experimental verification

8.1 Introduction

As the wise Tamil poet Avvaiyar suggested, one cannot make ropes out of sand. To draw a parallel, simulation studies are useful to establish the initial validity of experimental cases. Nevertheless, to be useful in the real world, theoretical work has to be translated into its practical counterpart to be beneficial to society, to make a meaningful contribution to knowledge and further research progress. Hence, to establish the rationality of conclusions from simulation studies in previous chapters, experimental work was undertaken. The full scale trials discussed in this chapter illustrate the autonomous operation with *Springer*. Specifically, the USV's capacity to cope with changes in dynamics whilst preserving robust performance was investigated. These trials were carried out at Roadford Reservoir in Devon (UK) during 2013/14. The first experiments used the conventional (i.e. non-adaptive) MPC implementation in *Springer*. The LOS guidance system was used to generate the reference trajectory and wIKF was used to provide an estimate of the vehicle's current position. These trials were then repeated with the aMPC implementation of the autopilot. The same two autopilots were then tested with a gradual change in additional mass (from 100 to 0kg). Finally, a series of trials using the two autopilots were conducted with a sudden change in mass. It is

important to note that the mass changes (gradual and sudden) were implemented midway whilst *Springer* was in operation.

8.2 *Springer* test site for control system trials

The waypoint mission trials, gradual change in mass and sudden change in mass trials were carried out at Roadford Reservoir as seen in Figure 8.1.

Figure 8.1: The test site, Roadford Reservoir, Devon , United Kingdom

8.3 Experimental results

To summarise briefly, complete autonomous way-point following missions using three buoys in a triangle formation were successfully accomplished. The results of the different experimental configurations are presented below.

8.3.1 Autonomous trial 1 - verification of MPC parameters

Up to this point MPC parameters have been obtained from simulation studies, thus it was necessary to run an initial set of trials to verify these settings in the field. It was found that the parameter set (H_p=50, H_c=3) was appropriate and performance translated effectively to the test environment as evident from the following results. Therefore, the same prediction horizon H_p and the control horizon H_c parameters were used for all subsequent trials.

8.3.2 Autonomous trial 2 - MPC

The following Figure 8.2 illustrates the experimental test platform with its original configuration. This trial was the first test of the conventional MPC applied to an USV autopilot to achieve an autonomous waypoint mission. The results can be seen in the following figures which demonstrate the ability of the autopilot to reach the predefined waypoints with a high degree of accuracy as shown in Figure 8.3.

Figure 8.2: Original configuration of *Springer*

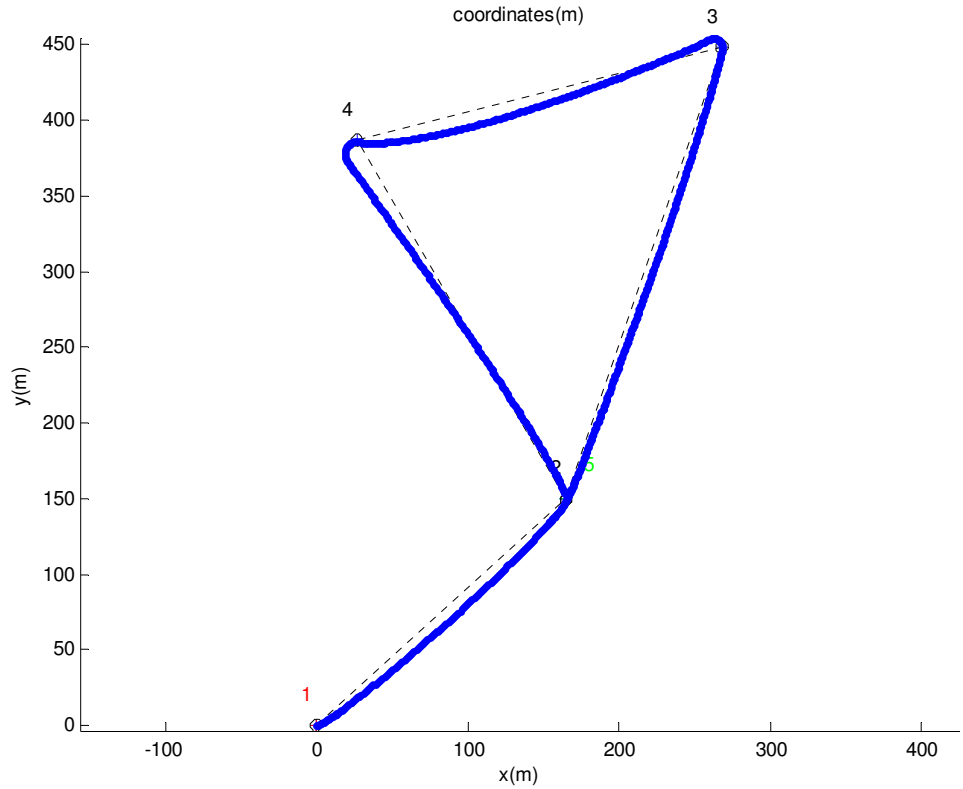

Figure 8.3: Waypoint following mission: conventional MPC

The following Figure 8.4 (a) shows the reference trajectory generated by the guidance systems (as explained in Chapter 5) and the actual heading of the USV. It is clear that there is very little deviation between the actual and reference trajectories. The second panel of this Figure 8.4 (b) shows the output of the gyroscope while the bottom panel of the Figure 8.4 (c) shows the output of the controller.

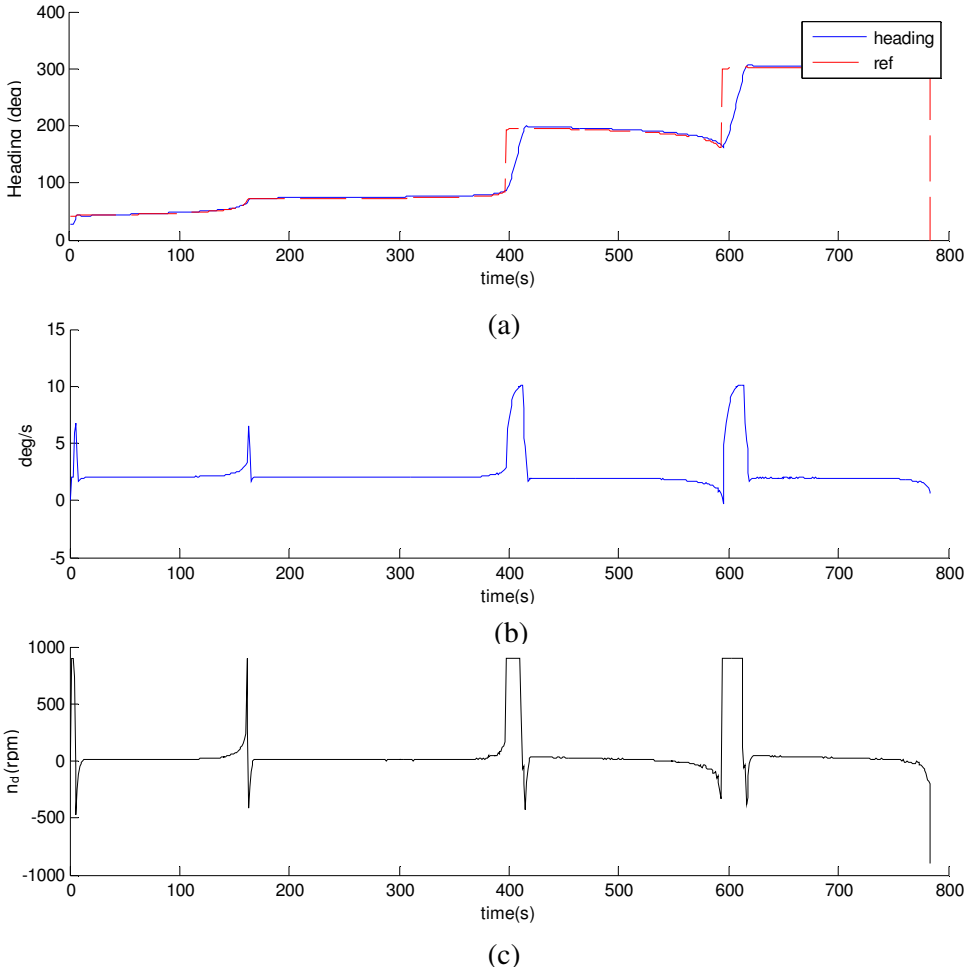

Figure 8.4: Outputs (a) reference and *Springer* heading (b) gyroscope output (c) controller output

In this trial the *Springer* utilised the conventional MPC and was able to reach all the pre-defined five waypoints. The total distance travelled by the vehicle was 1.0785e+03m. Average deviation from the reference trajectory was found to be 9.3959m. Average controller energy consumption was 11.7129 $(rps)^2/s$.

8.3.3 Autonomous trial 3 - aMPC

Here the aMPC controller was utilised for the autopilot. The same sets of predefined waypoints were chosen for the test in order to provide a framework for comparison of performance between the two controllers. Figures 8.5 and 8.6 (below) represent the same experimental parameters as in trial 2, waypoint following, reference and actual trajectories, outputs of the vessel, gyroscope and controller.

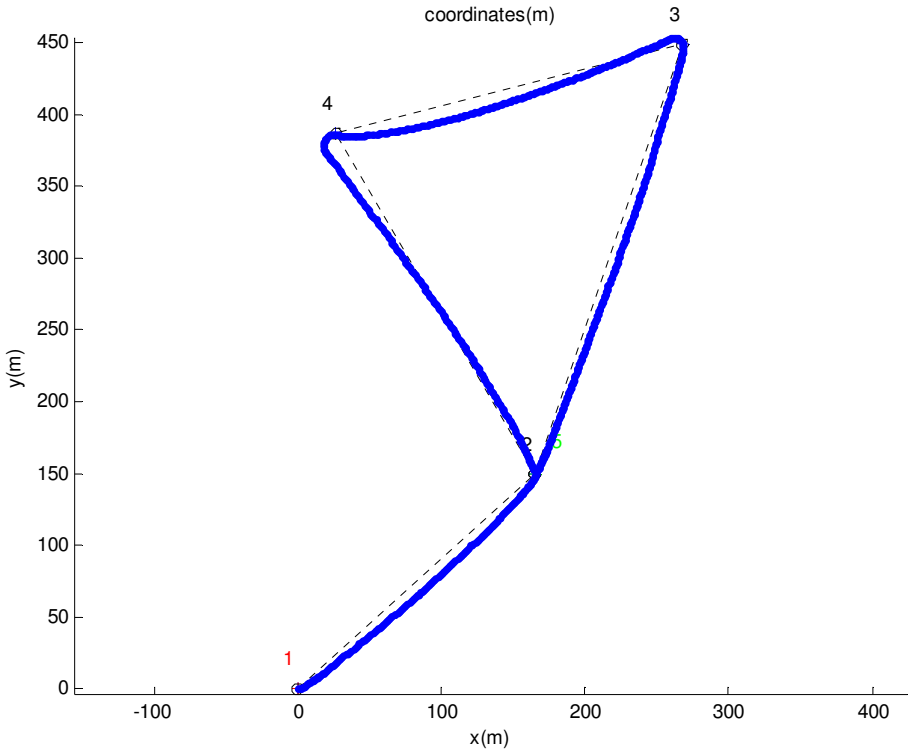

Figure 8.5: Waypoint following mission: aMPC

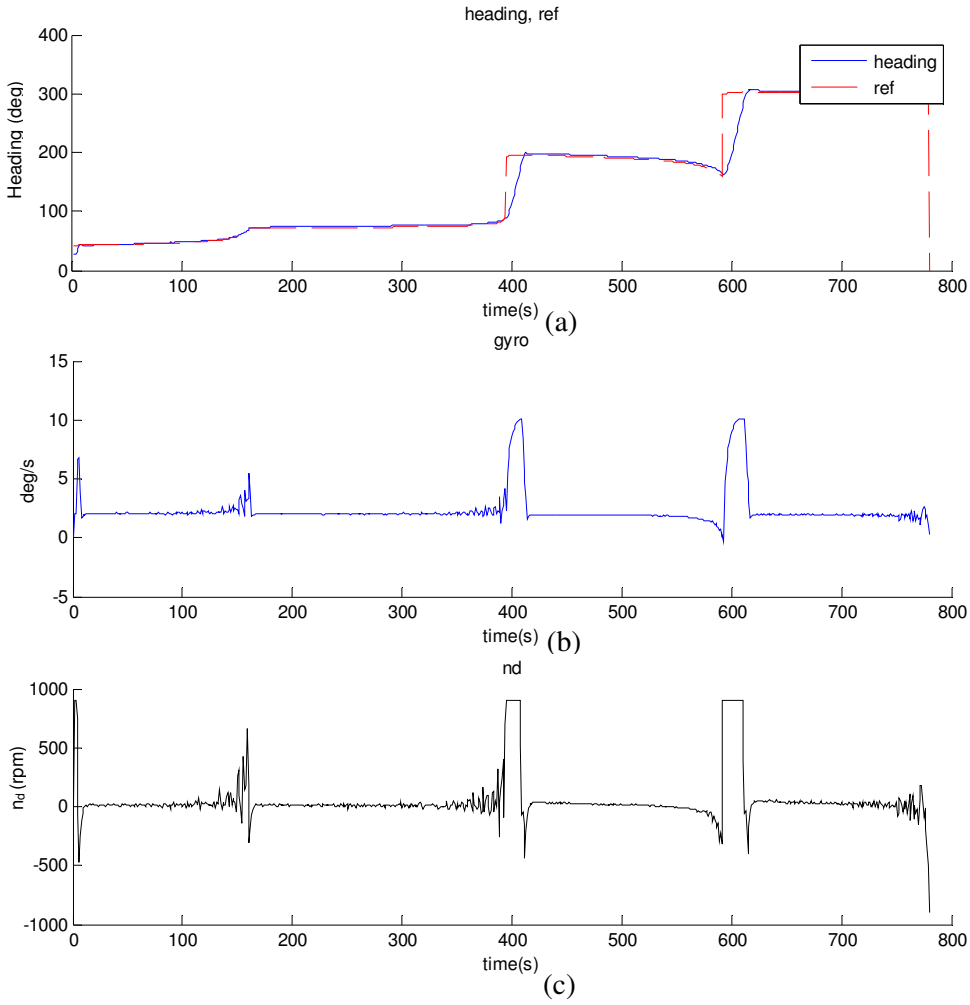

Figure 8.6: Outputs (a) reference and *Springer* heading (b) gyroscope output (c) controller output

In this trial the *Springer* utilised the aMPC algorithm and was able to reach all the pre-defined five waypoints, as previously with the standard MPC autopilot. The total distance travelled by the vehicle was 1.0804e+03m. Average deviation from the reference trajectory was found to be 9.4625m. Average controller energy consumption was 12.0036 $(rps)^2/s$.

As illustrated above, the difference in performance of the two controllers is seemingly marginal. However, at this juncture, it should be noted that the conventional MPC utilised an accurate model of *Springer* (0kg additional mass, 900rpm forward speed) as derived in Chapter 4. The level of performance of the conventional MPC was owing to the availability of a veridical model of the plant. Moreover, in this case there were no significant events (e.g. no change in mass) to test the adaptive capacities of the aMPC controller. Though the results from the two controllers were very similar, nevertheless this is the first time the aMPC has been implemented as an USV autopilot. Thus, these results function as a proof of concept and demonstrate the applicability of this controller to the problem of USV control and specifically it's potential as an autopilot for *Springer*.

8.3.4 Autonomous trial 4 - MPC (gradual change in mass)

In this trial a slow decrease in additional payload (from 100 to 0kg) was implemented with the MPC controller. The gradual change in mass was achieved by opening the taps in the jerry cans and allowing the water to flow out. The means for this procedure is illustrated below in Figure 8.7 (a) and (b).

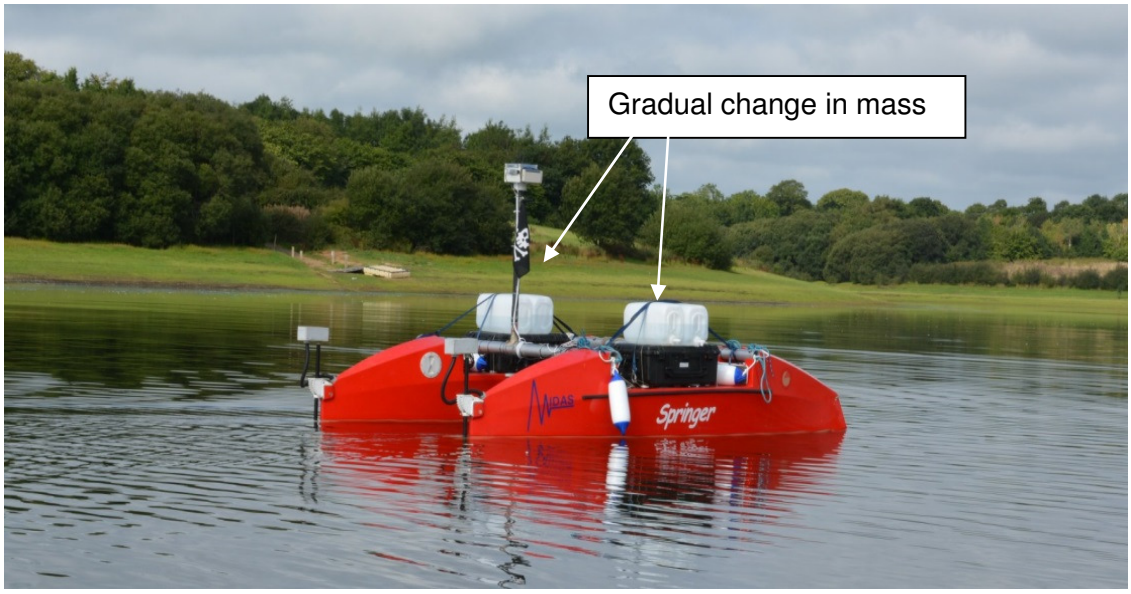

(a)

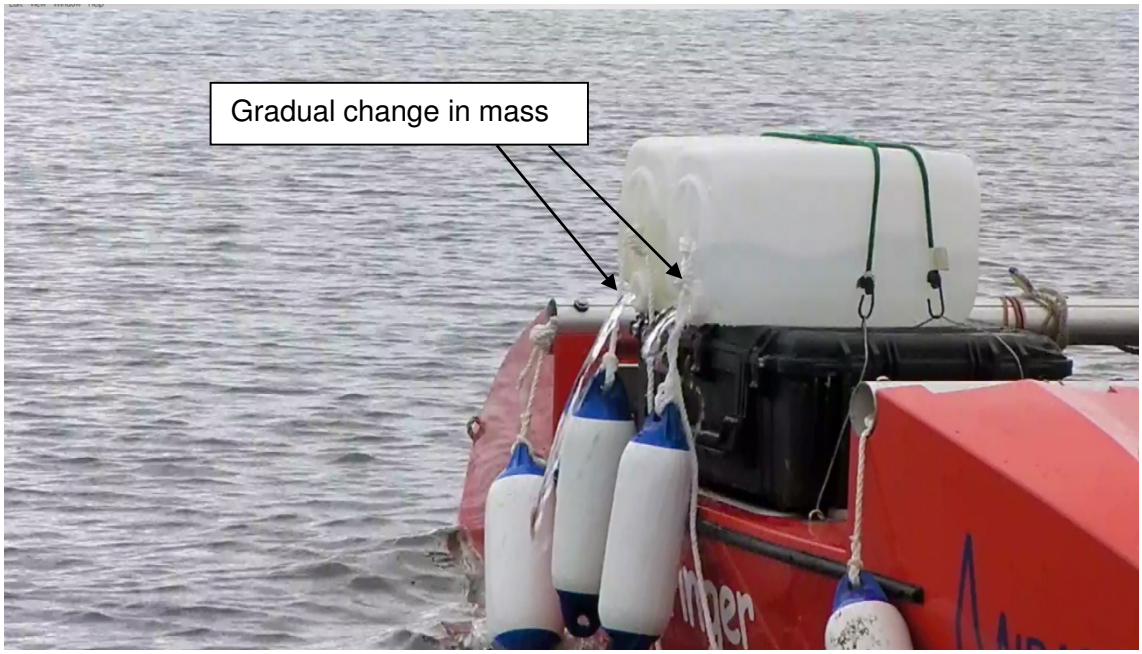

(b)

Figure 8.7: Experimental set up demonstrating gradual change in mass

(a) long distance (b) close up

The ability of the autopilot to reach a series of predefined waypoint/ follow a reference trajectory was established in trials 1-4. Thus, the focus of this experiment was to understand the behaviour of the autopilot with a gradual change in mass. Accordingly, the scope of this mission was limited to two waypoints. Figure 8.8 shows that although the vehicle eventually reached the predefined waypoint the performance of the controller was poor. The deviation from the reference trajectory is large and this implies a concomitant increase in energy consumption. It is clear that this would impose serious limitations on missions of longer duration.

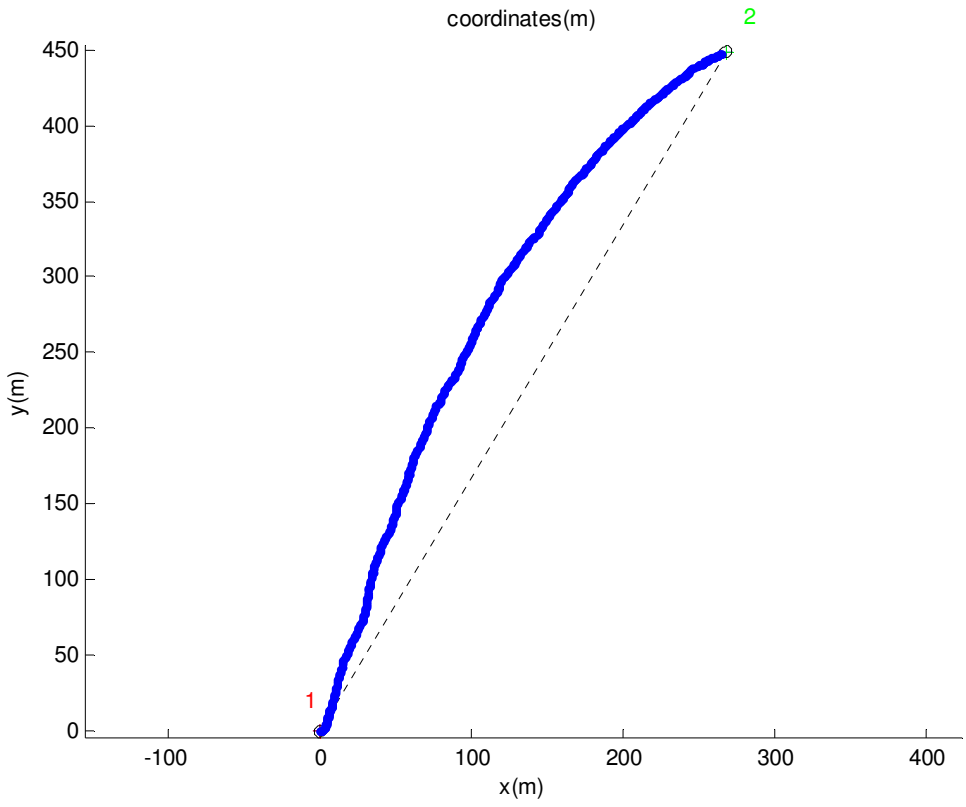

Figure 8.8: Gradual change in mass mission: conventional MPC

The following Figure 8.9 (a) shows the reference trajectory generated by the guidance systems and the actual heading of the USV. Figure 8.9 (b) shows the output of the gyroscope, whilst Figure 8.9 (c) shows the corresponding output of the controller.

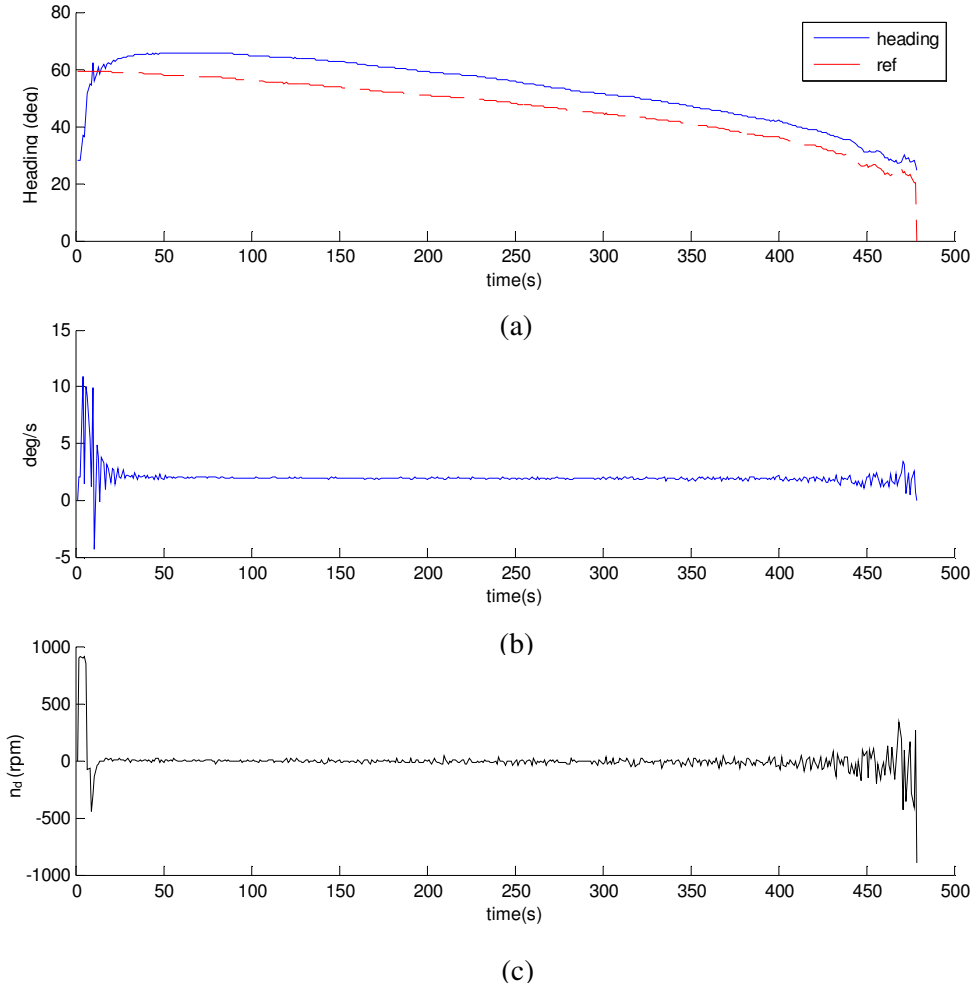

Figure 8.9: Outputs (a) reference and *Springer* heading (b) gyroscope output (c) controller output

In this trial the *Springer* utilised the conventional MPC and was able to reach two pre-defined waypoints, despite an intermediate gradual change in mass en route. The total distance travelled by the vehicle was 546.8731m. Average deviation from the

reference trajectory was found to be 142.2072m. Average controller energy consumption was 3.7636 $(rps)^2/s$.

8.3.5 Autonomous trial 5 - aMPC (gradual change in mass)

With the aMPC and a gradual change in payload mass, deviation from the reference trajectory is reduced and the actual trajectory of the vessel is thus more energy efficient. So with these innovations to the controller, longer missions become plausible. The following Figure 8.10 illustrates the gradual change in mass mission whilst using aMPC.

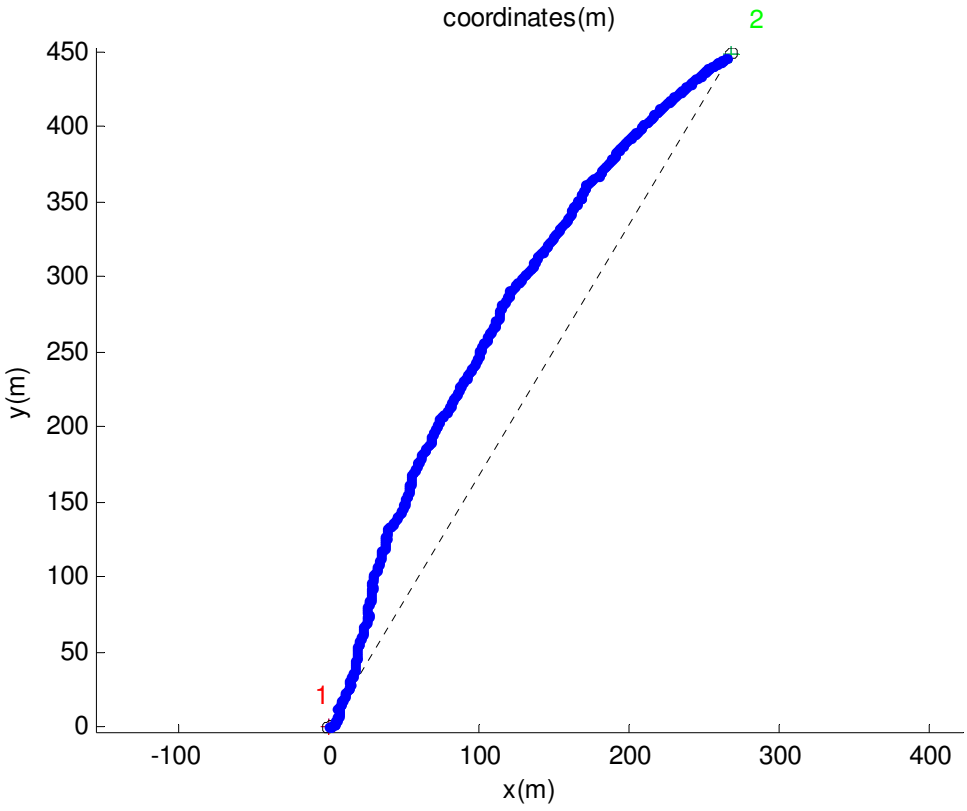

Figure 8.10: Gradual change in mass mission: aMPC

The output of the vehicle, the reference trajectory, the outputs from gyroscope and controller during this trial are summarised in the following Figure 8.11.

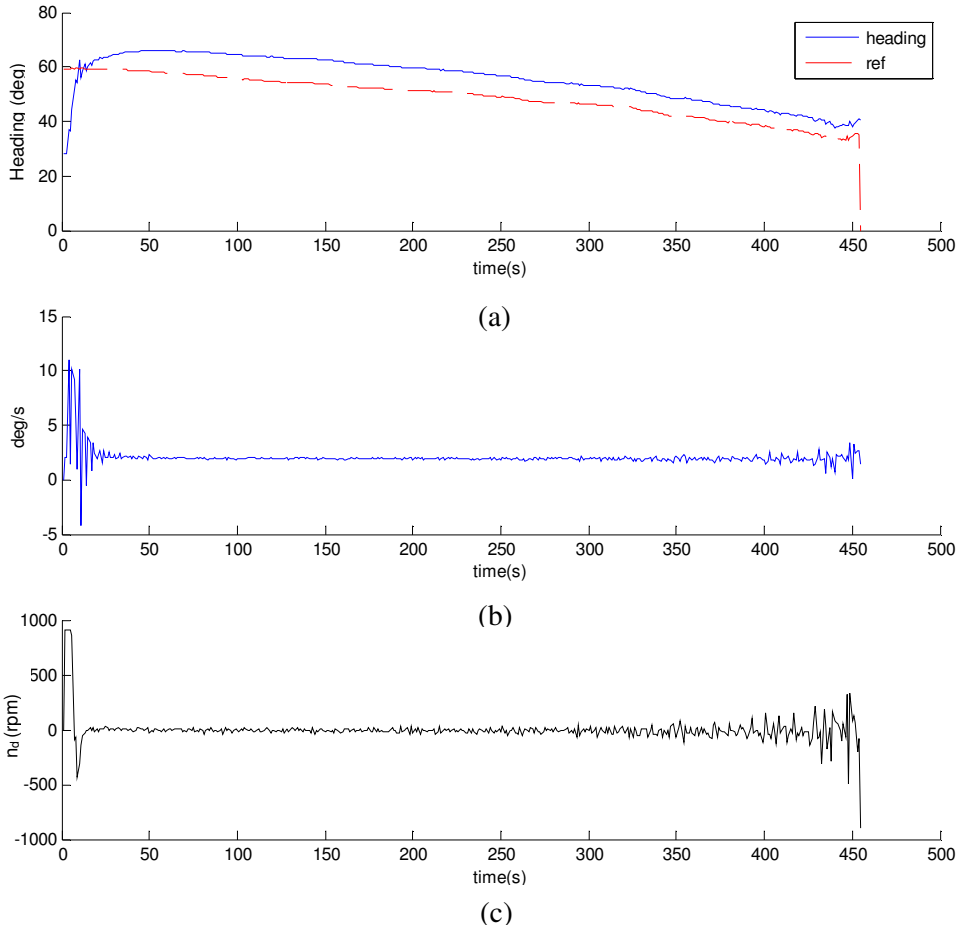

Figure 8.11: Outputs (a) reference and *Springer* heading (b) gyroscope output (c) controller output

In this trial the *Springer* utilised the aMPC and was able to reach two pre-defined waypoints, despite an intermediate gradual change in mass en route. The total distance travelled by the vehicle was 555.2682m. Average deviation from the reference trajectory was found to be 135.5705m. Average controller energy consumption was 3.9368 $(rps)^2/s$.

8.3.6 Autonomous trial 6 - MPC (sudden change in mass)

Designs for a number of mechanisms to obtain a sudden change in mass whilst *Springer* was in operation were investigated. Finally, it was decided to remove the additional mass on-board *Springer* at a pre-defined time in the mission by pulling the jerry cans off *Springer* by use of ropes attached to two adjacent RHIBs. This procedure is shown in Figure 8.12 (below). Whilst the results presented thus far show a relatively small difference in the performance of the two controllers, this experiment (with sudden change in mass) clearly demonstrates the significant improvement offered by the aMPC over the MPC. The following Figure 8.13 (a) and (b) shows the deviation of the actual trajectory from the reference under conditions of a sudden decrease in payload (from 100kg to 0kg). The deviation becomes very pronounced and remains so as the plant cannot adapt to the new vessel dynamics.

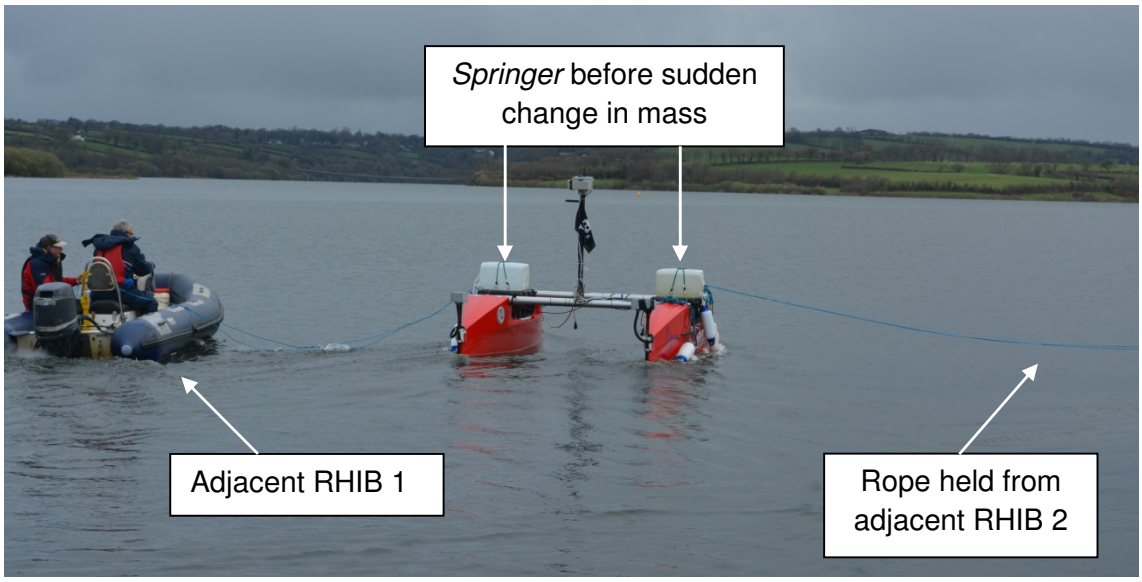

(a)

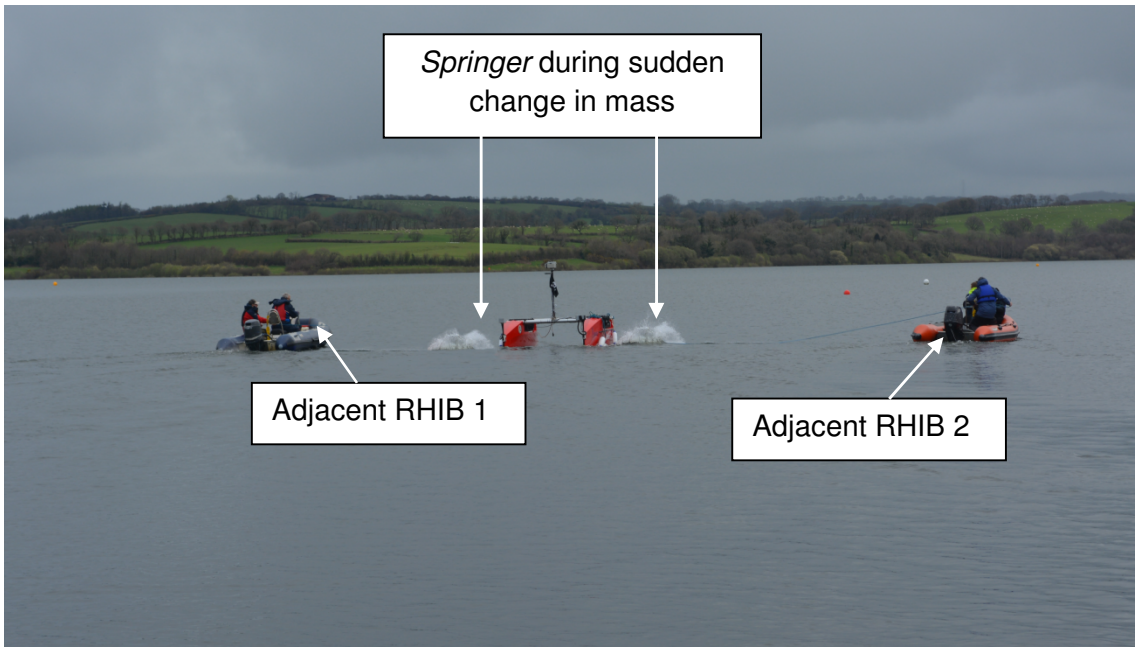

(b)

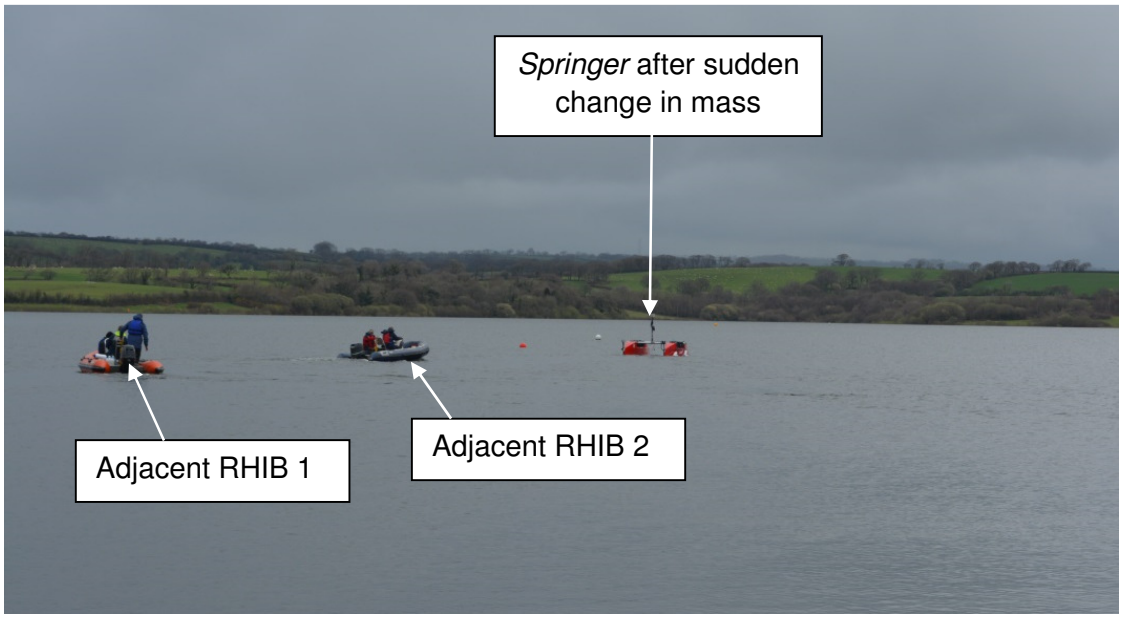

(c)

Figure 8.12: Experimental set up (a) *Springer* before change in mass (b) *Springer* during change in mass (c) *Springer* after change in mass

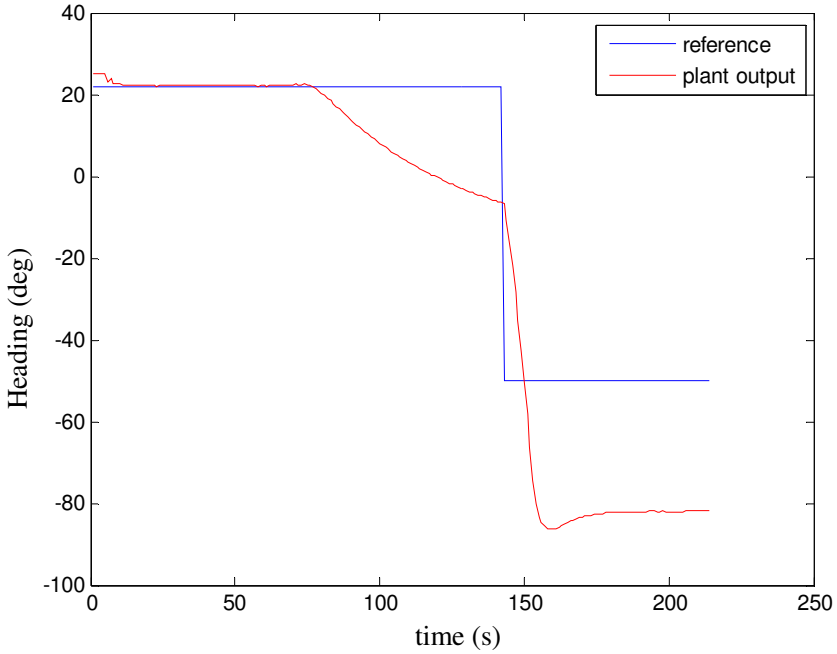

(a)

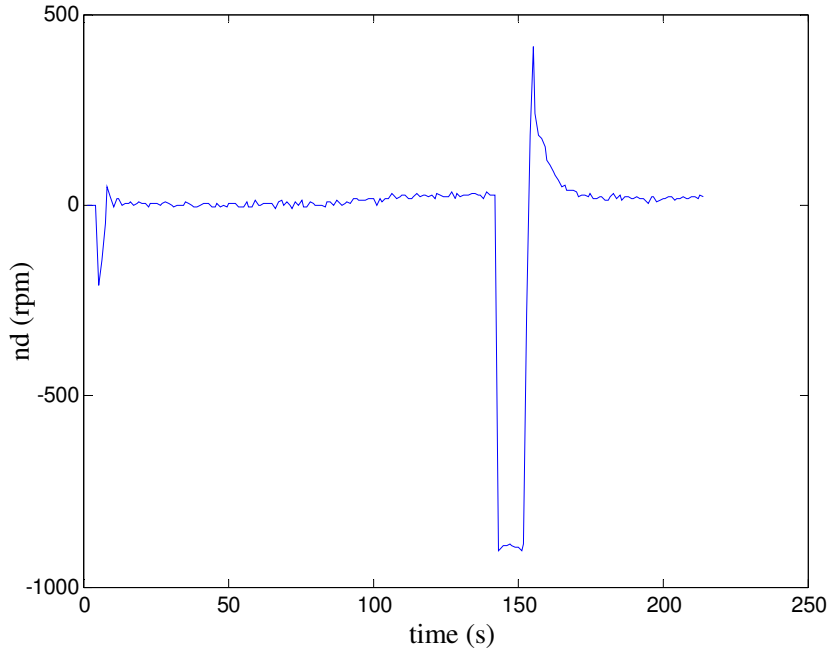

(b)

Figure 8.13: Sudden change in mass: conventional MPC

(a) reference and *Springer* heading (b) controller output

To reiterate, the focus of this experiment was to verify the performance of the autopilots under conditions of a sudden change in mass whilst the vehicle is attempting to follow a reference trajectory.

In this trial the *Springer* utilised conventional MPC. The root mean square value of the error in heading was 21.2525 degrees. Average controller energy consumption was 11.2701 $(\text{rps})^2/\text{s}$. From the above, it is evident that the vehicle is unable to recover after a sudden change in mass and loses its ability to track a given reference trajectory. This has serious implications. If such a change happens during a mission, subsequent to this event the vehicle will not be able to keep its course. This may result in untoward behaviour on the part of the vessel and potentially accidents involving other marine vehicles/obstacles. Hence, a mission may need to be aborted before accomplishment of the desired objectives if a sudden change in mass were to occur.

8.3.7 Autonomous trial 7 - aMPC (sudden change in mass)

This trial entails the same experimental set up as in trial 6. However, in this case the aMPC is used for the autopilot. As shown in Figure 8.14, the aMPC is able to respond to the sudden change in payload (Figure 8.14a and b) and to continue following the reference trajectory. There is an initial deviation from the reference trajectory followed by a rapid recovery. Thus, the adaptive controller demonstrates its capacity to respond efficiently and effectively to a sudden change in vessel dynamics.

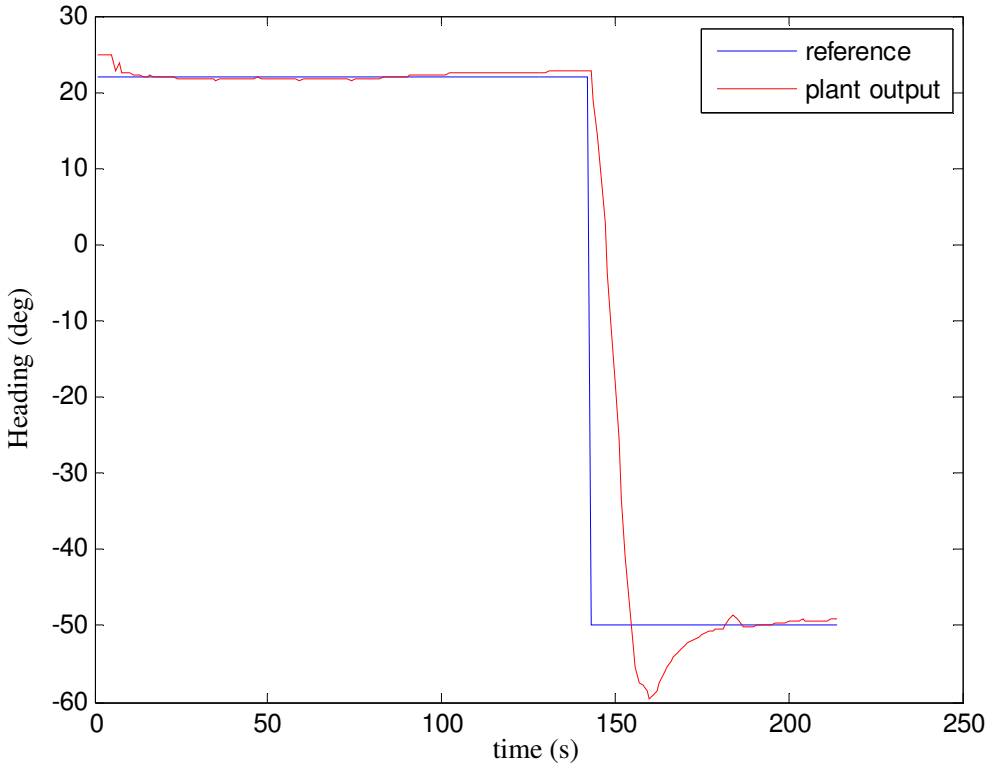

(a)

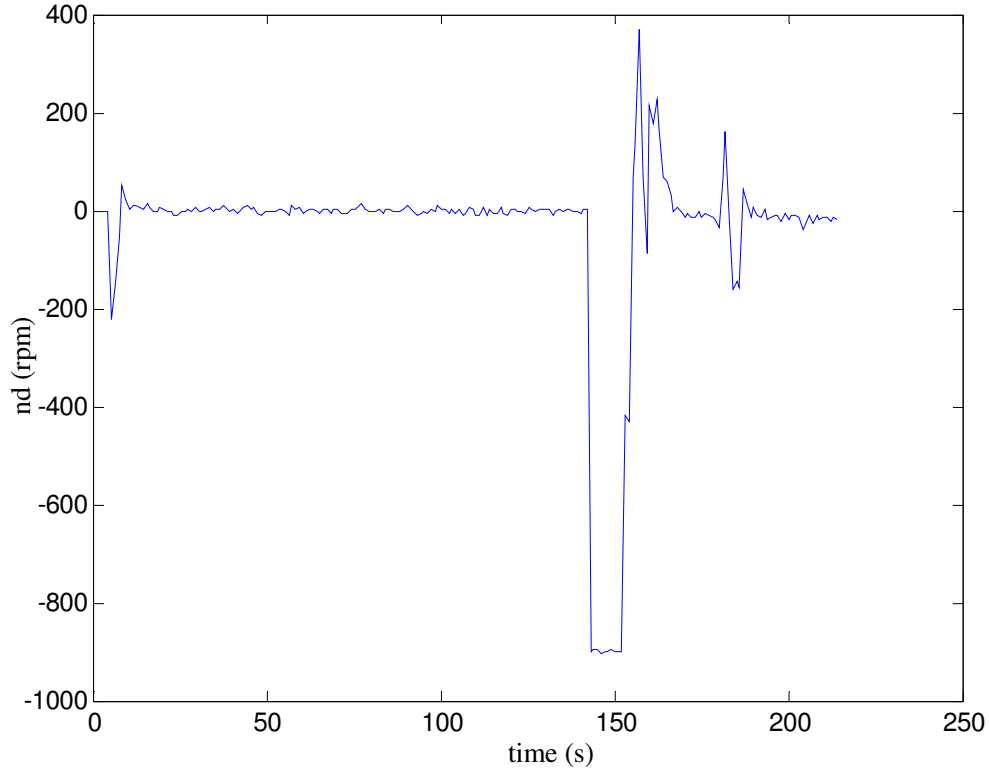

(b)

Figure 8.14: Sudden change in mass: aMPC (a) reference and *Springer* heading

(b) controller output

The aim of this trial was to verify the performance of aMPC autopilot under conditions of a sudden change in mass, whilst the vehicle is attempting to follow a reference trajectory.

The root mean square value of the error in heading was 11.2026 degrees. Average controller energy consumption was 11.7250 $(rps)^2/s$. Most importantly, the vehicle is able to follow the required reference trajectory, despite sudden change in mass. This is primarily due to the adaptive nature of the algorithm. The variation in parameters during the sudden change in mass trials is illustrated in Figure 8.15 (below). As explained in Chapter 4, the parameters a_1, a_2, a_3, a_4; b_1, b_2, b_3, b_4 represent the true dynamics of *Springer* at a given point in time. The simulation studies reported in Chapter 7 show that the sudden change in payload induces change in system dynamics (as represented by the parameters a_1, a_2, a_3, a_4; b_1, b_2, b_3, b_4). Similarly in field trials, changes in these parameters were observed following the sudden change in mass, as shown in Figures 8.15 and 8.16 (below).

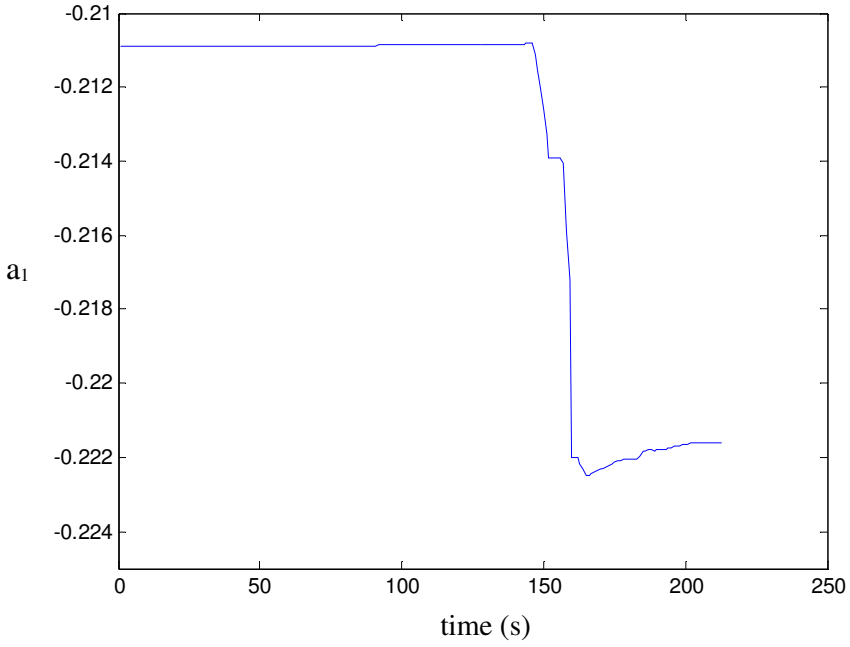
-0.21
-0.212
-0.214
-0.216
-0.218
-0.22
-0.222
-0.224
a1
0
50
100
150
200
250
time (s)

(a)

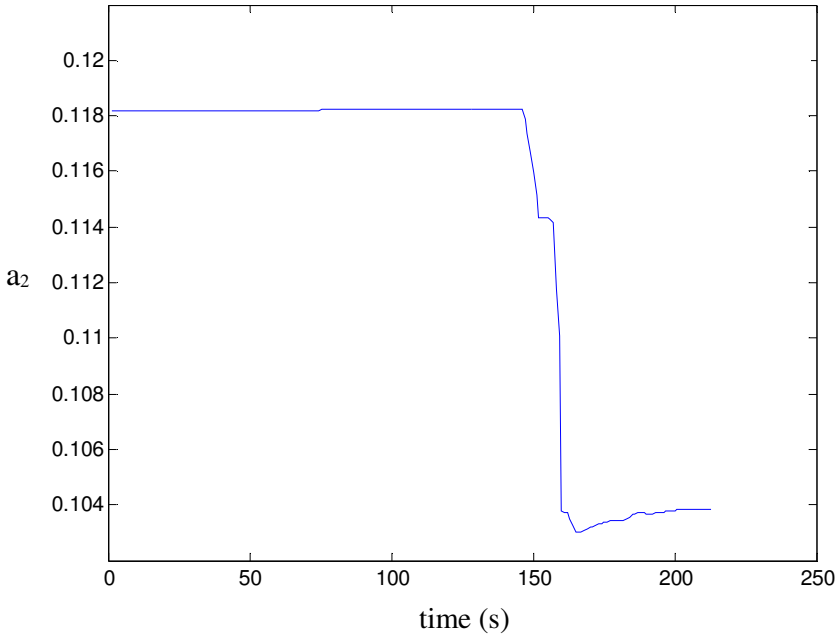
0.12
0.118
0.116
0.114
0.112
0.11
0.108
0.106
0.104
a2
0
50
100
150
200
250
time (s)

(b)

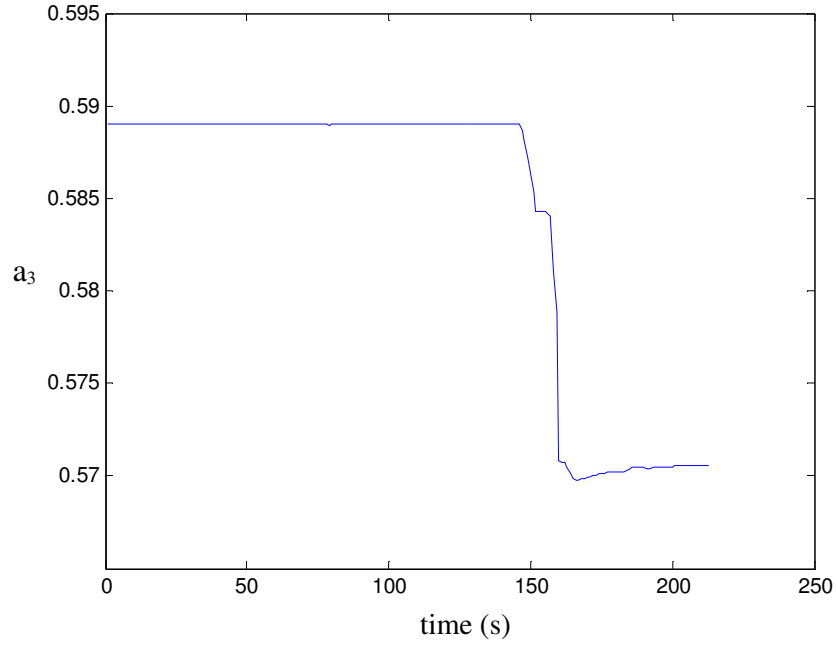

(c)

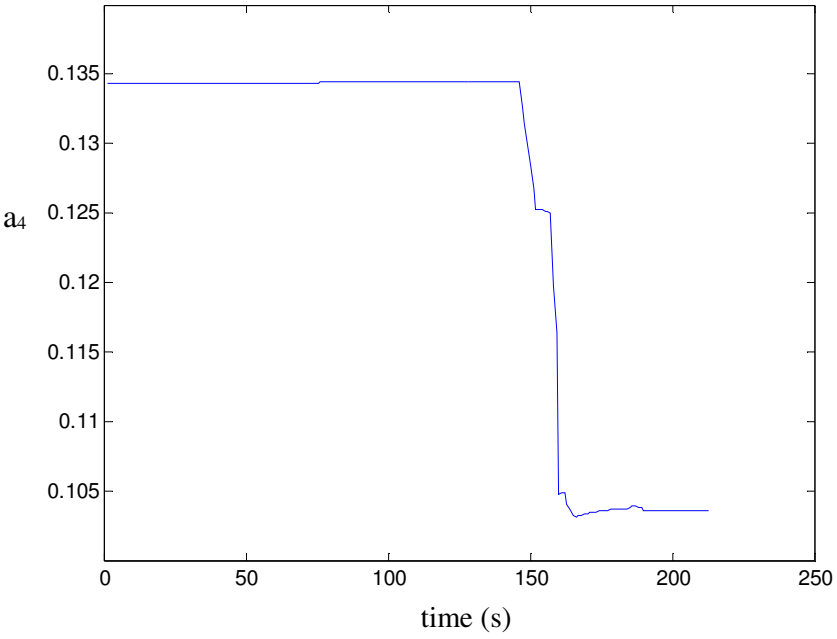

(d)

Figure 8.15: Variation in a parameters during sudden change in mass (a) parameter a_1 (b) parameter a_2 (c) parameter a_3 (d) parameter a_4

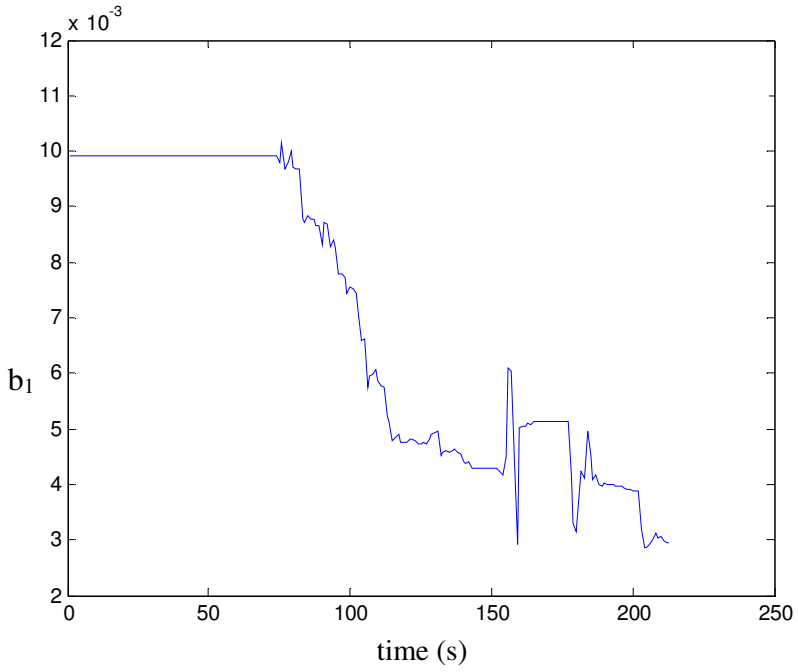
x 10^-3
12
11
10
9
8
7
6
5
4
3
2
b1
0
50
100
150
200
250
time (s)

(a)

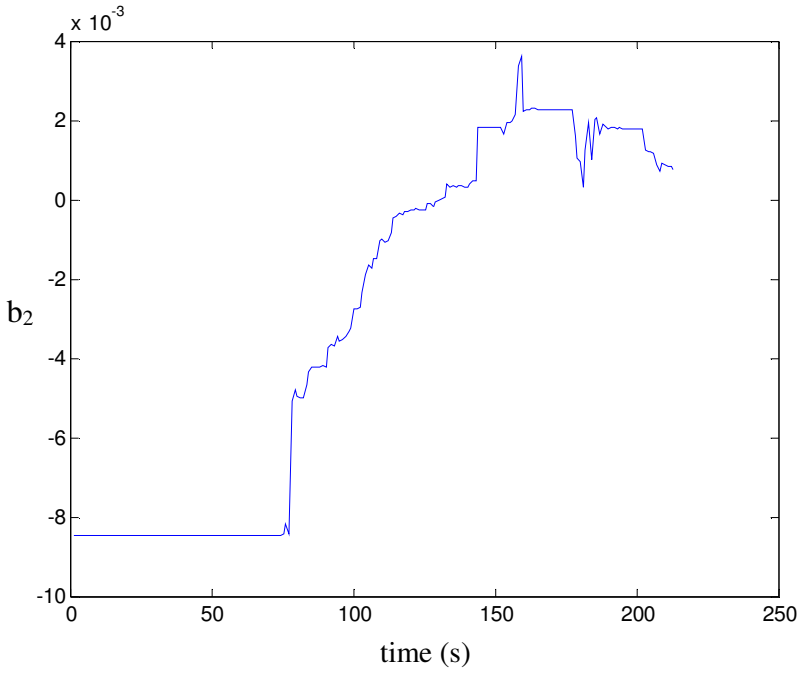
x 10^-3
4
2
0
-2
-4
-6
-8
-10
b2
0
50
100
150
200
250
time (s)

(b)

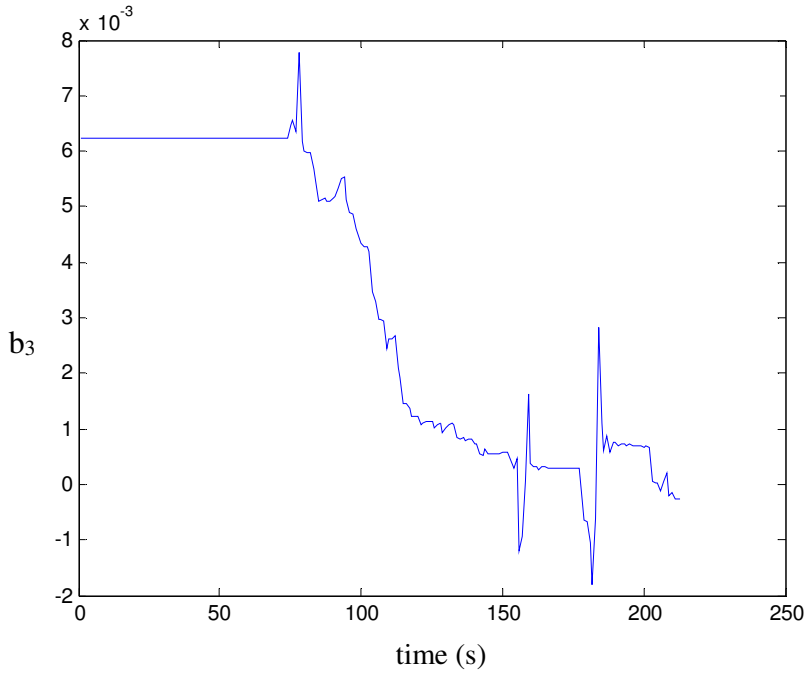

(c)

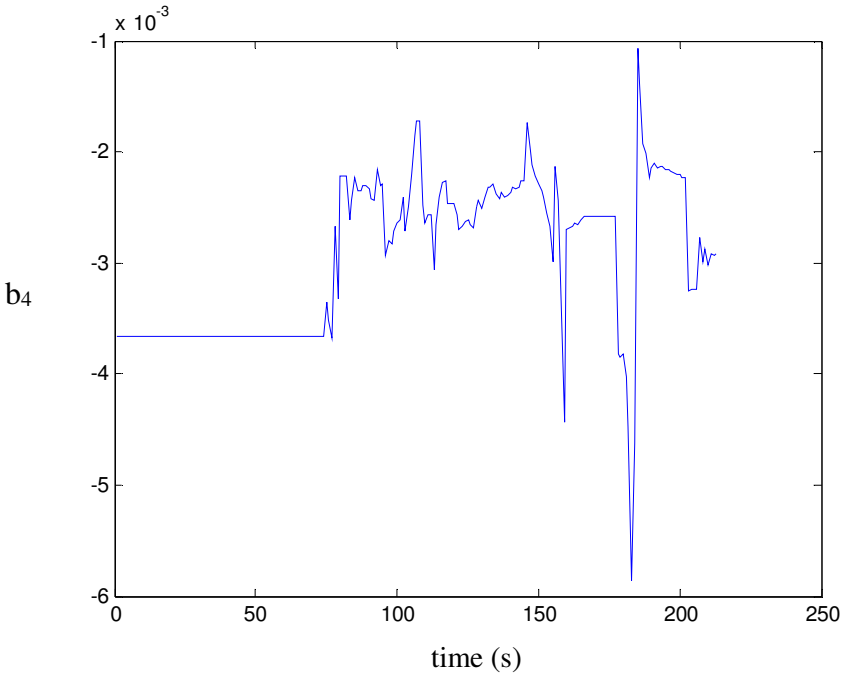

(d)

Figure 8.16: Variation in b parameters during sudden change in mass (a) parameter b_1 (b) parameter b_2 (c) parameter b_3 (d) parameter b_4

8.4 Discussion

The successful test results presented above were not achieved without difficulties. It is beyond the scope of this discussion to elaborate on all the practical and procedural issues encountered during the experimental phase. However, a brief overview of some of the major obstacles encountered and the corresponding solutions are detailed in this section.

There were several issues with the hardware/software which were not detected during dry trials, such as the main interface window leading to the autopilot action not being transferred adequately to the motors. On several occasions prior to the trials there were issues with the WiFi connectivity which had not appeared before, and during trials problems with access to a serial COMM port (one of the compasses), one of the GPS receivers, and the computer crashing on a couple of occasions. Though it was not always possible to fully regulate the test environment beyond human control, care was taken to ensure that the test conditions were as similar as possible in all the trials. Several autonomous missions were carried out via the successful integration of navigation, guidance and control systems. However, it was not possible to complete all the intended trials during the experimental phase owing to adverse weather conditions, unexpected issues, and the consequential operational difficulties. At this juncture, it is worth mentioning however, that some of these complications were useful in that they provided an opportunity to establish that *Springer* could operate under less than ideal circumstances.

An additional issue to be solved concerned some initial problems in connecting the RoboteQ controller to the laptop. The USB to serial port convertor and the electrical wiring of the propeller motors was identified as the problem. Subsequently, a solution was found and connection to the laptop was achieved. Thereafter the RoboteQ controller was tested for different settings.

Furthermore, it is interesting to note that the simulation studies were conducted with actuator saturation limits +/- 300 rpm and maximum step change was restricted to 20. These were values based on similar studies from the literature however during field experimentation it was soon realised that these parameters were overtly restrictive. This resulted in the vehicle being slow to follow the trajectory generated by the guidance system (as explained in Chapter 5). Heuristically, these parameters were altered at the test site, after a period of experimentation parameters were increased to +/- 900 rpm. Further details of motor saturation can be found in Chapter 4. Additionally, the rationale for choice of step change to be 20 during simulation studies was owing to concerns that too great a step change could damage the electrical circuitry for the motors. Conversely, this was not found to be the case in field tests conducted with *Springer* at Roadford Reservoir. In reality step changes of up to 500 were allowed to enable the motor to respond quickly so that the vehicle could follow the desired trajectory effectively.

It should also be noted that the result of the way-point following mission was hard to replicate for every trial. One of the problems encountered was that the trajectory followed is highly dependent on the initial heading of the vehicle at the first (starting) way point. It was necessary to start with the same heading angle, as well as the same position in each case in order to be able to compare one mission with the subsequent

mission. Further, it was challenging to manually control the vessel to follow a path owing to the unpredictable and ever changing currents.

One possible solution consisted of adding a fictitious "pre-initial way point" close to the first way-point. This ensured the alignment with the first two way-points to calculate the desired heading angle and manually steer the vehicle along the path from this "pre-waypoint" to the initial way-point before letting the autopilot take over. However, this did not work in practice because the variation in the initial heading angle of the vehicle affected the mission as a whole.

However, an easier and more practical solution was adopted which consisted in initiating the autonomous mission at launch of the vehicle from the same point of the jetty and facing in the same direction for each of the trials.

8.5 Conclusions

This chapter has described the test environment, modifications to the configuration of *Springer* and test procedures that were required for experimental verification. Integration of the NGC systems was achieved on-board *Springer* during full scale verification trials at Roadford Reservoir. This paved the way to conducting further experiments as described in this chapter. *Springer* proved capable of performing effective waypoint missions under a number of test scenarios. The aMPC based controller was found to be able to adapt to a sudden change in mass of the plant thus achieving a significant improvement in performance over the MPC controller and this satisfied a main objective of this research project as a whole.

Chapter 9
Summary, conclusions and recommendations for further work

Veritas Vos Liberabit

9.1 Summary

The overall aim and objectives of the *Springer* project and of this particular research were detailed in Chapter 1. The subsequent chapters sequentially elucidated the theoretical and experimental approaches entailed in achieving the stated aims and objectives for this research project.

Chapter 2 delineated historical developments with respect to USVs, MPCs and marine control systems. A number of USVs built by research institutions and marine companies are presented. It highlights recent interest in the application of modern controllers such as MPC to USVs - growing interest evidenced by the support provided by the ONR for studies in this area. At this juncture, it is interesting to note that research groups across the globe have begun to look at developing modern autopilots for USVs. In this thesis, work has been done to explicate a historical perspective on the origins and development of MPCs within the petrochemical industry. This approach has facilitated a deeper understanding of the challenges associated with innovative approaches to adapting MPC

technology to work with dynamic systems such as *Springer*. In addition, this chapter also highlights some gaps in the literature that warrant further investigation.

Having elucidated the theoretical background essential to the execution of this research project, thereafter in Chapter 3, the individual components used in the test platform *Springer,* were described. A number of innovations were made to the hardware setup of the research test platform, *Springer*. These advances served to increase mission duration, reliability of on board electronic systems and the overall performance of the test platform. One such modification comprised dispensing with the necessity for AC to DC conversion via the use of an Intense Pro PC. In addition an increase in feasible mission duration was obtained via improvements to heat dissipation within the system. Furthermore, the risk of system failure was reduced by the removal of mechanical moving components and potential hazards associated with the umbilical cord (required to enable manual override) were avoided through use of WiFi. Full details of the components on-board *Springer* are provided in Chapter 3 and the respective appendices.

Chapter 2 made clear that the success of utilising MPC as an autopilot for an USV was very much dependant on the accuracy on the model of the system. Hence, Chapter 4 is dedicated to understanding the different approaches to obtain a realistic, cost effective and accurate model of the vessel. Approaches such as rigid body modelling, CLID and SI were explored in Chapter 4. Owing to the complexity, time constraints and financial implications of the other approaches explored, it was decided to utilise SI for obtaining a suitable model of *Springer.* Hence, further trials were carried out at Roadford Reservoir where various tests were conducted for different forward speeds of 450 rpm, 900 rpm and 1200 rpm. Experiments were conducted for each of the forward speeds,

with three different cases of additional mass (0kg, 50kg and 100kg) in *Springer*. Thereafter, a new modelling technique is developed and the data collected from these experimental results are utilised to obtain a generalised ARX and ARMAX models of *Springer* by applying this innovative technique, which is detailed in Chapter 4.

Chapter 5 described the contemporary guidance and autopilot designs. This chapter covered the considerations that led to the adoption of waypoint LOS as a guidance system for *Springer*. Traditional autopilots based on PID techniques have been utilised in the shipping industry for many years. As the USV industry is still in its infant stage there is extensive scope for development of this technology. Hence, simulation studies were undertaken in Chapter 5 to explore the application of PID to *Springer*. Subsequently, the performance of modern controllers such as LQG was analysed and the results also presented in Chapter 5. Furthermore, different state estimation techniques, namely KF, IKF and wIKF were also presented. A wIKF navigation system was employed in field experiments conducted at Roadford Reservoir and this work was described in Chapter 8. The viability of innovative modifications such as a new combination of LQR and IKF was studied and the suitability of such a combination for USVs such as *Springer* was established. As far as the author is aware, this is a novel approach and as such comprises a useful new contribution to knowledge.

Elaborating on the ideas presented in Chapter 2, the important concepts of MPC were discussed in detail in Chapter 6. Application of MPC to *Springer* was analysed and the simulation results for a combination of various parameters were presented in this chapter. These results further reinforced the superior performance and suitability of MPC as an autopilot for *Springer* and other similar USVs.

Chapter 6 established the suitability of MPC to function as an autopilot however it also highlighted the inherent risks, as such a controller is highly reliant on the accuracy of the internal model to perform its pre-defined tasks. The need for adaptive autopilots was established in Chapter 7 and a solution to this problem provided. The suitability of different algorithms such as GD, LS and WLS for use in conjunction with MPC was also explored in this chapter. Further modifications were suggested and significant improvements were achieved with a combination of a novel WLS in conjunction with the MPC to work in coordination with navigation and guidance systems (as discussed in Chapter 5). To the best knowledge of the author, such an innovative adaptive autopilot for USVs did not previously exist; therefore this also comprises a novel contribution to knowledge in this domain.

The experimental site used for verification of autonomous missions is described in Chapter 8. Autonomous *Springer* mission experiments were conducted and the results presented in this chapter. Further experiments were carried out with a gradual change in payload mass from 100kg to 0kg and the performance of the aMPC and MPC autopilots were presented. Finally, experiments with a sudden change in mass were conducted and the performance of MPC and aMPC were also examined in this chapter. The superior performance of aMPC was clearly demonstrated by the experiments conducted and this is summarised in Chapter 8. Hence, this adaptive autopilot is recommended for USVs such as *Springer* to enable them to perform multi-various roles/missions.

9.2 Conclusions

Research was undertaken in the field of USVs, trends in marine control and different strategies of MPC to understand the background information essential to progress

further with this project. This provided an overview of current developments in a plethora of areas that had to be applied in this project and facilitated the identification of gaps in the research literature. Preliminary trials were conducted at Roadford Reservoir, Devon, United Kingdom and the yaw response of the *Springer* was examined and recorded. This data was utilised to derive a mathematical model from SI techniques. The models thus obtained were used in the autopilot design. Subsequently, integration between the NGC systems was achieved on-board *Springer*. This was verified by a series of full scale trials to evaluate the performance of autopilot.

The accuracy of the model of the plant is a critical component to the successful design of MPC. This became very evident when there was a sudden change in mass on-board *Springer*. It is important to note that while a sudden change in mass induces change in the system dynamics, this is not the only source of perturbation. Changes in wind direction, underwater currents and surface effects all contribute to changing system dynamics and the response of the vessel to the corresponding controller action. There is work being done to model such effects on system dynamics however this requires extensive use of additional expensive technology. In the work described here, this data is inferred from the relatively low-cost sensors on-board *Springer* and the aMPC is able to cope with such perturbations automatically and continuously.

Thus, the aims and objectives as in Chapter 1 were successfully achieved over a period of three years and are summarised through the various chapters of this thesis. Therefore, the primary aim, as set out at the beginning of this PhD study, which was to design and develop an autopilot with accompanying adaptive features for the USV *Springer* was

accomplished. The specific goal of this research was to implement an adaptive MPC based autopilot for an USV and to establish the robustness of its performance under a number of operating conditions. In the field experiments conducted at Roadford Reservoir various operating scenarios were set up including both gradual and sudden changes in on-board payload. This adaptive capacity opens up new mission capabilities for USVs and enables autonomous operation despite challenging mission requirements.

Field experiments at Roadford demonstrated that the MPC based autopilot was unable to adapt to changes in vessel dynamics (in this case induced by sudden decrease in payload). By contrast the aMPC autopilot was able to adapt to such perturbations and to maintain robust performance even under conditions of sudden alterations to system dynamics. Thus, this thesis has, to the best of the author's knowledge, presented the first known applications of a number of novel techniques to the domain of system modelling and autopilot design for USVs. The outcomes of this research have been disseminated through peer-reviewed journal papers and conference publications. A number of suggestions for future work to further advance this technology have also been made in the section that follows (9.3).

9.3 Recommendations for future work

In scientific research and advances in engineering, there is always scope for further development. Much of human progress has relied upon constant innovation and improvisation with existing technologies over extended periods of time. Hence, the following recommendations for further work are forwarded:

- The challenging primary task of reaching the desired destination by controlling the yaw angle has been the focus of this research. Another equally taxing and important area of research is the dynamic positioning of USVs, this can be investigated further.

- Significant improvements were made in developing hardware on-board *Springer* (as detailed in Chapter 3). Although, TCM2, HMR3000, KVH-C100 were satisfactory, the rapid progression of developments in the field of micro electromechanical components and nano technology have produced a plethora of new compact sensors that could be employed in further *Springer* development.

- Collision avoidance and path planning can be incorporated to form an advanced guidance system in *Springer.*

- A number of 'mini-USVs' could be built to perform operations which require mutual co-operation and co-ordination. Other allied projects to progress development of such portable USVs such as Sutton USV (as in appendix A5) could be pursued further.

- Maritime laws are carefully defined by international authorities to specify how commercial and military vessels should behave in international waters. The roles of USVs are still in a nascent stage. Hence, there are no clear rules and regulations pertaining to their operation. This necessitates further investigation to make USV autopilot designs compliant with the Convention on the International Regulations for Preventing Collisions at Sea (COLREGs).

"finito"

References

Åkesson, J., and Slätteke, O., (2006). Technical Report ISRN LUTFD2/TFRT-7615-SE, Department of Automatic Control, Lund University, Sweden.

Allgower, F., Glielmo, L., Guardiola, C., and Kolmanovsky, I., (2010). *Automotive model predictive control.* Springer-Verlag, Berlin, Germany.

Alves, J., Oliveira, P., Pascoal, A., Rufino, M., Sebastião, L., Silvestre, C., (2006). Vehicle and Mission Control of the *Delfim* Autonomous Surface Craft, Proceedings of the 14th Mediterranean conference on Control and Automation, 28-30 June, Ancona, Italy, pp.1-6.

Anderson, P., and Stone, H., (2007). Predictive guidance and control for a tail-sitting unmanned aerial vehicle. Proceedings of the Information Decision and Control, 12-14 February, Adelaide, Australia, pp. 148-153.

Annamalai, A.SK. and Motwani, A., (2013). A comparison between LQG and MPC autopilots for inclusion in a navigation, guidance and control system. Springer Technical Report, MIDAS SMSE.2013.TR.006, Plymouth University, Plymouth, United Kingdom.

Annamalai, A.SK., (2012). A review of model predictive control and closed loop system identification for design of an autopilot for uninhabited surface vehicles, Springer Technical Report*:* MIDAS.SMSE.2012.TR.005, Plymouth University, Plymouth, United Kingdom.

Annamalai, A.SK., Motwani, A., Sutton, R., Yang, C., Sharma, SK. and Culverhouse, P., (2013). Integrated navigation and control system for an uninhabited surface vehicle based on interval Kalman filtering and model predictive control. Proceedings of the 1st IET Control and Automation Conference*,* Conference Aston, Lakeside Centre*,* 4-5 June, Birmingham, United Kingdom.

Ashino, R., (2004). Wavelet analysis for system identification. Japan Society for the Promotion of Science, Japan-U.S. Cooperative Science Program (2003–2004), pp.1-16.

Ashrafiuon, H., Muske, K.R., McNinch, L.C. and Soltan, R.A., (2008). Sliding-mode tracking control of surface vessels. *IEEE Transactions on Industrial Electronics,* volume 55, issue 11, November, pp. 4004-4012 .

ASR Ltd., (2012) Fukushima radioactive Ocean impact map (www.asrltd.com/japan/plume.php accessed 27 March 2013).

Babuška,R.,and Verbruggen, H., (2003). Neuro-fuzzy methods for nonlinear system identification. *Annual Reviews in Control*, volume 27, pp. 73–85.

British Broadcast Corporation., (2013). Padstow speedboat deaths, 17 May. (www.bbc.co.uk/news/uk-england-cornwall-22560652 accessed 19 May 2013)

Bemporad, A., (2006). Model predictive control design: new trends and tools. Proceedings of the 45th IEEE Conference on Decision and Control, San Diego, California, United States of America, 13-15 December, pp. 6678-6683.

Bendtsen, J., Trangbaek, J., Stoustrup, J., (2008). Closed-loop system identification with new sensors. Proceedings of the 47th IEEE Conference on Decision and Control, Cancun, Mexico, 9-11 December, pp 2631-2636.

Bertram, V., (2008). Unmanned surface vehicles – A survey. Technical report, Ecole Nationale Suprieure des Ingnieurs des Etudes et Techniques d'armement (ENSIETA) (www.ensta-bretagne.fr/ accessed 07 January 2012).

Borrelli, F., Keviczky, T., and Balas, G.J., (2004). Collision-free UAV formation flight using decentralized optimization and invariant sets. Proceedings of the 43rd IEEE Conference on Decision and Control, 14-17 December, Paradise Island, Bahamas, pp.1099-1104.

Botto, M., and Costa, J., (1998). A comparison of nonlinear predictive control techniques using neural network models. *Journal of Systems Architecture*, volume 44, pp. 597-616.

Caccia, M., Bono, R., Bruzzone, Ga., Bruzzone, Gi., Spirandelli, E., Veruggio, G., Stortini, A.M., Capodaglio, G., (2005). Sampling sea surfaces with SESAMO. *Robotics and Automation Magazine*, volume 12, issue 3, pp.95-105.

Caccia, M., Bibuli, M., Bono, R., and Bruzzone, G., (2008). Basic navigation, guidance and control of an unmanned surface vehicle. *Autonomous Robots*, volume 25, issue 4, pp. 349-365.

Caccia, M., Bibuli, M., Bono, R., Bruzzone, Ga., Bruzzone, Gi., and Spirandelli, E., (2007). Unmanned surface vehicle for coastal and protected waters applications: The Charlie project. *Marine Technology Society Journal,* volume 41, issue 2, pp.62-71.

Canale, M., Fagiano,L., and Signorile, M.C., (2010a). Vehicle lateral stability using a front steer by wire device and set membership predictive control techniques. 2010 American Control Conference, Baltimore, MD, United States of America. June-July, pp.1483-1488.

Canale, M., Fagiano, L., and Milanese, M., (2010b). Efficient model predictive control for nonlinear systems via function approximation techniques. IEEE Transactions on Automatic Control, volume 55, issue 8, pp.1911-1916.

Carlos, E. G., Prett, D. M., and Morari, M., (1989). Model predictive control: Theory and practice – a survey. *Automatica*, volume 25, issue 3, pp. 335-348.

Carrasco, D.S., and Goodwin, G.C., (2011). Feedforward model predictive control. *Annual Reviews in Control*, volume 35, issue 2, pp.199-206.

Chen, C.L.P., Liu, Y.J. and Wen, G.X., (2013). Fuzzy neural network-based adaptive control for a class of uncertain nonlinear stochastic systems. *IEEE Transactions on Cybernetics*, volume 44, issue 5, pp. 583-593. doi: 10.1109/TCYB.2013.2262935

Chen, G., Wang, J., and Shieh, L. S., (1997). Interval Kalman filtering. *IEEE Transactions on Aerospace and Electronic Systems,* volume 33, issue 1, pp. 250–258.

Chen, M., Ge, S. S. and Ren, B., (2011). Adaptive tracking control of uncertain MIMO nonlinear systems with input constraints. *Automatica*, volume 47, issue 3, pp. 452-465.

Chen.H., and Allgower, F., (1998). A quasi-infinite horizon nonlinear model predictive control scheme with guaranteed stability. *Automatica*, volume 34, issue 10, pp. 1205-1217.

Chui, C.K. and Chen, G., (2008). *Kalman Filtering with Real-Time Applications*, 4th Edition. Springer, New York, United States of America.

Clarke, D.W., Mohtadi, C., and Tuff, P.S., (1987). Generalised predictive control. Part 1: The basic algorithm. *Automatica*, volume 23, issue 2, pp. 137-148.

Cortes, C. and Vapnik, V., (1995). Support-Vector Networks, *Journal of Machine Learning*, September, volume 20, issue 3, pp. 273-297.

Craven, P.J., (1999). Intelligent control strategies for an autonomous underwater vehicle, PhD. thesis, Plymouth University, United Kingdom.

Cui, R., Ge, S.S., How, V.E.B. and Choo, Y.S., (2010) Leader–follower formation control of underactuated autonomous underwater vehicles. *Ocean Engineering*, volume 37, issue 17-18, pp. 1491-1502.

Cui, R., Ren, B. and Ge, S.S., (2012). Synchronised tracking control of multi-agent system with high order dynamics. *IET Control Theory and Applications*, volume 6, issue 5, pp. 603-614.

Cutler, C. R., and Ramaker, B. L., (1980). Dynamic matrix control - a computer control algorithm. Proceedings of the Joint Automatic Control Conference, 13-15 August, San Francisco, CA, paper WP5-B.

De Souza, G., Odloak, D., and Zanin, A.C., (2010). Real time optimization (RTO) with model predictive control (MPC). *Computers and Chemical Engineering*, volume 34, issue 12, pp.1999-2006.

Desborough, L., and Harris, T., (1992). Performance assessment measures for univariate feedback control. *Canadian Journal of Chemical Engineering*, volume 70, pp.1186 - 1197.

Dynamical Systems and Ocean Robotics Laboratory., (2012). Welcome to DSOR lab. (http://dsor.isr.ist.utl.pt/index.html accessed 11 July 2012)

Elkaim, G.H. and Kelbley, R., (2006). Measurement based H infinity controller synthesis for an autonomous surface vehicle. Proceedings of the 19th International Technical Meeting of the Satellite Division of the Institute of Navigation, September, Fort Worth, United States of America.

Elkaim, G.H., (2009). System identification based control of an unmanned autonomous wind propelled catamaran, *Control Engineering Practice*, volume 17, pp.158-169.

Eshel, T., (2012). US Navy tests Rafael Spike missiles on unmanned vessels. (http:// defense-update.com, accessed 30 May 2013)

Faísca, N.P., Kouramas, K.I., Saraiva, P.M., Rustem, B., and Pistikopoulos, E.N., (2007). A multi-parametric programming approach for constrained dynamic programming problems. *Optimization Letters*, volume 2, issue 2, pp.267-280.

Farrell, J.A. and Barth. M., (1999). *The Global Positioning System and Inertial Navigation.* McGraw-Hill, New York, United States of America.

Ferreira, H., Martins, A., Dias, A., Almeida, C., Almeida, J. M. and Silva, E.P., (2006). ROAZ Autonomous Surface Vehicle Design and Implementation. *Encontro Científico - Robótica, Pavilhão Multi-usos*, Guimarães, Portugal.

Fossen TI., (2011). *Handbook of marine craft hydrodynamics and motion control*. John Wiley and Sons Ltd, Chichester, United Kingdom.

Fossen, T. I., (2000). A survey of nonlinear ship control: From theory to practice, Proceedings of the 5th IFAC Conference on Manoeuvring and Control of Marine Craft, 23-25 August, Aalborg, Denmark, pp. 1–16.

Fossen, T.I., Sagatun,S.I., and Scrensen, A.J., (1996). Identification of dynamically positioned ships. *Control Engineering Practice*, volume 4, issue 3, pp.369-376.

Freund, E., and Mayr, R., (1997). Nonlinear path control in automated vehicle guidance. *IEEE Transactions on Robotics*, volume 13, issue 1, pp. 49-60.

Gass, S.I., and Saaty, T.L., (1955). The computational algorithm for the parametric objective function. *Naval Research Logistics Quarterly*, volume 2, pp.39–45.

Ghaemi, R., Oh, S., and Sun, J., (2010). Path following of a model ship using model predictive control with experimental verification. American Control Conference, 30 June – 02 July, Baltimore, MD, United States of America, pp. 5236-5241.

Grewal, M.S., and Andrews, A.P., (2010). Applications of Kalman Filtering in Aerospace 1960 to the Present. IEEE control systems magazine, June, pp.69-78.

Guo, L., (1996). Self-convergence of weighted least squares with applications to stochastic adaptive control, *IEEE Transactions on Automatic Control*, volume 41, issue 1, January, pp. 79-89.

Harris, C.J., and Gan, Q., (2001). State estimation and multi-sensor data fusion using data-based neurofuzzy local linearisation process models. *Information Fusion*, volume 2, issue 1, pp.17-29.

Healey, A. J., and Lienard, D., (1993). Multivariable sliding model control for autonomous diving and steering of unmanned underwater vehicles. *IEEE Journal of Oceanic Engineering*, volume 18, issue 3, pp. 327-339.

Hill, D., (2011). MPC vs. ARC - not an 'either/or' decision. *Hydrocarbon Processing*, January, volume 90, issue 1, pp.13-13.

Hine, R., and McGillivary, P., (2007). Wave powered autonomous surface vessels as components of ocean observing systems. Proceedings of the 20th Pacific Congress on Marine Science and Technology, 24-27 June, Honolulu, Hawaii, United States of America, pp.1-9.

Hjalmarsson, H., Gevers, M., de Bruyne. F., (1996). Closed-loop identification gives better performance for model-based control design. *Automatica*, volume 32, issue 12, pp.1659-1673.

Hof, P.M.J.V., and Schrama, R.J.P., (1995). Identification and Control - Closed-loop Issues. *Automatica*, volume 31, issue 12, pp. 1751-1770.

Hof, P.M.J.V., and Gilson, M., (2001). Closed-loop system identification via a tailor-made IV method. Proceedings of the 40th IEEE Conference on Decision and Control, December, Orlando, Florida, United States of America, volume 5, pp. 4314-4319.

Holler, J., Longfield, S., Murphy, K., Striz, A., and Bingham, B., (2008). Unmanned surface vehicles for undergraduate engineering education. *Oceans*, 15-18 September, Québec, Canada, volume 1, issue 8, pp.15-18.

Hussain, A., Essounbouli, N., and Hamzaoui, A., (2007). Adaptive variable structure fuzzy wavelet network based controller for nonlinear systems. Proceedings of the 3rd IFAC Advanced Fuzzy and Neural Network Workshop, Valenciennes, France, October, pp.1-6.

Ippolitti, G., Jetto, L., and Longhi, S., (2006). Switching-based supervisory control of underwater vehicles. In G. N. Roberts & R. Sutton (Eds.), *Advances in Unmanned Marine Vehicles*. IEE Control Engineering Series, pp.105–121.

Jang, J-S.R., (1992). Neuro-fuzzy modelling: architecture, analysis and applications. PhD. thesis, University of California, Berkley, United States of America.

Jiang, H., Choudhury, S., and Shah, S., (2007). Detection and diagnosis of plant-wide oscillations from industrial data using the spectral envelope method, *Journal of Process Control*, volume 17, issue 2, pp. 143-155.

Jiang, H., Li, W. and Shah, S., (2006). Detection and isolation of model-plant-mismatch for multivariate systems. Proceedings of the Safe Process, August, Beijing, China, pp.1396-1401.

Jounela, S.L.J., (2007). Future trends in process automation. *Annual Reviews in Control*, volume 31, pp. 211-220.

Julien, R.H., Foley, M.W., and Cluett, W.R., (2004). Performance assessment using a model predictive control benchmark. *Journal of Process Control*, volume 14, issue 4, pp. 441-456.

Karimi, A., and Dorã, I., (1998). Comparison of the closed-loop identification methods in terms of the bias distribution. *Systems and Control Letters*, volume 34, pp.159-167.

Khare, N., and Singh, P., (2012). Modelling and optimization of a hybrid power system for an unmanned surface vehicle. *Journal of Power Sources*, volume 198, pp. 368-377.

Kim, B., Necsulescu, D., and Sasiadek, J., (2004). Autonomous mobile robot model predictive control. *International Journal of Control*, volume 77, issue 16, pp.1438-1445.

Kiran, S.R., Raju, S.S.N., Varadarajan, S., and Shankar, A., (2009). LTI system identification using wavelets. *Journal of Theoretical and Applied Information Technology*. December, volume 9, issue 2, pp.1-8.

de Klerk, E., Craig., I. K., (2004)., "A laboratory experiment to teach closed-loop system identification", *IEEE Transactions on Education*, May, volume 47, issue 2, pp.. 276-283.

de Klerk, E., and Craig, I.K., (2002). Closed loop system identification of a MIMO plant controlled by a MPC Controller. Proceedings of the 6th IEEE Africon Conference, 2-4 October, George, South Africa, volume 1, pp. 85-90.

Landau, I.D., and Rolland, F., (1994). An approach for closed loop system identification. Proceedings of the 33rd conference on decision and control, 4 December, Lake Buena Vista, Florida, United States of America, pp. 4164-4169.

Landau, I.D., (1999). From robust control to adaptive control. *Control Engineering Practice*, volume 7, pp.1113-1124.

Leavey, C.M., James, M.N., Summerscales, J., and Sutton, R., (2003). An introduction to wavelet transforms: a tutorial approach. The British Institute of Non-Destructive Testing. *Insight* volume 45, issue 5, pp. 344-353.

Li, Z., Ding, L., Gao, H., Duan, G. and Su, C.Y., (2013). Trilateral tele-operation of adaptive fuzzy force/motion control for nonlinear tele-operators with communication random delays. *IEEE transactions on Fuzzy Systems*, volume 21, issue 4, pp. 610-624.

Li, W.C., and Biegler, L.T., (1989). Multistep Newton-type control strategies for constrained nonlinear processes. *Chemical Engineering Research Design*, volume 67, pp. 562–577.

Li, Z. and Su, C.Y., (2013). Neural-adaptive control of single-master multiple slaves tele-operation for coordinated multiple mobile manipulators with time-varying communication delays and input uncertainty. *IEEE Transactions on Neural Network and Learning Systems*, volume 24, issue 9, pp. 1400-1413.

Li, Z., and Sun, J., (2012). Disturbance compensating model predictive control with application to ship heading control. *IEEE Transactions on Control Systems Technology*, volume 20, issue 1, January, pp. 257-265.

Li, Z., Cao X. and Ding, N., (2011). Adaptive fuzzy control for synchronization of nonlinear teleoperators with stochastic time-varying communication delays. *IEEE Transactions on Fuzzy Systems*, volume 19, issue 4, pp. 745-757.

Li, Z., Li, J. and Kang, Y., (2010). Adaptive robust coordinated control of multiple mobile manipulators interacting with rigid environments, *Automatica*, volume 46, issue 12, pp. 2028-2034.

Liu, J., Allen, R. and Yi, H., (2011c). Ship motion stabilizing control using a combination of model predictive control and an adaptive input disturbance predictor. *Proceedings of the Institution of Mechanical Engineers Part I: Journal of Systems and Control Engineering*, August, Volume 225, issue 5, pp. 591-602.

Liu, Y.J., Chen, C.L.P., Wen, G.X. and Tong, S., (2011a). Adaptive neural output feedback tracking control for a class of uncertain discrete-time nonlinear systems, *IEEE transactions on neural networks*, volume 22, issue 7, pp. 1162-1167.

Liu, Y.J., Tong, S. and Chen, C.L.P., (2013a). Adaptive fuzzy control via observer design for uncertain nonlinear systems with un-modelled dynamics. *IEEE Transactions on Fuzzy Systems*, volume 21, issue 2, pp. 275-288.

Liu, Y.J., Tong, S.C, Wang, D., Li, T.S. and Chen, C.L.P., (2011b). Adaptive neural output feedback controller design with reduced-order observer for a class of uncertain nonlinear SISO systems. *IEEE Transactions on Neural Networks*, volume 22, issue 8, pp. 1328-1334.

Ljung, L., (1999). *System Identification, Theory for the User*. Second Edition, Prentice Hall, New Jersey, United States of America.

Ljung, L., (2010). Perspectives on system identification. *Annual Reviews in Control*, volume 34, issue 1, pp.1-12.

Loebis, D., Naeem, W., Sutton, R., Chudley, J. and Tiano, A., (2006). Navigation, guidance and control of the Hammerhead autonomous underwater vehicle. In G. N. Roberts & R. Sutton (Eds.), *Advances in Unmanned Marine Vehicles*. IEE Control Engineering Series, pp.128–159.

Long, C.E., Polisetty, P.K., and Gatzke, E.P., (2006). Nonlinear model predictive control using deterministic global optimization. Journal of Process Control, volume 16, issue 6, pp. 635-643.

Maciejowski, J.M., (2002). *Predictive control with constraints.* Prentice Hall Inc, London, United Kingdom.

Majohr, J., Buch, T., and Korte, C., (2000). Navigation and automatic control of the measuring dolphin (*Messin^{TM}).* Proceedings of the 5th IFAC Conference on Manoeuvring and Control of Marine Craft, August, Aalborg, Denmark, pp.405-410.

Manley, J.E., (2008). Unmanned surface vehicles, 15 years of development. *Oceans Special Issue*, MTS IEEE Oceans Conference, 15-18 September, Quebec, Canada, pp.1-4.

Martensson, K., and Wernrud, A., (2008). Dynamic model predictive control. Proceedings of the 17th IFAC World Congress, July, Seoul, Korea, pp.13182-13187.

Mattingley, J., Wang, Y., and Boyd, S., (2010). Code Generation for Receding Horizon Control. Proceedings of the IEEE Multi-Conference on Systems and Control, Yokohama, Japan, September 2010. pp. 985–992.

Mayne, D.Q., Rawlings, J. B., Rao, C.V., and Scokaert, P.O.M., (2000). Constrained model predictive control: stability and optimality. *Automatica*, volume 36, pp. 789-814.

McNinch, L.C., and Ashrafiuon, H., (2011). Predictive and Sliding Mode Cascade Control for Unmanned Surface Vessels. American Control Conference, San Francisco, USA, 29 June – 01 July, pp. 184 – 189.

Micheal, P.A., and Cox, J.W., (2003). A practical approach for large-scale controller performance assessment, diagnosis, and improvement. *Journal of Process Control*. March, volume 13, issue 2, pp. 155-168.

Misra, J., and Saha, I., (2010). Artificial neural networks in hardware: A survey of two decades of progress. *Neurocomputing,* volume 74, issue 1-3, pp.239-255.

Morari, M., and Lee, J.H., (1999). Model predictive control: past, present and future. *Process Engineering*, volume 23, pp.667 - 682.

Moreira, L., Fossen, T., and Guedessoares, C., (2007). Path following control system for a tanker ship model. *Ocean Engineering*, volume 34, issue14-15, pp. 2074-2085.

Motwani, A., (2012). Survey of unmanned surface vehicles. *MIDAS Technical Report* MIDAS.SMSE.2012. TR.001, Plymouth University, United Kingdom.

Motwani, A., Sharma, S.K., Sutton, R., Culverhouse, P., (2013). Interval Kalman filtering in navigation system design for an uninhabited surface vehicle. *Journal of Navigation*, volume 6, pp. 639-652. doi: 10.1017/S0373463313000283

Motwani, A., Sharma, S., Sutton, R., and Culverhouse, P. (2014) Application of artificial neural networks to weighted interval Kalman filtering. *Proceedings of the Institution of Mechanical Engineers, Part I: Journal of Systems and Control Engineering* - Published online February 3, 2014,
` doi: 10.1177/0959651813520148

Naeem, W., Sutton, R., Ahmad, S.M., and Burns, R.S., (2003). A review of guidance laws applicable to unmanned underwater vehicles. *Journal of Navigation*, volume 56, issue 1, pp.15-29.

Naeem, W., (2004). Guidance and control of an autonomous underwater vehicle. PhD Thesis, Plymouth University, United Kingdom.

Naeem, W., Sutton, R. and Chudley, J., (2006). Soft computing design of a linear quadratic Gaussian controller for an unmanned surface vehicle. Proceedings of the 14th Mediterranean Conference on Control Automation, 1-6 June, Ancona, Italy.

Naeem, W., Sutton, R., Chudley J., Dalgleish F.R., and Tetlow, S., (2005). An online genetic algorithm based model predictive control autopilot design with experimental verification. *International Journal of Control*, volume 78, issue 14/20, September, pp. 1076-1090.

Naeem, W., Sutton, R., and Xu, T., (2012). An integrated multi-sensor data fusion algorithm and autopilot implementation in an uninhabited surface craft. *Ocean Engineering*, volume 39, pp. 43-52.

Naeem, W., Xu T., Sutton, R., and Tiano, A., (2008). The design of a navigation, guidance, and control system for an unmanned surface vehicle for environmental monitoring. *Proceedings of the Institution of Mechanical Engineers Part M: Journal of Engineering for the Maritime Environment*, volume 222, issue M2, pp. 67–80.

Naeem, W., Xu, T., Sutton, R., Tiano. A., (2008). The design of a navigation, guidance, and control system for an unmanned surface vehicle for environmental monitoring, *Proceedings of the Institution of Mechanical Engineers, Part M: Journal of Engineering for the Maritime Environment*, volume 222, issue 2, pp. 67-79.

Narendra, K. S., and Balakrishan, J. (1997). Adaptive control using multiple models. *IEEE Transactions on Automatic Control*, volume 42, pp.171–187.

O'Connor, N., and O'Dwyer, A., (2004). Control loop performance assessment: a classification of methods. Proceedings of the Irish Signals and Systems Conference, July, Queens University Belfast, pp. 530-535.

Oh, S.R., and Sun, J., (2010). Path following of under actuated marine surface vessels using line-of-sight based model predictive control. *Ocean Engineering*, volume 37, issue 2-3, pp. 289-295.

Oliveira, N.M.C., and Biegler, L.T., (1995). An extension of Newton-type algorithms for nonlinear process control, *Automatica*, volume 31, issue 2, pp. 281–286.

Pan, Y., and Wang, J., (2010). A neurodynamic optimization approach to nonlinear model predictive control. Proceedings of the IEEE International Conference on Systems Man and Cybernetics (SMC), 10-13 October, Istanbul, Turkey, pp.1597-1602.

Park, S., Kim, J., Lee, W., and Jang, C., (2005). A study on the fuzzy controller for an unmanned surface vessel designed for sea probes. Proceedings of the International Conference on Control, Automation and Systems, 1-4 June, Kintex, Korea.

Perez, T., (2005). *Ship motion: Course keeping and roll stabilisation using rudder and fins.* Springer-Verlag, London, United Kingdom.

Phillips, S., Hook, D., and Young, H., (2008). Remote Deployment of Commercial and Military Sensors at Sea, Proceedings of the UDT Europe, 10-12 June, Nexus Media, Glasgow, United Kingdom.

Piche, S., Sayyar-Rodsari, B., Johnson, D., and Gerules, M., (2000). Nonlinear model predictive control using neural networks. *IEEE Control Systems Magazine*, pp. 53–62.

Polkinghorne, M. N., Roberts, G. N., Burns, R. S., and Winwood, D., (1995). The implementation of fixed rulebase fuzzy logic to the control of small surface ships. *Control Engineering Practice*, volume 3, issue 3, pp. 321–328.

Privara, S., Široký, J., Ferkl, L., and Cigler, J., (2011). Model predictive control of a building heating system: The first experience. Energy and Buildings, volume 43, issue 2-3, pp. 564-572.

Qiaomei, S., Guang, R., Jin, Y. and Xiaowei, Q., (2010). SVM inverse model–based heading control of unmanned Surface vehicle. IEEE Youth Conference on Information Computing and Telecommunications (YC-ICT), 28-30 November, Beijing, pp. 138-141, doi: 10.1109/YCICT.2010.5713064.

Qiaomei, S., Guang, R., Jin, Y. and Xiaowei, Q., (2011). Autopilot design for unmanned surface vehicle tracking control. Proceedings of the 3rd International Conference on Measuring Technology and Mechatronics Automation, volume 1, January, Shangshai, China, pp. 610-613.

Qin, S.J., and Badgwell, T. A., (2003). A survey of industrial model predictive control technology. Control Engineering Practice, volume 1, issue 7, pp.733-764.

Rahideh,A., and Shaheed, M.H.,(2010). Real time nonlinear model predictive control for fast systems. Proceedings of the International Symposium on Power Electronics, Electrical Drives, Automation and Motion, Pisa, Italy, pp.1732-1737.

Rawlings, JB., and Mayne, DQ., (2009). *Model predictive control: Theory and design*. Nob Hill Publishing, Madison, United States of America.

Richalet, J. A., Rault, A., Testud, J. D., and Papon, J., (1978). Model predictive heuristic control: Applications to industrial processes. *Automatica*, volume 14, pp. 413–428.

Richards, A., Breger, L., and How, J.P., (2006). Analytical performance prediction for robust constrained model predictive control. *International Journal of Control*, volume 79, issue 8, pp.877-894.

Roberts, G. N., Sharif, M. T., Sutton, R., and Agarwal, A. (1997). Robust control methodology applied to the design of a combined steering/stabiliser system for warships. Control Theory and Applications, IEE Proceedings, volume 144, issue 2, pp. 128-136.

Roberts, G. N. and Sutton, R., (2012). *Further Advances in Unmanned Marine Vehicles*. The Institution of Engineering and Technology, London, United Kingdom.

Roberts, G.N., (2008). Trends in marine control systems. *Annual Reviews in Control*, volume 32, issue 2, pp.263-269.

Sakizlis, V., Kouramas, K. I., and Pistikopoulos, E. N., (2007). Linear Model Predictive Control via Multiparametric Programming. In *Multi-Parametric Model-Based Control: Theory and Applications, Volume 2*. E. N. Pistikopoulos, M. C. Georgiadis and V. Dua (Editors), Wiley-VCH Verlag GmbH and Co. Weinheim, Germany.

Sharma, S., and Sutton, R., (2012). Modelling the yaw dynamics of an uninhabited surface vehicle for navigation and control system design. Proceedings of *IMarEST - Part A: Journal of Marine Engineering and Technology*, September, volume 11, issue 3, pp. 9-20.

Sharma, S., Naeem, W. and Sutton, R., (2012). An autopilot based on a local control network design for an unmanned surface vehicle. *Journal of Navigation*, volume 65, issue 2, pp. 281-301.

Sharma, S., Sutton, R., Motwani, A. and Annamalai, A.S.K., (2013). Nonlinear control algorithms for an unmanned surface vehicle. *Proceedings of the Institution of Mechanical Engineers, Part M: Journal of Engineering for the Maritime Environment*, 5 November, doi: 10.1177/1475090213503630.

Sonnenburg, C., Gadre, A., Horner, D., Kragelund, S., Marcus, A., Stilwell, D.J., and Woolsey, C.A., (2010). Control-oriented planar motion modelling of unmanned surface vehicles, OCEANS, 20-23 September, Seattle, Washington, United States of America, pp.1-10.

Sosic G.V.,(1976). The Academy of Model Aeronautics history program presents: Biography of Nikola Tesla, Model aviation magazine. (https://www.modelaircraft.org/files/TeslaNikola.pdf accessed 10 June 2011)

Sotomayor, O.A.Z., Odloak, D., and Moro, L.F.L., (2009). Closed-loop model re-identification of processes under MPC with zone control. *Control Engineering Practice* volume 17, pp. 551–563.

Srinivasan, M.V., (2011). Visual control of navigation in insects and its relevance for robotics. *Current Opinion in Neurobiology*, volume 2, issue 4, pp.535-543.

Stafford, B., & Osborne, N. (2008). Technology development for steering and stabilizers, *Proceedings of the Institution of Mechanical Engineers Part M: Journal of Engineering for the Maritime Environment,* May, volume 222 issue M2, pp. 41-52.

Steimle, E.T., and Hall, M.L., (2006). Unmanned surface vehicles as environmental monitoring and assessment tools. Proceedings of OCEANS 2006, 18-21 September, Boston, Massachusetts, United States of America, pp.1-5.

Stovall, S.H., (1997). Basic inertial navigation. Naval Air Warfare Center Weapons Division, China Lake, California, Technical Memorandum 8128, September.

Sui, D., and Ong, C.J., (2008). Constrained piecewise linear systems: controller design via convex invariant sets. *International Journal of Robust and Nonlinear Control*, volume 18, issue 13, pp.1327-1347.

Sutton, R., Sharma, S., and Xu, T., (2011). Adaptive navigation systems for an unmanned surface vehicle. Proceedings of the IMarEST - Part A: *Journal of Marine Engineering and Technology*, September, volume 10, issue 3, pp.3-20.

Tatjewski, P., and Lawrynczuk, M., (2006). Soft computing in model–based predictive control. *International Journal of Applied Math and Computer Science*, volume 16, issue 1, pp.7-26.

Thornhill, N.F., Oettinger, M., and Fedenczuk, P., (1998). Performance assessment and diagnosis of refinery control loops, Proceedings of the Foundations of computer aided process operations conference, 5-9 July, Snowbird, Utah, United States of America, pp. 373-379.

Thornhill, N.F., Oettinger, M., and Fedenczuk, P.,(1999). Refinery-wide control loop performance assessment, *Journal of Process Control*, volume 9, pp.109-124.

Tian, X., Chen, G., and Chen, S., (2011). A data-based approach for multivariate model predictive control performance monitoring. *Neurocomputing*, volume 74, issue 4, pp. 588-597.

Tiano, A., Sutton, R., Lozowicki, A., and Naeem, W., (2007). Observer Kalman filter identification of an autonomous underwater vehicle. *Control Engineering Practice*, volume 15, issue 6, pp.727-739.

Tischler, M.B., (1995). System identification methods for aircraft flight control development and validation. NASA Technical memorandum 110369, United States of America ATCOM Technical Report 95-A-007

Tontiruttananon, C., Tugnait, J. K., (1998). Parametric identification of closed-loop linear systems using cyclic-spectral analysis. Proceedings of the American Control Conference, 24-26 June, Philadelphia, United States of America, pp. 3597-3601.

Wang L., (2009). Model predictive control system design and implementation using MATLAB. *Springer-Verlag*, Berlin, Germany.

Wang, J., Chen, C., Huang, P., Gu, W., and Chu, J., (2011). Modeling, simulating and experiment of an autonomous surface vehicle. *Energy Procedia*, volume 11, pp.314-318.

Wang, M., and Sutton, R., (2005). Closed loop identification of a remotely operated flight vehicle, *Journal of the Society for Underwater Technology*, volume 26, issue 2, pp.57-63.

Wang, Y., and Boyd, S., (2010). Fast model predictive control using online optimization. *IEEE Transactions on Control Systems Technology*, volume 18, issue 2, pp.267-278.

Wojsznis,W., Gudaz, J., Blevins, T., and Mehta, A., (2003). Practical approach to tuning MPC. *ISA Transactions*, volume 42, issue 1, pp.149-62.

Xiaofei,W., Baohua, Z., Deying, C., Huaming, W., (2011). Adaptive analytic model predictive controller for path following of underactuated ships. Proceedings of the 30th Chinese Control Conference, July, Yantai, China, pp. 5515-5521.

Xu, T., (2007). *An intelligent navigation system for an unmanned surface vehicle.* PhD thesis, Plymouth University, Plymouth, United Kingdom.

Yan, R.J., Pang, S., Sun, H.B., and Pang, Y.J., (2010). Development and missions of unmanned surface vehicle. *Journal of Marine Science and Application*, volume 9, issue 4, pp.451-457.

Zadeh, L.A., and Whalen, L.H., (1962). On optimal control and linear programming, *IRE Transactions on Automatic Control*, volume 7, issue 4, pp. 45-46.

Zanovello, R., and Budman, H., (1999). Model predictive control with soft constraints with application to lime kiln control. *Computers and Chemical Engineering*, volume 23, issue 6, pp.791-806.

Zhao, H., Guiver, J., Neelakantan, R., and Biegler, L.T., (2001). A nonlinear industrial model predictive controller using integrated PLS and neural net state-space model. *Control Engineering Practice*, volume 9, pp.125-133.

Zhao, Y., and Kearney, R.E., (2007). Closed-loop system identification of ankle dynamics with compliant loads, Proceeding of the 29th Annual International Conference of the IEEE Engineering in Medicine and Biology Society, 22-26 August, Lyon, France, pp. 4919-4922.

Zhu, Y.C., (1998). Multivariable process identification for MPC: the asymptotic method and its applications. *Journal of Process Control*, volume 8, issue 2, pp. 101-115.

Appendix A

Springer electronics and other hardware

The significant technical specifications of the major components on-board *Springer* are detailed by the following:

- A1. Intense PC Pro Technical Specifications
- A2. TCM2 Technical Specifications
- A3. HMR3000 Technical Specifications
- A4. KVH C100 Technical Specifications
- A5. m*ini-Springer* and *Sutton* Kayak trials
- A6. RoboteQ AX2850 Technical Specifications
- A7. *Springer* Hardware

Tiny Green PC

Impossibly small, fanless computers for 24/7

Intense PC
Powerful. Tiny. Fanless.

Product Specification

Rev7

Introduction

Based on the 3rd Generation Intel® Core™ i7 processor, the Intense PC is the most powerful miniature fanless PC ever! It is the first PC on the market that offers high end computing performance, low power consumption and the ability to extend and customise functionality, all within a tough enclosure.

Key Features

- Intel Core CPU up to 1.7GHz dual core
- Dual-head Intel HD graphics
- Low power consumption
- Ruggedised die-cast aluminium shell
- Innovative customisable modular FACE design

Tiny Green PC

Impossibly small, fanless computers for 24/7

System

Intense PC is designed around Intel Core CPU providing:

- Dual-core 64 bit x86 CPU @ 1.1-1.7 GHz
- Intel HD Graphics GPU

The CPU is supplemented by up to 16GB DDR3-1333

High Performance – Low Power

With a 3rd Generation Intel Core CPU, Intense PC delivers amazing fast performance - unprecedented for a miniature fanless system. Intense PC consumes under 10W when idle, yet for high workloads the two CPU cores provide up to 2.8 GHz of processing power with Intel® Turbo Boost Technology.

I/O

Out-of-the-box Intense PC provides interfaces unmatched by any computer of a similar size. Standard Back plate I/O include:

- Dual-head display HDMI + DisplayPort
- Digital 7.1 S/PDIF and analog 2.0 audio, both input and output
- Dual Gigabit Ethernet
- WiFi 802.11 b/g/n + BT combo with dual antennas
- 2 USB3 ports + 2 USB2 ports
- 2 eSATA ports
- Bay for 2.5" SATA HDD
- 2 mini-PCIe sockets
- Serial RS232 port

Tiny Green PC

Impossibly small, fanless computers for 24/7

Introducing FACE

FACE modules (Function And Connectivity Extension Module), are unique standard or custom extension boards that integrate seamlessly into the Intense PC to provide custom functionality and optional I/O extensions.

Example applications of **FACE**:

- A FACE Module with 4 GbE ports and 4 USB ports for networking applications
- Combine GPIOs, ADCs, DACs and serial ports for instrumentation applications
- Add multiple frame-grabbers for surveillance computing
- Enable Intense PC with cellular communication capabilities by adding an internal 3G or LTE modem

For Standard and Custom FACE solutions visit our dedicated FACE page or contact us.

Innovative Thermal Design

Intense PC is designed for fanless operation at the smallest possible form-factor using innovative thermal design and advanced power management technologies:

- Internal passive heat-spreader to eliminate hot-spots
- Power regulation based on both CPU and case temperature monitoring. If case temperature exceeds a threshold the CPU is underclocked until temperature is back within permitted range. The threshold can be configured in BIOS.

Ruggedised Industrial Design

Each part of the metal housing of Intense PC is 3D modelled and produced by die-casting for perfect fit. The streamlined design of the Intense PC makes it one of the toughest computers on the market, easily withstanding industrial, automotive and outdoor.

Tiny Green PC

Impossibly small, fanless computers for 24/7

System and Graphics

Feature	Specifications			Notes
	Value	Standard	Pro	
CPU	Intel Celeron 1047UE 64 bit dual core 1.4 GHz 17W TDP	Intel Core i3-2340UE 64 bit dual core 1.3 GHz 17W TDP	Intel Core i7-3517UE 64 bit dual core 1.7 GHz 17W TDP	
GPU	Intel HD Graphics 2500	Intel HD Graphics 4000	Intel HD Graphics 4000	
RAM	Up to 16 GB, DDR3-1333, dual channel (two SO-DIMM sockets)			Configurable
Storage	Internal 2.5" hard disk, up to 6 Gbit/s			Configurable
	Two eSATA ports, up to 3 Gbit/s			
HDMI	HDMI 1.4a, up to 1920 x 1200 @ 60 Hz			
DisplayPort	Up to 2560 x 1600 at 60Hz, dual mode support			

I/O

Feature	Specifications	Notes
Audio	Stereo line-out and stereo line-in	
	7.1 channel S/PDIF, (electrical through 3.5mm jack)	
Network	Two 1000 BaseT Ethernet port	
	802.11b/g/n Wi-Fi, 2 antennas, 150 Mbit/s	Optional half-size Mini PCIe module
	BT 3/4	
USB	Two USB 3.0 host ports, 5 Gbit/s	
	Two USB 2.0 host ports, 480 Mbit/s	
	Four USB 2.0 host ports, 480 Mbit/s in front	Optional FACE Module
RS232	Partial modem controls, ultra mini serial connector	
IR	Consumer IR receiver	
Expansion	Mini PCIe socket, half-size	Used for wireless module
	Mini PCIe socket, full-size	
	Proprietary **FACE Module** (Function and Connectivity Extension Module): 2x PCIe x1, 1x PCIe x 2, 1x PCIe x8 5x USB2 3x SATA 7x GPIOs SMBus LPC LVDS	

Electrical and Mechanical

Feature	Specifications			Notes
Supply Voltage	Unregulated 8 to 16 volt input			
Power Consumption	Value	Standard	Pro	Depends on System load
	9W – 19W	10W – 23W	10W – 26W	
Dimensions	19cm x 16cm x 4cm			
Operating Temp	0-70°C (with SSD), 0-50°C (with HDD), -20-70°C (Optional Extra)			
MTBF	100,000 Hours			

Tiny Green PC

Impossibly small, fanless computers for 24/7

Block Diagram

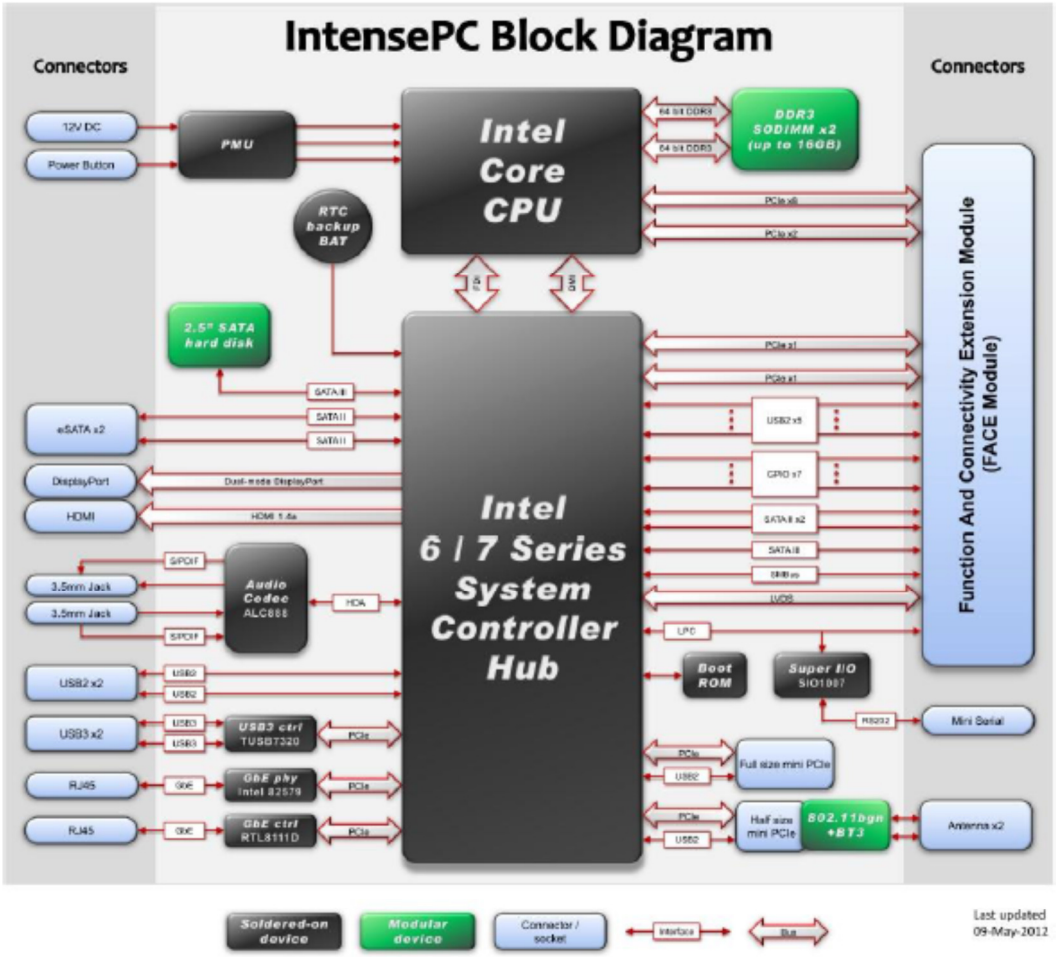

Tiny Green PC

Impossibly small, fanless computers for 24/7

Meet the Models

Model	CPU	RAM	Storage	WiFi & BT	FACE Module	O/S
Intense PC Value Barebone	Intel Celeron 1047UE (17W) 1.4 GHz dual core HD Graphics 2500	-	-	+	4 USB	-
Intense PC Value 4GB Linux	Intel Celeron 1047UE (17W) 1.4 GHz dual core HD Graphics 2500	4GB (2GB DDR3 SODIMM x 2)	HDD 320GB	+	4 USB	Linux Mint
Intense PC Standard Barebone	Intel Core i3-2340UE (17W) 1.3 GHz dual core HD Graphics 3000	-	-	+	4 USB	-
Intense PC Standard 4GB Linux	Intel Core i3-2340UE (17W) 1.3 GHz dual core HD Graphics 3000	4GB (2GB DDR3 SODIMM x2)	HDD 500GB	+	4 USB	Linux Mint
Intense PC Standard 4GB Windows 7 Home Premium	Intel Core i3-2340UE (17W) 1.3 GHz dual core HD Graphics 3000	4GB (2GB DDR3 SODIMM x2)	HDD 500GB	+	4 USB	Windows 7 Home Premium
Intense PC Pro Barebone	Intel Core i7-3517UE (17W) 1.7 GHz dual core HD Graphics 4000	-	-	+	4 USB	-
Intense PC Pro 8GB Linux	Intel Core i7-3517UE (17W) 1.7 GHz dual core HD Graphics 4000	8GB (4GB DDR3 SODIMM x2)	HDD 500GB	+	4 USB	Linux Mint
Intense PCPro 8GB Win7 Pro	Intel Core i7-3517UE (17W) 1.7 GHz dual core HD Graphics 4000	8GB (4GB DDR3 SODIMM x2)	HDD 500GB	+	4 USB	Windows 7 Pro

Package Content

Item	Description
1	Intense PC Computer
2	Power Supply. Input 100-240V AC 50/60Hz. Output 12V DC 5A. DC plug with locking mechanism. DC cord length – 150cm.
3	AC cord.
4	HDMI to DVI adapter
5	3.5mm to RCA cable for S/PDIF
6	2 WiFi antennas

TCM2™ ELECTRONIC COMPASS, MAGNETOMETER, AND TILT SENSOR MODULE

—Data Sheet—

TCM2-20

TCM2 electronic compass sensor module with tilt compensation of ±20°.

Heading Information

Accuracy when level:	0.5° RMS
Accuracy when tilted:	1.0° RMS
Resolution:	0.1°
Repeatability:	±0.1°

Tilt Information

Accuracy:	±0.2°
Resolution:	0.1°
Repeatability:	±0.2°
Range:	±20°

TCM2-50

TCM2 electronic compass sensor module with tilt compensation of ±50°.

Heading Information

Accuracy when level:	1.0° RMS
Accuracy when tilted:	1.5° RMS
Resolution:	0.1°
Repeatability:	±0.3°

Tilt Information

Accuracy:	±0.4°
Resolution:	0.3°
Repeatability:	±0.3°
Range:	±50°

PERFORMANCE OF THE TCM2-20 AND TCM2-50

Magnetic Field Information

Absolute Accuracy:	±1 µT up to 70 µT ±5 µT from 70 µT to 80 µT
Resolution:	0.01 µT
Repeatability:	±0.2 µT
Range:	±80 µT

Temperature Information (sensor is uncalibrated)

Accuracy after calibration:	±1° C, ±2° F
Resolution:	±1° C, ±2° F
Range:	-20° to 70° C

Power Requirements

Supply Voltage:	+5 VDC regulated or 6 to 18 VDC unregulated
Current:	*Note: This is for version 2.82K only* Operating standard mode: 15-20 mA (depending on user configuration) Operating low power mode: 7-13 mA (depending on user configuration) Sleep mode: 2.5 mA

CHARACTERISTICS OF THE TCM2-20 AND TCM2-50

Physical Measurements

Dimensions:	2.50" x 2.00" x 1.25"
Weight:	1.6 ounces

Environmental Characteristics

Operating Temperature:	-20° to 70° C
Storage Temperature:	-30° to 90° C

Interfaces

Digital:	RS232C NMEA0183
Analog:	0-5 V linear, 19.53 mV resolution (256 discrete levels) 0-5 V quadrature (sine and cosine)

FEATURES OF THE TCM2-20 AND TCM2-50

- Built-in hard iron distortion correction system with advanced automatic hard iron calibration algorithms. Soft iron correction system available if needed.
- Compass heading, pitch, roll, 3-axis magnetometer and temperature outputs are all available from the TCM2.
- Distortion Detection: raises a warning flag when magnetic disturbances, such as nearby ferrous metals and electrical currents, compromise accuracy.
- User selectable sampling rate of 1Hz to 30Hz.
- Optional heading damping.

Specifications subject to change without notice

PNI CORPORATION
5464 Skylane Blvd., Suite A • Santa Rosa, CA • 95403 • USA
(707) 566-2260 • FAX (707) 566-2261
http:\\www.pnicorp.com

Honeywell

Digital Compass Solution HMR3000

The Honeywell HMR3000 is a digital compass module that provides heading, pitch, and roll outputs for navigation. The three of Honeywell's magneto-resistive sensors are oriented in orthogonal directions plus a fluid tilt sensor are employed to measure the vector components of the earth's magnetic field and a gravitational reference. These solid-state sensors create a strapdown compass that is both rugged and reliable. The data output is serial full-duplex RS-232 or half-duplex RS-485 with 1200 to 19,200 data rates.

Applications include: Compassing & Navigation, Dead Reckoning Backup to GPS Systems, Marine Navigation, Antenna Positioning, and Land Surveying

A RS-232 development kit version is available that includes a windows compatible demo program, interface cable, AC adapter, and carrying case.

Honeywell continues to maintain product excellence and performance by introducing innovative solid-state magnetic sensor solutions. These are highly reliable, top performance products that are delivered when promised. Honeywell's magnetic sensor solutions provide real solutions you can count on.

FEATURES & BENEFITS

- High Accuracy, <0.5° with 0.1° Resolution
- Wide Tilt Range of ±40°
- Up to 20 Updates per Second
- NMEA Standard Sentence Outputs
- Hard Iron Calibration Routine
- RS-232 or RS-485 Serial Data Interfaces
- PCB or Aluminum Enclosure Options
- 6-15 volt DC Unregulated Power Supply Interface

BLOCK DIAGRAM

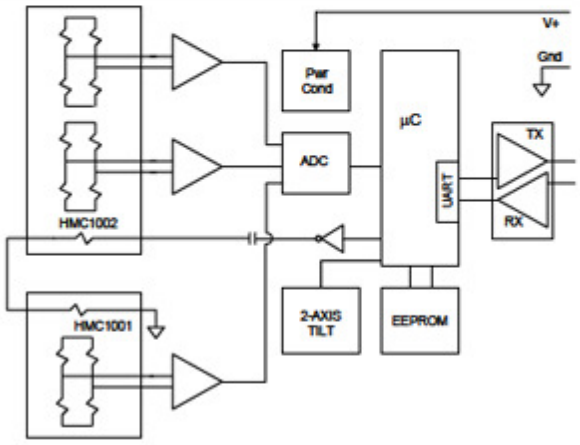

HMR3000

SPECIFICATIONS

Characteristics	Conditions	Min	Typ	Max	Units
Power Supply					
Supply Voltage	Pin 9 referenced to Pin 5 (Ground) Pin 8 referenced to Pin 5 (Ground)	+6.0 +4.75	 +5.0	+15 +5.25	Volts
Supply Current	Vsupply = +6V (Pin 9) Normal Operation STOP Mode SLEEP Mode		 35 13 2.0		mA
Temperature					
Operating	Ambient	-20		+70	°C
Storage	Ambient, Unpowered	-35		100	°C
Heading					
Accuracy	Dip < 50°, Tilt < 20° Dip < 75°, Tilt < 20°			0.5 (1) 1.5	°RMS
Resolution			0.1		degrees
Repeatability			±0.3		degrees
Magnetic Field					
Dynamic Range	Adjustable		±1.0		gauss
Resolution	±0.5 gauss range		1.0		milli-gauss
Tilt					
Range	Pitch, Roll			±40	degrees
Accuracy (2)	Tilt < 20° Tilt >= 20°		±0.4 ±0.6		degrees
Repeatability			±0.2		degrees
Resolution			0.1		degrees
Interface					
Format	RS-232 Full Duplex or RS-485 Half Duplex				
Baud Rate	Full or Half Duplex	1200		19,200	bps
Update Rate	Continuous, per NMEA Sentence	1		20	Hz
Mechanical					
Weight	PCB Only PCB and Flanged Enclosure		22 92		grams
Shock	MIL-STD-810E; TM 516.4 drop test		30		inches
Vibration	20 to 2000Hz, Random for 2 Hours/axis MIL-STD-810E; TM514.4				

*Notes: (1) Calculated values. (2) Device tilt not to exceed 75 degrees, or temporary loss of accuracy occurs.

www.honeywell.com

HMR3000

PIN CONFIGURATION

Pin Number	Pin Name	Description
1	OP/CAL	Operate/Calibrate (open = operate)
2	TD	Transmit Data, RS-485 (B+)
3	RD	Receive Data, RS-485 (A-)
4	RDY/SLP	Ready/Sleep Input (open = ready)
5	GND	Power and Signal Ground
6	RN/STP	Run/Stop Input (open = run)
7	CT/RST	Continue/Reset (open = continue)
8	+5V	Regulated Power Input (+5 volts)
9	V+	Unregulated Power Input (+6 to +15 VDC)

Pin assignments for 9-pin "D" connector. Power input shall be either regulated +5VDC (pin 8) or unregulated +6 to +15VDC (pin 9). Only one of the two pins shall be connected in a given installation to prevent HMR3000 damage.

RS-232 UNBALANCED I/O INTERCONNECTS

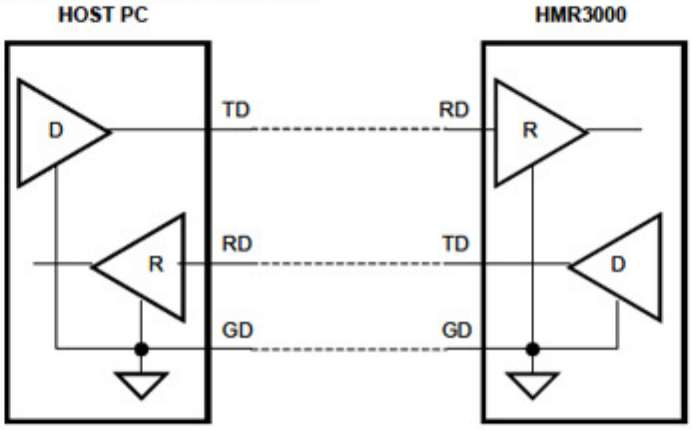

RS-485 BALANCED I/O INTERCONNECTS

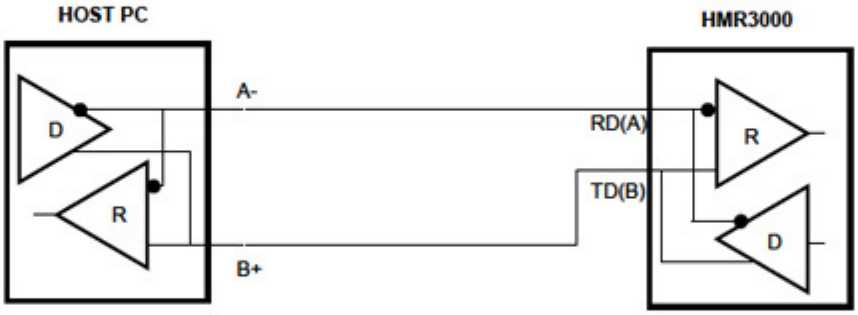

DATA COMMUNICATIONS

The HMR3000 serial communications are governed by a simple asynchronous, ASCII protocol modeled after the NMEA 0183 standard. Either an RS-232 or an RS-485 electrical interface can be ordered. ASCII characters are transmitted and received using 1 start bit, 8 data bits (LSB first), no parity (MSB always 0), and 1 stop bit; 10 bits total per character. The baud rate defaults to 19,200 and can be reconfigured to 1200, 2400, 4800, 9600, 19200, 38400 bits per second. The

www.honeywell.com

HMR3000

HMR3000 supports both standard NMEA 0183 and proprietary messages. Unsolicited NMEA messages are sent by the HMR3000 in Continuous Mode at the rates programmed in the EEPROM. HMR3000 also responds to all input messages from the host. An HMR3000 response to a command input may be delayed due to transmission of an unsolicited output. The host computer must wait for HMR3000 to respond to the last command input before sending another command message. All communication from and to HMR3000 contain a two-character Checksum Field at the end of the data fields, and are denoted in the sentences by 'hh'. The checksum assures the accuracy of the message transmitted. This checksum is also calculated per NMEA 0183 Standard.

The RS-232 signals are single-ended undirectional levels that are sent received simultaneously (full duplex). One signal is from the host personal computer (PC) transmit (TD) to the HMR3000 receive (RD) data line, and the other is from the HMR3000 TD to the PC RD data line. When a logic one is sent, either the TD or RD line will drive to about +6 Volts referenced to ground. For a logic zero, the TD or RD line will drive to about –6 Volts below ground. Since the signals are transmitted and dependent on an absolute voltage level, this limits the distance of transmission due to line noise and signal to about 60 feet.

When using RS-485, the signals are balanced differential transmissions sharing the same lines (half-duplex). This means that logic one the transmitting end will drive the B line at least 1.5 Volts higher than the A line. For a logic zero, the transmitting end will drive the B line at least 1.5 Volts lower than the A line. Since the signals are transmitted as difference voltage level, these signals can withstand high noise environments or over very long distances where line loss may be a problem; up to 4000 feet. Note that long RS-485 lines should be terminated at both ends with 120-ohm resistors.

Specific measurement descriptions and interface commands are not included in this datasheet but are included in the companion HMR3000 User's Guide document.

CIRCUIT DESCRIPTION

The HMR3000 Digital Compass Module contains all the basic sensors and electronics to provide digital indication of heading and tilt. The HMR3000 has all three axis of magnetic sensors on the far end of the printed circuit board, away from the connector interface. The HMR3000 uses the circuit board mounting holes or the enclosure surfaces as the reference mechanical directions. The complete HMR3000 PCB assembly consists of a mother board and the 9-pin D-connector.

The HMR3000 circuit starts with the Honeywell HMC1001 1-Axis Magnetic Sensor and the HMC1002 2-Axis Magnetic Sensor elements to provide the X, Y, and Z axis magnetic sensing of the earth's field. These sensor output voltages are then amplified and converted to a digital representation. A microcontroller integrated circuit receives the digitized magnetic field values (readings) by periodically querying the Analog to Digital Converter (ADC) and performs the necessary offset value corrections provided by the EEPROM via the calibration routine. This microcontroller also performs the external serial data interface and other housekeeping functions. The onboard EEPROM integrated circuit also is employed to retain necessary setup variables for best performance.

A liquid filled two-axis (pitch, roll) tilt sensor is also used to create tilt compensated heading data. This tilt sensor performs an electronic gimballing function and is normally mounted flat (PCB horizontal) for maximum tilt range.

APPLICATIONS PRECAUTIONS

Several precautions should be observed when using magnetic compasses in general:

- The presence of ferrous materials, such as nickel, iron, steel, and cobalt near the magnetometer will create disturbances in the earth's magnetic field that will distort the X, Y, and Z field measurements.
- Perming effects on the HMR3000 circuit board need to be taken into account. If the HMR3000 is exposed to fields greater than 10 gauss, then it is recommended that the enclosure/circuit boards be degaussed for highest sensitivity and resolution. A possible result of perming is a high zero-field output indication that exceeds specification limits. Degaussing wands are readily available from local electronics tool suppliers and are inexpensive. Severe field offset values could result if not degaussed.

NON-FERROUS MATERIALS

Materials that do not affect surrounding magnetic fields are: copper, brass, gold, aluminum, some stainless steels, silver, tin, silicon, and most non-metals.

HMR3000

HANDLING PRECAUTIONS

The HMR3000 Digital Compass Module measures fields within 1 gauss in magnitude. Computer floppy disks (diskettes) store data with field strengths of approximately 10 gauss. This means that the HMR3000 is many times more sensitive than common floppy disks. Please treat the compass with at least the same caution as your diskettes by avoiding motors, CRT video monitors, and magnets. Even though the loss of performance is recoverable, these magnetic sources will interfere with measurements.

The fluidic tilt sensor works best when kept near level, and in calm to moderate vibration conditions. If turned upside down or violently jarred, not all the fluid will immediately return to the bottom of the tilt sensor's glass ampoule. Accurate tilt and tilt compensated headings may be unavailable for a minute or two to allow for the fluid to transit to the bottom of the ampoule.

PCB DIMENSIONS AND PINOUT

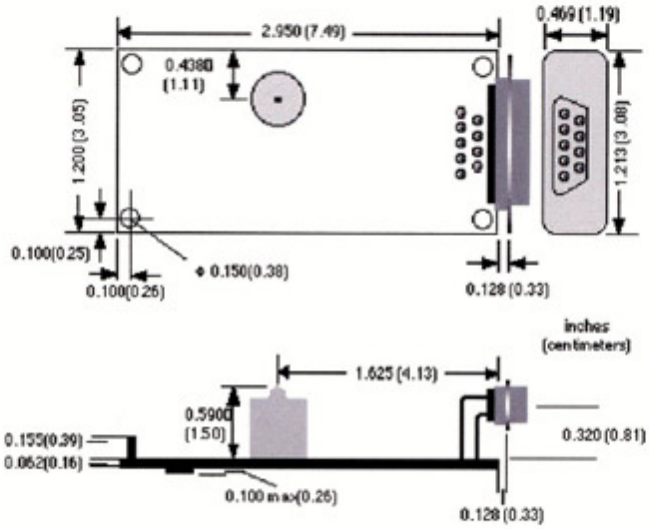

CASE DIMENSIONS

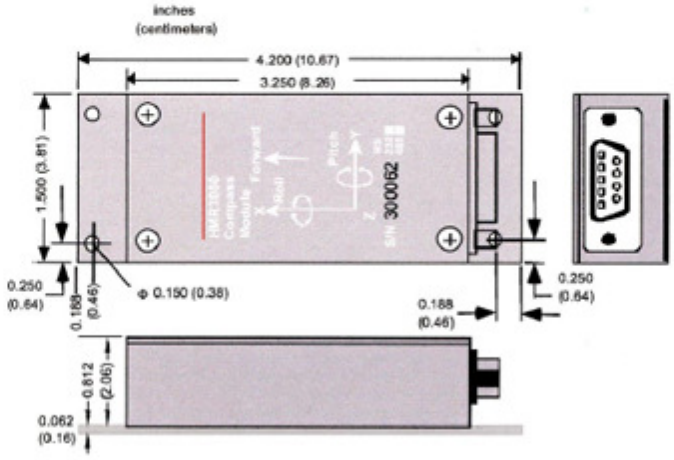

HMR3000

DEMONSTRATION PCB MODULE KIT

The HMR3000 Demonstration Kit includes additional hardware and Windows software to form a development kit for the digital compass module. This kit includes the HMR3000 PCB and enclosure, serial port cable with attached AC adapter power supply, and demo software plus documentation on a compact disk (CD). The figure below shows the schematic of the serial port cable with integral AC adapter. There will be three rotary switches on the AC adapter. These should be pointed towards the positive (+) polarity, +9 volts, and 120 or 240 VAC; depending your domestic supply of power.

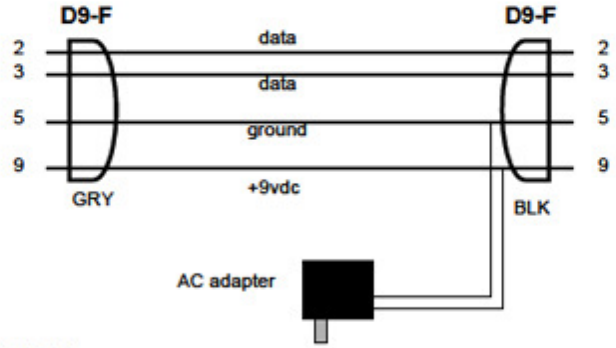

ORDERING INFORMATION

Ordering Number	Product
HMR3000-D00-232	PCB Only (No Enclosure), RS-232 I/O
HMR3000-D00-485	PCB Only (No Enclosure), RS-485 I/O
HMR3000-D21-232	Extended-Base Enclosure, RS-232 I/O
HMR3000-D21-485	Extended-Base Enclosure, RS-485 I/O
HMR3000-D21-232-DEMO	Demo Kit, Extended-Base Enclosure, RS-232 I/O

FIND OUT MORE

For more information on Honeywell's Magnetic Sensors visit us online at www.magneticsensors.com or contact us at 800-323-8295 (763-954-2474 internationally).

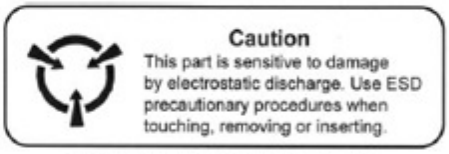

CAUTION: ESDS CAT. 1B

Honeywell
12001 Highway 55
Plymouth, MN 55441
Tel: 800-323-8295
www.honeywell.com/magneticsensors

Honeywell

Form #900204 Rev D
September 2006

C100™ Compass Engine

Innovative Stand-alone Heading Sensor

Key Features

- 3 unhoused variants, 1 housed version
- Extremely reliable, stand-alone sensor
- Multiple digital and analog user selectable outputs
- Automatic compensation for hard and soft iron errors
- Operates accurately in latitudes up to 80° magnetic dip
- Compact design
- Detachable sensor element for remote mounting (unhoused units)
- Industrial grade, extended temperature components rated at -40°C to +65°C and built to military quality standards
- Operating tilt range options:
  ±16° housed or unhoused versions
  ±30° unhoused version
  ±45° unhoused version

A Compass Engine to Meet Your Demanding Heading Sensor Applications

The KVH C100 is a complete stand-alone sensor that outputs extremely accurate heading data in any of six user-selectable digital or analog formats. Compact and affordable, the C100 was designed with flexibility in mind, facilitating integration into your system.

How the C100 Works

The C100 microprocessor-controlled fluxgate compass consists of a toroidal fluxgate sensor element and a small electronics board. Each C100 has a saturable ring core in a Lexan cylinder, free floating in an inert fluid to keep it horizontal with respect to the earth. Windings surround the Lexan housing, electrically driving the ring core into saturation and measuring the amplitude of induced pulses which are proportional to the earth's magnetic field. This data is then sent to the microprocessor, which compensates for the hard and soft iron magnetic interference of the host platform. The resulting output is translated into extremely accurate heading data.

The C100 calibration process provides a "score" of the quality of the compensation and the magnitude of magnetic interference present from the host platform. This information helps identify the optimal mounting location, ensuring the best performance in a wide range of applications.

Accurate and Versatile

To facilitate integration of the C100 into your application, a variety of analog and digital outputs may be accessed. A menu-driven software kit allows you to configure the C100's output for your product, or to connect it to your PC for prototype testing.

The unhoused C100's mechanical design permits one-piece mounting for simple installations as well as a detachable sensor element for applications where space restrictions or sources of magnetic interference (deviation) require remote sensor mounting. The aluminum-housed C100 (±16° of tilt only) has been designed to meet military specification shock (40G, 3 axes) and vibration (18G RMS, 30 minutes).

System Diagram

Unhoused Units
(SE-15 coil not shown)

The red line indicates where the sensor element may be "broken away" from the electronics portion for remote mounting.

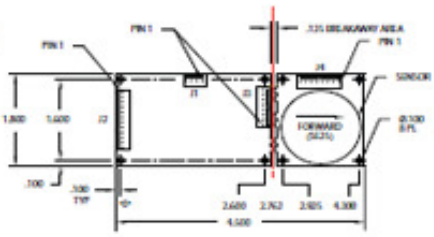

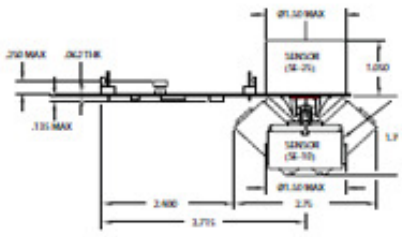

Aluminum Housed Unit
(SE-25 coil only)

Coil Operating Tilt Ranges:
SE-25: ±16°
SE-15: ±30°
SE-10: ±45°

Technical Specifications

Physical

Dimensions:	114.3 mm(l) x 45.72 mm(w) x 27.94 mm(h) (4.5" x 1.8" x 1.1")
Weight (unhoused):	64 g (2.25 ounces) – with SE-25 coil
Input Voltage:	+8 to +18 VDC or +18 to +28 VDC (user selectable)
Current Drain:	40 mA DC; maximum

Optional Aluminum Housing[1]

Dimensions:	80 mm(l) x 74.93 mm(w) x 57.15 mm(h) (3.15" x 2.95" x 2.25")
Weight (housed):	400 grams (14 oz.) – excluding cable

Environmental

Operating Temperature:	-40°C to +65°C (-40°F to +150°F)
Storage Temperature:	-57°C to +71°C (-71°F to +160°F)
Shock/Vibration:	Designed to meet MIL-STD-810 shock and vibration requirements
Altitude:	Designed to meet 12,192 meters (40,000 ft.) MSL
Reliability:	MTBF calculated to >30,000 hours

Performance

Accuracy[2]:	±0.5° or ±10 mils RMS (SE-25 coil and digital outputs)
Repeatability:	±0.2° or ±5 mils RMS (SE-25 coil and digital outputs)
Resolution:	0.1° or 1 mil
Dip Angle:	±80° (maintains stated accuracy after auto-compensation
Tilt Angle:	±16°; Dev = ±0.3° RMS (SE-25) ±30°; Dev = ±0.5° RMS (SE-15) ±45°; Dev = ±0.5° RMS (SE-10)
Response Time:	0.1 to 24 seconds (user selectable)

Digital Interface[3]

RS232 Compatible:	Bidirectional Serial Data, UART format w/ASCII characters, 300-9600 baud (user selectable)
Serial Input:	Accepts RS232 levels or 0 to +5V logic levels
Serial Output:	Same as RS232 except for 0 to +5V logic levels; (Logic "0"= +5V) 10K Ohm - min. load
Inv. Serial Output:	Same as Serial Output except logic "1" = +5V
NMEA 0183:	NMEA 0183 compatible bidirectional data/levels/formats
Synchronous:	Strobe Input: Ground momentarily to obtain data output Clock Output: 0 to +5V sq.wave @ 10 KHz rate Data Output: 0 to +5V levels Data Format: 4 digit BCD, 16 bit binary or 16 bit serial gray code – user selectable through serial port 10K Ohm minimum load on output signals

Analog Outputs

Sine/Cosine:	Output Voltage: +1.5V ±1.0V Reference Voltage: +1.5 VDC; 20K Ohm minimum load capability
Linear Voltage:	0.1 to 1.9 VDC into 20K Ohm minimum load

[1] SE-25 coil option only
[2] Accuracy measurements apply to a level compass module after compensation in a free magnetic field. After installation and auto-compensation, typical accuracies of ±0.5° are achievable on most platforms.
[3] Digital outputs can be user-configured to provide strobed or free running data at up to a 10 Hz message rate.

ISO 9001 CERTIFIED SYSTEM

KVH NASDAQ LISTED

KVH

Visit www.kvh.com

Made in the U.S.A.

DS_C100_A4_611

KVH Industries, Inc. • 50 Enterprise Center • Middletown, RI 02842-5279 • U.S.A. • Phone: +1 401 847-3327 • Fax: +1 401 845-2410

***mini-Springer* USV**

It was necessary to run an initial series of trials with a minimal platform, thus the mini-*Springer* was employed for these early tests. The first trials were attempted at test facilities in Brunel laboratories. It was not possible to get a GPS fix inside the labs hence the trials were conducted in an open water surface in Plymouth city centre where the *mini-Springer* performs a manoeuvre as shown in Figures A and B.

During these trials the initial readings from the sensors were spurious, predominantly due to the electromagnetic interference from the electric motors. To an extent this problem was tackled by housing the sensors as far away from the electric motors as practically possible. The major advantage of the *mini-Springer* was the portability, less man power intensive, cost effective and flexible to conduct experiments. Prior to this, attempts were made to modify a couple of model warships and other scaled versions of ships to enable the progress of further research. This was abandoned due to the limitations posed by the propulsion units, the reliance on rudder for controlling the heading, *et cetera*. Finally, *mini-Springer* offered a relatively similar test platform to the full scale *Springer* as it is also powered by twin motors.

A number of trials were conducted that enabled the cognition and practical aspects of the project. Some of the data collected during these trials are presented as follows. The path followed by the *mini-Springer* during trials 1, is shown in Figure C (i) and the heading angle of the *mini-Springer* is represented by Figure C (ii).

Figure A: Experiments with *mini-Springer* in front of Plymouth Civic centre

Figure B: The *mini-Springer* performing a manoeuvre

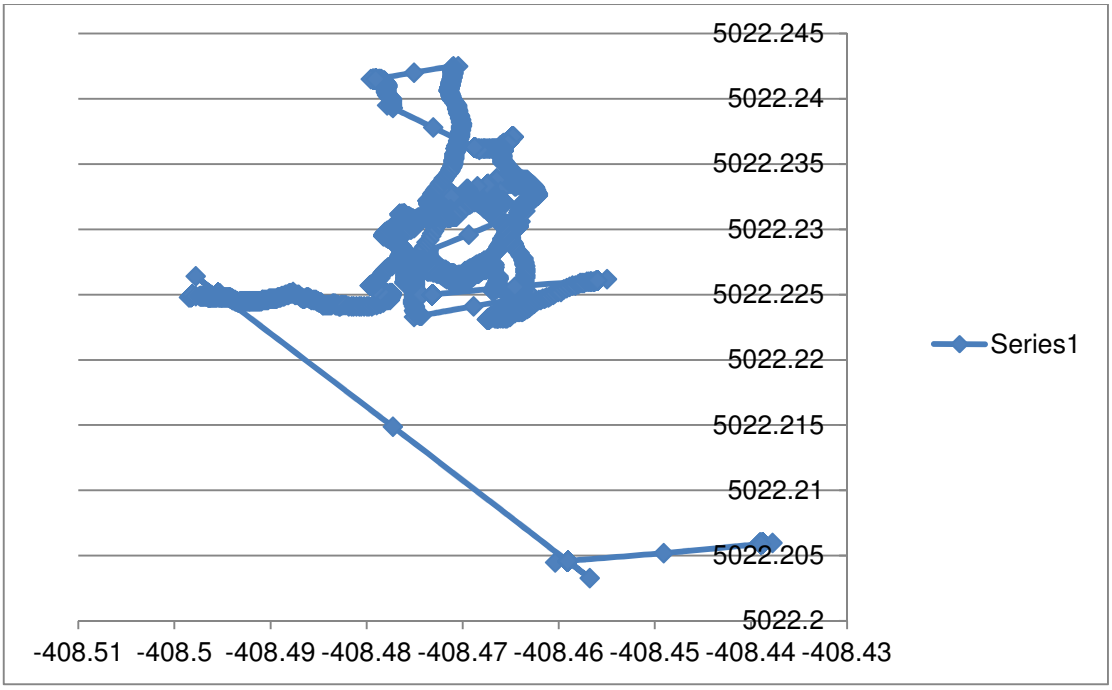

(i)

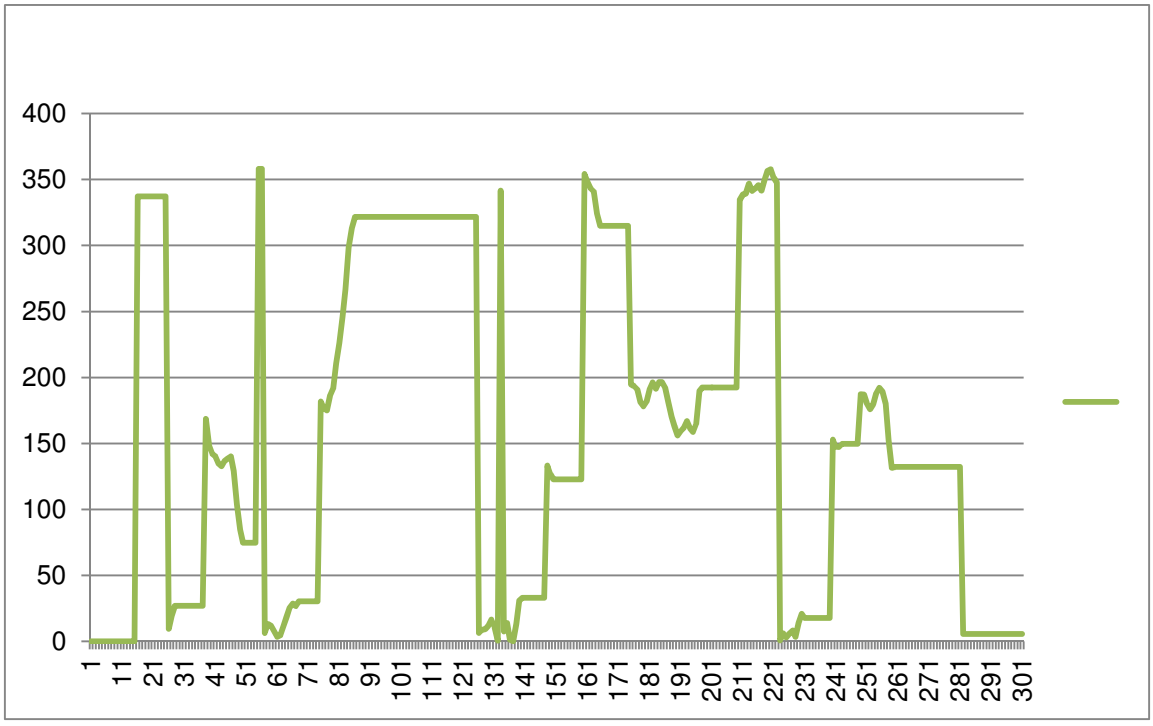

(ii)

Figure C: *mini-Springer* trials 1 (i) path followed (ii) heading angle

Furthermore, the path followed by the *mini-Springer* during trials 2, is shown in Figure D (i) and the heading angle of the *mini-Springer* is represented by Figure D (ii).

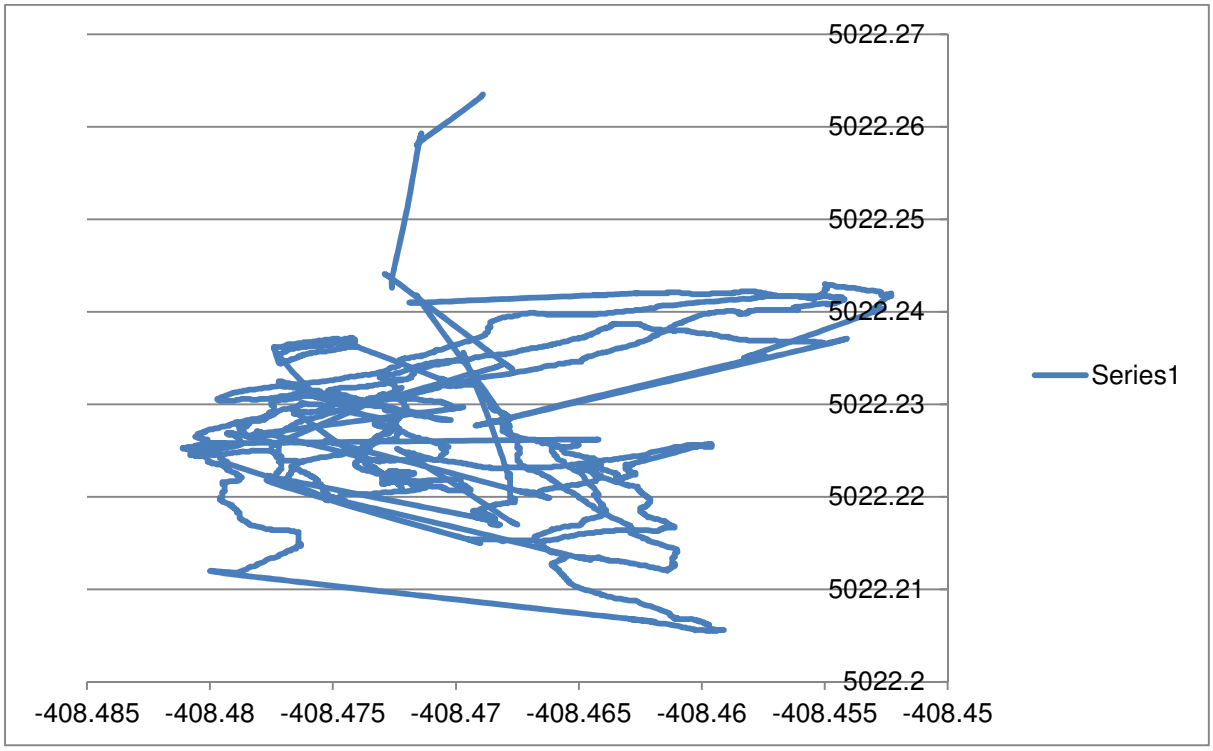

(i)

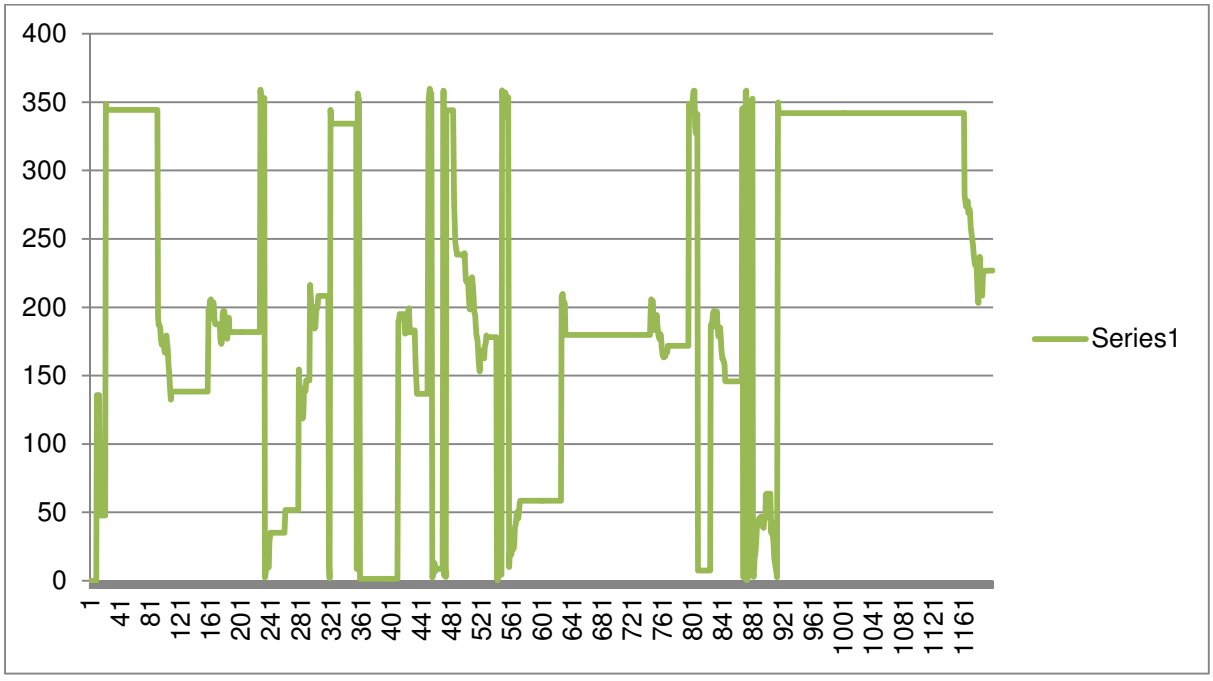

(ii)

Figure D: *mini-Springer* trials 2 (i) path followed (ii) heading angle

The *mini-Springer* was useful as it introduced the practical challenges encountered during experimentation and provided clearer understanding of the project. Nevertheless, it soon became obvious that the space avaiable in this test vessel was very restritive and it was forseen to build a bigger model (approx 90cm to 102cm). Initially equipments were anticipated to be onboard to perform closed loop system identification. A model fiberglass monohull of approximately 1m long was fabricated in the Brunel Laboritories with the help of Mr. Richard Cullen. This solved the problem of space available to house the sensors. However, owing to the constraints of available resources it was not practically feasible to make it operational. Hence, this issue was raised in a *Springer* technical meeting. The chair of the meeting, Professor Sutton was smitten by the idea and other researchers were also keen on utilising such a scaled down model of *Springer* to conduct their initial experiments. At this juncture, it is worth mentioning that to launch the full scale *Springer* it requires a team of 12-15 members, difficulty in finding a suitable water test site for a vehicle of 4.2m long, local transportation of at least one hour to reach the test site, the costs and timescales involved made it prohibitive for the researchers to conduct trials at short notice of time and it was not viable to test all ideas as and when they occurred. Despite the limitations of full scale *Springer* and other team members willingness to develop a scaled down version of *Springer*, Dr. Phillip Culverhouse disagreed and all further official progress along these lines were stalled.

Sutton **USV**

In spite of all the obstacles encountered, the promise of a portable and practical test platform propelled the development of *mini-Springer* in private. This resulted in the development of *Sutton* USV as shown in the following Figure E (i) and (ii).

(i)

(ii)

Figure E: *Sutton* Kayak USV (i) facing the Royal William Yard (ii) operating along the Cremyll Ferry Port, Plymouth, United Kingdom

The dimensions of *Sutton* USV is approximately 3m in length and 50cm in width. Initially it was envisaged to have two Kayaks and two motors to replicate the dynamics of *Springer*. However, the financial limitations meant that it was not practical. After a temporary time delay, further progress was resumed by modifying a wiper motor to provide the heading angle and utilising an electric motor to provide the thrust. Surprisingly, it was plausible to make this test platform operational. Additionally, it could also carry a weight of 100kg. Hence, there was no restriction in the amount of sensors and other electronic equipment that could be housed in such a facility. It was utilised as a test platform for a period of time. Further development and trials were undertaken with the full scale *Springer.*

This appendix A5 encapsulates time over a period of three years and shows the progression of various tests conducted on *mini-Springer* and *Sutton*.

RoboteQ

AX2550
AX2850

Dual Channel High Power Digital Motor Controller

v1.9b, June 1, 2007

visit www.roboteq.com to download the latest revision of this manual

	AX2550 AX2560	AX2550HE	AX2550SC AX2560SC	AX2550HESC	AX2850 AX2860	AX2850HE	AX2850SC AX2860SC	AX2850HESC
Power Stage								
Operating Voltage	2550 and 2850: 12V to 40V DC 2560 and 2860: 12V to 60V DC							
Number of Channels	2	2	1	1	2	2	1	1
Max Current 30s 1min 3 min 1h & more	120A 100A 80A 60A	140A 120A 100A 80A	240A 200A 160A 120A	280A 240A 200A 160A	120A 100A 80A 60A	140A 120A 100A 80A	240A 200A 160A 120A	240A 200A 160A 120A
Surge Current	>250A	>500A	>500A	>1000A	>250A	>500A	>500A	>1000A
MOSFETs per Channel	8	16	2 x 8	2 x 16	8	16	2 x 8	2 x 16
ON Resistance	5 mOhm	2.5 mOhm	2.5 mOhm	1.25 mOhm	5 mOhm	2.5 mOhm	2.5 mOhm	1.25 mOhm
Synchronous Rectification	Yes - Allows regenerative braking							
Current Limiting	By automatic power output reduction according to user preset limit and temperature							
Temperature protection	Automated current limit reduction starting at 80o C (175o F) case temperature							
Voltage protection	Output shut off below 12V and above 43V							
Power Wiring	8 AWG wires		8 AWG wire pairs		8 AWG wires		8 AWG wire pairs	
Command								
R/C Inputs	2 + 1 accessories (1.0ms - 1.5ms center - 2ms, Adjustable)				2 inputs (1.0ms - 1.5ms center - 2ms, Adjustable)			
Serial Interface	RS232. 9600 bauds							
Analog Interface	2 inputs (0V - 2.5V center - 5V)							
Input Corrections	Ch1 & Ch2 mixing for tank steering. Programmable deadband. 4 Exponent & Logarithmic command curves.							
Input/Outputs								
Optical Encoder Interface	May be added as option				4 Inputs for 2 incremental encoders. 125kHz max			
Analog Inputs	2 inputs, 8-bit resolution							
Digital Outputs	1 output, 24V 2A max.							
Digital Inputs	3 general purpose inputs				2 general purpose inputs.			
5V Supply Output	100mA max for Radio or other devices				100mA max for Encoders, Radio or other devices			
Operating Modes								
Open Loop Speed	Forward & Reverse Speed Control. Separate or Mixed							
Closed Loop Speed	Use Tachometer on analog inputs & PID				Use Tachometer on analog inputs or Optical Encoder & PID			
Position Mode	Use Potentiometer on analog inputs & PID				Use Potentiometer on analog inputs or Optical Encoder &PID			
Controller Configuration	Jumper-less. Configuration using built-in switch and LED display or PC utility							
Physical								
Operating Temperature	-40 to +85oC case temperature							
Enclosure	Heat-sinking Aluminum Extruded Case							
Controller size	5.5" (140mm) wide x 1.6" (40mm) tall x 9" (228mm) long including mounting brackets							
Cables	10" (25cm) RC cable to Radio. 4' (1m) RS232 cable for PC connection							
Weight	3.3lbs (1.5kg)							

On-board vehicle

Item	Acquired during current project	Qty	further details
Trolling motors with optical encoders	N	2	
ROBOTEQ motor controller	N	1	
RC signal receiver	N	1	
12VDC lead gel batteries	N	8	main batteries for motor power
12VDC lead acid gel batteries	Y	2	batteries for on-board electronics
Pelican Case Peli1650 Case	N	2	
leak sensors	N	2	within motor housings
speed sensor	N	1	paddle wheel sensor
depth sensor	N	1	
power electronics box	N	1	custom made to commute between RC and serial modes

Mast

Item	Acquired during current project	Qty	further details
shaft with mounted housing	N	1	
LynkSys WRT54GX router	N	1	for communication between Peli-cases and wireless comms with external laptop
pirate flag	Y	1	
cable with 2.1mm DC power plug to 2-pin Bulgin plug	N	1	for powering LynkSys WRT54GX router from STARBOARD Peli-Case
cable with RJ232 and no end connector (old router ehternet conection)	Y	1	

cable with RS232 and 8 way-pin plug for ethernet	Y	2	for connecting LynkSys WRT54GX router PCs in Peli-cases
cable with USB female to 4-pin Bulgin plug	Y	2	for connecting PCs in Peli-cases to GPS units on mast
G-Star IV USB GPS receiver	Y	2	

Pelican Cases

Starboard Pelican Case			
Item	Acquired during current project	Qty	further details
Intense PC Pro i7 (16 GB RAM, 300 GB SSD, 6 Serial Port Face Module)	Y	1	
TCM2 electronic compass unit	N	1	
TCM2 compass PVC housing	N	1	
TCM2 molex to serial connector cable (custom made)	Y	1	
KVH C100 electronic compass unit (in two parts)	N	1	
KVH C100 compass PVC housing	N	2	
KVH mokex to serial connector cable (custom made)	Y	1	
HMR 3000 electronic compass unit	N	1	
HMR 3000 compass housing	N	1	
HMR 3000 breadboard wiring to serial connector cable	Y	1	
serial male to female custom made cables	Y	3	for connecting compasses to PC
serial female to RJ-11 plug	Y	3	for connecting compasses to PC via serial face module
Arduino Mega 2560	Y	1	Used as A/D converter for gyroscope
Arduino Mega power supply wiring via 2.1mm jack to chocolate block	Y	1	
TinkerKit Gyroscope 2 Axis sensitivity 4X	Y	1	

sixteen terminal chocolate block	Y	1	Power distribution within Peli-case
twenty-four terminal chocolate block	Y	1	Power distribution within Peli-case
cable: mini-serial to serial female	Y	1	
cable: serial male to 3-pin Bulgin socket	Y	1	for connection of Intense-PC to Peli-case panel
cable : RJ45 to 8-way Bulgin socket	Y	1	for connection of Intense-PC to Peli-case panel
cable : USB to 4-way Bulgin socket	Y	2	for connection of Intense-PC to Peli-case panel
cable : 2.1 jack to open-ended wires	Y	1	for connection of Intense-PC power input to chocolate block
2-way Bulgin plug	N	1	for power to Peli-Case
2 way Bulgin socket	N	2	for power from Peli-Case
12-pin Bulgin socket	N	1	
MDF fibreboard customised platform	Y	1	for placing/attaching components, cables, etc.
metallic raised platform for Intense PC	Y	1	
Switches	N	2	embedded in front of Peli-case, formerly used to power on internal PCs
Heat sink fins screwed on Peli Case	N	2	
metallic brackets connecting heat sink to PC platform	Y	2	
Port-Side Pelican-case			
Intense PC i7 (16 GB RAM, 300 GB SSD, standard Face Module)	Y	1	
3 meter USB 3.0 Type-A to Micro-B cable with locking screws.	Y	1	Cable for camera

Other items

Item	Acquired during current project	Qty	further details
Futaba mains charger 230V	N	1	for charging remote control unit and RC receiver
AC adapter 230VAC to 12V DC, 800mA	N	1	for powering Springer router (LynkSys WRT54GX) from mains
Sanyo Xacti VPC-CA 100 Handheld Camera	Y	1	for documenting Springer trials
2-pin Bulgin plug to 2-pin connector compatible with KEEPOWER battery charger socket	Y	2	for charging 12VDC batteries on Springer from panel sockets
keepower 12V 4Amp battery charger	N	2	for charging Springer 12V batteries
USB to serial (DB9) cables	Y	9	
Futaba radio control unit	N	1	for mechanical manual remote control of Springer
Anemometer	Y	1	
orange Bulgin tool designed by Mike and Bill	N	1	for unscrewing Bulgin sockets
3-pin Bulgin plug to DB9 male serial cable	Y	1	for connecting the ROBOTEQ controller to a computer serial port from the Springer panel
GARMIN GPS 76 handheld GPS unit in box	N	1	
3-pin Bulgin plug to 3-pin Bulgin socket short cable	Y	2	for connecting STARBOARD Peli-Case to ROBOTEQ controller
2-pin Bulgin plug to 2-pin Bulgin socket short cable	Y	3	for connecting STARBOARD Peli-Case to 12VDC battery within Springer Hull
2-pin Bulgin socket to Banana terminals short cable	Y	1	for powering STARBOARD Peli-Case from a DC power supply unit or external car battery
OS map of Launceston & Holsworthy	Y	1	used for landmarking Roadford Lake
Keyboard protective film	Y	4	protection against light rain
Raymarine E85001 Interface. ST40	N	1	
ND-100S GPS Dongle	Y	2	
Belkin N150 wireless modem router	Y	1	router for communication with Intese PC in office enviroment

winch straps with hooks	N	4	for securing Jerry-cans when on Springer
HMC5883L Electronic Compass 3-Axis Magnetoresistive Sensor	N	1	
GY-521 MPU-6050 Module 3 axial gyroscope accelerometer	N	1	
MBC24-63/3 24 V 60Amp battery charger	N	2	chargers for Springer motor batteries
Chemtronics Heat Sink grease tube	Y	1	
Waders	Y	4	
jerry cans (25 litres)	Y	4	
Fenders	Y	4	
canvas tarpaulin sheet (white)	Y	1	small sheet
umbilical cord with floaters, attached to cable1: 3-pin Bulgin socket to 3-pin Bulgin plug; cable 2: RJ45 to 8 pin Bulgin socket	N	1	
Laptop Dell Inspiron 15R 7520	Y	1	
Laptop Toshiba Satellite P775-10K	Y	1	
TOSHIBA PA3817U-1BRS replacement Battery	Y	3	
Seagate USB 2.0 1TB Portable HDD (White Colour)	Y	2	
BlackMagic Intensity Shuttle (USB 3.0)	Y	1	
2 Port USB 3.0 PCI Express Card	Y	1	
Buffualo Ministation 500 GB USB 2.0 HDD (Black Colour)	Y	1	
Walimex Pop-Up 50cm Laptop Tent Super – Black	Y	1	
Targus Carry Case/XXL for Notebook	Y	1	
PointGrey Flea3 FL3-U3-32S2C-CS USB 3.0 Vision System	Y	1	
UTC Aerospace IMU02	Y	1	
universal laptop power supply	Y	1	For powering laptop from DC battery
Tarpaulin tent	Y	2	For housing *Springer*
Rigid-frame garage	Y	1	For housing *Springer*

Plan details	Purpose	Actions
Initial seaworthy test on remote control operation. Data logging (compasses, GPS, motor rpm)	To make sure systems are operative and solve any arising issues.	Short trial (maybe just several minutes) guiding the vessel via remote control, after which it will be verified that systems have been running correctly and that data has been logged correctly by the on-board computers.
Assess wind and current conditions.	Measure drift speed of the vehicle under no motor thrust. This will provide an idea of the current speed and direction, and its variability along the reservoir.	Position the vehicle where it can drift freely, whilst collecting data (mainly GPS). Repeat at several different locations. Prepare anemometer and take measurements of wind speed and direction, to correlate with drift speed.
Manual control through umbilical cable.	Be able to manoeuvre the vessel from the general purpose laptop connected to the RoboteQ controller via umbilical cable. Verify relationship between n_1, n_2 and n_c, n_d (make sure sign of n_d as function of n_1 and n_2 is correct).	Short trial. Run the vehicle with constant n_c and gradually apply n_d in one direction and then the other. Verify that the vehicle turns as expected (in the right direction!)
Data collection for n_c – forward speed static relationship.	To model the static (steady-state) relationship between n_c and forward speed of the vehicle. This relationship will be graphed and used when dynamic steering models are obtained for different constant values of n_c. This trial will also enable the range of n_c to be determined.	Perform several trials, under umbilical control mode, maintaining a constant heading and each trial at constant forward speed. This will enable to vehicle to reach a steady forward speed. GPS and compass data to be collected during these trials. Wind speed to be measured using anemometer (if available). In the case of

		significant current drift, to factor this out several trials in different directions for the same n_c should be conducted.
Data collection for dynamic steering models.	Data collection for obtaining steering dynamic models maintaining n_c constant.	Perform several trials under umbilical control mode. Each trial will have a constant value of n_c. To be decided how many models are required depending on the range of n_c. Each trial should be conducted with steering manoeuvres which excite the steering dynamics (appropriate n_d signals). Wind speed should be measured (if possible). Data collected will include GPS and compass readings stored on NGC PC.
Open loop control with NGC PC	Realise some basic manoeuvres pre-programmed on the NGC PC to verify open loop control functionality.	The vehicle will be placed in an open area void of obstacles. A simple open loop control sequence will be applied from the NGC PC (pre-programmed to realise a small closed route).
Vision Based Odometry with constant velocity ("narrow" localisation up-to-scale).	Use optical flow to track points in multiple frames in order to infer self-motion (as a rotation translation) up-to-scene scale. The velocity value is used to scale the estimates.	Provide pose estimates at any time while *Springer* is running at constant velocity.
Vision based odometry with IMU readings (refined scaled "narrow" localisation).	Again, use optical flow to infer self-motion in terms of rotation and translation from some original coordinate frame and fuse with IMU readings in order to obtain	Provide pose estimates at any time while *Springer* is performing motion with arbitrary characteristics.

	scale and refine odometry.	
Video collection of data of the coastal area combined with GPS (and possibly now, IMU) in order to acquire scene descriptors for wide localisation.	Interpolate depth information using odometry and scene (using possibly some sparse modelling technique – AKA dimensionality reduction) to produce scene descriptors for "wide" localisation.	Record video and GPS (and/or IMU) data from coastal areas of all sorts.
"Wide" area localisation	Localise roughly with respect to a scene (i.e., a descriptor).	Build a map of visited areas during a mission.
SLAM	Localise both in the narrow and wide sense. In other words, the vehicle will not only be self-aware of its odometry, but will also be incrementally building a map (of scene descriptors) against which, it will attempt to do loop closure.	Run the *Springer* without GPS in "roaming" mode, during which, a map will be built. Then run a mission in which the vehicle finds its way to a desired area in the map.

As seen by Figure A (ii) the signal from the GPS receiver was intermittent. Hence, the path was not a trajectory as expected. During this trial a wind speed of 2-4 m/s (4-8 knot) in a south westerly direction was observed.

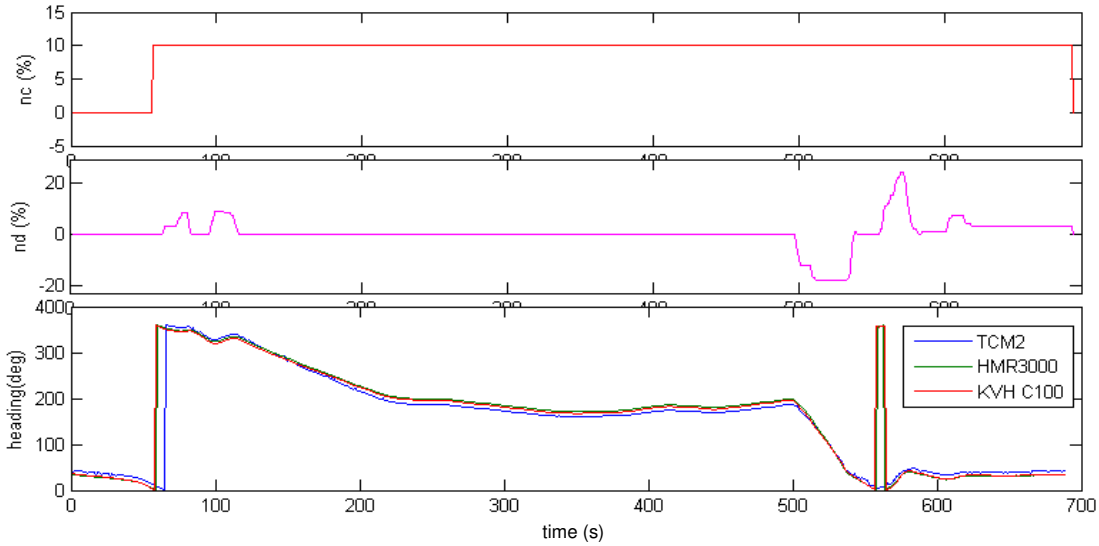

(i)

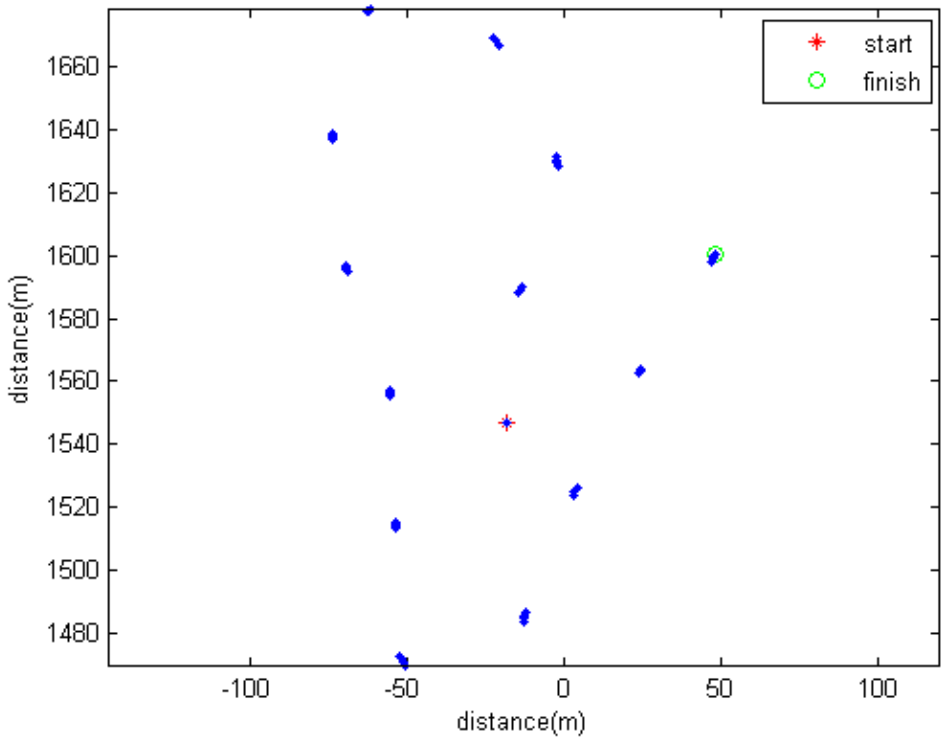

(ii)

Figure A: Data set 1 (i) n_c, n_d and heading (ii) actual trajectory

Data set 2 was collected under the following conditions: n_c 20% , wind speed 1-3 m/s (2-6 knots), south westerly direction. The results can be found from the following Figure 4.7.

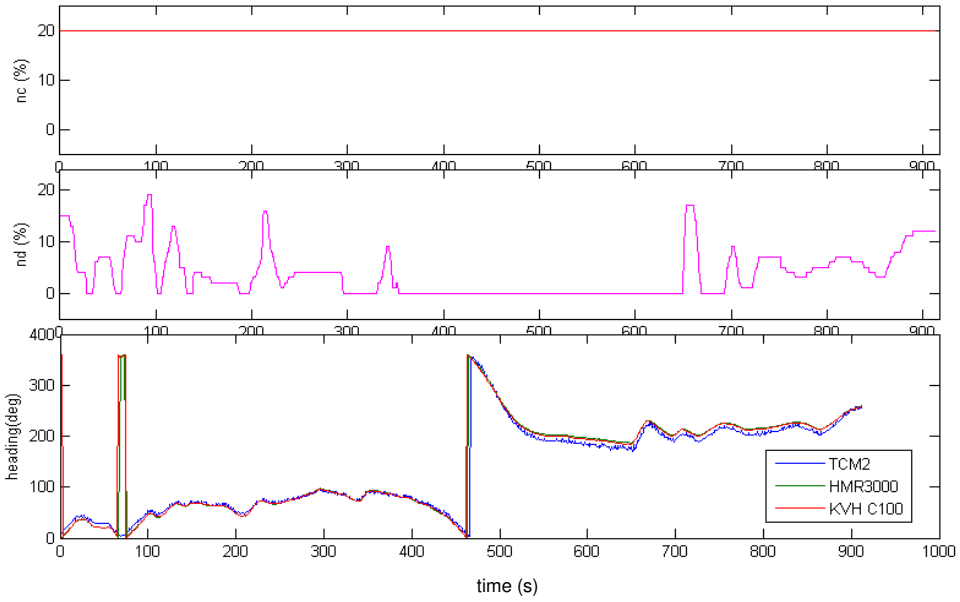

(i)

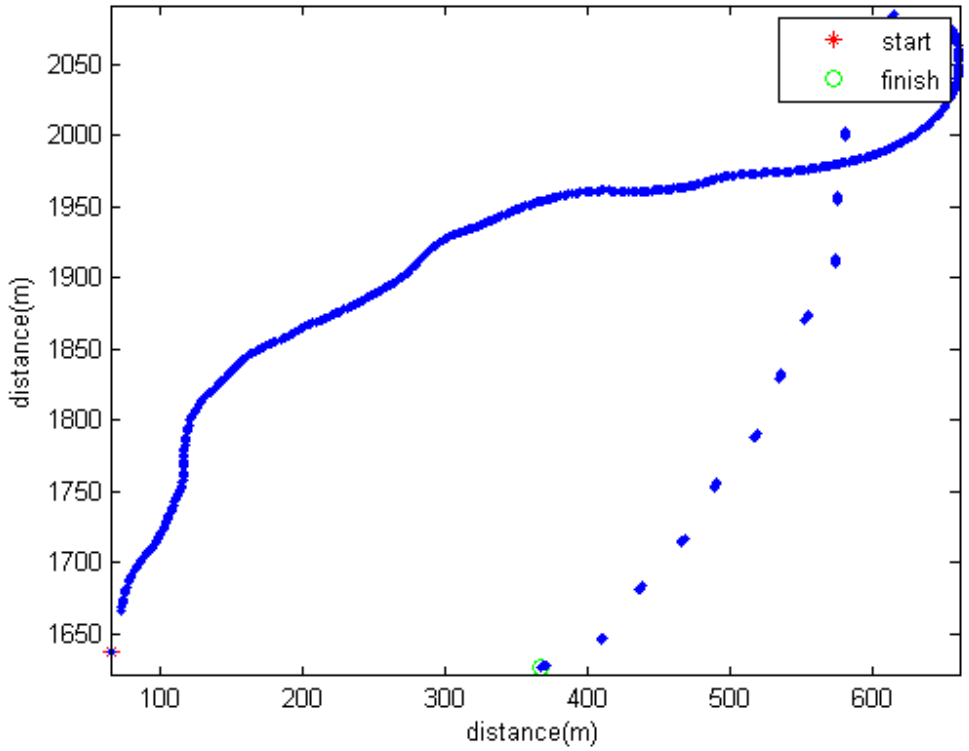

(ii)

Figure B: Data set 2 (i) n_c, n_d and heading (ii) actual trajectory

Data set 3 was incongruent because the compasses were not calibrated appropriately. The results can be found from the following Figure C.

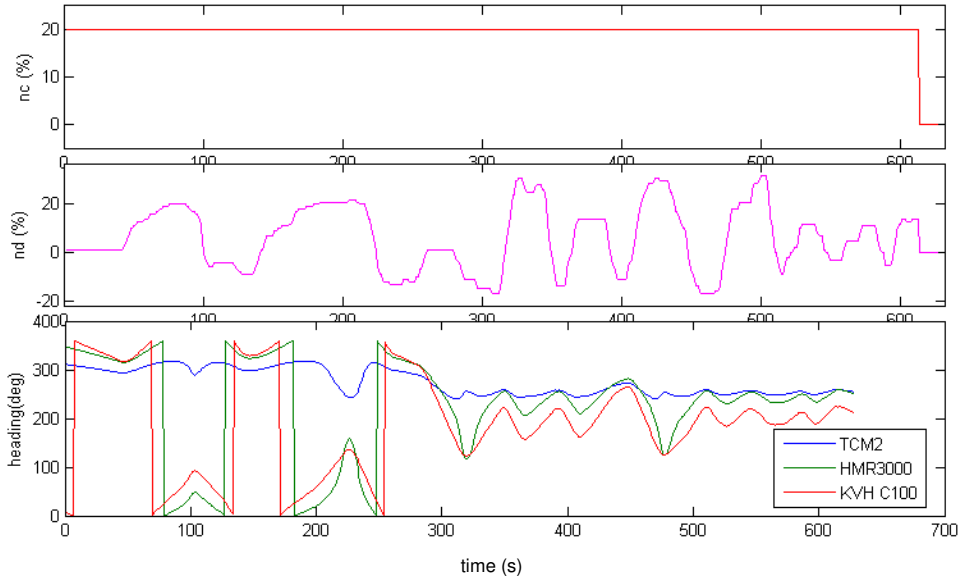

(i)

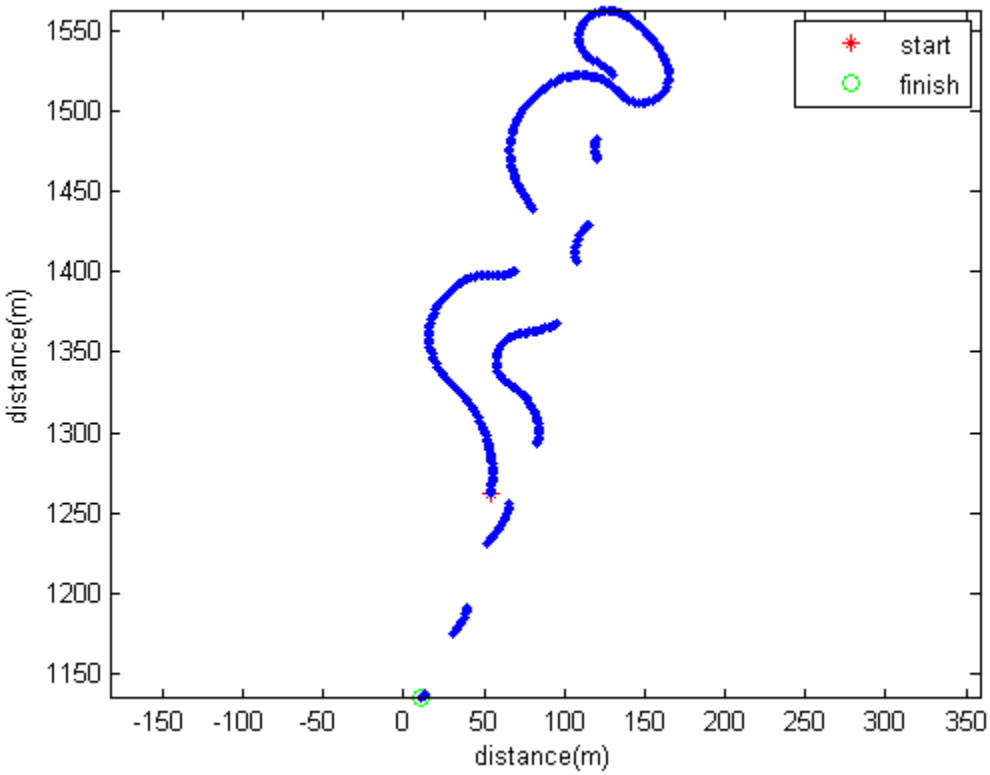

(ii)

Figure C: Data set 3 (i) n_c, n_d and heading (ii) actual trajectory

Data set 4 was collected under the following conditions: n_c = 20%, n_d superimposed with PRBS of ±2 %, wind speed 1.75 m/s (3.5 knots) in a northerly direction. The results can be found from the following Figure D.

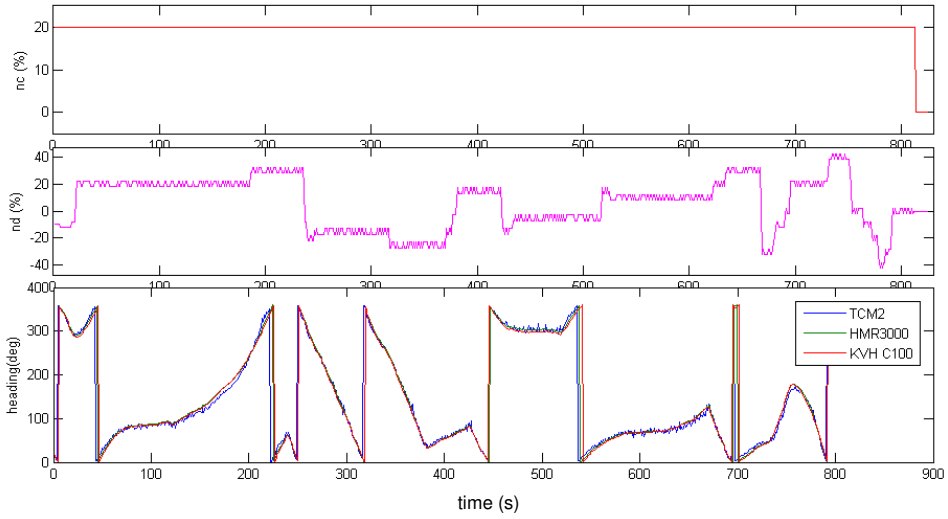

(i)

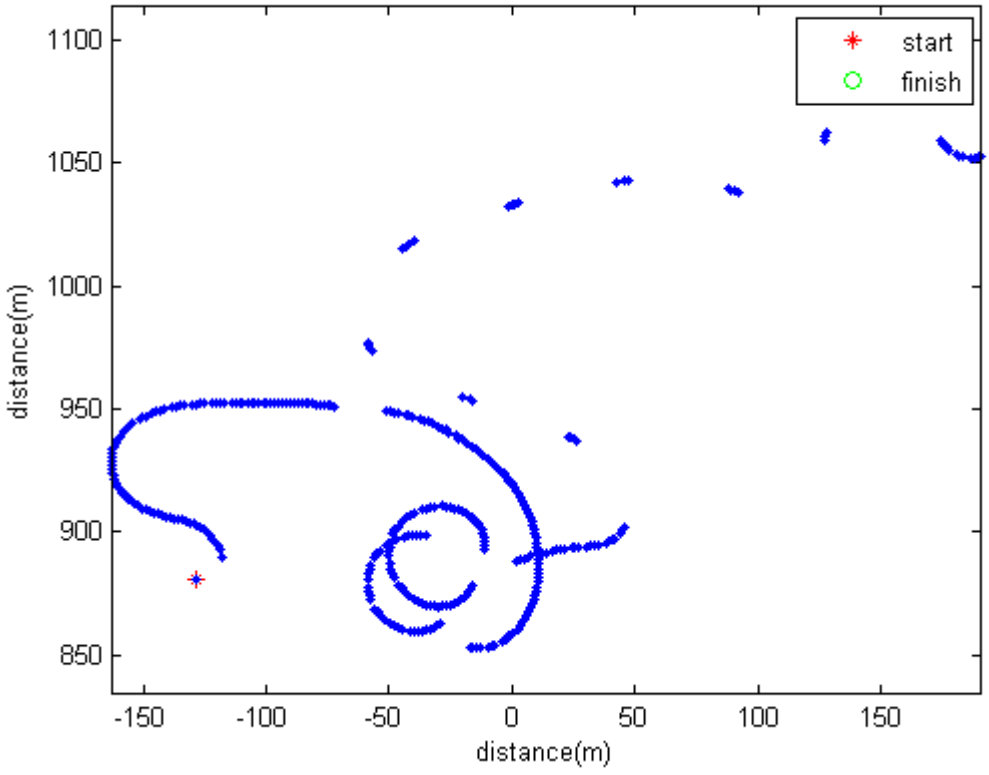

(ii)

Figure D: Data set 4 (i) n_c, n_d and heading (ii) actual trajectory

Data set 5 was collected under the following conditions: n_c=30%, n_d with superimposed PRBS of ±3% , wind speed of 1.5-3 m/s (3-7 knots) in a north and north-easterly direction . The results can be found from the following Figure E.

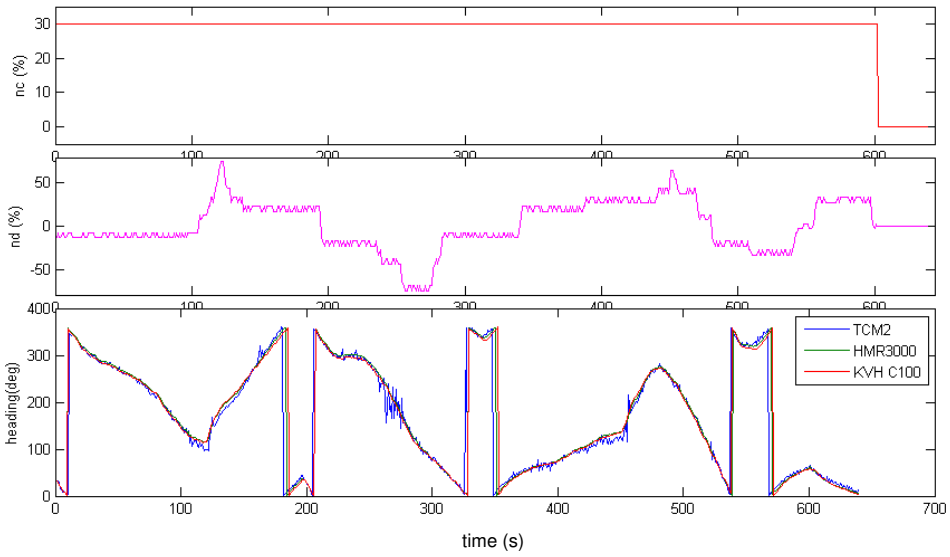

(i)

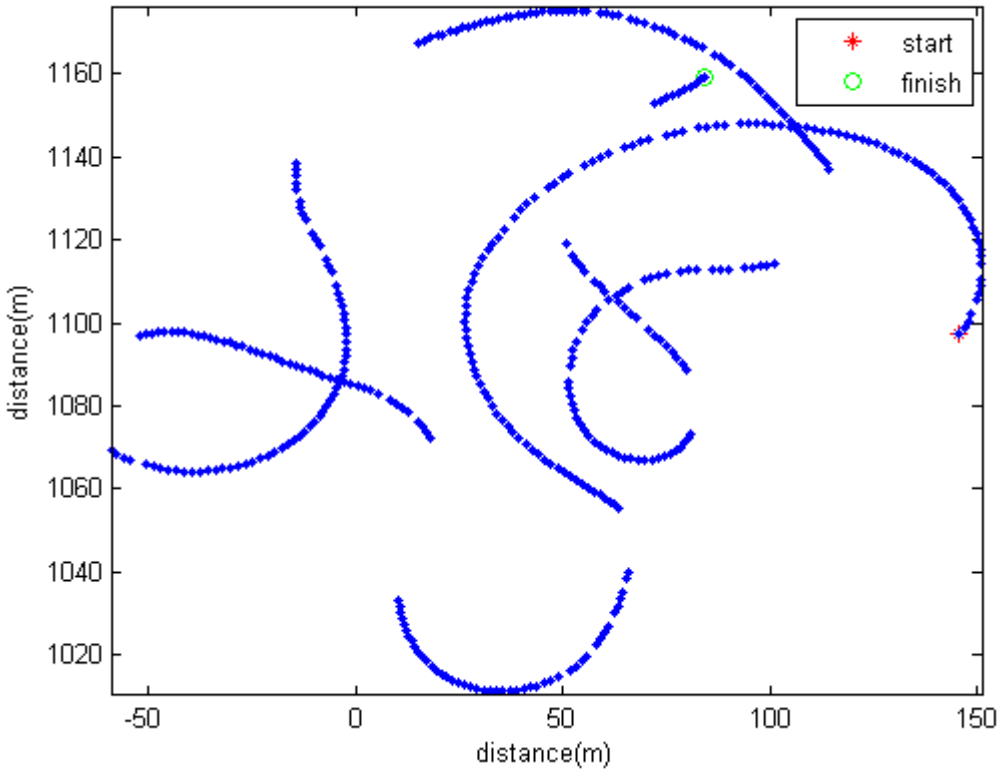

(ii)

Figure F: Data set 5 (i) n_c, n_d and heading (ii) actual trajectory

Data set 6 was incongruent because the compasses were not calibrated appropriately. The results can be found from the following Figure G.

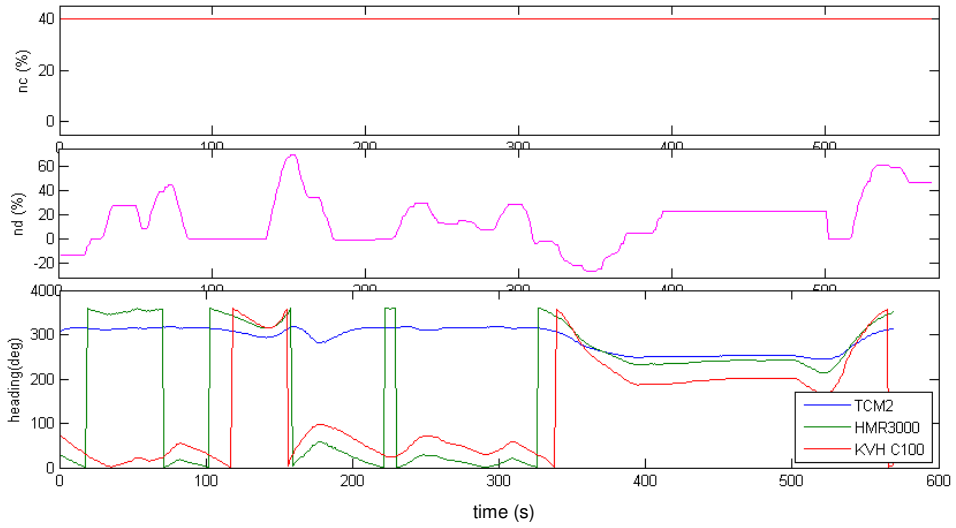

(i)

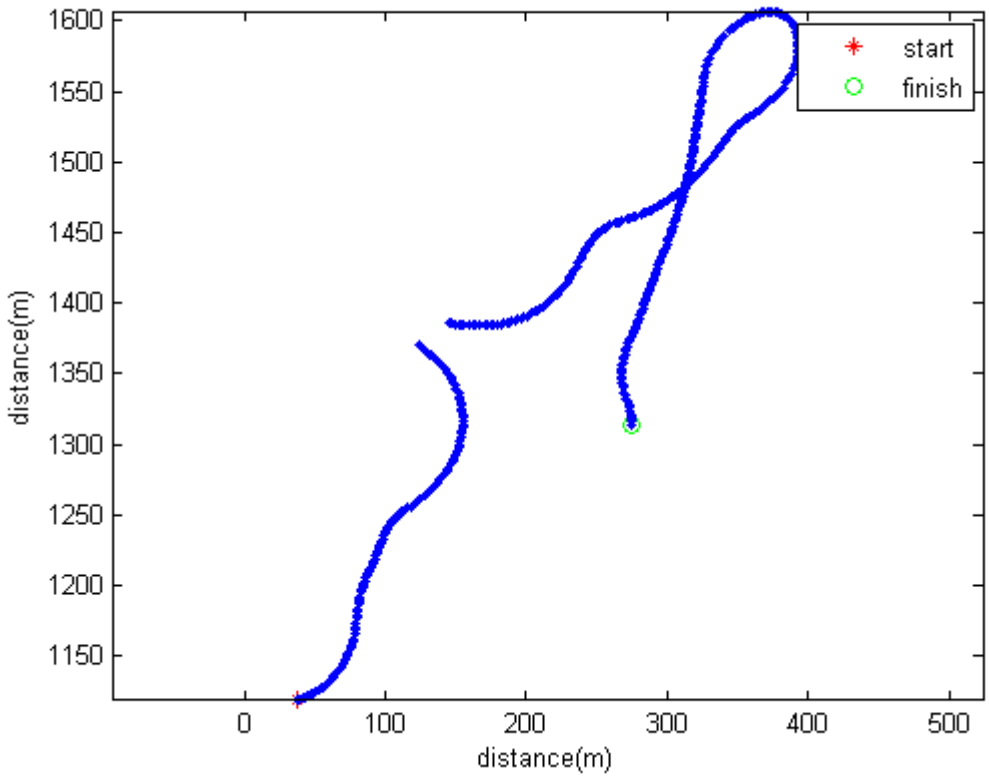

(ii)

Figure G: Data set 6 (i) n_c, n_d and heading (ii) actual trajectory

Data set 7 was collected and the results can be found from the following Figure H.

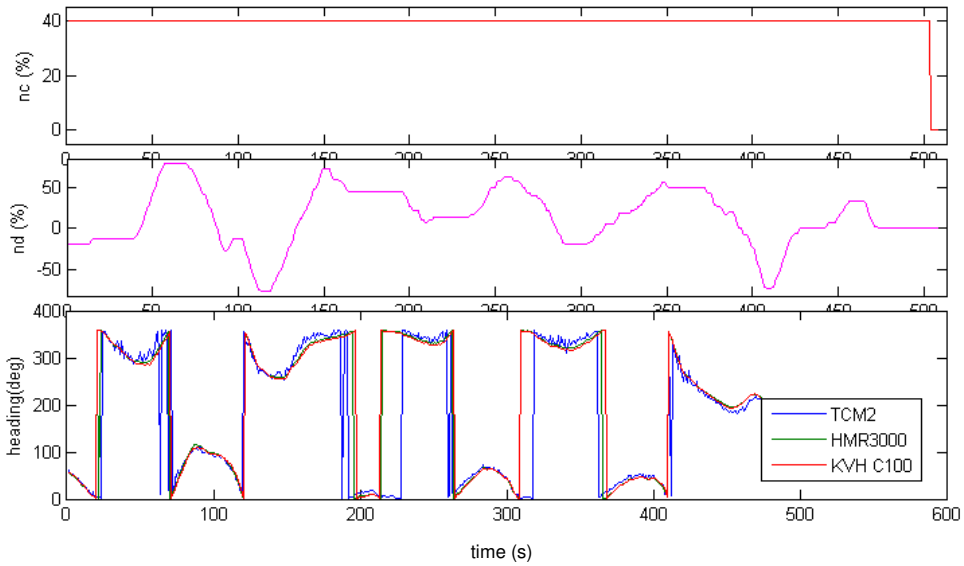

(i)

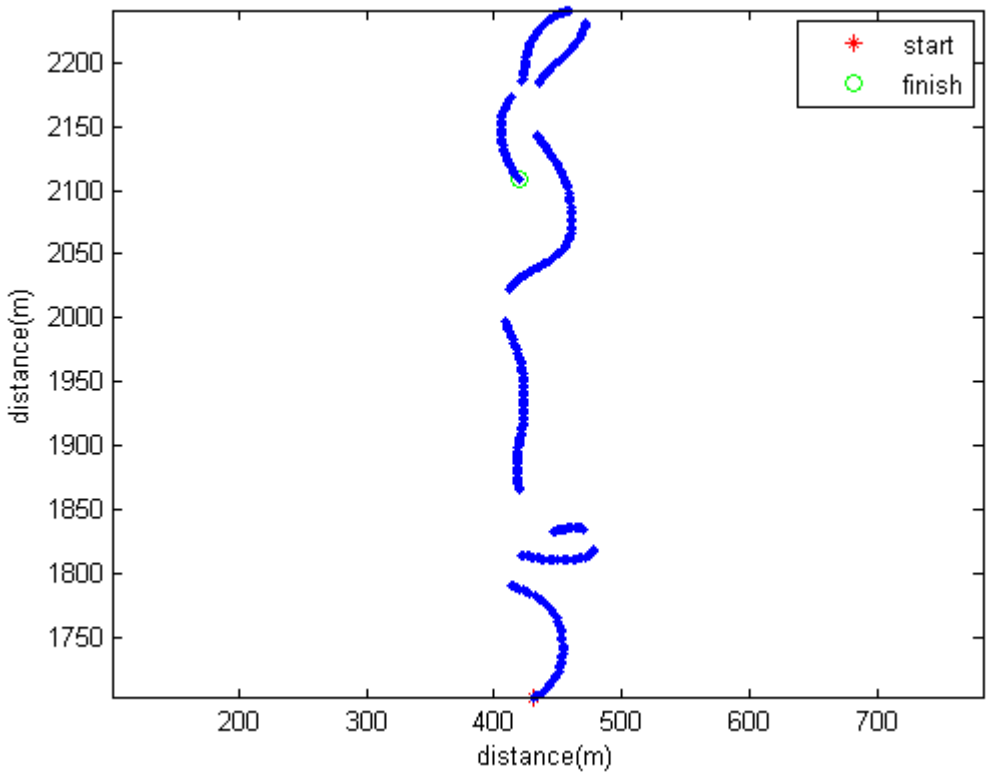

(ii)

Figure H: Data set 7 (i) n_c, n_d and heading (ii) actual trajectory

Data set 8 was collected under the following conditions: n_c=40%, n_d with superimposed PRBS of ±3%. The results can be found from the following Figure I.

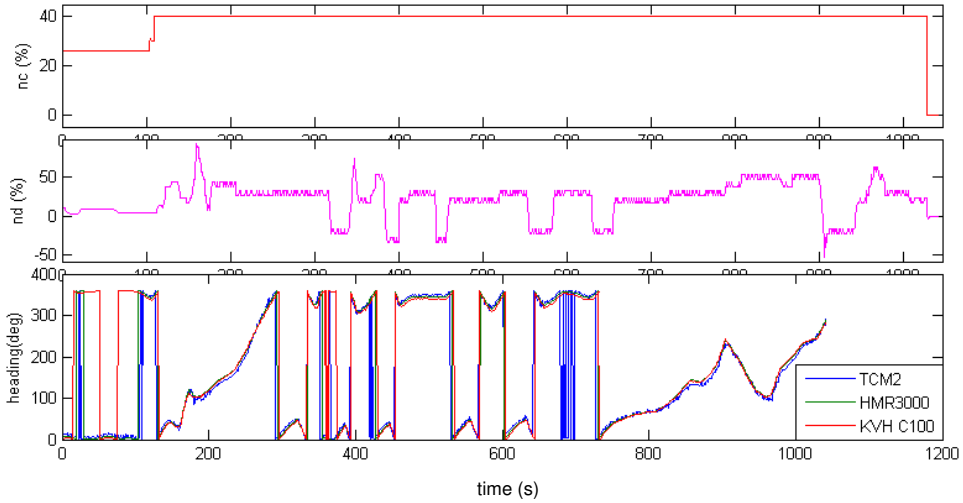

(i)

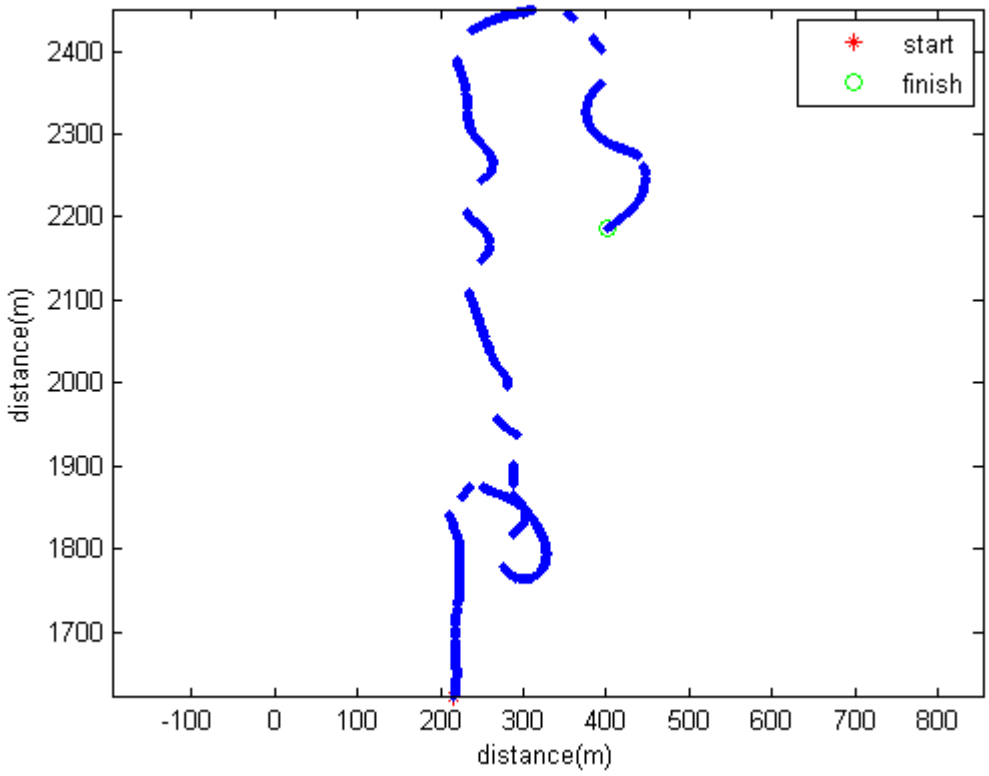

(ii)

Figure I: Data set 8 (i) n_c, n_d and heading (ii) actual trajectory

Data set 9 was collected and the results can be found from the following Figure J.

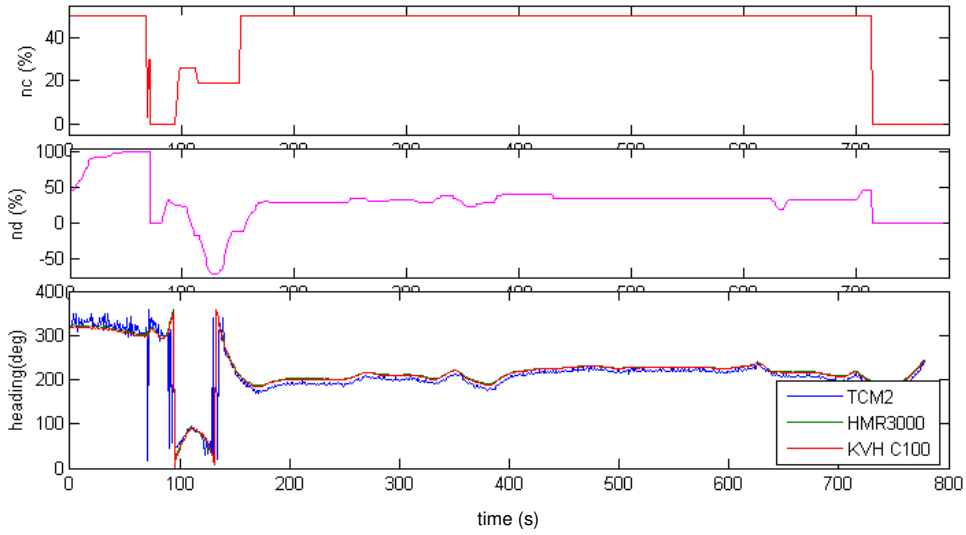

(i)

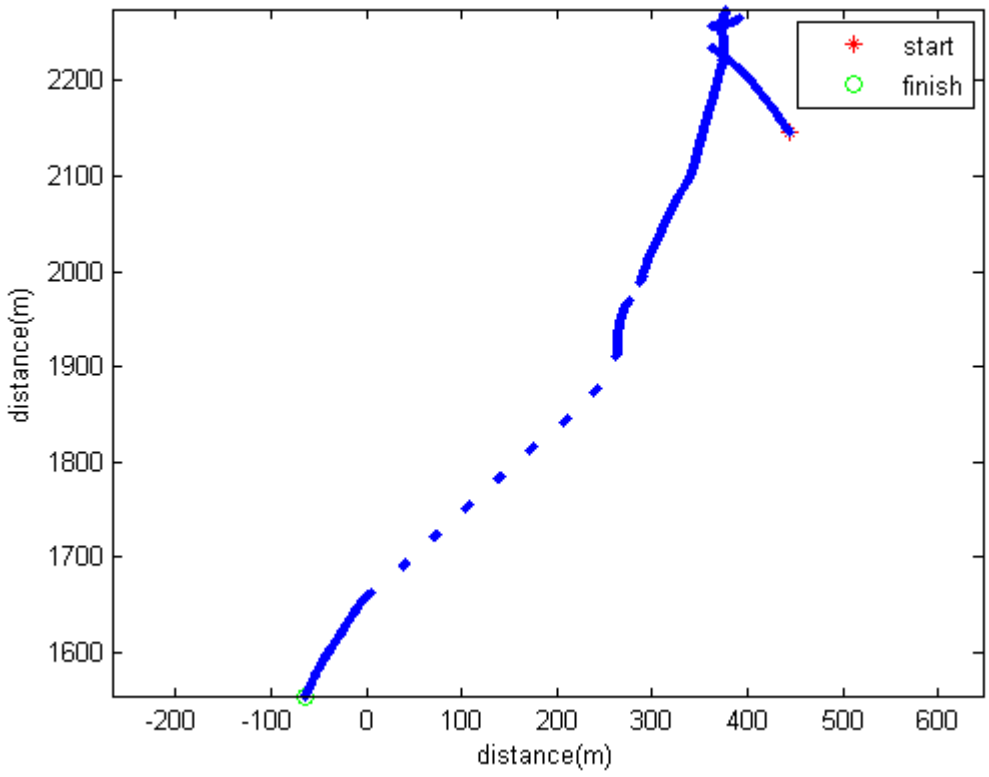

(ii)

Figure J: Data set 9 (i) n_c, n_d and heading (ii) actual trajectory

Data set 10 was incongruent because the compasses were not calibrated appropriately. The results can be found from the following Figure K.

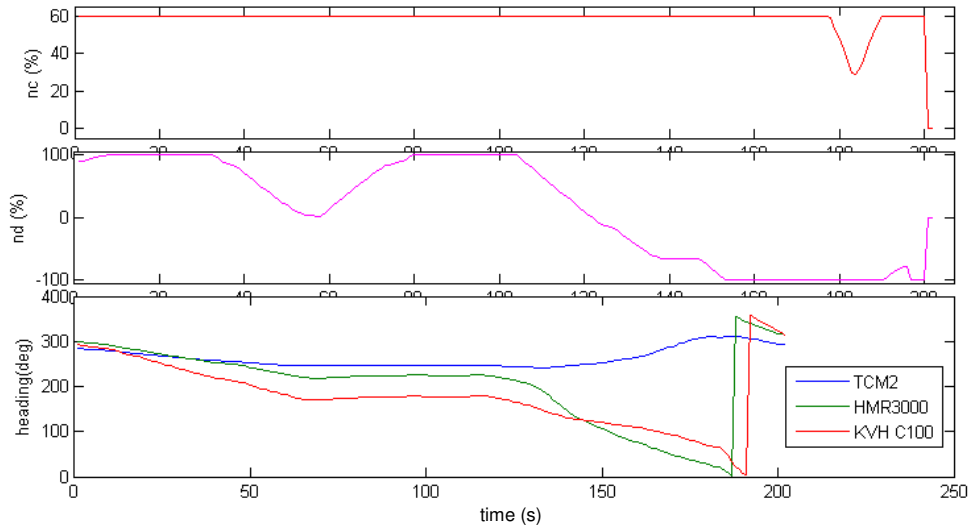

(i)

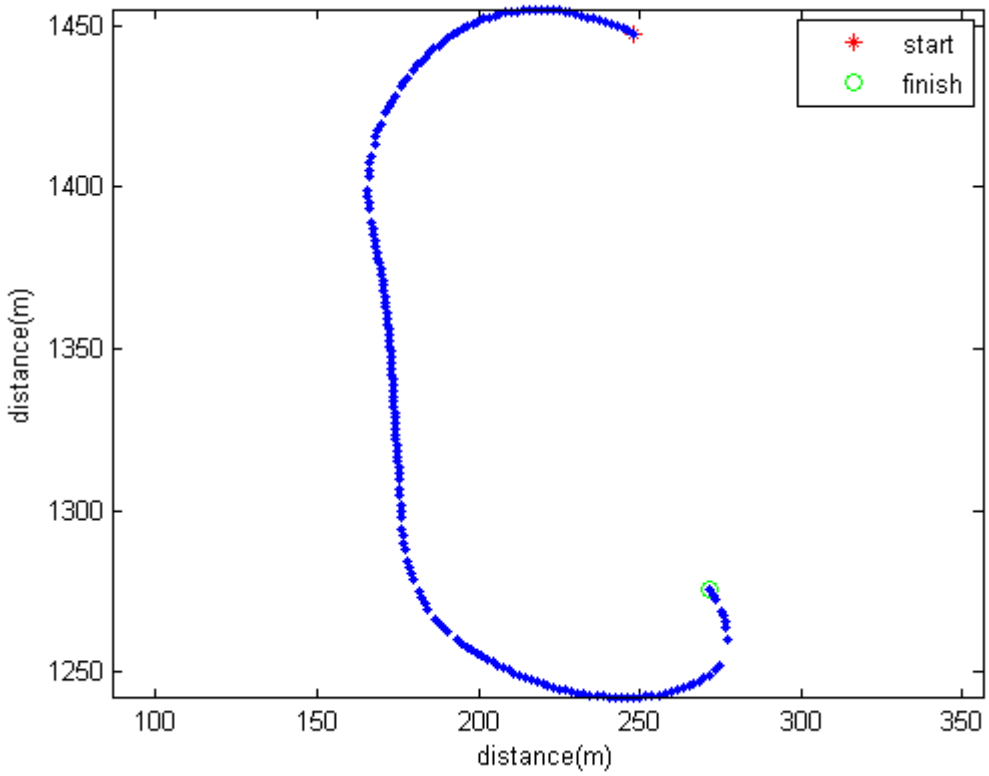

(ii)

Figure K: Data set 10 (i) n_c, n_d and heading (ii) actual trajectory

Appendix D

Publications

Significant contributions have been made through the course of this research and the newly acquired knowledge has been disseminated via journal articles, conference papers and technical reports as follows:

Journal papers

- Annamalai, A.S.K., Sutton, R., Yang, C., Culverhouse P., Sharma, S., (2014). Robust Adaptive Control of an Uninhabited Surface Vehicle, Journal of Intelligent & Robotic Systems, Springer Netherlands, issue May.

- Annamalai, A.SK., Motwani, A., Sutton, R., Yang, C., Sharma, SK. and Culverhouse, P., (2013). A robust navigation technique for integration in the guidance and control of an uninhabited surface vehicle, Journal of navigation, 11 October (under review).

- Sharma, S., Sutton, R., Motwani, A. and Annamalai, A.SK., (2013). Nonlinear control algorithms for an unmanned surface vehicle, Proceedings of the Institution of Mechanical Engineers, Part M: Journal of Engineering for the Maritime Environment, 5 November, doi: 10.1177/1475090213503630.

Conference publications and presentations

- Annamalai, A.S.K., Sutton, R., Yang, C., Culverhouse P. and Sharma, S., (2014). Innovative adaptive autopilot design for uninhabited surface vehicles, Twenty fifth Irish Signals and Systems Conference, 26-27 June, Limerick, Ireland.

- Motwani, A. and Annamalai, A.SK., (2013). Autonomous environmental monitoring, Making Waves Conference, 28 November, Plymouth Marine Laboratories, Plymouth, Devon, United Kingdom.

- Annamalai, A.SK., Sutton, R., (2013). An adaptive autopilot design for an uninhabited surface vehicle, Fourth UK Marine Technology Conference, 11-12 June, University College London, United Kingdom.

- Annamalai, A., Motwani, A., Sutton, R., Yang, C., Sharma, SK. and Culverhouse P., (2013). Integrated navigation and control system for an uninhabited surface vehicle based on interval Kalman filtering and model predictive control, Proceedings of the First IET Control and Automation Conference, 4 - 5 June, Conference Aston, Lakeside Centre, Birmingham, United Kingdom.

- Annamalai, A., Yang, C. and Sutton, R., (2013). Closed loop identification of an uninhabited surface vehicle, Proceedings of the 1st IET Control and Automation Conference, 4 - 5 June, Conference Aston, Lakeside Centre, Birmingham, United Kingdom.

- Annamalai, A.SK., (2012). Guidance and control of an USV, Making Waves Conference, 18 December, Plymouth Marine Laboratories, Plymouth, Devon, United Kingdom.

- Annamalai, A.SK., (2012). Guidance and control of an USV, Plymouth University projects showcase, 11 September, Plymouth, Devon, United Kingdom.